

Final Report to the
Air Resources Board
Contract No. 04-326

**Analyses of PM-Related Measurements
for the Impacts of Ships**

by
Philip K. Hopke
InJo Hwang
Eugene Kim, and
Jong Hoon Lee
Clarkson University
Center for Air Resources Engineering and Science
Box 5708
Potsdam, NY 13699-5708

Disclaimer

The statements and conclusions in this Report are those of the contractor and not necessarily those of the California Air Resources Board. The mention of commercial products, their source, or their use in connection with material reported herein is not to be construed as actual or implied endorsement of such products.

Acknowledgment

This Report was submitted in fulfillment of contract number 04-326, Analyses of PM-Related Measurements for the Impacts of Ships by Clarkson University under the sponsorship of the California Air Resources Board. Work was completed as of September 1, 2006.

Table of Contents

List of Figures	vi
List of Tables	xii
ABSTRACT	xiv
EXECUTIVE SUMMARY	xv
INTRODUCTION	1
Ship Emission Characteristics	2
Prior Analysis of IMPROVE Data	2
DATA ANALYSIS METHODS	3
Positive Matrix Factorization	3
Conditional Probability Function	5
Variable Selection Criteria	5
STUDY RESULTS	5
IMPROVE Data	6
Aqua Tibia	6
San Gabriel	12
San Rafael	18
Pinnacles National Monument	24
Yosemite National Park	32
Point Reyes National Seashore	39
Redwood National Park	46
Kalmiopsis	53
Olympic National Park	62
Effect of Changing Analytical Methodology on Ship Emissions Apportionment	70
Aqua Tibia	70
Point Reyes	71
STN Data	74
Anchorage, AK	74
Seattle, WA	80
Beacon Hill IMPROVE	113
Comparison of Beacon Hill Site Results	121
Portland, OR	122
San Jose, CA	130
4 th Street.	130
Jackson Street.	137
Comparison of the 4 th Street and Jackson Street Results.	141
Los Angeles, CA	145
San Diego, CA	166
Escondido.	169
El Cajon.	176
Relationship of Primary Combustion Emissions to Other Species	184
CONCLUSIONS	187
REFERENCES	189

List of Figures

Figure ES1. Map showing the locations of the IMPROVE (yellow dots) and STN (green dots) sites that were used to assess the impacts of ship emissions on PM _{2.5} concentrations along the west coast of the United States.	xv
Figure ES2. The oil combustion contributions obtained at the Beacon Hill STN site in Seattle, WA plotted against the sulfate contributions at this site.	xvi
Figure ES3. The residual oil combustion contribution at the Olive St. site in Seattle plotted against the secondary sulfate contributions.	xviii
Figure ES4. The residual oil combustion contribution at the Duwamish site in Seattle plotted against the secondary sulfate contributions.	xviii
Figure ES5. Plot of the residual oil contributions against the secondary sulfate contributions for the El Cajon STN site.	xviii
Figure ES6. Plot of the residual oil contributions against the secondary sulfate contributions for the Escondito STN site.	xviii
Figure ES7. Residual oil combustion contributions plotted against the corresponding secondary sulfate contributions at Point Reyes National Seashore.	xix
Figure ES8. Residual oil combustion contributions plotted against the corresponding secondary sulfate contributions at Olympic National Park.	xix
Figure 1 Estimated NO _x emissions in the US from shipping in 1997. Figure taken from Corbett and Fishbeck (2000).	2
Figure 2 Oil combustion emissions profiles derived from IMPROVE data.	3
Figure 3 Map showing coastal and near-coastal IMPROVE sites in California.	6
Figure 4 Predicted mass concentrations compared to the measured mass concentrations for the Aqua Tibia IMPROVE site.	7
Figure 5 Source profiles derived from the PMF2 analysis of the IMPROVE data from the Aqua Tibia site.	9
Figure 6 Source contribution time series derived from the IMPROVE data from the Aqua Tibia site.	10
Figure 7 HYSPLIT trajectory calculated for noon on November 25, 2002.	12
Figure 8 HYSPLIT trajectory calculated for noon on October 30, 2003.	12
Figure 9 Map of the Los Angeles area showing the location of the San Gabriel IMPROVE site.	13
Figure 10 Predicted mass concentrations plotted against the measured mass concentrations.	13
Figure 11 Source profiles derived from the San Gabriel IMPROVE site data.	15
Figure 12 Source contributions derived from the San Gabriel IMPROVE site data.	16
Figure 13 Back trajectory from San Gabriel on August 18, 2002.	17
Figure 14 Back trajectory from San Gabriel on September 28, 2002.	17
Figure 15 Source profiles of the resolved PM _{2.5} sources for the San Rafael IMPROVE site. ..	21
Figure 16 Time series plots of the resolved PM _{2.5} source contributions for the San Rafael IMPROVE site.	22
Figure 17 Predicted PM _{2.5} mass concentration versus measured PM _{2.5} mass concentration ...	23
Figure 18 10 day HYSPLIT backward trajectory on 04/16/2001	23
Figure 19 The location of the Pinnacles National Monument sampling site	24
Figure 20 Profiles for the sources resolved for the Pinnacles National Monument.	27
Figure 21 Time series of source contributions to the PM _{2.5} observed at the Pinnacles National Monument.	28
Figure 22 Comparison of seasonal (summer: June to August, winter: December to February) and overall contributions of the sources to the PM _{2.5} at the Pinnacles National Monument	29
Figure 23 Average source contributions for weekdays and weekends at the Pinnacles National Monument.	30

Figure 24. Conditional Probability Function (CPF) results based on source contributions obtained by the PMF analysis of the data from the Pinnacles site.	31
Figure 25. HYSPLIT back trajectories calculated for April 24, 1998.	31
Figure 26 Comparison of the predicted total PM _{2.5} mass concentrations with the PM _{2.5} concentrations measured at the Pinnacles National Monument.	32
Figure 27 Location of the IMPROVE monitoring sites at the Yosemite National Park, CA. . .	32
Figure 28 Measured versus PMF predicted PM _{2.5} mass concentrations at the Yosemite National Park.	35
Figure 29 The seasonal comparison of source contributions to PM _{2.5} mass concentration at the Yosemite National Park (mean ± 95 % distribution).	35
Figure 30 Source profiles deduced from PM _{2.5} samples measured at the Yosemite National Park (prediction ± standard deviation).	36
Figure 31 Time series plot of source contributions at the Yosemite National Park.	37
Figure 32 Weekday/weekend variations at the Yosemite National Park (mean ± 95% distribution).	38
Figure 33 CPF plots for the highest 25% of the mass contributions at the Yosemite National Park.	39
Figure 34 View of the area surrounding the Point Reyes National Seashore IMPROVE site. .	39
Figure 35 Source Profiles Derived from the Data from the Point Reyes National Seashore National Park IMPROVE Site	43
Figure 36 Source Contributions Derived from the Data from the Point Reyes National Seashore IMPROVE Site	44
Figure 37 CPF Plots for the factor contributions derived from the Point Reyes National Seashore IMPROVE Site Data	45
Figure 38 Apportionment of the PM _{2.5} mass concentrations at the Point Reyes National Seashore IMPROVE Site	46
Figure 39. The location of the Redwood National Park sampling site.	47
Figure 40. Source profiles for the Redwood National Park IMPROVE site constructed using the PMF model.	49
Figure 41. Temporal variation of source contribution for the Redwood National Park site constructed using the PMF2 model.	49
Figure 42. Comparison of the seasonal (summer: June to August, winter: December to February) contributions for each source in Redwood National Park site.	50
Figure 43. The average source contributions for weekdays and weekend days in Redwood National Park site.	51
Figure 44. Conditional Probability Function (CPF) results based on source contributions obtained by the PMF analysis of the data from the Redwood National Park site.	52
Figure 45. HYSPLIT back trajectories calculated for April 16, 2001, April 22, 2001, and April 20, 2002	52
Figure 46. Average source contribution for the sampling period at Redwood National Park IMPROVE site.	53
Figure 47. Comparison of the predicted PM _{2.5} mass concentrations with the measured PM _{2.5} mass concentrations for the Redwood National Park site.	53
Figure 48. The location of the Kalmiopsis IMPROVE site.	53
Figure 49. Source profiles for the Kalmiopsis IMPROVE site derived using the PMF2 model.	55
Figure 50. Temporal variation of source contributions for the Kalmiopsis site constructed using the PMF model.	56
Figure 51. Seasonal and annual mean contributions of the various sources to the PM _{2.5} mass at Kalmiopsis.	57
Figure 52. The average source contributions for weekdays and weekend days at the Kalmiopsis site.	58

Figure 53. Comparison of the predicted total PM _{2.5} mass concentrations from the PMF analysis with the measured PM _{2.5} mass concentrations for the Kalmiopsis IMPROVE site.	59
Figure 54. Comparison of wood/field burning source contributions and TC, K, SO ₄ ²⁻ concentrations during the Biscuit wildfire period.	59
Figure 55. PSCF plots for the source contributions resolved from the PM _{2.5} composition data obtained at the Kalmiopsis IMPROVE site.	60
Figure 56. Map showing the location of the Olympic National Park IMPROVE sampling site.	63
Figure 57. Measured versus PMF predicted PM _{2.5} mass concentrations at the Olympic National Park site.	66
Figure 58. The seasonal comparison of source contributions to PM _{2.5} mass concentration at the Olympic National Park site (mean ± 95 % distribution).	66
Figure 59. Source profiles deduced from PM _{2.5} samples measured at the Olympic National Park site (prediction ± standard deviation).	67
Figure 60. Time series plot of source contributions at the Olympic National Park site.	68
Figure 61. Weekday/weekend variations at the Olympic National Park site (mean ± 95 % distribution).	69
Figure 62. CPF plots for the highest 25 % of the mass contributions at the Olympic National Park site.	69
Figure 63. Uncertainties in the V concentrations measured at Point Reyes National Seashore as a function of the date on which the sample was collected.	70
Figure 64. The pairwise comparisons of the contribution values derived from the Aqua Tibia data for the four defined cases.	72
Figure 65. The pairwise comparisons of the contribution values derived from the Point Reyes data for the four defined cases.	73
Figure 66. Location of the three STN monitoring sites.	74
Figure 67. Measured versus PMF predicted PM _{2.5} mass concentrations.	76
Figure 68. The seasonal comparison of source contributions to PM _{2.5} mass concentration (mean ± 95% distribution).	76
Figure 69. Source profiles deduced from PM _{2.5} samples measured at Garden monitoring site (prediction ± standard deviation).	77
Figure 70. Time series plot of source contributions at Garden monitoring site.	78
Figure 71. Weekday/weekend variations at Garden monitoring site (mean ± 95% distribution).	79
Figure 72. CPF plots for the highest 25% of the mass contributions at Garden monitoring site.	79
Figure 73. Location of the STN monitoring sites: 1. Lake Forest, 2. Olive St., 3. Beacon Hill, 4. Duwamish, and 5. Georgetown.	80
Figure 74. Measured versus PMF predicted PM _{2.5} mass concentrations.	89
Figure 75. The seasonal comparison of source contributions to PM _{2.5} mass concentration (mean ± 95% distribution)	90
Figure 76. Source profiles deduced from PM _{2.5} samples measured at Lake Forest (prediction ± standard deviation).	91
Figure 77. Source profiles deduced from PM _{2.5} samples measured at Olive St. (prediction ± standard deviation).	92
Figure 78. Source profiles deduced from PM _{2.5} samples measured at Beacon Hill (prediction ± standard deviation).	93
Figure 79. Source profiles deduced from PM _{2.5} samples measured at Duwamish (prediction ± standard deviation).	94
Figure 80. Source profiles deduced from PM _{2.5} samples measured at Georgetown (prediction ± standard deviation).	95

Figure 81. Time series plot of source contributions at Lake Forest.	96
Figure 82. Time series plot of source contributions at Olive St.	97
Figure 83. Time series plot of source contributions at Beacon Hill.	98
Figure 84. Time series plot of source contributions at Duwamish.	99
Figure 85. Time series plot of source contributions at Georgetown.	100
Figure 86. Weekday/weekend variations at Lake Forest (mean \pm 95% distribution).	101
Figure 87. Weekday/weekend variations at Olive St. (mean \pm 95% distribution).	102
Figure 88. Weekday/weekend variations at Beacon Hill (mean \pm 95% distribution).	103
Figure 89. Weekday/weekend variations at Duwamish (mean \pm 95% distribution).	104
Figure 90. Weekday/weekend variations at Georgetown (mean \pm 95% distribution).	105
Figure 91. CPF plots for the highest 25% of the mass contributions at Lake Forest.	106
Figure 92. CPF plots for the highest 25% of the mass contributions at Olive St.	107
Figure 93. CPF plots for the highest 25% of the mass contributions at Beacon Hill.	108
Figure 94. CPF plots for the highest 25% of the mass contributions at Duwamish.	109
Figure 95. CPF plots for the highest 25% of the mass contributions at Georgetown.	110
Figure 96. The comparison of average source contributions to PM _{2.5} mass concentrations (mean \pm 95% distribution).	111
. Backward trajectories for days with high impacts of airborne soil arriving at Beacon Hill on Apr. 12, 2000 (circle), Apr. 22, 2001 (triangle), and Apr. 20, 2002 (square) calculated from NOAA Air Resource Laboratory.	112
Figure 98. Source directions of oil combustion identified by PMF and CPF analyses.	112
Figure 99. Location of the IMPROVE monitoring sites at Beacon Hill, Seattle.	113
Figure 100. Measured versus PMF predicted PM _{2.5} mass concentrations at Beacon Hill, Seattle.	116
Figure 101. The seasonal comparison of source contributions to PM _{2.5} mass concentration at Beacon Hill, Seattle (mean \pm 95 % distribution).	116
Figure 102. Source profiles deduced from PM _{2.5} samples measured at Beacon Hill, Seattle (prediction \pm standard deviation).	117
Figure 103. Time series plot of source contributions at Beacon Hill, Seattle.	118
Figure 104. Weekday/weekend variations at Beacon Hill, Seattle (mean \pm 95 % distribution).	119
Figure 105. CPF plots for the highest 25 % of the mass contributions at Beacon Hill, Seattle.	120
Figure 106. Location of the Roselawn monitoring site in Portland, OR..	122
Figure 107. Measured versus PMF predicted PM _{2.5} mass concentrations at the Roselawn site in Portland, OR.	125
Figure 108. The seasonal comparison of source contributions to PM _{2.5} mass concentration at the Roselawn site in Portland, OR (mean \pm 95 % distribution).	125
Figure 109. Source profiles deduced from PM _{2.5} samples measured at the Roselawn site in Portland, OR (prediction \pm standard deviation).	126
Figure 110. Time series plot of source contributions at the Roselawn site in Portland, OR. . .	127
Figure 111. Weekday/weekend variations at the Roselawn site in Portland, OR (mean \pm 95 % distribution).	128
Figure 112. CPF plots for the highest 25 % of the mass contributions at the Roselawn site in Portland, OR.	129
Figure 113. The location of the sampling site.	130
Figure 114. Source profile for the 4th Street STN site.	133
Figure 115. Temporal variation of source contribution for the 4th Street STN site.	134
Figure 116. The average source contributions for weekdays and weekend days in 4th Street (gray bar) and Jackson Street (white bar).	135
Figure 117. Source profiles for the Jackson Street STN site.	138
Figure 118. Temporal variation of source contribution for the Jackson Street STN site.	139

Figure 119. Conditional Probability Function (CPF) results based on source contributions obtained by the PMF analysis of the data from the 4th Street (dark line) and Jackson Street (gray line) in San Jose (gray area denote overlap area between the 4th Street and Jackson Street).	142
Figure 120. Comparison of the predicted total PM _{2.5} mass concentrations from the PMF analysis with measured PM _{2.5} mass concentrations for the 4th Street and Jackson Street sites.	143
Figure 121. Comparison of average source contributions for the each sampling site during summer and winter periods.	144
Figure 122. Measured versus PMF predicted PM _{2.5} mass concentrations.	150
Figure 123. The seasonal comparison of source contributions to PM _{2.5} mass concentration (mean ± 95% distribution).	151
Figure 124. Source profiles deduced from PM _{2.5} samples measured at Simi Valley (prediction ± standard deviation).	152
Figure 125. Source profiles deduced from PM _{2.5} samples measured at LA (prediction ± standard deviation).	153
Figure 126. Source profiles deduced from PM _{2.5} samples measured at Rubidoux (prediction ± standard deviation).	154
Figure 127. Time series plot of source contributions at Simi Valley.	155
Figure 128. Time series plot of source contributions at LA.	156
Figure 129. Time series plot of source contributions at Rubidoux.	157
Figure 130. Weekday/weekend variations at Simi Valley (mean ± 95% distribution).	158
Figure 131. Weekday/weekend variations at LA (mean ± 95% distribution).	159
Figure 132. Weekday/weekend variations at Rubidoux (mean ± 95% distribution).	160
Figure 133. CPF plots for the highest 25% of the mass contributions at Simi Valley.	161
Figure 134. CPF plots for the highest 25% of the mass contributions at LA.	162
Figure 135. CPF plots for the highest 25% of the mass contributions at Rubidoux.	163
Figure 136. Backward trajectories for days with high impacts of airborne soil arriving at LA and Rubidoux on Jan. 3, 2003 (square and triangle, respectively) calculated by the HYSPLIT model (NOAA Air Resource Laboratory).	164
Figure 137. Map of sampling location for STN PM _{2.5} measurements. Symbol (*) indicates the NOAA meteorological station near the sites.	166
Figure 138. Source profiles of 8-factor solution deduced from PMF modeling for Escondido PM _{2.5} .	170
Figure 139. Source contributions of 8-factor solution deduced from PMF modeling for Escondido PM _{2.5} .	171
Figure 140. Seasonal average mass contributions (mean ± 95% standard error) of each source to total PM _{2.5} mass concentration. Summer is from May to October, and winter is from November to April.	172
Figure 141. Comparison of measured versus predicted PM _{2.5} mass concentrations for Escondido data.	173
Figure 142. Average mass contributions (mean ± 95% confidence interval) of the PMF sources for weekday and weekend PM _{2.5} mass concentration at Escondido.	174
Figure 143. CPF plots of PMF-resolved sources at Escondido.	175
Figure 144. Source profiles of 8-factor solution deduced from PMF modeling for El Cajon PM _{2.5} .	177
Figure 145. Source contributions of 8-factor solution deduced from PMF for El Cajon PM _{2.5} .	178
Figure 146. Seasonal average mass contributions (mean ± 95% standard error) of each source to total PM _{2.5} mass concentration. Summer is from May to October, and winter is from November to April.	179
Figure 147. Comparison of measured versus predicted PM _{2.5} mass concentrations for El Cajon	

data.	179
Figure 148. Average mass contributions (mean \pm 95% confidence interval) of the PMF sources for weekday and weekend PM _{2.5} mass concentration at El Cajon.	179
Figure 149. CPF plots of PMF-resolved sources at El Cajon.	180
Figure 150. Comparison of the estimated source contributions between the sites. The diesel at El Cajon was compared to the mixed motor vehicle at Escondido.	182
Figure 151. Back trajectories on days showing high residual oil mass concentrations at Escondido and El Cajon sites.	183
Figure 152. Plot of the contributions of oil combustion against the secondary sulfate contributions at the Beacon Hill site in Seattle.	184
Figure 153. The residual oil combustion contribution at the Olive St. site in Seattle plotted against the secondary sulfate contributions.	185
Figure 154. The residual oil combustion contribution at the Duwamish site in Seattle plotted against the secondary sulfate contributions.	185
Figure 155. Plot of the residual oil contributions against the secondary sulfate contributions for the El Cajon STN site.	185
Figure 156. Plot of the residual oil contributions against the secondary sulfate contributions for the Escondido STN site.	185
Figure 157. Residual oil combustion contributions plotted against the corresponding secondary sulfate contributions at Point Reyes National Seashore.	186
Figure 158. Residual oil combustion contributions plotted against the corresponding secondary sulfate contributions at Olympic National Park.	186

List of Tables

Table ES-1. Summary of the average source apportionments for the IMPROVE sites along the west coast of the United States.	xvi
Table ES-2. Summary of the average source apportionments for the STN sites along the west coast of the United States.	xvii
Table 1. Summary Statistics of the Chemical Composition and Overall Mass for City of Agua Tibia, CA Samples Collected from 12/20/2000 to 12/29/2003	8
Table 2. Source Apportionment for the PM _{2.5} measures at Aqua Tibia	11
Table 3. Summary statistics for data from the San Gabriel IMPROVE site.	14
Table 4. Average source contributions to the PM _{2.5} samples collected at San Gabriel	18
Table 5. Summary Statistics for PM _{2.5} and 33 Species Mass Concentrations used for PMF Analysis of the San Rafael IMPROVE Site.	20
Table 7. Summary statistics for the PM _{2.5} and species concentrations at Pinnacles National Monument.	26
Table 8. Average seasonal source contributions at the Pinnacles National Monument IMPROVE site	29
Table 9. Summary of PM _{2.5} species mass concentrations at the Yosemite National Park, CA.	34
Table 10. Average source contributions (µg/m ³) to PM _{2.5} mass concentration at the Yosemite National Park, CA.	38
Table 11. List of excluded species for the data from Point Reyes National Seashore	40
Table 12. Summary statistics for the species used in this study of Point Reyes National Seashore (µg/m ³)	41
Table 13. Summary statistics for the PM _{2.5} and species concentrations in the Redwood National Park site.	48
Table 14. Average seasonal source contributions for the Redwood National Park site.	51
Table 15. Summary statistics for the PM _{2.5} and species concentrations at the Kalmiopsis (ng/m ³) site.	54
Table 16. Average seasonal source contribution using the PMF model in Kalmiopsis IMPROVE site.	57
Table 17. Summary of PM _{2.5} species mass concentrations at the Olympic National Park site.	64
Table 18. Average source contributions (µg/m ³) to PM _{2.5} mas concentration at the Olympic National Park site.	66
Table 19. Comparison of the PIXE and XRF V values from the Case 1 and 2 analyses.	71
Table 20. Summary of PM _{2.5} species mass concentrations at Garden site.	75
Table 21. Average source contributions (µg/m ³) to PM _{2.5} mas concentration.	76
Table 22. Summary of STN sites in Seattle, Washington	81
Table 23. Summary of OC blank concentrations estimated from regression of PM _{2.5} mass concentrations against OC concentrations.	81
Table 24. Summary of PM _{2.5} species mass concentrations at Lake Forest.	82
Table 25. Summary of PM _{2.5} species mass concentrations at Olive St.	83
Table 26. Summary of PM _{2.5} species mass concentrations at Beacon Hill.	84
Table 27. Summary of PM _{2.5} species mass concentrations at Duwamish.	85
Table 28. Summary of PM _{2.5} species mass concentrations at Georgetown.	86
Table 29. Average source contributions (µg/m ³) to PM _{2.5} mass concentration.	88
Table 30. Summary of PM _{2.5} species mass concentrations at Beacon Hill, Seattle.	114
Table 31. Average source contributions (µg/m ³) to PM _{2.5} mas concentration at Beacon Hill, Seattle.	115
Table 32. Comparison of the source apportionments from samples collected at the Beacon Hill	

Site in both the STN and IMPROVE networks.	121
Table 33. Summary of PM _{2.5} species mass concentrations at Roselawn site.	123
Table 34. Average source contributions (µg/m ³) to PM _{2.5} mas concentration at Roselawn site.	124
Table 35. Summary statistics for the PM _{2.5} and species concentrations in the 4 th Street, San Jose.	131
Table 36. Summary statistics for the PM _{2.5} and species concentrations at the Jackson Street, San Jose.	132
Table 37. Average seasonal source contribution using the PMF model in 4th Street, San Jose.	136
Table 38. Average seasonal source contributions in Jackson Street, San Jose.	140
Table 39. Average source contributions to PM _{2.5} mass concentration in 4th Street and Jackson Street.	144
Table 40. Summary of STN sites in South Coast Air Basin.	145
Table 41. Summary of OC blank concentrations estimated from regression of PM _{2.5} mass concentrations against OC concentrations.	145
Table 42. Summary of PM _{2.5} species mass concentrations at Simi Valley.	147
Table 43. Summary of PM _{2.5} species mass concentrations at Los Angeles.	148
Table 44. Summary of PM _{2.5} species mass concentrations at Rubidoux.	149
Table 45. Average source contributions (µg/m ³) to PM _{2.5} mass concentration.	165
Table 46. Summary statistics of the Escondido PM _{2.5} mass and species concentrations	167
Table 47. Summary statistics of the El Cajon PM _{2.5} mass and species concentrations	168
Table 48. Average source contributions from PMF to measured PM _{2.5} mass concentration at Escondido	172
Table 49. Average source contributions from PMF to measured PM _{2.5} mass concentration at El Cajon	176
Table 50. Summary of the average source apportionments for the IMPROVE sites along the west coast of the United States.	187

ABSTRACT

The objective of this project is to resolve the sources of $PM_{2.5}$ along the western coast of the United States with a particular emphasis on the impacts of ship emissions on the mass concentrations observed. Ship engines burn low cost, residual oil similar to that used in oil-fired power plants. The ability of these analyses to separately apportion the impacts of ships, spark- and compression-ignition vehicle emissions as well as the formation of secondary particles will be important to permit the assessment of the effects of ship emissions on air quality along this coast.

The data that are available for these analyses include results from a number of sites that might be affected by ship emissions. Along the west coast, there are data available from three monitoring programs, IMPROVE, Speciation Trends Network (STN), and PM_{10} Technical Enhancement Program (PTEP). However, problems were found in the PTEP data and they were not analyzed. The IMPROVE and STN data were analyzed using positive matrix factorization. Applying these approaches to the PM -related measurements to identify PM sources was the goal of this study so that ship emission impacts can be quantitatively assessed. Primary emissions from the combustion of residual oil produce particles containing Ni and V. Source profiles for residual oil could be observed in Seattle, Los Angeles, and San Diego. They could not be identified at the other STN sites (Anchorage, Portland, and San Jose). There were high Ni concentrations in San Jose, but no V and thus, it is highly unlikely that this source is residual oil.

The clearest influence of ship emissions was in Seattle where multiple site results point clearly to the Port of Seattle as a likely source area. The situation in the Los Angeles area is unclear. A residual oil profile could not be extracted from any of the three STN sites although Ni and V could be observed in approximately the ratio seen in the residual oil combustion profiles from other locations. The average Ni and V concentrations at Rubidoux were approximately 66% of those observed at the downtown LA site. If the source was ship emissions at the Port of Los Angeles and the Port of Long Beach, there should have been a much larger decrease in the Ni and V concentrations as the air moved eastward to Rubidoux. In addition, experiments performed in Rubidoux in the summer of 2005 found high concentrations of V-bearing particles and high mercury concentrations suggesting that there is significant residual oil combustion in the Riverside-Rubidoux area even though it does not appear in the emissions inventory. In addition, there is the potential confounding of the ship emissions by the refineries in the Torrance area. The emissions inventory indicates an emission rate for Ni of 750 pounds per year and no report of V emissions. However, it is likely that the Ni comes from residual oil combustion to produce the energy needed for the refinery operations. At all three sites, the Ni and V appear most strongly in the aged sea salt factor so that it appears there is sufficient covariance among these elements and Na and nitrate that they cannot be separated. At the two San Diego area sites, residual oil could be separated.

At some of the rural IMPROVE sites (Aqua Tibia, San Rafael, Point Reyes, and Olympic), oil combustion source profiles can be identified. The clearest influence is at the Point Reyes National Seashore where it appears that the ships approaching San Francisco influence this site to the northwest of the city. However, primary ship emissions do not represent a large source of $PM_{2.5}$ at any site with a maximum mean value of the order of $1 \mu\text{g}/\text{m}^3$.

A correlation between the primary oil combustion particles and secondary sulfate could be identified at a number of sites. In Seattle, there appears to be $0.82 \mu\text{g}/\text{m}^3$ of sulfate for every $1 \mu\text{g}/\text{m}^3$ of primary oil combustion particles. However, in San Diego, a similar correlation could not be observed. At Point Reyes National Seashore, the relationship between the ship emission primary particles and secondary sulfate is less well defined as observed in Seattle. If there is a relationship, it has similar magnitude to that was more clearly seen in Seattle. The results for the Aqua Tibia, San Rafael, and Olympic sites are more equivocal. Thus, the presence of other sources of secondary sulfate tend to mask the production of sulfate aerosol arising from ship emissions.

EXECUTIVE SUMMARY

Increased trade with the countries on the Pacific Rim and transport of crude oil from Alaska results in significant ship traffic along the west coast of North America. Ship engines typically burn the lowest cost fuel possible and thus, commonly use residual oil as their primary fuel. Residual oil is also referred to as No. 6 or Bunker-C oil. Residual oil can contain significant concentrations of sulfur as well as trace metals, particularly vanadium and nickel. Now that the U.S. Environmental Protection Agency in conjunction with state and local air quality agencies have been operating $PM_{2.5}$ monitoring networks since 2000 that provide composition data at sites across the country, there is data available for receptor modeling that could potentially resolve the direct contributions from ship emissions to the measured $PM_{2.5}$ concentrations. It is the purpose of this project to apply the state-of-the-art multivariate receptor model, positive matrix factorization (PMF), to the data from sites selected because of their proximity to the west coast in order to ascertain the impact of the ship emissions on particulate air quality.

There are two networks in which particle samples are routinely collected and analyzed for their constituents, the Speciation Trends Network (STN) and the Interagency Monitoring of Protected Visual Environments Network (IMPROVE). Coastal sites from Anchorage, AK to San Diego, CA were selected from these networks and data from the sites shown in Figure ES1 were analyzed to identify the $PM_{2.5}$ sources and apportion the mass concentrations to those sources.

The results of these apportionment studies are presented in Tables ES1 and ES2. Table ES1 provides the mean mass concentration apportionments for the IMPROVE sites while Table ES2 gives the analogous results for the STN sites as well as the IMPROVE-protocol site in Seattle, WA.

The clearest influence of ship emissions was in Seattle where multiple site results point clearly at the Port of Seattle as a likely source area. However, the ship primary emissions represent a small source of $PM_{2.5}$. The average mass contributions ranged from $0.20 \mu\text{g}/\text{m}^3$ at Aqua Tibia to $0.60 \mu\text{g}/\text{m}^3$ at the Beacon Hill site in Seattle, WA. However, the STN data at the Beacon Hill site suggested that the mean contribution was $0.43 \mu\text{g}/\text{m}^3$. The differences appear to arise primarily from the difference in the measurement method for organic and elemental carbon as measured in the two networks.

Sulfate sources could be identified at all of the sites. It is expected that oil combustion in an internal combustion engine will result in a lower maximum temperature than would occur in a stationary source burning residual oil. Since the equilibrium between SO_2 and SO_3 favors more SO_3 at lower temperatures, it is anticipated that the ship emissions will include SO_3 that will appear as sulfate in the $PM_{2.5}$ samples. However, factor analysis is not likely to be able to

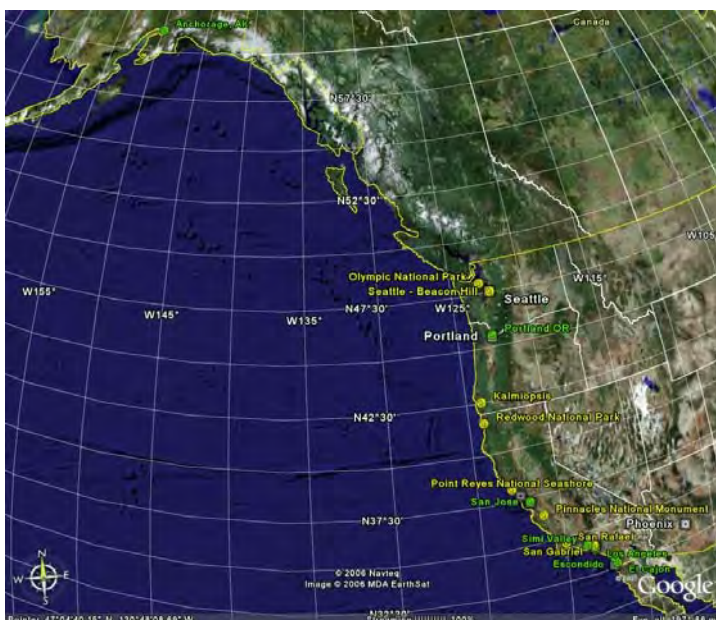


Figure ES1. Map showing the locations of the IMPROVE (yellow dots) and STN (green dots) sites that were used to assess the impacts of ship emissions on $PM_{2.5}$ concentrations along the west coast of the United States.

separate the relatively weak sulfate signal from the ship emissions from the larger background of regionally transported secondary sulfate.

Table ES-1. Summary of the average source apportionments for the IMPROVE sites along the west coast of the United States.

Site	Sulfate	Nitrate	Gasoline	Diesel	Residual Oil	Soil	Wood smoke	Sea Salt	Other
Aqua Tibia	2.67	1.44	1.28	0.26	0.20	0.80		0.94	
San Gabriel	1.04	1.05	0.50	0.08		0.37		0.28	1.34
San Rafael	1.63	0.55	1.40	0.09	0.26	0.79		0.32	0.08
Pinnacles	1.46	0.57	1.87	0.26		0.13	0.37	1.01	
Yosemite	0.89	0.20	0.23 ^a			0.73	1.11	0.65	0.23
Point Reyes	1.53	0.90	0.72	0.04	0.44	0.06	0.31	1.89	
Redwoods			1.58			0.15	0.71	1.97	
Kalmiopsis	0.85	0.24	0.06	0.04		0.27	1.22	0.33	0.16
Olympic	0.54	0.25	0.47		0.50	0.18	0.33	0.25	0.08

a. Combined contribution of motor vehicles (gasoline and diesel)

Figure ES1 shows a plot of the oil combustion contributions plotted against the corresponding secondary sulfate contributions at the Beacon Hill STN site. It can be seen that there is a relationship between the secondary sulfate and the primary V-Ni bearing particles. The line represents an “edge” that demonstrates this relationship (Henry, 2003). The slope of this line is 1.213 so that there appears to be 0.82 $\mu\text{g}/\text{m}^3$ of sulfate for every 1 $\mu\text{g}/\text{m}^3$ of primary oil combustion particles. Similar plots can be derived at the other two Seattle STN sites where a residual oil combustion factor was resolved as shown in Figures ES3 and ES4. A line with the same slope as seen in the Beacon Hill results is shown in each plot.

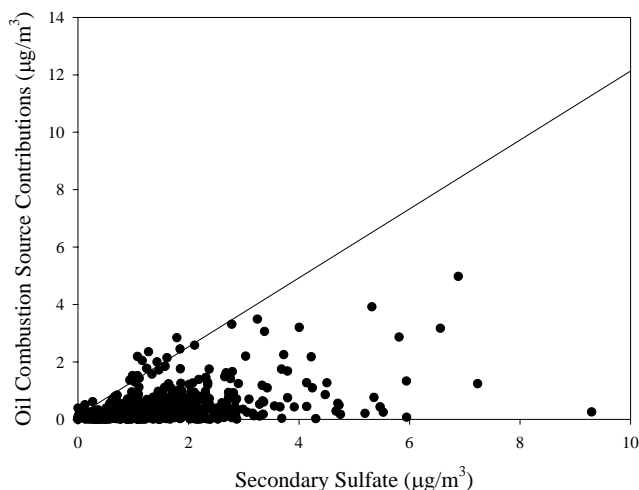


Figure ES2. The oil combustion contributions obtained at the Beacon Hill STN site in Seattle, WA plotted against the sulfate contributions at this site.

Table ES-2. Summary of the average source apportionments for the STN sites along the west coast of the United States.

Site	Sulfate	Nitrate	Gasoline	Diesel	Residual Oil	Soil	Wood smoke	Sea Salt	Other
Anchorage	0.89	0.91	2.66	0.33		0.32		0.33	0.67
Seattle - Beacon Hill STN	1.51	1.50	2.51	0.21	0.43	0.22	0.65	0.98	0.65
Seattle - Beacon Hill IMPROVE	1.92	1.66	0.85	0.14	0.60	0.32	1.40	1.05	0.19
Seattle - Olive Street	1.84	2.70	1.38	0.91	0.43	0.99	0.75	0.99	0.50
Seattle - Duwamish	2.48	2.87	1.59	0.65	0.44	0.70	1.21	0.92	1.38
Seattle - Georgetown	1.77	2.00	1.80	0.18		0.49	1.86	1.39	0.14
Seattle - Lake Forrest	1.70	1.19	2.67			0.23	3.07	1.20	
Portland	1.84	1.62	0.97	0.41		0.58	2.82	1.25	0.23
San Jose - 4 th St	1.58	3.29	1.07	0.57		0.99	4.73	2.14	0.37
San Jose- Jackson St	1.99	2.92	1.20	0.45		0.27	4.84	2.52	0.18
Los Angeles Downtown	4.49	6.30	4.50	4.50	2.13	1.45	0.79	1.48	0.77
Simi Valley	3.58	4.51	2.90	2.90	1.09	1.79		1.94	
Rubidoux	3.68	14.06	3.52	3.52	2.27	1.86		3.49	
El Cajon	2.62	3.39	3.23	0.15	0.44	0.43		1.77	
Escondido	2.60	2.92	3.38	0.15	0.57	1.48		1.87	

a. Combined contribution of motor vehicles (gasoline and diesel)

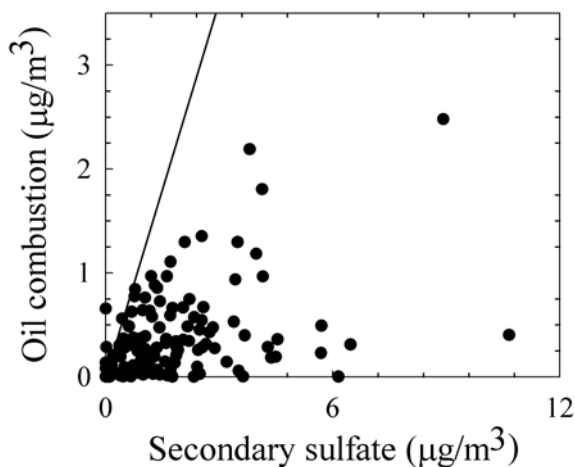


Figure ES3. The residual oil combustion contribution at the Olive St. site in Seattle plotted against the secondary sulfate contributions.

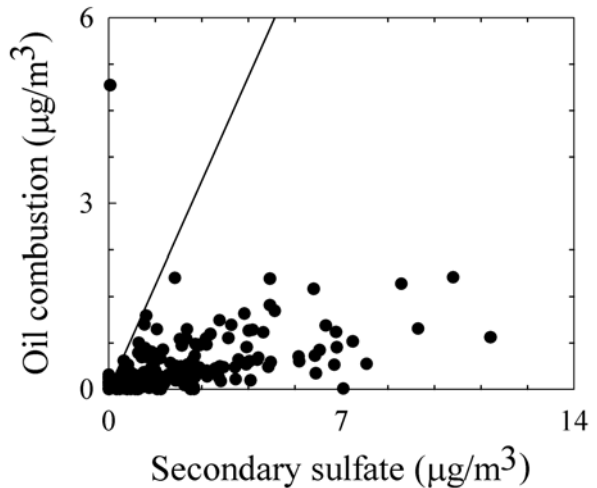


Figure ES4. The residual oil combustion contribution at the Duwamish site in Seattle plotted against the secondary sulfate contributions.

At the two San Diego area sites, residual oil could be separated and the residual oil contributions are plotted against the secondary sulfate concentrations in Figures ES5 and ES6. It can be seen that there are no obvious edges in either of these plots. The 1.2 slope line was included as a point of comparison. At these two sites, there does not appear to be any correlation between the residual oil combustion emissions and sulfate formation.

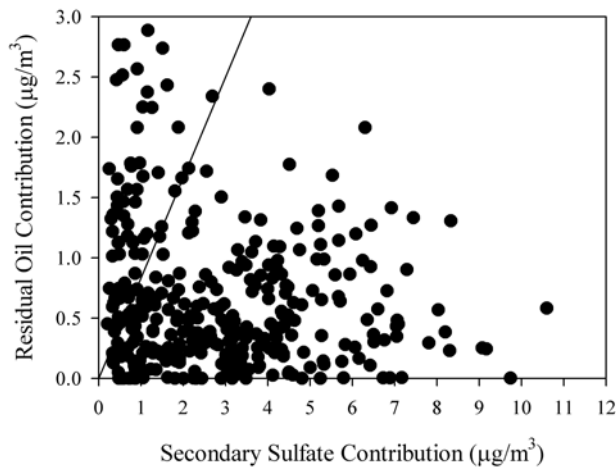


Figure ES5. Plot of the residual oil contributions against the secondary sulfate contributions for the El Cajon STN site.

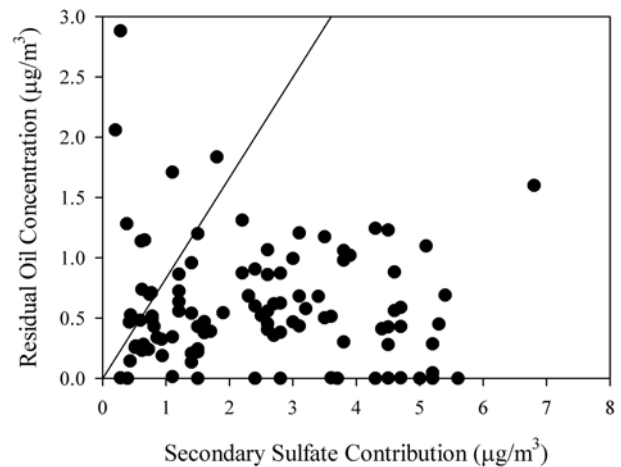


Figure ES6. Plot of the residual oil contributions against the secondary sulfate contributions for the Escondito STN site.

The situation in the Los Angeles area is unclear. A residual oil profile could not be extracted from any of the three STN sites although Ni and V could be observed in approximately the ratio seen in the residual oil combustion profiles from other locations. The average Ni and V concentrations at Rubidoux were approximately 66% of those observed at the downtown LA site. If the source was ship emissions at the Port of Los Angeles and the Port of Long Beach,

there should have been a much larger decrease in the Ni and V concentrations as the air moved eastward to Rubidoux. In addition, experiments performed in Rubidoux in the summer of 2005 found high concentrations of V-bearing particles and high mercury concentrations suggesting that there is significant residual oil combustion in the Riverside-Rubidoux area even though it does not appear in the emissions inventory. In addition, there is the potential confounding of the ship emissions by the refineries in the Torrence area. The emissions inventory indicates an emission rate for Ni of 750 pounds per year and no report of V emissions. However, it is likely that the Ni comes from residual oil combustion to produce the energy needed for the refinery operations. At all three sites, the Ni and V appear most strongly in the aged sea salt factor so that it appears there is sufficient covariance among these elements and Na and nitrate that they cannot be separated.

At some of the rural IMPROVE sites (Aqua Tibia, San Rafael, Point Reyes, and Olympic), oil combustion source profiles can be identified. The clearest influences are at the Point Reyes National Seashore and Olympic National Park. Point Reyes is likely to be affected by the ships approaching San Francisco. At Point Reyes, the relationship between the ship emission primary particles and secondary sulfate (Figure ES7) is less well defined as observed in Seattle with the edge plot shown in Figure ES1. A line with the same slope as in Seattle is shown in the figure suggesting that if there is a relationship, it has similar magnitude to that which was more clearly seen in Seattle. The plots for the other sites are more equivocal. Figure ES8 shows the plot for the Olympic National Park site. In this case there is no clear edge in the plot. Thus, it is difficult to conclude that it is possible to associate a specific contribution of secondary sulfate that is clearly associated with ship diesel emissions at these sites.

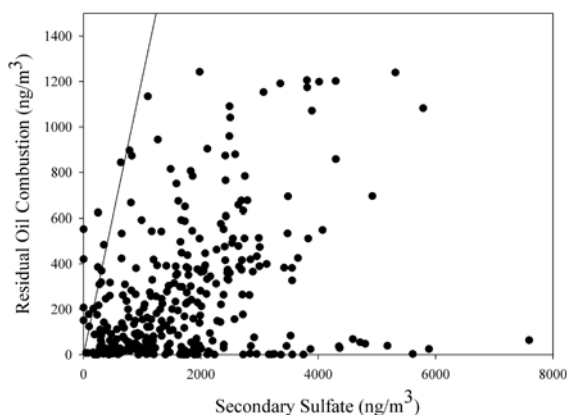


Figure ES7. Residual oil combustion contributions plotted against the corresponding secondary sulfate contributions at Point Reyes National Seashore.

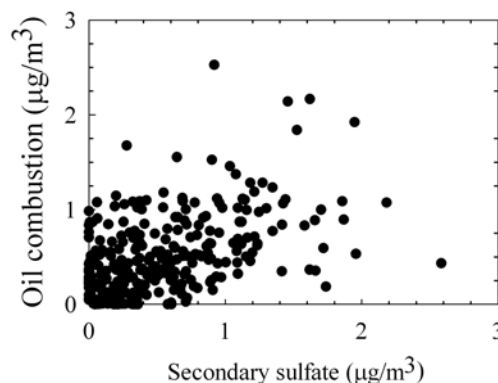


Figure ES8. Residual oil combustion contributions plotted against the corresponding secondary sulfate contributions at Olympic National Park.

Overall, the impacts of the ship emissions of primary particles tend to be relatively small compared to the full suite of sources identified at the sites along the western coast of the United States. It is possible that there is an additional direct contribution of sulfate from the SO₃ emitted by the ships. However, it appears that at most it doubles the mass contributions from the primary particle emissions. It is not possible in these analyses to determine the extent of secondary sulfate that is associated with the ship emissions of SO₂.

INTRODUCTION

Over the past few years, we have been developing and applying new approaches to multivariate receptor modeling based on explicit least-square techniques called Positive Matrix Factorization (PMF). PMF (Paatero, 1997) has been shown to be a powerful technique relative to traditional multivariate receptor modeling of airborne PM (Huang *et al.*, 1999; Willis, 2000; Qin *et al.*, 2002). It has been successfully used to assess ambient PM source contributions in the Arctic (Xie *et al.*, 1999; Polissar *et al.*, 1998), in Hong Kong (Lee *et al.*, 1999), in Thailand (Chueinta *et al.*, 2000), in Finland (Yli-Tuomi *et al.*, 2004), in Bangladesh (Begum *et al.*, 2004), in Phoenix (Ramadan *et al.*, 2000), in Vermont (Polissar *et al.*, 2001), in three northeastern U.S. cities (Song *et al.*, 2001), in Brigantine, NJ (Lee *et al.*, 2002), in Spokane, WA (Kim *et al.*, 2003a), and in Atlanta (Kim *et al.*, 2003b). Also, PMF has been applied to particle size distribution data measured in Seattle (Kim *et al.*, 2004a) and Pittsburgh (Zhou *et al.*, 2004).

To improve source identification as well as to separate primary sources of carbonaceous particles into traffic-related carbonaceous particle sources, and residual oil combustion, we have recently begun using the IMPROVE temperature resolved carbon fractions in PMF analysis for PM data from Atlanta, GA (Kim *et al.*, 2004b), Washington, DC (Kim and Hopke, 2004a), Brigantine, NJ (Kim and Hopke, 2004b), and Seattle, WA (Maykut *et al.*, 2003; Kim *et al.*, 2004a).

We have been the first group to analyze data from the U.S. Environmental Protection Agency's Speciation Trends Network (STN). As will be discussed below, there are a number of problems associated with the use of these data. We have developed an approach to deal with these problems (Kim *et al.*, 2005a). We have not yet published results from these analyses, but we will shortly submit a manuscript on the data from sites in the New York City metropolitan area. Several other papers are in preparation based on work done for sites in New Jersey, Delaware, and across the LADCO region (Chicago, St. Louis, Indianapolis, Cleveland, and Detroit). The PMF analyses successfully separated diesel emissions, gasoline emissions, and oil combustion sources using data from both PM_{2.5} composition monitoring networks.

The objective of this project is to resolve the sources of PM_{2.5} with a particular emphasis on the impacts of ship emissions on the mass concentrations observed along the west coast of the United States. Ship engines burn low cost residual oil similar to that used in oil-fired power plants. The ability of these analyses to separately apportion the impacts of ships, spark- and compression-ignition vehicle emissions, as well as the formation of secondary carbon will be important to permit the assessment of the effects of ship emissions on air quality along the coasts. The nature of these various carbonaceous aerosol emissions will be reviewed below.

In terms of the data that are available for these analyses, there are a number of sites that might be affected by ship emissions. For the west coast studies, there are data available from three monitoring programs: the Interagency Monitoring of Protected Visual Environments (IMPROVE), the Speciation Trends Network (STN), and the PM₁₀ Technical Enhancement Program PTEP. Examination of the PTEP data suggested problems with the elemental values and thus, only the IMPROVE and STN data were analyzed using positive matrix factorization. Particular emphasis in this proposal are on approaches to source apportionment studies for different types of data obtained at a variety of locations. Applying these approaches to the PM-related measurements to identify PM sources was the goal of this study so that ship emission impacts can be quantitatively assessed.

Ship Emission Characteristics

There is relatively little reported in the literature on the nature of the emissions from compression ignition ship engines (Corbett and Fishbeck, 2000). Ship diesels can utilize a wide range of quality fuels and will typically utilize the lowest cost fuels available. Thus, they utilize low volatility residual oil, often referred to No. 6 or bunker-C oil. This material tends to be enriched in porphyrins that contain Ni and V (Osan *et al.*, 2000). These oils are used in the northeastern US in oil-fired power plants (Hopke *et al.*, 1976; Alpert and Hopke, 2000). These oils are generally high in sulfur as well and have been reduced in sulfur since the early 1970s. The primary ship emissions that have been examined include SO₂ and NO_x because of their potential for cloud formation in “ship trails.” For example, Corbett and Fishbeck (2000) examine the impacts of ship emissions on NO_x and SO₂. Figure 1 shows the effect of ships on NO_x in the US.

They also provide estimates of particulate matter and hydrocarbons to the coastal regions. However, all of their results are based on emissions models. Globally, there are a number of similar modeling efforts (e.g., Corbett *et al.*, 1999; Endresen *et al.*, 2003; Song *et al.*, 2003). Some information on polycyclic aromatic hydrocarbons in the clouds of ship tracks has been reported (Russell *et al.*, 2000), but there is no direct information on the elemental composition of typical ship emissions.

The ships generally burn fuel as they enter and leave the ports, but do not generally run their engines while docked for loading and unloading so there are limited emissions during this period. However, there would be significant emissions from support vehicles, trucks and railroad engines, as well as cargo handling systems during the loading/unloading operations.

Prior Analysis of IMPROVE Data

In order to identify ship diesel emissions, it is necessary to separate the various fuel combustion emission types including motor vehicle emissions. In previous analyses of ambient PM_{2.5} (particulate matter ≤ 2.5 μm in aerodynamic diameter) compositional data from Atlanta, GA including total OC and EC (Kim *et al.*, 2003b), diesel emissions could not be separated from gasoline emission sources. Eight sources were identified by the PMF including a motor vehicle source that appears to be a mixture of gasoline and diesel emissions. They were not separated because of their similar chemical profiles and daily emission patterns were not different enough to be extracted separately by PMF. However, re-analysis of the Atlanta data including eight temperature resolved carbon fractions analyzed via Interagency Monitoring of Protected Visual Environments / Thermal Optical Reflectance (IMPROVE/TOR) protocol (Chow *et al.*, 1993) showed improved source identification (Kim *et al.*, 2004b). PMF identified eleven sources in this study. PMF derived four traffic-related combustion source profiles (gasoline vehicle, on-road diesel, railroad, and bus maintenance facility/highway traffic) containing high carbon fractions whose abundance was different between the sources. Similar results were obtained for compositional data from Brigantine, NJ (Kim and Hopke, 2004b), Washington, DC (Kim and Hopke, 2004 a), and Seattle, Washington (Maykut *et al.*, 2003).

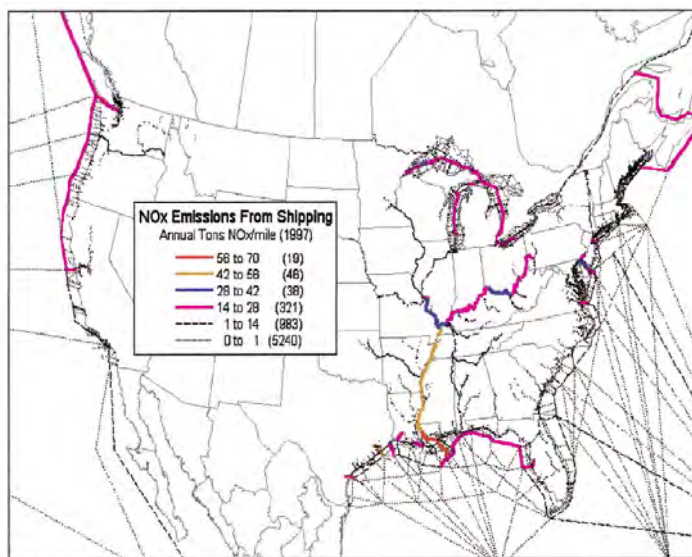


Figure 1 Estimated NO_x emissions in the US from shipping in 1997. Figure taken from Corbett and Fishbeck (2000).

“Oil combustion” profiles were derived from the Seattle, WA, Brigantine, NJ, and Washington, DC IMPROVE site data. These profiles are shown in Figure 2. In most cases, emissions inventories would suggest that more V comes from airborne soil than other sources. However, the correlation between Ni and V and between these two metals and the particulate carbon species permits the separation of these profiles. We clearly see differences in the carbonaceous species among these profiles. In Seattle, there is more

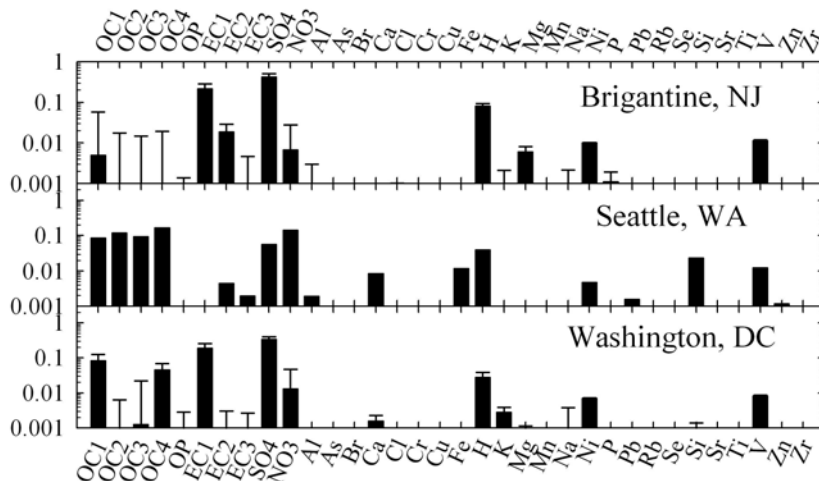


Figure 2 Oil combustion emissions profiles derived from IMPROVE data.

organic carbon than elemental carbon. This result would appear to be consistent with the results of Russell *et al.* (2000). The east coast sites show the opposite behavior. These differences may be helpful in distinguishing ship emissions from oil-fired power plants since the combustion conditions would be quite different.

In the case of the two east coast sites (Brigantine and Washington), there are much higher sulfur concentrations than in the Seattle profile. In both east coast sites, the oil fired power plants are at a sufficient distance that there can be conversion of the emitted SO_2 into sulfate. In Seattle, there are no oil-fired power plants in the emissions inventory and thus, it is likely these are ship emissions. In this case, there would be relatively little time for the SO_2 emissions to undergo transformation to particulate sulfate. These PMF2 studies using carbon fractions demonstrated that the temperature-resolved fractional carbon data can enhance source apportionment of the carbonaceous aerosol including the separation of diesel emissions, gasoline vehicle emissions and residual oil combustion.

DATA ANALYSIS METHODS

Positive Matrix Factorization

Multivariate approaches are based on the idea that the time dependence of a chemical species at the receptor site will be the same for species from the same source. Chemical species are measured in a large number of samples gathered at a single receptor site over time. Species of similar variability are grouped together in a minimum number of factors that explain the variability of the data set. It is assumed that each factor is associated with a source or source type. Among the multivariate receptor modeling used for aerosol source identification, positive matrix factorization (PMF) developed by Paatero and Tapper (1993, 1994) and Paatero (1997) is a relatively new technique. PMF features the use of realistic error estimates to weight the data values and the imposition of non-negativity constraints in the factor computational process. PMF has been successfully applied in many atmospheric studies [Juntto and Paatero, 1994; Anttila *et al.*, 1995; Polissar *et al.*, 1996, 1998, 2001; Xie *et al.*, 1999; Paterson *et al.*, 1999; Chueinta *et al.*, 2000; Song *et al.*, 2001a; Polissar *et al.*, 2001; Lee *et al.*, 2002; Kim *et al.*, 2003a, b, 2004; Kim and Hopke, 2004].

In this study, PMF was applied to the various IMPROVE data sets. PMF is a described in detail by Paatero [1997]. Only a brief description of the technique is given here. PMF uses a weighted least-squares fit with the known error estimates of the elements of the data matrix used

to derive the weights. The factor model (PMF2) can be written as

$$X = GF + E \quad (1)$$

where X is the known $n \times m$ matrix of the m measured chemical species in n samples. G is an $n \times p$ matrix of source contributions to the samples (time variations). F is a $p \times m$ matrix of source compositions (source profiles). Both G and F are factor matrices to be determined. E is the residuals matrix, i.e., the difference between the measurement X and the model Y as a function of factors G and F .

$$E = X - Y = X - G \times F \quad (2)$$

The "object function," Q , that is to be minimized as a function of G and F is given by

$$Q(E) = \sum_{i=1}^m \sum_{j=1}^n \left[\frac{e_{ij}}{s_{ij}} \right]^2 \quad (3)$$

where s_{ij} is an estimate of the "uncertainty" in the i th variable measured in the j th sample. The factor analysis problem is then to minimize $Q(E)$ with respect to G and F with the constraint that each of the elements of G and F is to be non-negative.

The solution to the PMF problem depends on estimating uncertainties for each of the data values used in the PMF analysis. There are three types of values that are typically available. Most of the data points have values that have been determined, x_{ij} , and their associated uncertainties, s_{ij} . There are samples in which the particular species cannot be observed because the concentration is below the method detection limit. Finally, there are samples for which the values were not determined. These latter two types of data are often termed "missing" data. However, there are qualitative differences between them. In the below detection limit samples, the value is known to be small, but the exact value is not known. In the case where values could not be determined, the value is totally unknown. Polissar *et al.* (1998) has suggested an approach for estimating the concentration values and their associated error estimates including values below detection limits or missing for IMPROVE data from Alaska and we have used this approach in this study.

Another important aspect of weighting of data points is the handling of extreme values. Environmental data typically shows a positively skewed distribution and often with a heavy tail. Thus, there can be extreme values in the distribution as well as true "outliers." In either case, such high values would have significant influence on the solution (commonly referred to as leverage). This influence will generally distort the solution and thus, an approach to reduce their influence can be a useful tool. Thus, PMF offers a "robust" mode. The robust factorization based on the Huber influence function [Huber, 1981] is a technique of iterative reweighting of the individual data values. The least squares formulation, thus, becomes

$$Q = \sum_{i=1}^m \sum_{j=1}^n (e_{ij}/h_{ij}s_{ij})^2 \quad (4)$$

where

$$h_{ij}^2 = \begin{cases} 1 & \text{if } |e_{ij}/s_{ij}| \leq \alpha, \text{ and} \\ |e_{ij}/s_{ij}|/\alpha & \text{otherwise} \end{cases} \quad (5)$$

where α = the outlier distance and the value of $\alpha = 4.0$ was chosen. It is generally advisable to use the robust mode when analyzing environmental data. Our experience has generally found that the robust mode provides the best results for typical particulate composition data.

Conditional Probability Function

The conditional probability function (Kim *et al.*, 2003) analyzes local source impacts, especially gasoline vehicle and diesel emissions, from varying wind directions using the source contribution estimates from PMF coupled with the time resolved wind directions. The CPF estimates the probability that a given source contribution from a given wind direction will exceed a predetermined threshold criterion. CPF is defined as

$$CPF = \frac{m_{\Delta\theta}}{n_{\Delta\theta}} \quad (6)$$

where $m_{\Delta\theta}$ is the number of occurrences from wind sector $\Delta\theta$ that exceeded the threshold criterion, and $n_{\Delta\theta}$ is the total number of data from the same wind sector. The same daily contribution was assigned to each hour of a given day to match to the hourly wind data. In this study, 24 sectors were used ($\Delta\theta = 15$ degrees). Calm winds (< 1 m/sec) were excluded from this analysis due to the isotropic behavior of wind vane under calm winds. From the tests with several different percentiles of the fractional contribution from each source, the threshold criterion of upper 25% was chosen to clearly show the directionality of the sources. The sources are likely to be located to the direction that have high conditional probability values.

Variable Selection Criteria

All measurements contain uncertainty in the reported values. For environmental data, the noise content in some variables is much higher than in other variables (Paatero and Hopke, 2003). For example, the noise level in some variables may be well below 10% of the signal. In other variables, there may be more noise than signal, or no signal at all. A variable will be called "a weak variable" if it contains signal and noise in comparable amounts. Similarly, variables containing more noise than signal are termed "bad variables." It is problematic to give precise definitions of terms weak and bad variables. Minimum detective limit (MDL) is an important parameter to assess signal and noise for a variable.

A tentative definition of weak elements for censored data can be based on the number of concentration data below MDL (N_{DL}). Denote the variable j (average) MDL as δ_j , defining the ratio of signal and noise (SN) as:

$$SN = \frac{\sum_{(i|X_{ij} > \delta_j)} X_{ij}}{\delta_j N_{DLj}} \quad (7)$$

Then variable j may defined to be good, weak or bad if $SN \geq 2$, $0.2 < SN < 2$, $SN \leq 0.2$, respectively. Variables with more than 90% of concentrations lower than MDL are regarded as bad variables and are not selected for analysis. For each data set, the SN values are calculated for each variable and the data downweighted as recommended by Paatero and Hopke (2003).

STUDY RESULTS

There are three types of data available for analysis including IMPROVE, Speciation Trends Network (STN) and PTEP data. The studies have focused on the IMPROVE and STN site data because of problems that were found in the PTEP data that are described in a subsequent section of this report. The IMPROVE site results are presented first followed by the STN data analyses.

IMPROVE Data

Previously data from several IMPROVE sites have been analyzed including Crater Lake National Park and Lassen Volcanic National Park (Liu *et al.*, 2003) and San Geronio National Wilderness (Zhao and Hopke, 2004). In both cases, it was not possible to extract factors that could be assigned to residual oil combustion. A map showing the location of the near shore IMPROVE sites in California is shown in Figure 3. As a comparison site, Yosemite National Park has been studied. In addition to these California sites, the data from Olympic National Park in Washington is reported below.

Aqua Tibia

This site was established in 2000 and data from samples collected between December 2000 and December 2003 at the Aqua Tibia IMPROVE site (latitude: 33°27'49.32" N, longitude: 116° 58'14.16" W, elevation: 507 m) were analyzed. In the original measurement data set, 16% out of 375 samples had more than 50% missing values, so they were deleted from analysis. Examination of the time series plots for the various elements clearly indicates the presence of fireworks on July 4 events, so the 3 additional samples around July 4 were also deleted from the data set. Based on the S/N ratio, nitrite, and phosphorus were deleted as "bad" variables. The reported EC1 concentration in IMPROVE/TOR protocol includes the OP concentration. In this paper, the OP was subtracted from EC1 and utilized as an independent variable in the PMF analysis. In addition, some elements have more than 50% 0 values. For these elements, half of DL (detection limit) is used as replacing value and 4 times of DL is used to downweight these elements. XRF sulfur and SO₄²⁻ showed excellent correlations (slope = 0.316, r² = 0.97), S was excluded from the analysis since sulfate provided better mass closure. Thus a total of 312 samples and 33 species were used in this study. A summary of PM_{2.5} speciation data used in this analysis is shown in Table 1.

In choosing the number of factors, there are a number of indicators that can be reviewed, but there is no definitive method for identifying the "correct" factor number. In this case, factor numbers between 4 and 12 were considered. The 7-factor model was found to generate the most reasonable results. Reducing to fewer factors produced combinations of potential sources, such as the combination of diesel and gasoline emissions. Increasing the number of factors did not significantly improve the fit to the data and the factors were not easily interpreted. Therefore, a 7-factor model was chosen.

Factor analysis solutions have rotational ambiguity (Paatero *et al.*, 2002), so the parameters FPEAK and FKEY are used to control the rotation problem and find the optimal solution. By setting a positive/negative value of FPEAK, the routine is forced to add/subtract G factor vectors to/from each other and subtract/add the corresponding F factors from/to each other and thereby yield more physically realistic solutions. There is no certain rule for selecting FPEAK to produce the best solution. Usually PMF is run with different FPEAK values to find



Figure 3 Map showing coastal and near-coastal IMPROVE sites in California.

the range within which the objective function Q does not show significant changes. The optimal solution should lie in this range (Paatero *et al.*, 2002). Examining Q as a function of FPEAK, it was found that Q was stable in the range of FPEAK from -0.1 to 0.1. Thus, the FPEAK value was set to 0. All of the FKEY values were also set to 0.

The PM_{2.5} was regressed against the 7-source contributions. The resulting predicted mass from the PMF correlated well with the observed mass ($r^2 = 0.966$, slope = 0.94), as shown in Figure 4. The source profiles are shown in Figure 5 while the source contributions are shown in Figure 6. The apportioned mass contributions are provided in Table 2.

Vehicle emissions were separated into gasoline and diesel. Gasoline vehicle and diesel emissions have high carbon concentrations where the OC and EC abundances differ. Gasoline vehicles emissions have high concentrations of the OC fractions. In contrast, diesel emissions were higher in concentration of EC (Zhao and Hopke, 2004). The EC2 fraction in the diesel emissions is significantly higher than that in the gasoline emissions. Thus, source 6 is assigned as gasoline emission with high concentrations of OC while source 1 with high concentrations of OC1, EC1, and EC2 and EC1 appears to represent diesel emissions. Gasoline vehicles and diesel emissions account for 23.0% and 1.7% of the PM_{2.5} mass concentration, respectively.

Source 2 represents secondary nitrate. Clearly, this material is secondary ammonium nitrate originating from the oxidation products of NO_x and subsequent reaction with NH₃. The main sources of NO_x are motor vehicle and power plants. Secondary nitrate contributes 20.4% to the total PM_{2.5} mass. This source shows a seasonal pattern with its highest contributions in

winter although with some summer peaks were seen similar to those observed by Liu *et al.* (2000) at Riverside, CA.

A sulfate factor was obtained in this analysis. Secondary sulfate contributes 31.0% of the total PM_{2.5} mass. It contains sulfate and very low concentrations of any other species. It has its maximum contributions during the summer with very low winter values. It appears that this source could include non-sea salt sulfate produced by the oxidation of dimethyl sulfide and dimethyl disulfide that is produced by oceanic phytoplankton. In earlier work, off-shore sources of SO₂ were observed in the study of the Los Angeles basin (Gao *et al.*, 1993, 1994) that were not directly related to emissions from ships. It is also possible that there was transport from the Los Angeles basin. A back trajectory on September 15, 2003 shows

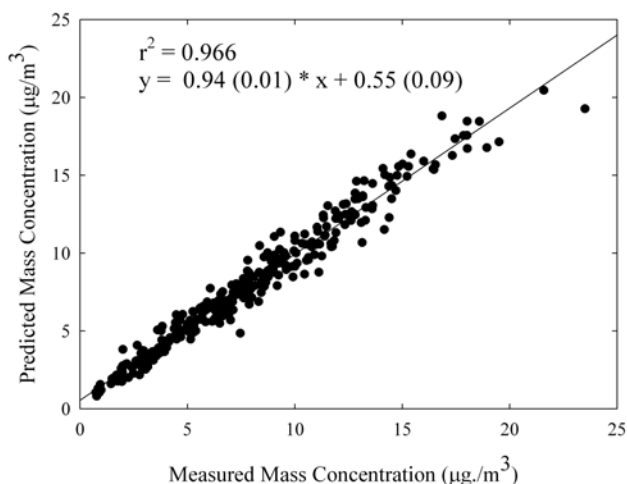


Figure 4 Predicted mass concentrations compared to the measured mass concentrations for the Aqua Tibia IMPROVE site.

transport from the South Coast Air Basin and prior studies of ozone in nearby Temcula have suggested transport from the western end of the basin. Another possible source area for the sulfate is Mexico as suggested by the trajectory on October 6, 2003. Thus, these different peak concentration days may arise from transport from different source areas.

Table 1. Summary Statistics of the Chemical Composition and Overall Mass for City of Agua Tibia, CA Samples Collected from 12/20/2000 to 12/29/2003

component	Concentration ($\mu\text{g}/\text{m}^3$)					Bad values			DL ($\mu\text{g}/\text{m}^3$) (Median)
	median	average	min	max	missing (%)	0 value (%)	other BDL (%)	total (%)	
PM _{2.5}	7.5000	4.7506	0.0000	32.2982	0.32%	0.00%	0.00%	0.32%	0.3073
Al	0.0000	0.0565	0.0000	1.2243	0.00%	52.06%	0.32%	52.38%	0.0066
As	0.0000	0.0001	0.0000	0.0021	0.00%	59.68%	0.00%	59.68%	0.0002
Br	0.0033	0.0035	0.0002	0.0107	0.00%	0.00%	0.00%	0.00%	0.0001
Ca	0.0425	0.0533	0.0000	0.3865	0.00%	0.32%	0.00%	0.32%	0.0002
Cl	0.0000	0.0056	0.0000	0.2836	0.00%	88.89%	0.00%	88.89%	0.0007
Cr	0.0000	0.0001	0.0000	0.0033	0.00%	66.67%	0.00%	66.67%	0.0001
Cu	0.0009	0.0010	0.0000	0.0074	0.00%	0.95%	0.95%	1.90%	0.0001
EC1	0.3626	0.3828	0.0146	1.7603	0.00%	0.00%	0.00%	0.00%	0.0177
EC2	0.0496	0.0591	0.0000	0.3059	0.00%	0.63%	17.14%	17.78%	0.0211
EC3	0.0000	0.0044	0.0000	0.0626	0.00%	71.75%	5.71%	77.46%	0.0052
Fe	0.0559	0.0675	0.0044	0.6714	0.00%	0.00%	0.00%	0.00%	0.0001
H	0.2782	0.3167	0.0436	1.4856	0.00%	0.00%	0.00%	0.00%	0.0050
K	0.0450	0.0628	0.0068	0.6927	0.00%	0.00%	0.00%	0.00%	0.0004
Mg	0.0000	0.0056	0.0000	0.1170	0.00%	86.35%	2.54%	88.89%	0.0199
Mn	0.0010	0.0013	0.0000	0.0128	0.00%	17.78%	0.32%	18.10%	0.0001
Na	0.0000	0.1708	0.0000	1.6810	0.00%	50.48%	1.27%	51.75%	0.0761
Ni	0.0005	0.0006	0.0000	0.0047	0.00%	11.75%	0.95%	12.70%	0.0001
NO3	1.2177	1.6858	0.0381	8.0857	0.00%	0.00%	0.00%	0.00%	0.0252
OC1	0.0694	0.0977	-0.0272	2.2093	0.00%	0.63%	42.54%	43.17%	0.0580
OC2	0.2422	0.2756	0.0000	3.4755	0.00%	0.32%	8.89%	9.21%	0.0578
OC3	0.5592	0.6779	0.0408	5.6428	0.00%	0.00%	5.08%	5.08%	0.1333
OC4	0.4321	0.4880	0.0370	4.5672	0.00%	0.00%	0.63%	0.63%	0.0461
OP	0.0121	0.0462	-0.0124	0.3203	0.00%	34.92%	23.81%	58.73%	0.0239
Pb	0.0015	0.0016	0.0000	0.0073	0.00%	0.63%	0.00%	0.63%	0.0001
Rb	0.0001	0.0002	0.0000	0.0019	0.00%	29.21%	0.32%	29.52%	0.0001
Se	0.0003	0.0003	0.0000	0.0011	0.00%	4.44%	0.32%	4.76%	0.0000
Si	0.1593	0.1958	0.0000	2.7017	0.00%	0.95%	0.00%	0.95%	0.0030
SO4	1.5223	1.9364	0.0819	7.8969	0.00%	0.00%	0.00%	0.00%	0.0266
Sr	0.0005	0.0007	0.0000	0.0073	0.00%	2.86%	2.54%	5.40%	0.0001
Ti	0.0054	0.0069	0.0000	0.0640	0.00%	3.17%	0.00%	3.17%	0.0001
V	0.0021	0.0027	0.0000	0.0175	0.00%	9.84%	0.00%	9.84%	0.0001
Zn	0.0036	0.0041	0.0004	0.0198	0.00%	0.00%	0.00%	0.00%	0.0001
Zr	0.0000	0.0000	0.0000	0.0008	0.00%	78.10%	8.25%	86.35%	0.0002

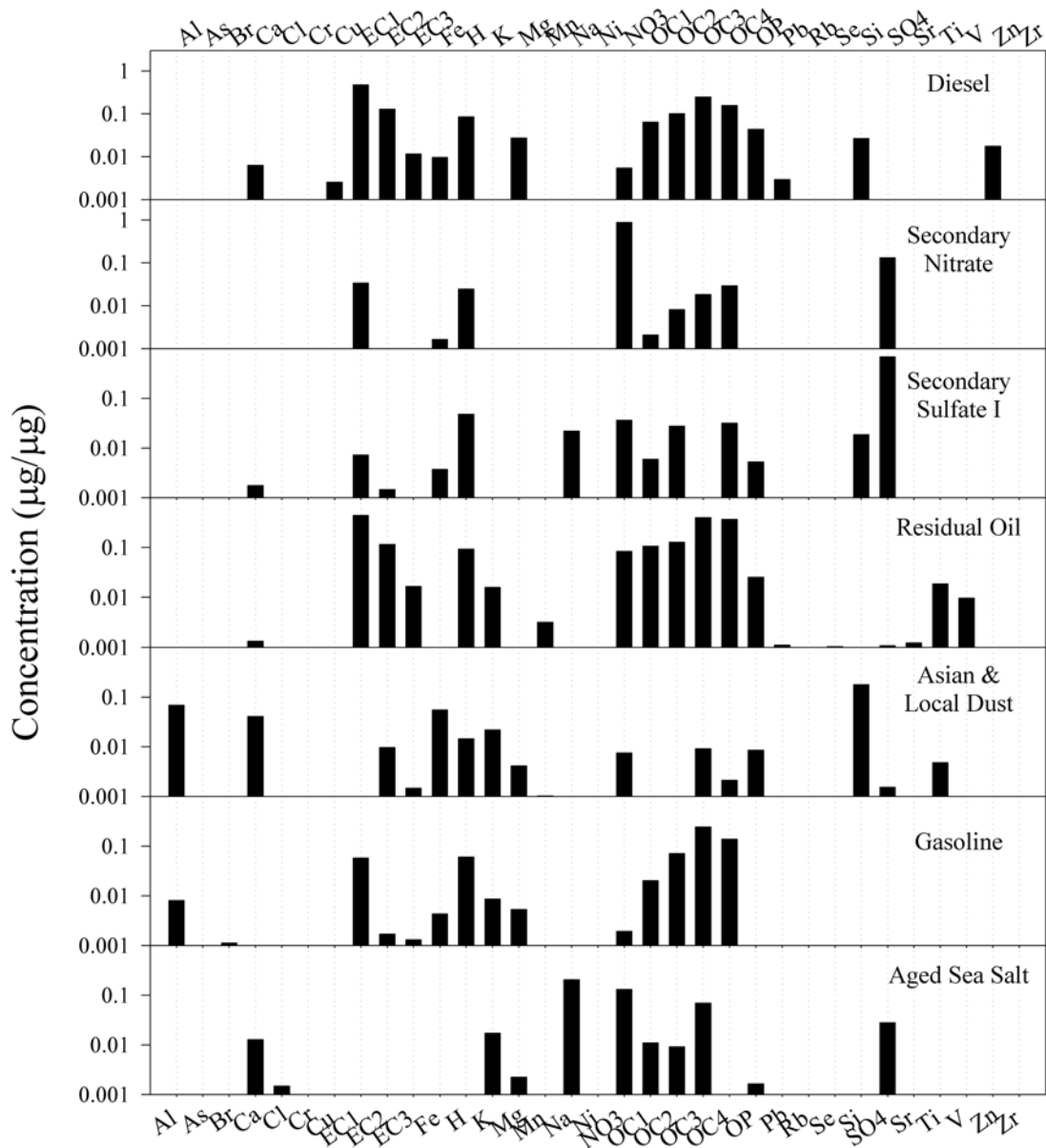


Figure 5 Source profiles derived from the PMF2 analysis of the IMPROVE data from the Aqua Tibia site.

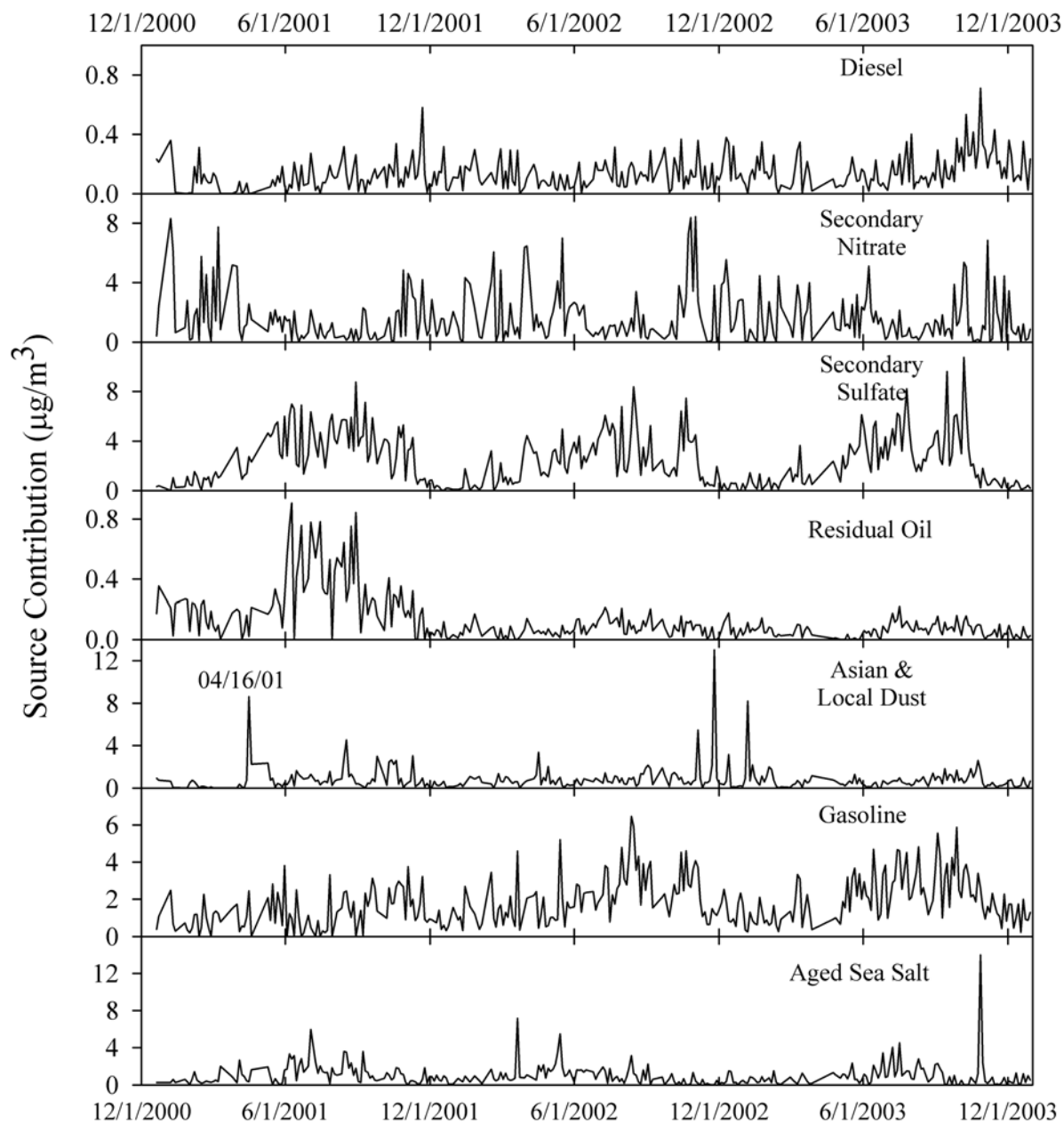


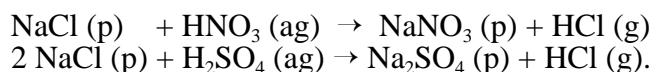
Figure 6 Source contribution time series derived from the IMPROVE data from the Aqua Tibia site.

The next source includes organic and elemental carbon as well as the highest concentrations of Ni and V and thus is assigned to be residual oil combustion. This source contributes relatively little mass (1.6%) and its mass contributions were concentrated in the middle to the end of 2001 with very low contributions before or after this period. This source could represent some influence of ship emissions. However, the profile also shows a relatively high Ti value and the temporal pattern is not consistent with routine ship traffic in the off-shore area. Thus, the exact nature of this weak source is not yet clear.

The next source represents airborne soil dust with high concentrations of Al, Si, Ca, and Fe, and contributes 6.3% to the total PM_{2.5} mass. The ratio of Al to Si in this source is 0.40, somewhat higher than the typical ratio observed in soils, 0.293 (Mason, 1966). From the time serial contribution plot of this source, we can see a high peak in the spring of 2001. This peak is likely caused by Asian desert dust. Dust storms occur almost every spring in the deserts of Western China, such as Taklamakan, Gobi and Ordos Deserts (Zhao and Hopke, 2004). Especially, the storm in April 2001 was strong and the dust cloud crossed the Pacific and reached much of the west coast of North America. Thus, the peak on 16 April 2001 in the contribution plot of this source is likely to correspond to this sand storm.

On the other hand, there are three major peaks and several lesser ones in the fall of 2003 and small peaks in the other fall seasons are clearly local dust brought to the area on the Santa Ana winds that are typical of the fall weather patterns. A back trajectory for November 28, 2003 corresponding to the largest peak in the contribution time series is shown in Figure 7. It clearly shows the influence of the inland areas of California and adjacent locations as the source of the airborne dust. In San Geronio, it was possible to separate two soil factors, but such a separation could not be achieved in this study.

Source 5 appears to be aged sea salt with high concentrations of Na, SO₄ and NO₃. This source contributes 12.7% to the total PM_{2.5} mass. The low concentration of chloride in this source is likely to be due to chloride loss reactions in the atmosphere such as



Both HNO₃ and H₂SO₄ appear to have participated in the chloride loss. Figure 8 shows the back trajectory on October 30, 2003 corresponding to the day with the highest contribution of aged sea salt.

Table 2. Source Apportionment for the PM_{2.5} measures at Aqua Tibia

Source	Mean Contribution ($\mu\text{g}/\text{m}^3$)
Diesel Emissions	0.26
Secondary Nitrate	1.44
Secondary Sulfate	2.67
Residual Oil	0.20
Asian and Local Dust	0.76
Gasoline Emissions	1.28
Aged Sea Salt	0.94

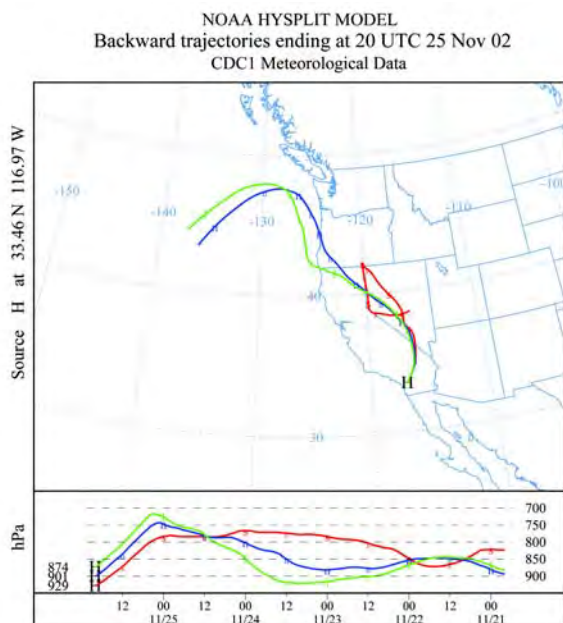


Figure 7 HYSPLIT trajectory calculated for noon on November 25, 2002.

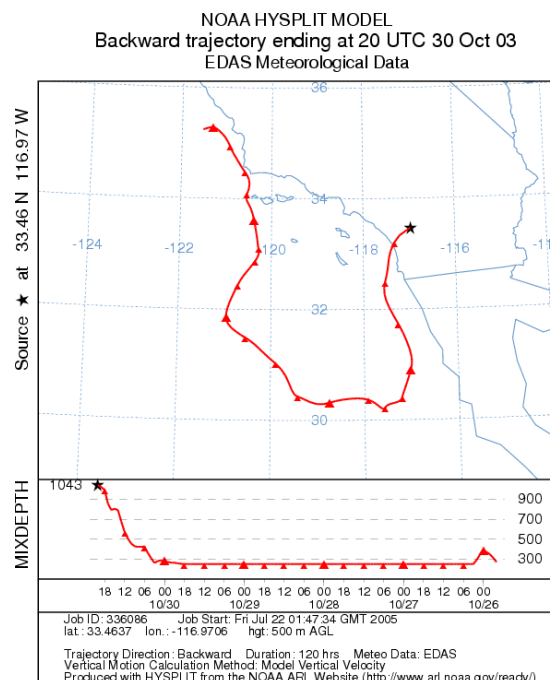


Figure 8 HYSPLIT trajectory calculated for noon on October 30, 2003.

San Gabriel

The San Gabriel Site is at latitude: 34° 12' 0" N, longitude: 118° 18' 0" W (Figure 9). This site has been in service since December 2001. Data were available through June 2004. The data are summarized in Table 2. The average mass concentration is 4.74 $\mu\text{g}/\text{m}^3$. This value is substantially lower than the STN site data in the Southern California Air Basin. As will be seen in the discussion of the STN sites in this region, the mean mass concentration values for Simi Valley, Los Angeles, and Rubidoux were 16.01, 21.07, and 31.01 $\mu\text{g}/\text{m}^3$, respectively. It is clear from the low mass concentration that there is relatively limited transport from the populated areas of the Basin to this site.

More than 90% of the values for Mo, P and NH_4^+ were missing. Therefore, these species were excluded from the analyses. The S/N of Cl^- was greater than that of XRF Cl. Similarly, the S/N ratio for S was greater than that for SO_4^- . CHL and SO_4^- were therefore excluded. The S/N ratios of As, EC3, Cl, Mg, N2, Na and Zr were between 0.2 and 2. These species were downweighted and their uncertainties were increased 3 fold. A sea salt factor was not identified in any of the solutions. Although this failure might have been due to the downweighting of both Cl and Na ions, but the analysis without downweighting Cl and Na provided source profiles that were not significantly different from the downweighted solution. Solutions were examined for 6 to 9 factors and a seven factor solution was chosen. It provided a good fit to the data as shown in Figure 10 and reasonably interpretable factors.

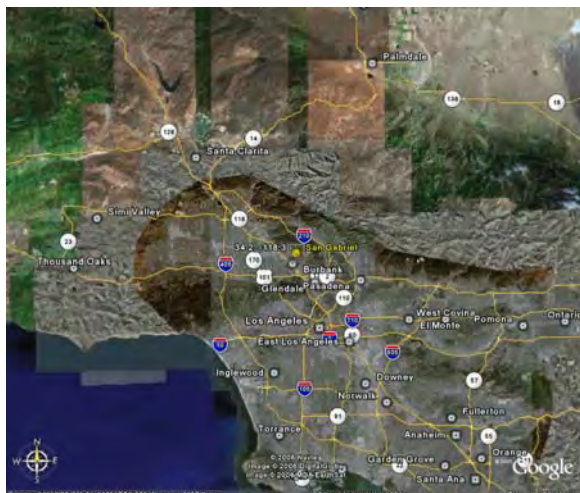


Figure 9 Map of the Los Angeles area showing the location of the San Gabriel IMPROVE site.

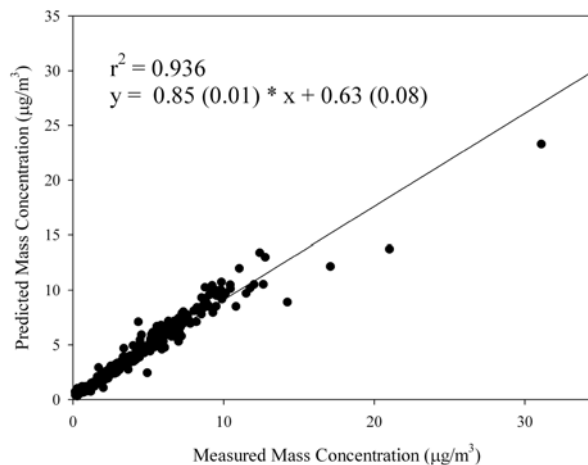


Figure 10 Predicted mass concentrations plotted against the measured mass concentrations.

The source profiles are shown in Figure 11, and the time series of contributions are presented in Figure 12. The first factor has high concentrations of EC with lower OC values. It also includes Zn, Cu, and Fe suggesting diesel emissions. It also includes Na that is not typically observed in diesel emission profiles. Efforts to pull the Na value down using FKEY did not result in any substantial change. The next profile shows OC with little EC and low concentrations of the other species. Both contribution time series for these factors show considerable day to day variation. This profile also includes what little Ni and V concentrations are observed at this site. At this site, the mean Ni and V concentrations are of the order of hundreds of picograms per cubic meter so that there is little influence from ship emissions on the total mass. This second profile appears to be an admixture of local gasoline emissions admixed with other source materials.

The next profile has high concentrations of Na, NO₃, S and OP. It contributes relatively little mass. There are peaks in the time series in May 2003 and 2004. Back trajectories on these days point back to the ocean with the trajectories arriving from the north and west without passing through the populated areas of the basin.

The fourth profile appears very similar to that which has typically been identified as gasoline emissions. However, it has a very unusual time series with a few very high concentrations values in August and September 2002. The back trajectories for September 26 and August 18, 2002 are shown in Figures 13 and 14. As can be seen, these trajectories pass through the area of San Francisco and thus, this profile appears to be the urban plume from the San Francisco Bay area. These trajectories run parallel to the coast, but do not appear to represent any significant accumulation of ship emissions.

Table 3. Summary statistics for data from the San Gabriel IMPROVE site.

Species	Mean ($\mu\text{g}/\text{m}^3$)	Std Dev ($\mu\text{g}/\text{m}^3$)	Geo Mean ($\mu\text{g}/\text{m}^3$)	Geo Std	Samples Missing	Values BDL	% BDL
PM _{2.5}	4.740	3.524	3.452	2.497	13	4	1.4%
EC1	0.236	0.183	0.178	2.318	15	0	0.0%
EC2	0.056	0.035	0.047	1.802	15	0	0.0%
EC3	0.005	0.006	0.003	2.167	15	220	76.1%
OC1	0.078	0.099	0.051	2.593	34	7	2.6%
OC2	0.182	0.209	0.130	2.282	15	0	0.0%
OC3	0.478	0.616	0.298	2.714	16	0	0.0%
OC4	0.296	0.388	0.196	2.495	15	0	0.0%
OP	0.075	0.075	0.050	2.714	30	28	10.2%
NO ₃ ⁻	1.243	1.382	0.688	3.484	18	0	0.0%
NO ₂ ⁻	0.019	0.017	0.014	2.438	72	74	31.9%
Al	0.056	0.067	0.018	6.061	13	108	37.1%
As	0.000	0.000	0.000	2.171	13	154	52.9%
Br	0.002	0.001	0.002	2.366	13	1	0.3%
Ca	0.043	0.035	0.030	2.513	13	0	0.0%
Cl	0.001	0.002	0.000	2.219	13	256	88.0%
Cr	0.000	0.000	0.000	2.940	13	110	37.8%
Cu	0.001	0.002	0.001	2.689	13	10	3.4%
H	0.187	0.150	0.141	2.174	13	0	0.0%
Fe	0.051	0.037	0.038	2.453	13	0	0.0%
Pb	0.001	0.001	0.001	2.251	13	3	1.0%
Mg	0.015	0.018	0.011	2.042	13	236	81.1%
Mn	0.001	0.001	0.001	3.144	13	13	4.5%
Ni	0.0003	0.0005	0.0002	3.319	13	47	16.2%
K	0.040	0.056	0.027	2.393	13	0	0.0%
Rb	0.000	0.000	0.000	2.621	13	87	29.9%
Se	0.000	0.000	0.000	3.245	13	40	13.7%
Si	0.155	0.136	0.103	2.960	13	4	1.4%
Na	0.076	0.092	0.047	2.474	13	190	65.3%
Sr	0.001	0.001	0.000	2.969	13	10	3.4%
S	0.289	0.214	0.207	2.438	13	0	0.0%
Ti	0.005	0.004	0.003	2.931	13	4	1.4%
V	0.0009	0.0010	0.0005	4.068	13	25	8.6%
Zn	0.003	0.002	0.002	2.330	13	1	0.3%
Zr	0.000	0.000	0.000	1.836	13	226	77.7%

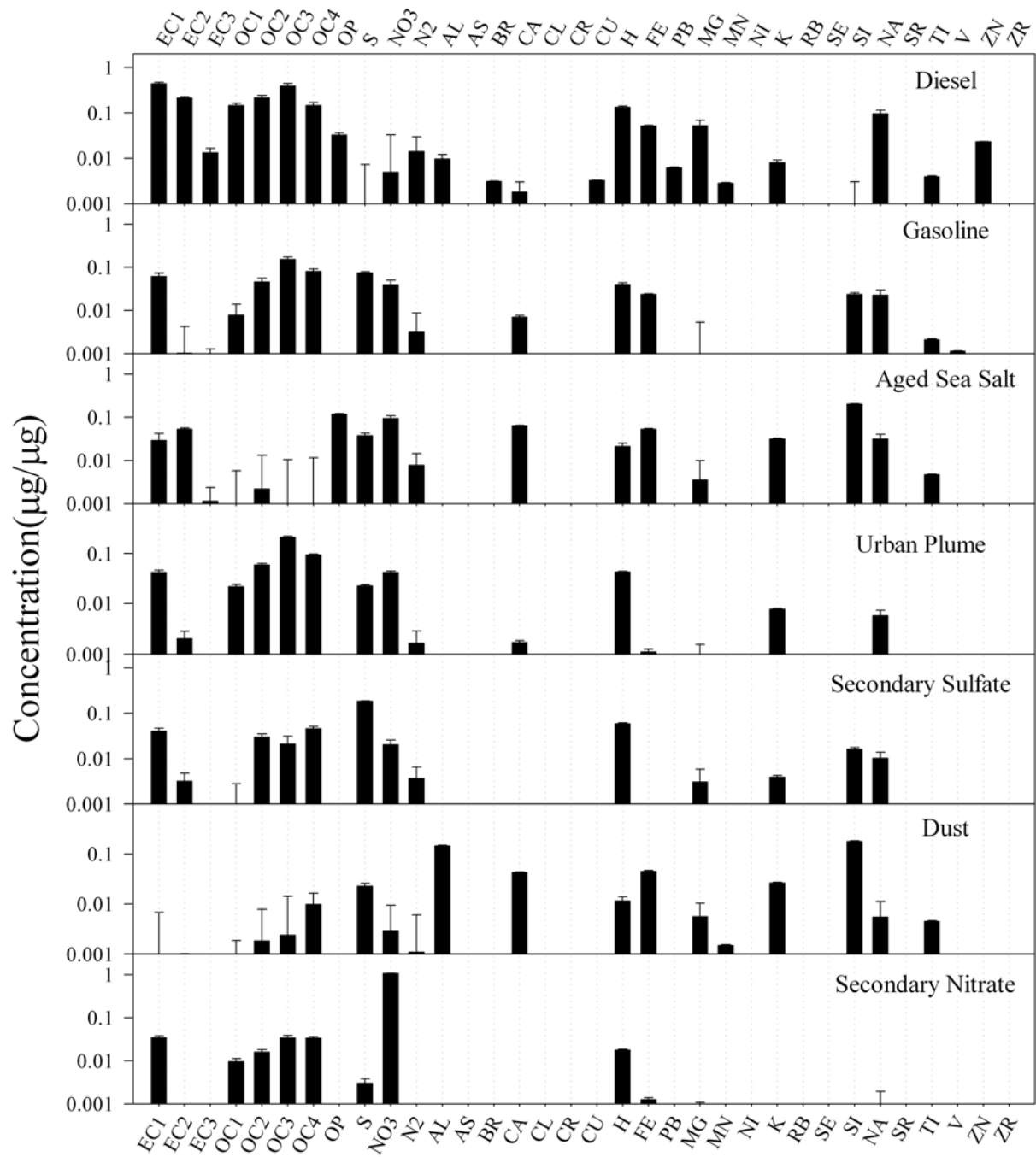


Figure 11 Source profiles derived from the San Gabriel IMPROVE site data.

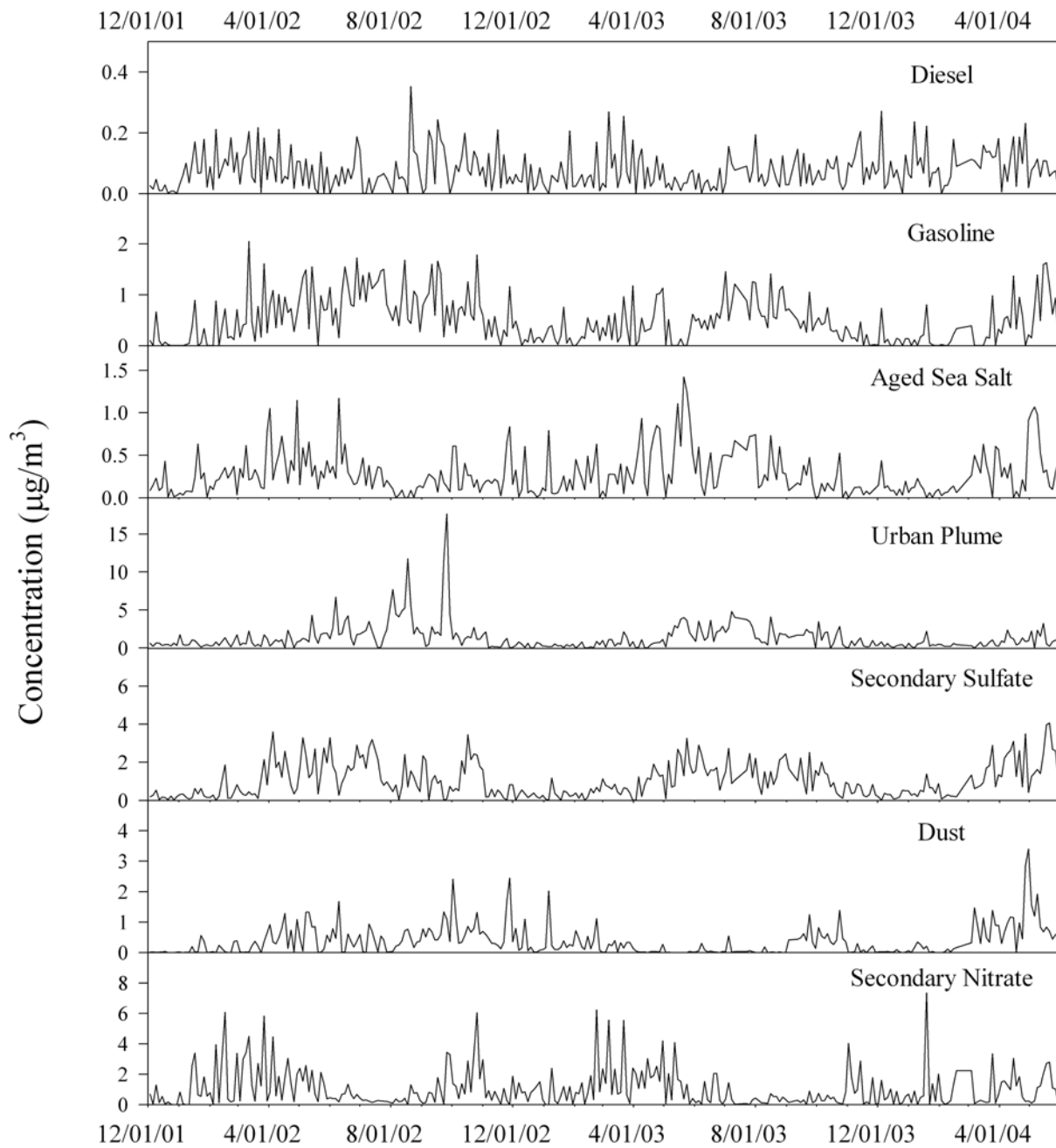


Figure 12 Source contributions derived from the San Gabriel IMPROVE site data.

The next profile is a typical secondary sulfate profile with relatively low associated carbon concentrations. These sulfate profiles are quite different from those observed in the eastern US in that there is essentially no selenium associated with the sulfate and much lower carbon concentrations. These differences reflect the absence of coal-fired power plants and the relatively limited transport over areas with significant organic carbon emissions. The lack of Se results in the observation of only a single sulfate factor since there is not the S-Se variation with seasonal photochemical activity that requires two factors to fit the data.

The next factor is attributed to wind-blown dust. In this case there is no significant influence of the Asian dust episode of late April 2001. There is a late April 2004 peak that appears to be associated with intercontinental transported Asian dust. The other major peaks observed in the time series of source contributions are associated with trajectories from the east that transport dust from inland areas of the western U.S.

The final profile is associated with secondary nitrate. It has peak contributions in the winter through spring. It represents one of the larger contributions to the PM_{2.5} at this site. The contributions to the average PM_{2.5} mass are summarized in Table 4.

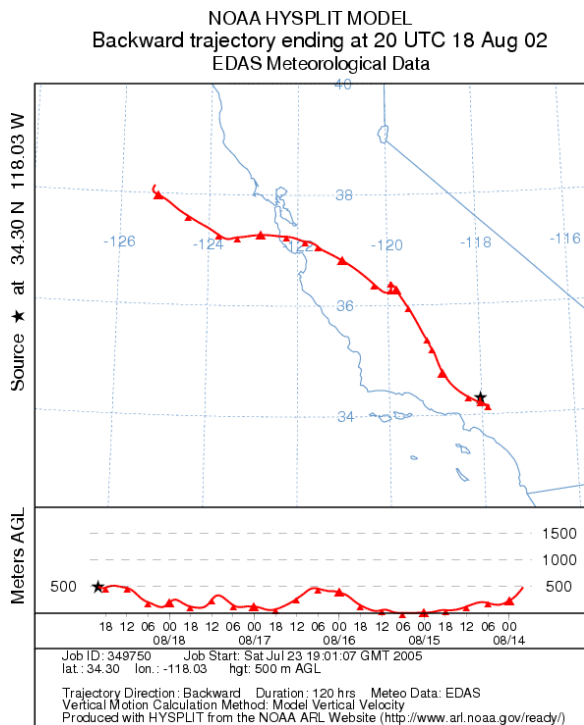


Figure 13 Back trajectory from San Gabriel on August 18, 2002.

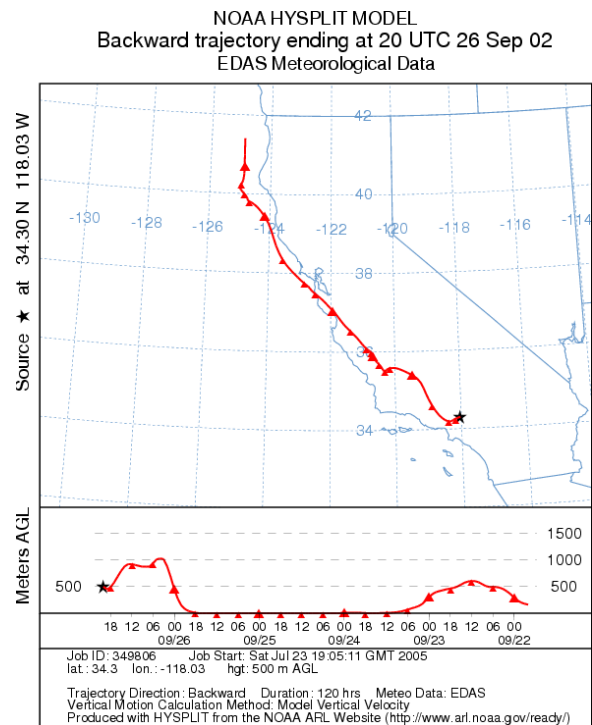


Figure 14 Back trajectory from San Gabriel on September 28, 2002.

Table 4. Average source contributions to the PM_{2.5} samples collected at San Gabriel

Source	Contribution (µg/m ³)
Diesel Emissions	0.08
Gasoline Vehicles	0.50
Aged Sea Salt	0.28
Urban Plume	1.34
Secondary Sulfate	1.04
Asian and Local Dust	0.37
Secondary Nitrate	1.05

San Rafael

Samples were collected at the IMPROVE monitoring site in San Rafael, California. The San Rafael site (34°43' 48" N and 120° 0' 36" W) is located in southern California in the vicinity of Santa Barbara. The site is located near the crest of a low ridge a few kilometers outside the southern wilderness boundary of the San Rafael wilderness area at an elevation of 953 m above sea level.

The reported EC1 concentration included the OP concentration. Thus, it was subtracted from the EC1 concentration and used as a separate variable, while the EC1 used for the data analysis was the difference between the reported EC1 and OP. The uncertainty associated with the EC1 used in the analysis was computed by error propagation. OC1 was downweighted by a factor of two, since OC1 includes adsorption artifacts onto the quartz filter. In addition to examining the percentage missing and below detection limit (BDL) values, the signal to noise (S/N) ratio was also calculated to choose the variables that could be included in the analysis. This approach to screen data allows inclusion of variables with high missing or BDL values having a few, but high quality data points. The S/N ratio was calculated for each variable and they were suitably downweighted following the procedure outlined in Paatero and Hopke, 2003. The XRF S and IC SO₄²⁻ showed an excellent correlation. In view of the potential for a positive artifact in SO₄²⁻ measurement due to the dissolution of SO₂ in the leaching medium, sulfate was excluded from the analysis and only XRF S was used. Cl⁻ was chosen over Cl for inclusion in the analysis because both variables had comparable BDL values, but the S/N ratio for Cl⁻ was very high. The measured PM_{2.5} mass was regressed against the reconstructed mass and was calculated following the procedure outlined in Malm *et al.*, 1994 to check for anomalies in the data. PM_{2.5} speciation data used in this study and calculated S/N ratios are summarized in Table 5. Variables which had BDL and missing values greater than 90% were excluded from the analysis. Samples which had missing PM_{2.5} mass concentration values and those that did not have all eight carbon fractions were excluded from the analysis. Samples which had error flags other than normal (“NM”) for PM_{2.5} concentration were also not included. Thus a total of 34 variables and 339 samples were retained for analysis.

In this study, the scaled residuals for a nine factor model were found reasonable for most of the variables. Based on the usual diagnostic steps, the number of factors was ultimately decided based on the physical interpretability of the resolved sources.

As with all bilinear factor analysis models, PMF also suffers from rotational ambiguity (Paatero *et al.*, 2002). One way of controlling rotational ambiguity is by fixing suitable FPEAK values in the PMF program. The Q value is determined as a function of FPEAK and the region

in which it is stable is examined. In this study, the Q value appeared stable for FPEAK values between -0.1 and 0.1. However, based on the physical interpretability of the resolved sources, FPEAK was set to zero.

Nine sources were resolved for the ambient particulate matter in San Rafael CA. The robust mode was used in this analysis to decrease the influence of extreme values in the solution. The final solution was determined by experimenting with different factors and the use of FPEAK and FKEY. In the nine source model, an additional source was resolved compared to the eight source model. However, the nine source model itself appears to have a source that is a combination of two sources. When the ten source model was tried to resolve this mixed source, an additional factor was created in a way that did not address the required source resolution, but resulted in the creation of two identical sources which appear as just one source in the nine factor model. Thus, the nine factor solution was selected. The sources resolved include gasoline vehicle, oil combustion, nitrate, resuspended soil mixed with traffic, secondary sulfate, sea salt (fresh and aged), diesel emissions, Asian dust and OP enriched sulfate. Figure 15 presents the source profiles derived from the San Rafael data while Figure 16 shows the time series of contributions. Figure 17 shows the comparison between predicted $PM_{2.5}$ mass concentration and the observed $PM_{2.5}$ mass concentration. The slope is 0.8 ± 0.01 , the intercept is 0.85 ± 0.09 , with a correlation coefficient of 0.90. Thus, the nine factor model explains the variability in the data set reasonably.

A combination of source profiles, time series of source contributions, and back trajectories were used for source identification. The gasoline vehicle and diesel sources were resolved utilizing the temperature-resolved carbon fraction information. It has been observed that in general the diesel OC1 and EC2 abundance is higher than that of gasoline. It has also been suggested that the gasoline EC1 abundance is greater than that of diesel. Further, both diesel and gasoline have very little or no EC3. The carbon fraction profiles meet the criteria with a small deviation in the EC1 abundance. In this study, the EC1 diesel abundance is greater than that of gasoline. However, it must be noted that elsewhere (Kim *et al.*, 2004), diesel and gasoline emission profiles obtained are similar to those obtained in this study. Further, the diesel source profile indicated the presence of Zn which is likely to be from engine lubrication oil in diesel trucks. There is a possibility though, that some of the mass apportioned to gasoline vehicles may include diesel traffic since the carbon fraction profiles depend to a large extent on whether the traffic is continuous or 'stop and go' traffic (Shah *et al.*, 2004).

The oil combustion source was identified based on the presence of the marker elements vanadium and nickel. The nitrate source is clearly indicated by the presence of nitrate in high concentrations and does not co-vary with other chemical species. A mixed source of resuspended soil and traffic was identified by presence of Ca, Fe, Si, Ti, and high carbon fraction concentrations co-varying with nitrate, respectively.

Table 5. Summary Statistics for PM_{2.5} and 33 Species Mass Concentrations used for PMF Analysis of the San Rafael IMPROVE Site.

Species	Concentration (µg/m ³)							
	Mean	Geometric mean	Minimum	Maximum	# BDL	# Missing	%(BDL+ Missing)	S/N
PM _{2.5}	5.11	4.00	0.25	27.30	2	106	22.22	16.42
Al	0.44	0.35	0.11	1.00	227	103	67.90	17.59
As	0.29	0.24	0.10	0.90	196	103	61.52	2.31
Br	0.33	0.28	0.10	0.99	0	103	21.19	60.10
Ca	0.43	0.36	0.11	1.00	5	103	22.22	68.46
EC1	0.36	0.29	0.11	1.00	1	98	20.37	5.95
EC2	0.45	0.40	0.11	0.98	6	98	21.40	1.90
EC3	0.40	0.31	0.12	0.92	284	98	78.60	2.02
OC1	0.43	0.36	0.11	1.23	93	98	39.30	1.02
OC2	0.36	0.28	0.11	2.13	1	98	20.37	2.22
OC3	0.51	0.39	0.11	5.46	2	98	20.58	3.47
OC4	0.40	0.33	0.11	3.81	0	98	20.16	6.60
OP	0.40	0.31	0.11	1.00	38	98	27.98	3.57
Cl	0.40	0.31	0.10	2.14	332	103	89.51	167.8
Cr	0.36	0.27	0.10	0.93	232	103	68.93	1.92
Cu	0.40	0.34	0.10	0.98	60	103	33.54	8.68
H	0.36	0.30	0.11	1.28	0	103	21.19	63.19
Fe	0.43	0.37	0.11	1.00	0	103	21.19	508.4
Pb	0.45	0.36	0.10	0.99	21	103	25.51	14.08
Mg	0.29	0.26	0.12	0.75	329	103	88.89	1.77
Mn	0.37	0.30	0.10	0.98	108	103	43.42	5.18
Ni	0.36	0.30	0.10	0.98	148	103	51.65	4.96
NO ₃ ⁻	0.83	0.62	0.11	4.52	0	100	20.58	28.75
K	0.42	0.35	0.11	1.00	3	103	21.81	53.78
Rb	0.31	0.25	0.10	0.9	113	103	44.44	3.04
Se	0.34	0.29	0.10	0.98	27	103	26.75	8.15
Si	0.35	0.28	0.11	1.74	8	103	22.84	70.91
Na	0.39	0.32	0.11	1.00	170	103	56.17	6.30
Sr	1.20	0.91	0.11	4.73	22	103	25.72	7.58
S	0.46	0.39	0.12	1.98	0	103	21.19	252.9
Ti	0.44	0.38	0.11	1.00	36	103	28.60	9.96
V	0.37	0.30	0.10	0.99	97	103	41.15	3.80
Zn	0.31	0.26	0.10	0.98	2	103	21.60	42.98
Zr	0.29	0.24	0.10	0.80	299	103	87.72	1.70

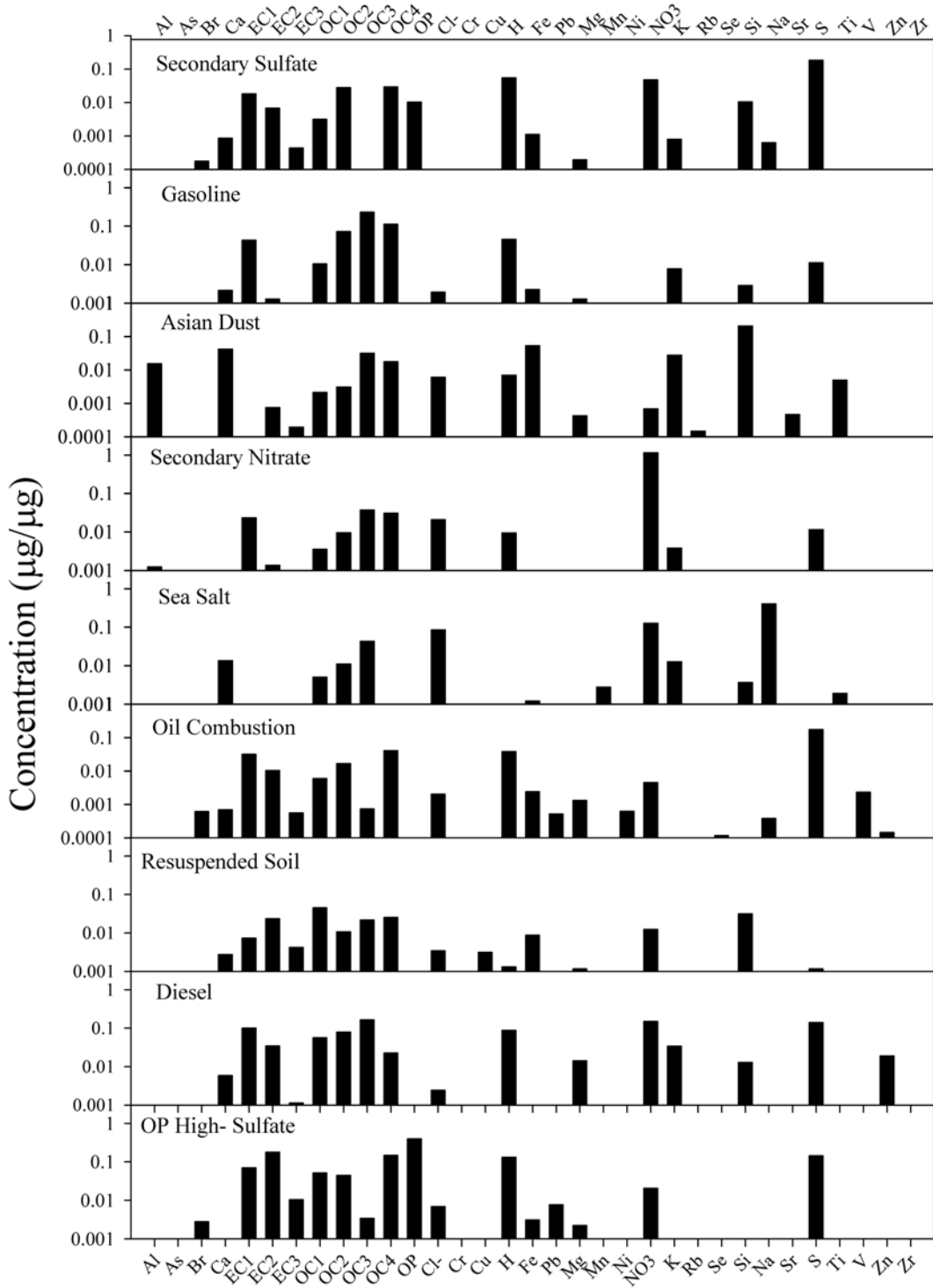


Figure 15 Source profiles of the resolved PM_{2.5} sources for the San Rafael IMPROVE site.

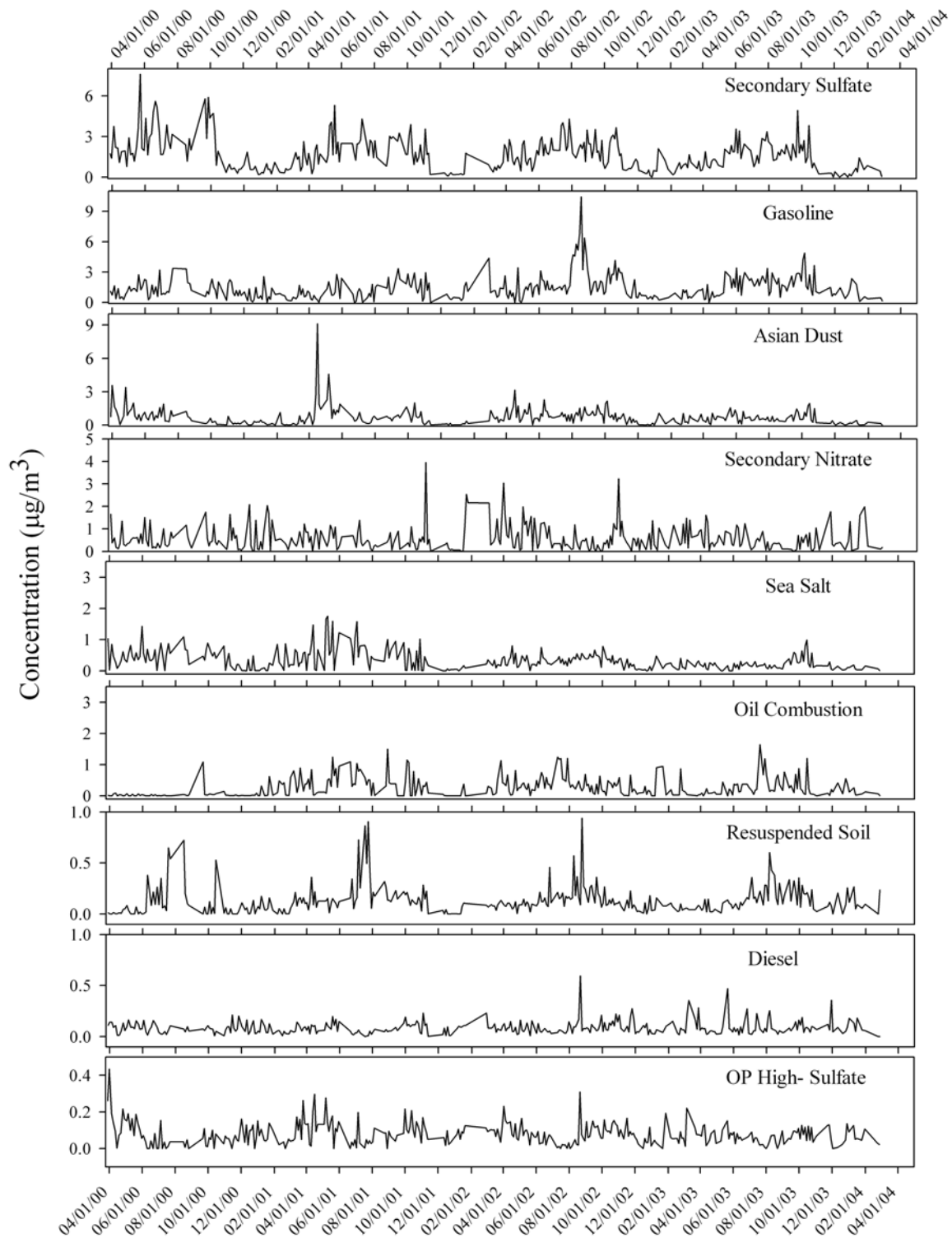


Figure 16 Time series plots of the resolved $\text{PM}_{2.5}$ source contributions for the San Rafael IMPROVE site.

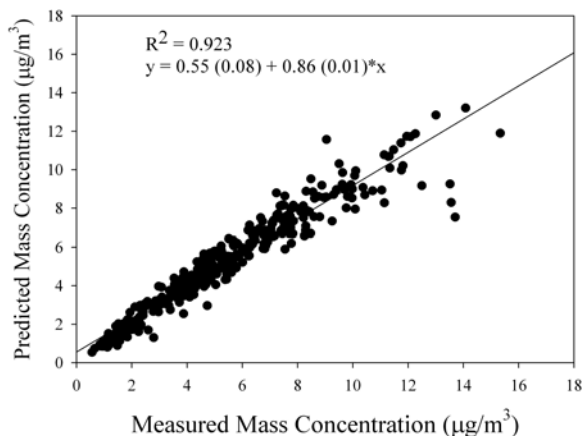


Figure 17 Predicted PM_{2.5} mass concentration versus measured PM_{2.5} mass concentration

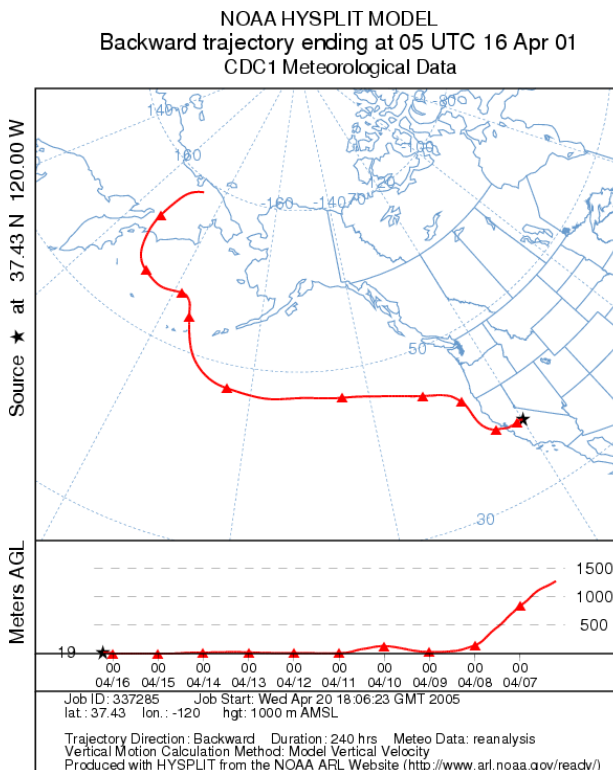


Figure 18 10 day HYSPLIT backward trajectory on 04/16/2001

The secondary sulfate source was identified due to the presence of high concentrations of sulfur with the time series plot for this source showing clear summer highs. A sea salt source was identified due to the presence of high concentrations of Na and somewhat moderate concentrations of chloride ion. However, this source also has considerable amounts of sulfur and nitrate present. This is indicative of the fact that the source is a mixture of fresh sea salt and aged sea salt. It is likely that some of the chloride in the fresh sea salt, during the course of aging, was replaced by sulfate or nitrate.

The Asian dust source was identified by the presence of crustal elements Al, Ca, Fe, K, Si, and Ti and the presence of a peak on 16 April 2001 in the time series of the source contribution. This peak corresponds to the Asian dust event identified using the HYSPLIT back trajectory model shown in Figure 18. This peak may also correspond to a major sand storm which occurred in China on 13 April 2001 (Zhao and Hopke, 2004).

A resolved source was characterized by the presence of all carbon fractions, with OP high, Fe, Mg, Pb and high concentration of S. It is not entirely clear what this source is. OP enriched sulfate sources have been reported in literature (Kim *et al.*, 2004), but it appears that some industrial source emissions may be combined with this source.

The model resolved percentage source contributions of all the sources to PM_{2.5} mass are shown in Table 6. Secondary sulfate is the highest contributor at 31.84% followed by gasoline vehicle emissions at 27.31%. The Asian dust source contributes as much as 13.22%. Considering that the site is located some distance from major cities such as Los Angeles and San Francisco, a nitrate contribution of 10.81%, although low, seems reasonable. Sea salt contributes 6.28%. Diesel emissions contribute only 1.66% to PM_{2.5} mass. Some of the diesel contributions, especially the ‘stop and go’ diesel traffic may be apportioned to the gasoline vehicle source.

Table 6. Average mass contributions of the sources of PM_{2.5} at the San Rafael IMPROVE site.

Source	Contribution (µg/m ³)
Gasoline Emissions	1.40
Residual Oil Combustion	0.26
Secondary Nitrate	0.55
Local Dust	0.12
Secondary Sulfate	1.63
Sea Salt	0.32
Diesel Emissions	0.09
Asian Dust	0.67
OP High Sulfate	0.08

PM_{2.5} speciation data for samples collected at San Rafael, CA, were analyzed. A total of nine sources were resolved. Gasoline emissions and diesel emissions were separated using the carbon fraction data. In general, gasoline appears OC enriched while diesel seems to be EC enriched. Secondary sulfate was the highest contributor to PM_{2.5} mass closely followed by gasoline emissions. It also appears that crustal material and sea salt contribute a significant fraction to PM_{2.5} mass at San Rafael.

Pinnacles National Monument

PM_{2.5} samples were collected at Pinnacles National Monument in California (Figure 19). The location of the Pinnacles National Monument site is latitude 36°29' 0" N, longitude 121° 9' 24" W. The Pinnacles site is surrounded by mountains. A total of 1634 samples were obtained from 3/2/1988 to 5/30/2004 at the Pinnacles National Monument site that were analyzed with 32 species (OC1, OC2, OC3, OC4, OP, EC1, EC2, EC3, SO₄²⁻, NO₃⁻, Al, As, Br, Ca, Cl, Cr, Cu, Fe, H, K, Mg, Mn, Na, Ni, Pb, Rb, Se, Si, Sr, Ti, V, Zn) selected for the PMF modeling. Table 7 presents the arithmetic mean, standard deviation, geometric mean, minimum and maximum values for the measured species.

The optimal solution was determined to have 7 sources with an FPEAK equal to zero. Figure 20 shows the source profiles for the 7 factor PMF solution for the Pinnacles National Monument data. Figure 21 presents temporal variations in the contribution of each source that occurred in the sampling site. Figure 22 and Table 8 show the seasonal contributions of each source at the Pinnacles National Monument site. The average source contributions for weekdays and weekend days are presented in Figure 23. The CPF plots are presented in Figure 24.



Figure 19 The location of the Pinnacles National Monument sampling site

Table 7. Summary statistics for the PM_{2.5} and species concentrations at Pinnacles National Monument.

	Arithmetic Mean	Standard Deviation	Geometric Mean	Min.	Max.	NO. of BDL (%)
PM _{2.5} *	5.58	2.94	4.83	0.50	20.13	-
OC1	109.51	127.56	59.09	1.50	1174.30	1113(68.1)
OC2	228.17	153.88	182.22	3.10	1333.30	272(16.6)
OC3	520.67	407.94	392.42	7.90	3914.40	135(8.3)
OC4	320.58	238.28	254.36	9.10	2353.40	55(3.4)
OP	146.89	128.05	97.19	2.80	926.90	480(29.4)
EC1	399.08	302.53	301.57	2.90	2657.20	54(3.3)
EC2	60.94	41.23	47.53	1.60	442.70	562(34.4)
EC3	17.09	12.34	13.17	1.50	66.70	1257(76.9)
Al	54.08	57.44	38.23	2.18	750.62	833(51.0)
As	0.51	2.38	0.30	0.05	57.11	1078(66.0)
Br	2.14	1.15	1.84	0.14	8.06	6(0.4)
Ca	29.90	23.32	23.49	1.19	369.13	12(0.7)
Cl	228.54	269.83	97.45	0.83	1649.98	1276(78.1)
Cr	0.87	0.75	0.51	0.02	3.80	1314(80.4)
Cu	0.58	0.52	0.47	0.04	8.83	351(21.5)
Fe	30.34	29.57	21.00	0.19	438.42	0(0.0)
H	203.55	115.79	174.79	28.59	898.12	1(0.1)
K	45.51	34.05	37.20	5.45	418.69	1(0.1)
Mg	52.11	38.99	39.79	2.87	296.66	1276(78.1)
Mn	1.26	0.99	0.94	0.03	10.25	911(55.8)
Na	272.18	262.65	178.56	6.99	2091.41	329(20.1)
Ni	0.45	0.55	0.32	0.04	5.48	855(52.3)
NO ₃ ⁻	841.39	768.97	605.67	1.60	9602.50	36(2.2)
Pb	1.57	1.43	1.17	0.10	19.69	98(6.0)
Rb	0.25	0.22	0.20	0.01	2.80	1232(75.4)
Se	0.36	0.21	0.30	0.03	1.64	321(19.6)
Si	96.29	101.66	66.04	2.40	1668.87	35(2.1)
Sr	0.44	0.37	0.33	0.03	4.96	613(37.5)
SO ₄ ⁻	1003.18	642.57	805.85	58.30	3978.80	65(4.0)
Ti	3.70	3.04	2.82	0.07	42.31	322(19.7)
V	1.43	1.06	1.10	0.06	8.78	925(56.6)
Zn	2.71	3.01	2.03	0.14	75.41	16(1.0)

*units are µg/m³

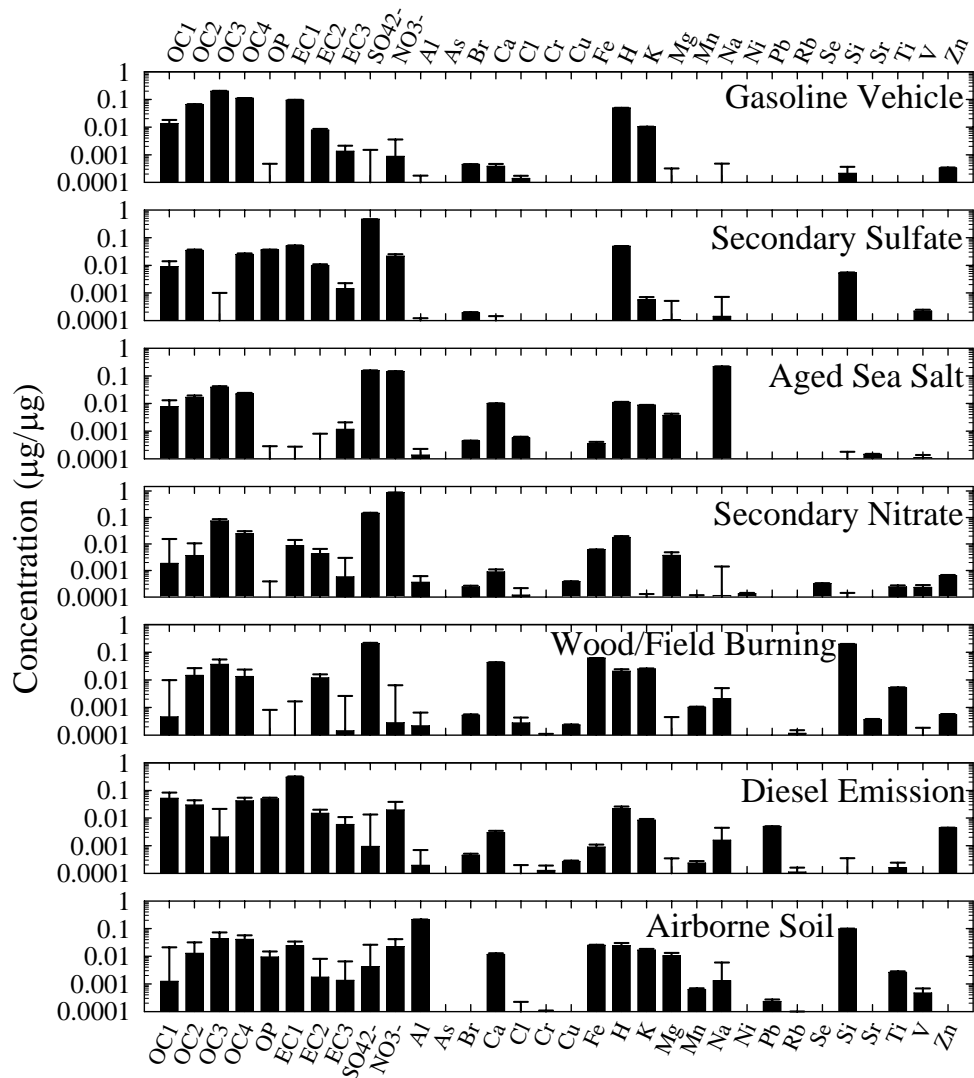


Figure 20 Profiles for the sources resolved for the Pinnacles National Monument.

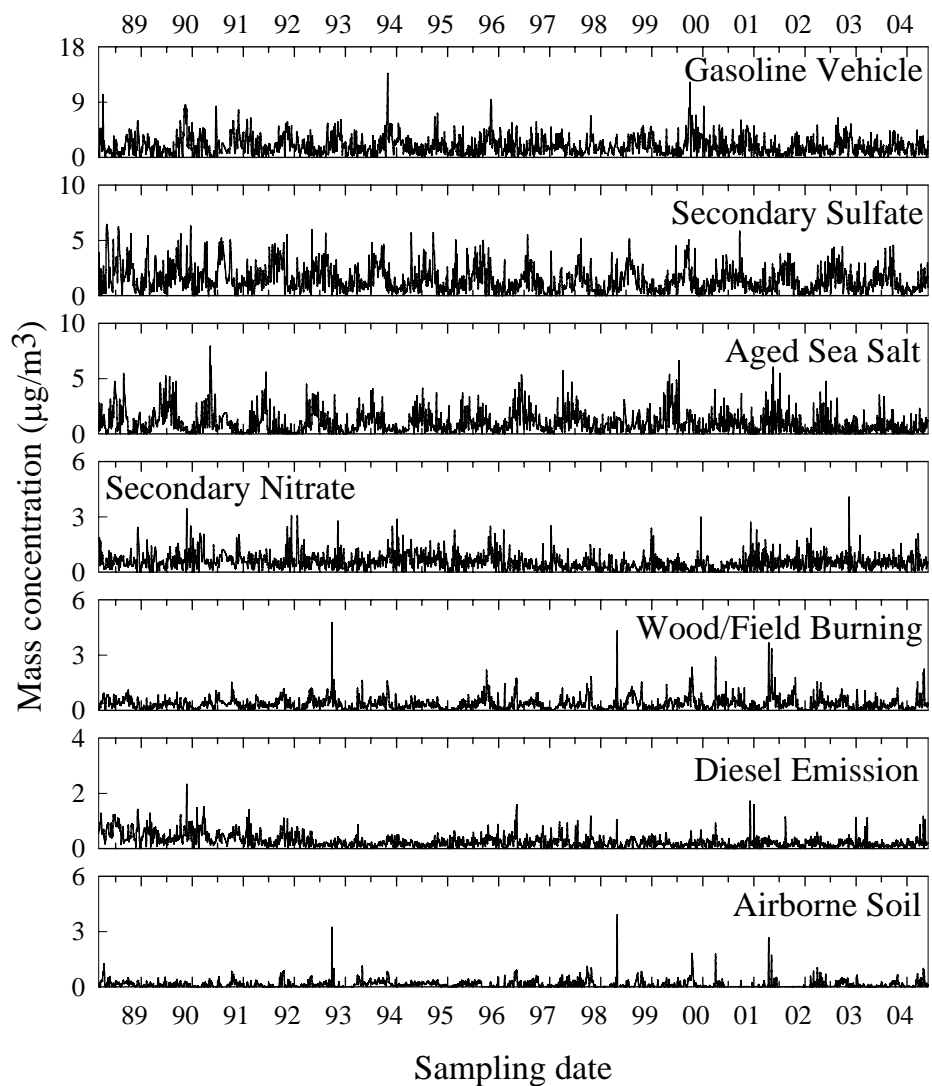


Figure 21 Time series of source contributions to the PM_{2.5} observed at the Pinnacles National Monument.

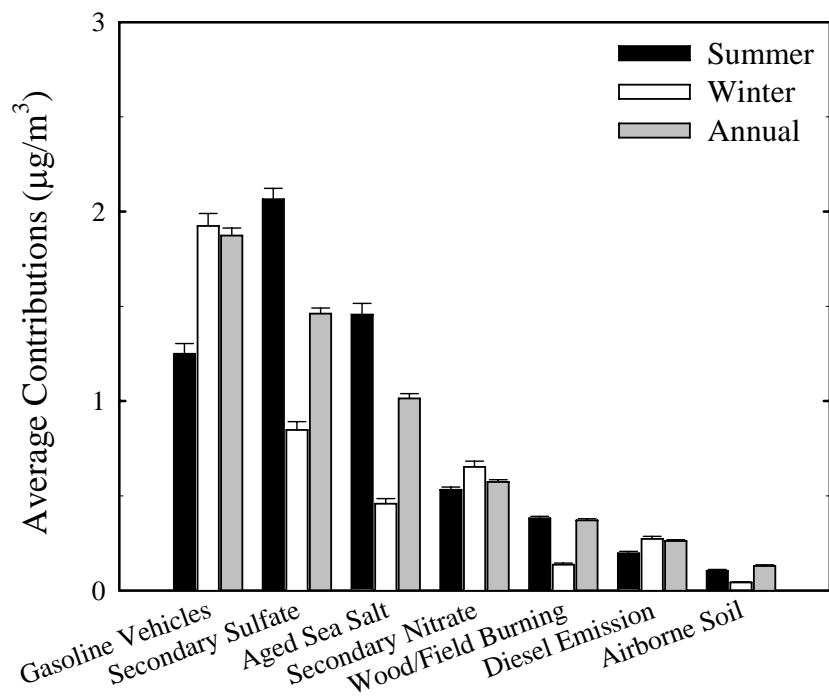


Figure 22 Comparison of seasonal (summer: June to August, winter: December to February) and overall contributions of the sources to the PM_{2.5} at the Pinnacles National Monument

Table 8. Average seasonal source contributions at the Pinnacles National Monument IMPROVE site

	Winter		Spring		Summer		Fall		AVG.	
	µg/m ³	%								
Gasoline Vehicle	1.92	44.4	1.57	28.2	1.25	20.9	2.79	41.2	1.87	33.0
Secondary Sulfate	0.85	19.6	1.24	22.2	2.06	34.5	1.68	24.8	1.46	25.7
Aged Sea Salt	0.46	10.5	1.32	23.7	1.46	24.3	0.75	11.1	1.01	17.8
Secondary Nitrate	0.65	15.1	0.53	9.5	0.53	8.9	0.59	8.7	0.57	10.1
Wood/ Field Burning	0.14	3.1	0.45	8.0	0.38	6.4	0.50	7.3	0.37	6.5
Diesel Emission	0.27	6.3	0.29	5.2	0.20	3.3	0.28	4.2	0.26	4.6
Airborne Soil	0.04	1.0	0.18	3.2	0.10	1.8	0.18	2.7	0.13	2.3
Sum	4.33	100.0	5.58	100.0	5.98	100.0	6.79	100.0	5.68	100.0

The first source was determined to be gasoline vehicle emissions. OC3, OC4, and EC1 were major species contributing to the first source along with minor species such as NO₃, Br, Ca, K, and Zn. This source was identified on the basis of high levels of OC that was higher than the EC concentration. In tailpipe emission tests, gasoline vehicle emissions included the lower temperature carbon fractions, and the diesel emissions contain large amounts of elemental carbon

(Watson et al., 1994; Kim and Hopke, 2004). For gasoline vehicle emissions, the fall contributions ($2.79 \mu\text{g}/\text{m}^3$, 41.2 %) were higher than for the other seasons (winter $1.92 \mu\text{g}/\text{m}^3$, spring $1.57 \mu\text{g}/\text{m}^3$, and summer $1.25 \mu\text{g}/\text{m}^3$). The mean weekend contribution was higher than the mean weekday contribution. This trend was attributed to an increase in visitors to this site on weekend days more than on weekdays.

The major marker species contributing to the second and fourth source profiles are SO_4^- and NO_3^- . These factors were classified as secondary sulfate and secondary nitrate. The mean seasonal mass contributions for secondary nitrate were: winter (15.1 %, $0.65 \mu\text{g}/\text{m}^3$), fall (8.7 %, $0.59 \mu\text{g}/\text{m}^3$), spring (9.4 %, $0.53 \mu\text{g}/\text{m}^3$), and summer (8.9 %, $0.53 \mu\text{g}/\text{m}^3$), showing the expected winter peak. The seasonal variation in secondary sulfate were; summer (34.5 %, $2.06 \mu\text{g}/\text{m}^3$), fall (24.8 %, $1.68 \mu\text{g}/\text{m}^3$), spring (22.2 %, $1.24 \mu\text{g}/\text{m}^3$), and winter (19.6 %, $0.85 \mu\text{g}/\text{m}^3$), showing the peak in summer. This result corresponds with the maximum in photochemical activity during the summer. Secondary sulfate and nitrate were not significantly different between weekdays and weekends. The CPF plots indicated secondary nitrate coming from the northeast and east and secondary sulfate was highest with winds from the northwest, west, and southwest.

The species contributing to the third source mainly included Na, SO_4^{2-} , NO_3^- , Ca, K, and Mg. This profile was identified as aged sea salt. Among the main sea salt species, Na^+ , Cl, SO_4^{2-} , K, and Ca (Hopke, 1985), only Na^+ showed a high concentration. Cl was depleted and replaced by SO_4^- and NO_3^- . Aged sea salt showed moderate to high contributions in all seasons compared with other source contributions (winter $0.46 \mu\text{g}/\text{m}^3$, spring $1.32 \mu\text{g}/\text{m}^3$, summer $1.46 \mu\text{g}/\text{m}^3$, and fall $0.75 \mu\text{g}/\text{m}^3$, respectively). Aged sea salt source was not significantly different between weekdays ($0.97 \mu\text{g}/\text{m}^3$) versus weekends ($1.07 \mu\text{g}/\text{m}^3$). The CPF plot indicated that the aged sea salt originated to the southwest.

The fifth source was assigned to wood/field burning. The species in this profile included OC (OC2 to OC 4), EC2, SO_4^- , Ca, Fe, K, and Si. The mean seasonal mass contributions of wood/field burning were: fall (7.3 %, $0.50 \mu\text{g}/\text{m}^3$), spring (8.0 %, $0.45 \mu\text{g}/\text{m}^3$), summer (6.4 %, $0.38 \mu\text{g}/\text{m}^3$), and winter (3.1 %, $0.14 \mu\text{g}/\text{m}^3$). Wood/field burning showed no significant differences between the contributions on weekdays ($0.38 \mu\text{g}/\text{m}^3$) versus weekends ($0.35 \mu\text{g}/\text{m}^3$) (Figure 23).

The species contributing to the sixth source included EC1, EC2, EC3, OC1, OC2, OC4, OP, NO_3^- , K, Pb, and Zn. The sixth factor at Pinnacles was identified as diesel vehicle emissions. The mean seasonal mass contributions for diesel emissions were: spring (5.2 %, $0.29 \mu\text{g}/\text{m}^3$), fall (4.2 %, $0.28 \mu\text{g}/\text{m}^3$), winter (6.3 %, $0.27 \mu\text{g}/\text{m}^3$), and summer (3.3 %, $0.20 \mu\text{g}/\text{m}^3$). The mean weekend contributions

of diesel emissions were slightly higher than the weekday contribution and may reflect some off-road 2-stroke vehicle emissions. The CPF plot indicates this source is to the east of the sampling site as shown in Figure 24. Since the major highway is located to the east of sampling site, this result supports the assignment of this factor to diesel emissions.

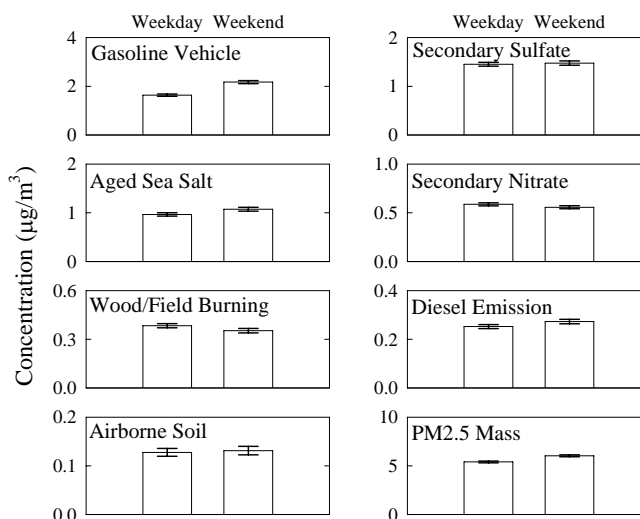


Figure 23 Average source contributions for weekdays and weekends at the Pinnacles National Monument.

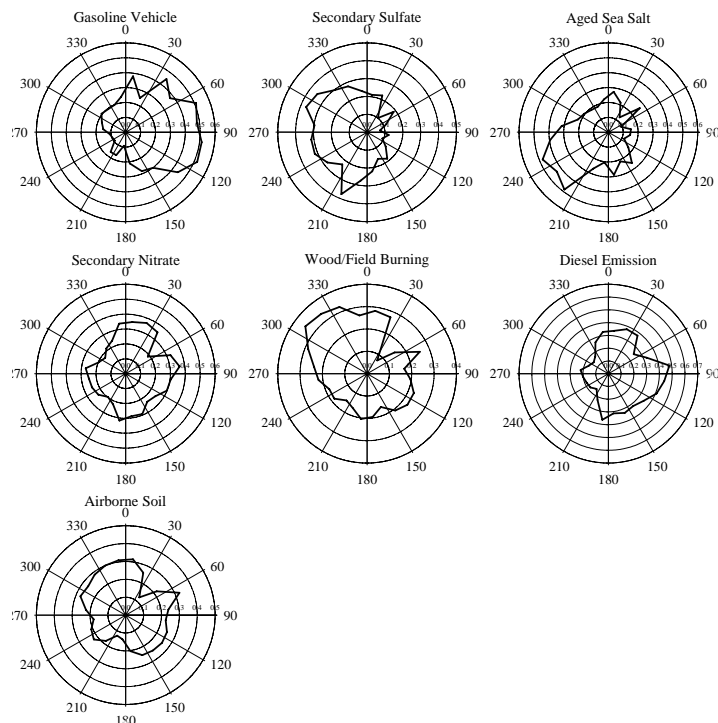


Figure 24. Conditional Probability Function (CPF) results based on source contributions obtained by the PMF analysis of the data from the Pinnacles site.

Finally, the major species contributing to the seventh source included Al, Si, Fe, Ca, K, Mg and Ti. These species were classified as the airborne soil. The seasonal mean mass contributions for airborne soil were: spring (3.2 %, 0.18 $\mu\text{g}/\text{m}^3$), fall (2.7 %, 0.18 $\mu\text{g}/\text{m}^3$), summer (1.8 %, 0.10 $\mu\text{g}/\text{m}^3$), and winter (1.0 %, 0.04 $\mu\text{g}/\text{m}^3$). The temporal variation of source contribution plot shows very strong contributions in March 1998 (3.91 $\mu\text{g}/\text{m}^3$), September 1992 (3.23 $\mu\text{g}/\text{m}^3$), and April 2001 (2.65 $\mu\text{g}/\text{m}^3$), respectively. These high values were attributed to high contributions of soil from the long range transport of dust from China during Asian dust storms (Figure 25). The relatively high fall concentration may arise from the Santa Ana winds from the east that are typical of the fall. The soil source contribution was marginally higher on weekends than on weekdays possibly reflecting the increased level of visitors on the weekends producing increased road dust.

Table 8 presents the average contribution of all the sources identified during the sampling period. The average concentration of $\text{PM}_{2.5}$ for all the sources observed during the period was 5.58 $\mu\text{g}/\text{m}^3$, whereas

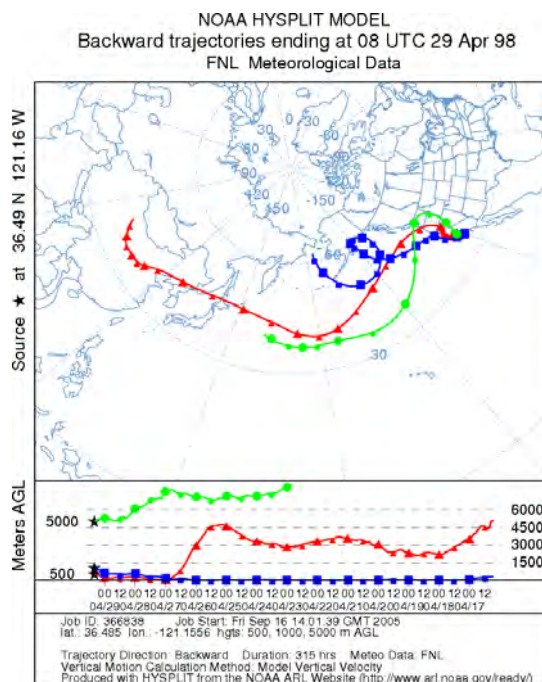


Figure 25. HYSPLIT back trajectories calculated for April 24, 1998.

the concentration calculated through the PMF modeling was $5.68 \mu\text{g}/\text{m}^3$. The contribution of gasoline vehicle emissions was 33.0 % ($1.87 \mu\text{g}/\text{m}^3$). This source had the greatest effect on the local ambient air quality, followed by secondary sulfate (25.7 %, $1.46 \mu\text{g}/\text{m}^3$), aged sea salt (17.8 %, $1.01 \mu\text{g}/\text{m}^3$), secondary nitrate (10.1 %, $0.57 \mu\text{g}/\text{m}^3$), wood/field burning (6.5 %, $0.37 \mu\text{g}/\text{m}^3$), diesel emissions (4.6 %, $0.26 \mu\text{g}/\text{m}^3$), and the airborne soil (2.3%, $0.13 \mu\text{g}/\text{m}^3$), respectively.

In Figure 28, a comparison of the predicted $\text{PM}_{2.5}$ contributions from all sources with measured $\text{PM}_{2.5}$ concentrations shows that the PMF resolved sources effectively reproduce the measured values and account for most of the variation in the $\text{PM}_{2.5}$ concentrations ($R^2 = 0.904$) and a slope of 0.8752.

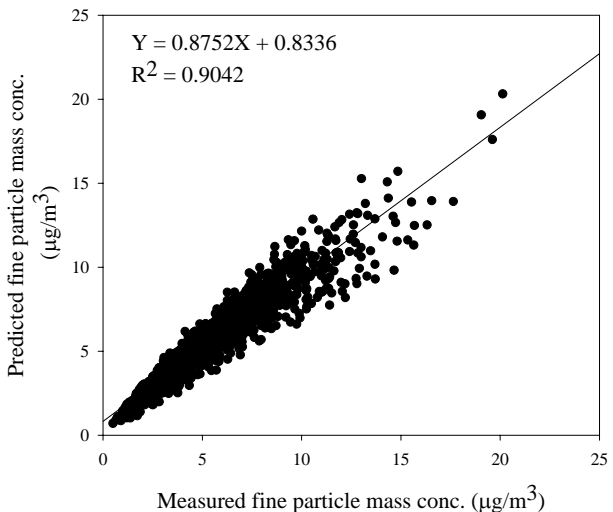


Figure 26 Comparison of the predicted total $\text{PM}_{2.5}$ mass concentrations with the $\text{PM}_{2.5}$ concentrations measured at the Pinnacles National Monument.

Yosemite National Park

$\text{PM}_{2.5}$ samples collected Wednesdays and Saturdays (Jan. 1989 - Aug. 2000) and on every third day (Sep. 2000 - May 2004) at the IMPROVE monitoring site located in the Yosemite National Park, CA were analyzed in this study (latitude: $37^\circ 42' 48'' \text{N}$; longitude: $119^\circ 42' 22'' \text{W}$; elevation: 1600 m). As shown in Figure 27, the monitoring site is located at Turtleback Dome about 1.7 km west of Tunnel View. It is 250 km east of San Francisco, and 210 km southeast of Sacramento. Highways 41 and 140 are closely situated to the west and north of the site. Wind data measured at the site were used in this study.

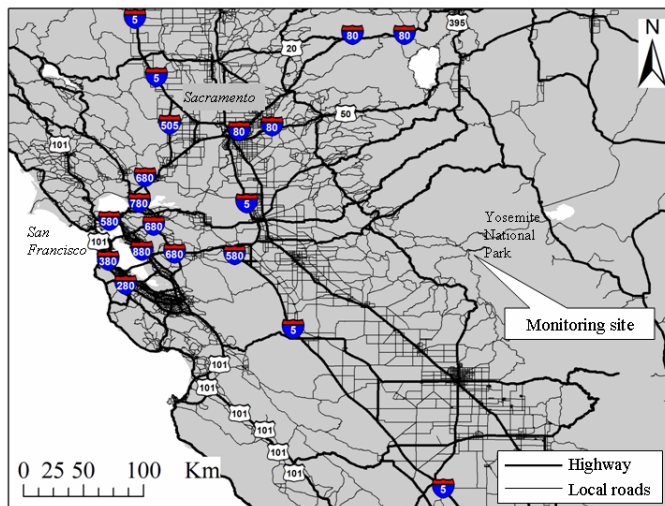


Figure 27 Location of the IMPROVE monitoring sites at the Yosemite National Park, CA.

Samples for which $\text{PM}_{2.5}$ were not available or below aero, or for which $\text{PM}_{2.5}$ had error flag were excluded from data set.

Samples for which eight carbon fractions were not available were also excluded. Overall, 21.9 % of the original data were not included in this study. SO_4^{2-} was not included and only S was used in this study because they showed good correlations ($slope = 3.0 \pm 0.02$, $r^2 = 0.97$). The reported EC1 concentration in IMPROVE/TOR method includes the OP concentration. In this study, the OP was subtracted from EC1 and utilized as an independent variable. Chemical species that have missing values more than 80 % or below MDL values more than 90 % were excluded. The chemical species that have S/N ratio below 0.2 (defined as bad variables) were not included in this study. A total of 1308 samples collected between March 1988 and May 2004 and 33 species including $\text{PM}_{2.5}$ were used in this study. Table 9 provides a summary of

PM_{2.5} species analyzed in this study. The estimated uncertainties of species that have *S/N* ratio between 0.2 and 2 (weak variable) and species that have below MDL values more than 50 % were increased by a factor of five and a factor of three, respectively, to reduce their weight in the solution. In addition, to obtain physically reasonable PMF solution, it was found necessary to increase three times the estimated uncertainties of Pb and Zn. The estimated uncertainties of OC1 were increased by a factor of three to reduce the influence of the positive artifact from the adsorption of gaseous OC. The estimated uncertainties of EC1 were increased by a factor of three to account for the additional uncertainty from the subtraction of OP. Table 9 provides a summary of PM_{2.5} speciation data and *S/N* ratios

A seven-source model with FPEAK = - 0.1 and a FKEY matrix provided the most interpretable solution. For the FKEY matrix, values of all elements were set to zero, except for a value of 6 for NO₃⁻ in secondary nitrate and a value of 7 for Na in OP-high source.

Comparisons of the daily reconstructed PM_{2.5} mass contributions from all sources with measured PM_{2.5} mass concentrations shows that the resolved sources effectively reproduce the measured values and account for most of the variation in the PM_{2.5} mass concentrations in Figure 28 (*slope* = 0.81 ± 0.01 and *r*² = 0.92). The averaged seasonal contributions are compared (summer: April - September; winter: October - March) in Figure 29. Source profiles, source contributions, weekday/weekend variations, and CPF plots are presented in Figures 30, 31, 32, and 33. The average mass contributions for the identified sources is presented in Table 10

Wood smoke is characterized by large amount of higher temperature carbon fractions, especially OC3 and OC4, and K. It contributed the most mass accounting for 27% of the PM_{2.5} mass concentration. Wood smoke has a strong summer-high seasonal trend, especially August and September and suggesting that there are wildfires in the dry summer as major sources of wood smoke in this area. There are no weekday/weekend variations in the wood smoke contributions. The CPF plot for wood smoke points to the northwest, northeast and southwest as major source directions.

Secondary sulfate has a high concentration of S and NH₄⁺ accounts for 22% of the PM_{2.5} mass concentration. As shown in Figure 29, the secondary sulfate shows a strong seasonal variation with higher concentrations in summer when the photochemical activity is highest.

Airborne soil is represented by Si, Fe, Al and Ca contributing 18% to the PM_{2.5} mass concentration. Crustal particles could be contributed by wind-blown soil dust and re-suspended by road traffic. Airborne soil shows strong summer-high seasonal variation. In Figure 31, the elevated airborne soil contributions in April (April 16, 1994, April 1, 2000, April 16, 2001, April 23, 2002) indicated that the high airborne soil contributions in this area were likely caused by Asian dust storm. It does not show a weekday/weekend variation. The CPF plot of airborne soil points to the northeast and southwest.

Aged sea salt is characterized by its high concentration of S, NO₃⁻, and Na⁺. The lack of Cl⁻ in the profile is caused by Cl⁻ displacement by acidic gases. Aged sea salt accounts for 16% of the PM_{2.5} concentrations. It shows a strong summer-high seasonal pattern. Aged sea salt does not show a weekday/weekend variation. The CPF plot points to the north and southwest as major source directions.

Table 9. Summary of PM_{2.5} species mass concentrations at the Yosemite National Park, CA.

Species	Arithmetic mean (µg/m ³)	Geometric mean (µg/m ³)	Minimum (µg/m ³)	Maximum (µg/m ³)	Number of below MDL values (%)	S/N ratio
PM _{2.5}	4.5566	3.3221	0.0600	20.1040	0.8	1741.3
OC1	0.1426	0.0832	0.0014	2.5040	63.3	1.7
OC2	0.2549	0.1618	0.0015	3.2554	24.5	9.6
OC3	0.5461	0.3448	0.0030	4.4032	12.4	38.0
OC4	0.2945	0.1899	0.0039	3.1410	7.4	87.7
OP	0.2064	0.1460	0.0028	2.0863	8.9	48.6
EC1	0.1505	0.0946	0.0027	1.1134	25.6	11.4
EC2	0.0703	0.0554	0.0016	0.2600	19.7	8.5
EC3	0.0164	0.0129	0.0015	0.1524	70.2	0.6
Al	0.0676	0.0495	0.0028	0.5470	34.9	34.7
As	0.0003	0.0002	0.0000	0.0016	59.4	1.7
Br	0.0016	0.0013	0.0001	0.0060	0.6	3870.4
Ca	0.0282	0.0190	0.0008	0.3915	1.3	2365.0
Cl-	0.0363	0.0228	0.0001	0.4579	78.1	0.2
Cr	0.0010	0.0006	0.0000	0.0045	68.9	0.7
Cu	0.0006	0.0004	0.0000	0.0056	21.3	25.0
Fe	0.0343	0.0205	0.0003	0.3430	0.1	304443.0
H	0.2008	0.1520	0.0156	1.1734	0	NA ¹
K	0.0377	0.0275	0.0014	0.2071	1.0	3254.7
Mg	0.0316	0.0222	0.0018	0.1664	81.2	0.8
Mn	0.0014	0.0010	0.0000	0.0079	44.3	2.8
Na	0.1075	0.0740	0.0036	0.7188	43.7	5.3
Ni	0.0002	0.0001	0.0000	0.0016	73.5	0.7
NO ₃ ⁻	0.3406	0.1902	0.0013	4.0203	5.5	234.8
Pb	0.0009	0.0007	0.0001	0.0064	7.4	83.7
Rb	0.0002	0.0002	0.0000	0.0012	49.5	1.5
Se	0.0002	0.0002	0.0000	0.0007	36.4	5.6
Si	0.1196	0.0808	0.0014	1.1163	1.8	2717.6
Sr	0.0004	0.0003	0.0000	0.0032	29.5	5.6
S	0.2418	0.1740	0.0055	0.9643	0	NA ¹
Ti	0.0047	0.0035	0.0000	0.0273	13.9	25.6
V	0.0012	0.0008	0.0000	0.0088	58.9	1.0
Zn	0.0018	0.0014	0.0001	0.0193	0.8	2965.2

¹ not available(infinite S/N ratio caused by no below MDL value)

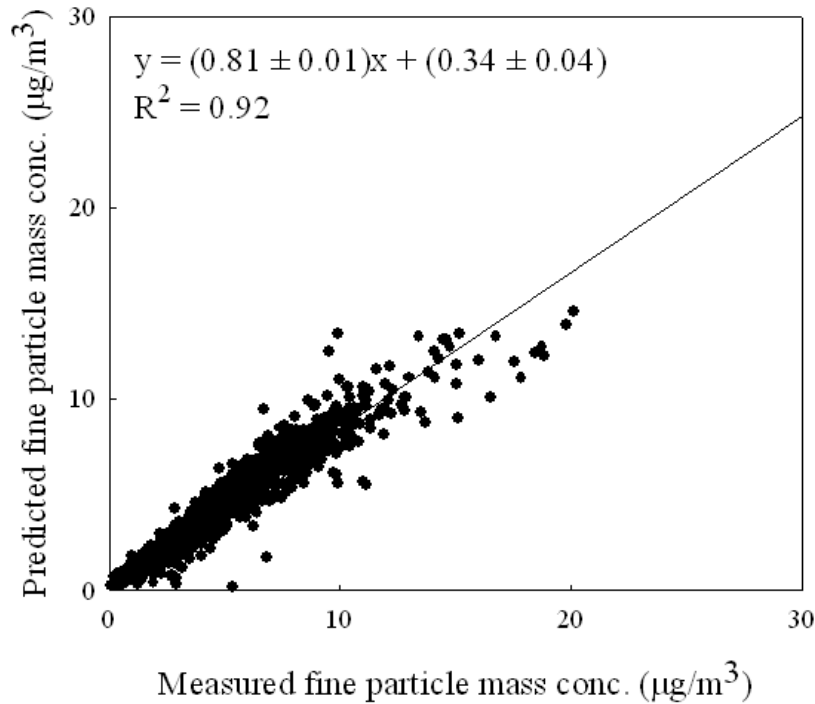


Figure 28 Measured versus PMF predicted $PM_{2.5}$ mass concentrations at the Yosemite National Park.

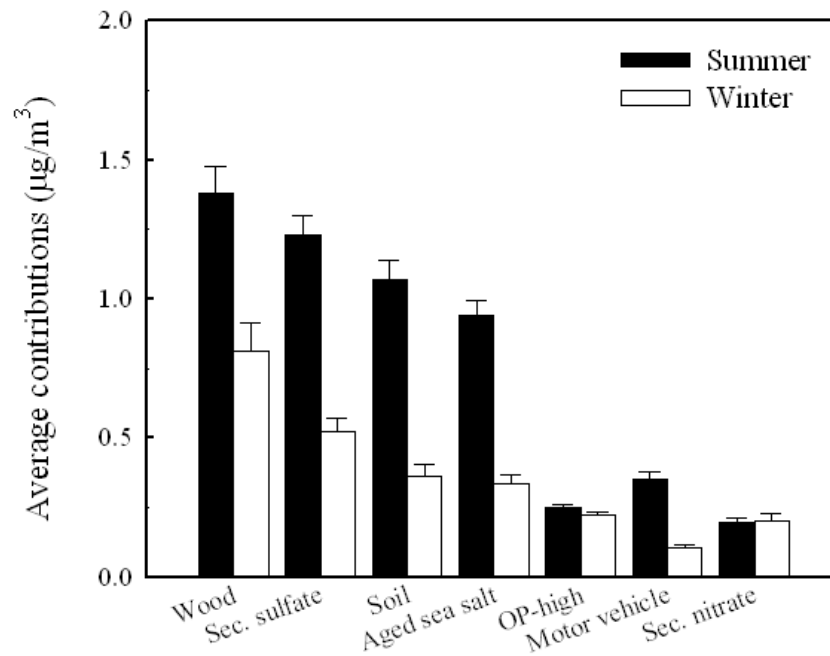


Figure 29 The seasonal comparison of source contributions to $PM_{2.5}$ mass concentration at the Yosemite National Park (mean \pm 95 % distribution).

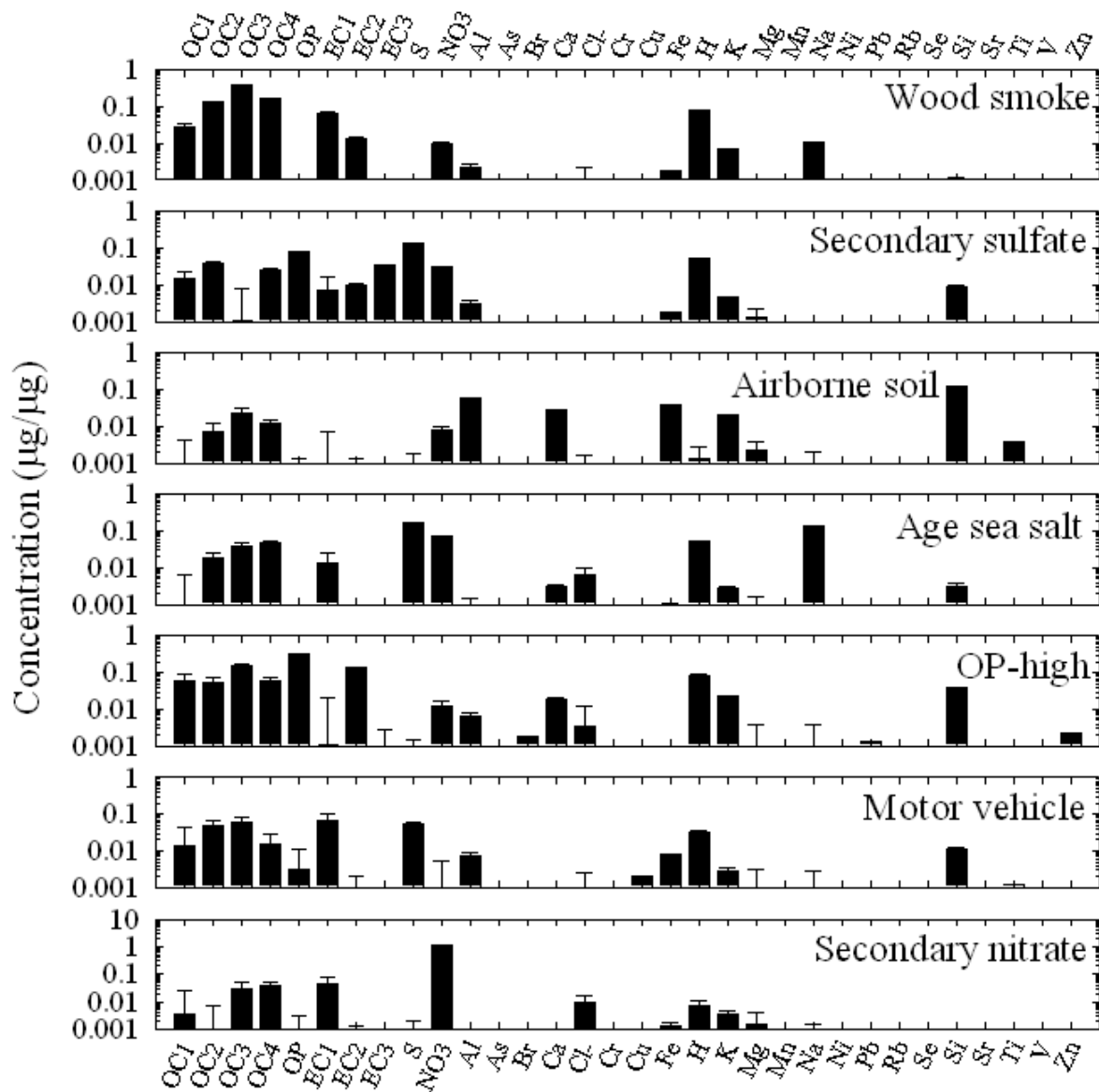


Figure 30 Source profiles deduced from PM_{2.5} samples measured at the Yosemite National Park (prediction ± standard deviation).

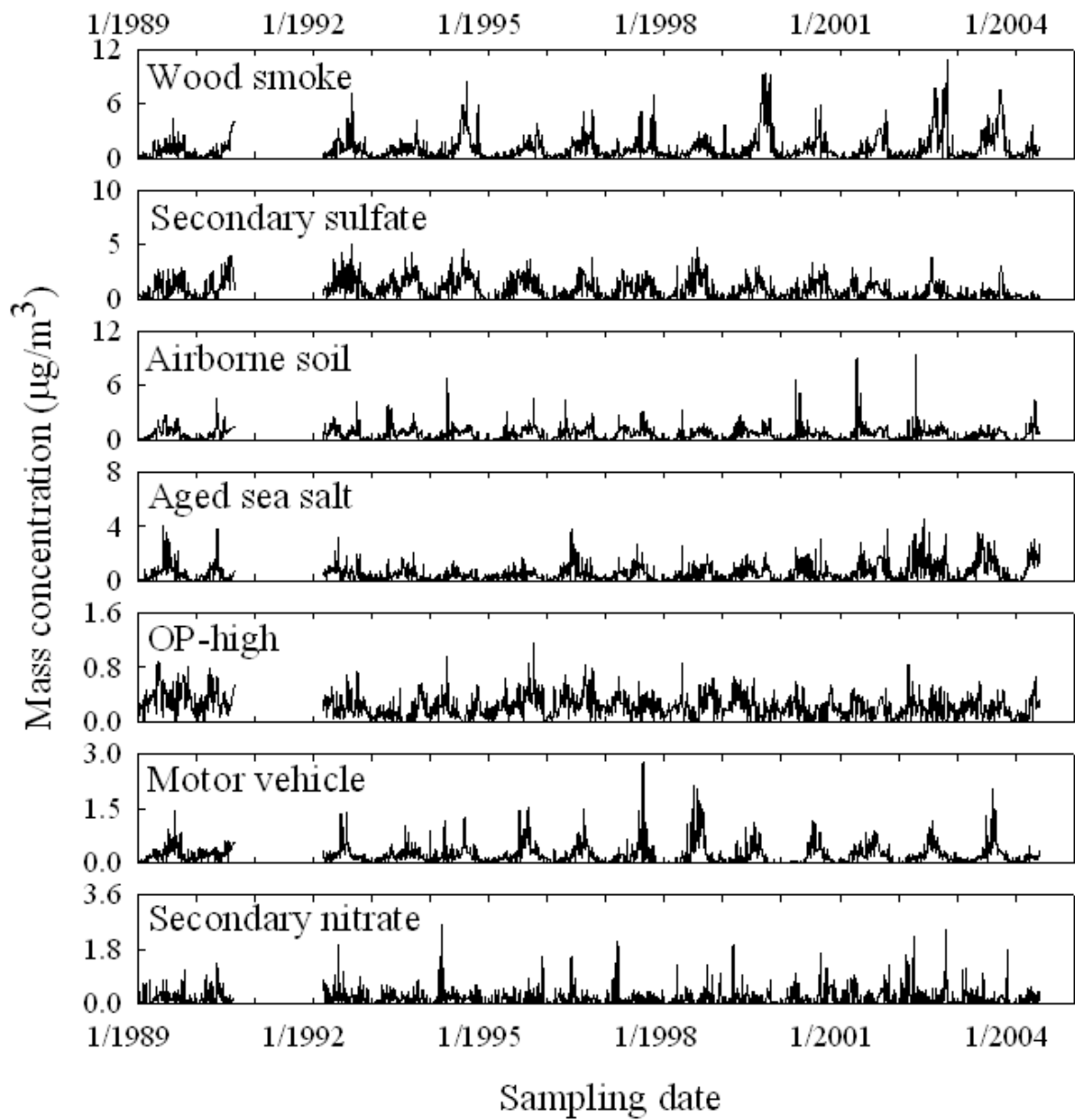


Figure 31 Time series plot of source contributions at the Yosemite National Park.

The OP-high source with large amount of lower temperature carbon fractions (OC2, OP, EC1), K, and Si was extracted in this study. It is likely to include contributions from both primary and secondary particles, i.e. secondary organic aerosol, wood smoke, and crustal materials. The detailed nature of this source are uncertain and need more investigation. It contributed 6% of the PM_{2.5} mass concentrations. It does not show a clear seasonal variation, a weekday/weekend variation, or directionality as shown in Figures 29, 32, and 33.

Motor vehicle emissions were identified by higher concentrations of OC and EC (Watson et al., 1994). It contributed 6% of the PM_{2.5} mass concentrations. In Figure 29, motor vehicle emissions show string summer-high seasonal variation. It does not show a weekday/weekend variation. The CPF plot shows the major contributions from northeast, northwest, and southeast.

Secondary nitrate is represented by its high concentration of NO₃⁻ and NH₄⁺. It accounts for 5% of the PM_{2.5} mass concentration. It does not show a seasonal variation, weekday/weekend variation, or source directions as shown in Figures 29, 32, and 33.

Table 10. Average source contributions (µg/m³) to PM_{2.5} mass concentration at the Yosemite National Park, CA.

Sources	Average source contribution (µg/m ³)	% Contribution
Wood smoke	1.11 (27.3)	27.3
Secondary sulfate	0.89 (22.0)	22.0
Airborne soil	0.73 (18.1)	18.1
Aged sea salt	0.65 (16.1)	16.1
OP-high	0.23 (5.8)	5.8
Motor vehicle	0.23 (5.8)	5.8
Secondary nitrate	0.20 (4.9)	4.9

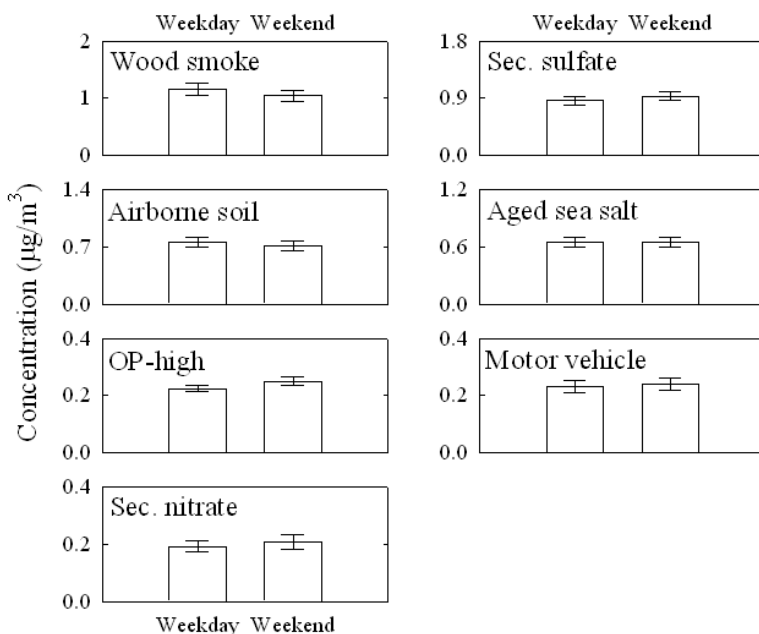


Figure 32 Weekday/weekend variations at the Yosemite National Park (mean ± 95% distribution).

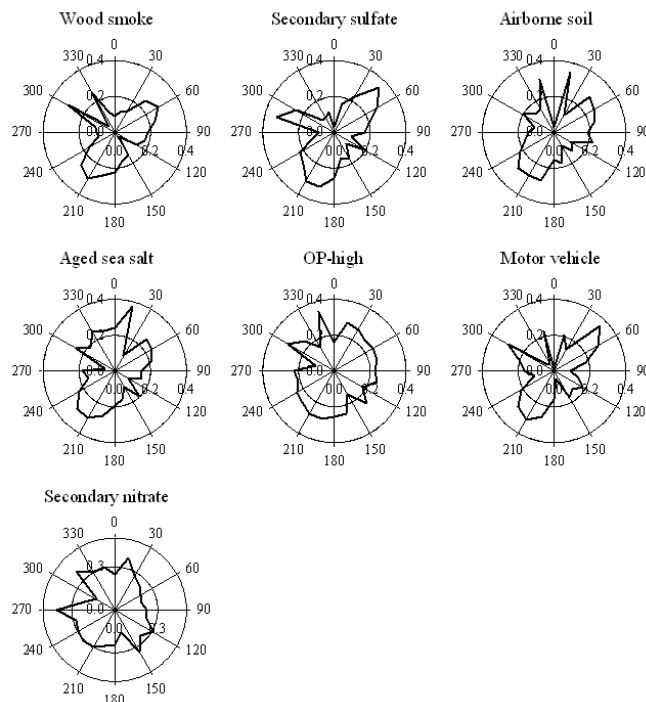


Figure 33 CPF plots for the highest 25% of the mass contributions at the Yosemite National Park.

Point Reyes National Seashore

Point Reyes National Seashore is located to the northwest of San Francisco. The sampling site is at latitude $38^{\circ} 7' 21''$ N and longitude $122^{\circ} 54' 31''$ W. The location is shown in Figure 34. Samples collected from January 1, 2000 to February 27, 2004 were used in this study. The data were pre-treated to remove variables that would otherwise distort the analysis. Consequently, several species were discarded from the analysis. These species, together with the reasons for discarding them, are listed in Table 11. In addition, the Cl^- ion, SO_4^{2-} showed strong correlations with Cl and S, respectively. As a result, the Cl and SO_4^{2-} values were also excluded from the analysis. Na exhibited an unusual time series that suggested high analytical uncertainty. Thus, Na was also omitted from this analysis. A total of 496 samples were used in this analysis. The final species used in this study are summarized in Table 12.

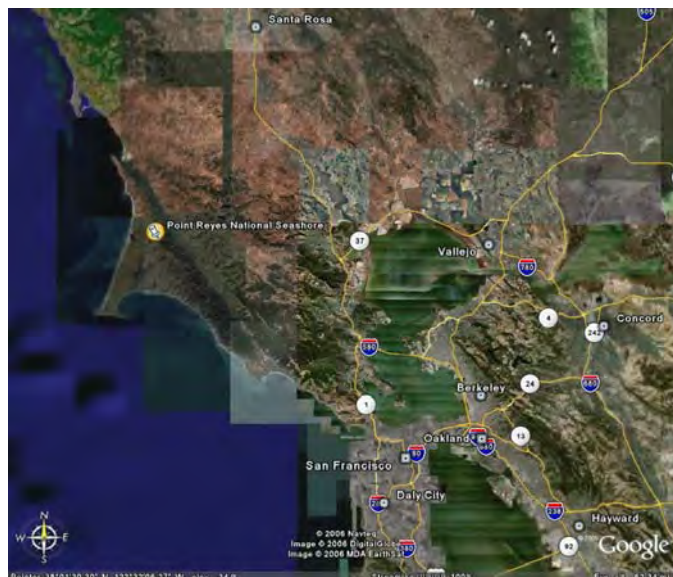


Figure 34 View of the area surrounding the Point Reyes National Seashore IMPROVE site.

The method of G Space plotting described by Paatero *et al* (2005) was used to check for rotational ambiguity of the obtained solutions. The rotational parameter, FPEAK (Paatero *et al.*,

2002) was set to 0.0 because it gave the most interpretable eight-factor solution.

Table 11. List of excluded species for the data from Point Reyes National Seashore.

Species Discarded	# Missing	% Missing	# BDL	% BDL	(S/N) _j ratio	Main reason for discarding
NH ₄	390	78.6	106	21.4	N/A ⁽¹⁾	Species consists entirely of Missing or BDL values
EC3	61	12.3	414	83.5	4.12	Species consists entirely of BDL values
Mo	496	100.0	0	0.0	N/A	Species consists entirely of Missing values
Mg	74	14.9	318	64.1	5.18	Species consists mainly of BDL values
NO ₂	66	13.3	334	67.3	1.96	High% of BDL values; S/N < 2 (~weak variable)
P	74	14.9	406	81.9	12.01	Species consists mostly of Missing or BDL values
SO ₂	496	100.0	0	0.0	N/A	Species consists entirely of Missing values
Zr	74	14.9	373	75.2	2.04	Species consists mostly of Missing or BDL values; S/N = 2 (~weak variable)

An eight-factor model was found to provide the most physically interpretable solution as well as satisfy the source apportionment conditions. The pollution sources were identified through (1) correlation of the PMF-resolved source contributions with all the chemical species, (2) observation of the relative abundance of each species in the source profiles, (3) observation of the time series plots to determine the locations of concentration peaks, if any, and calculating air parcel back trajectories ending at the times of those peaks, and (4) qualitative estimation of the location of the sources using a probability distribution function. The eight sources were identified as: wood burning, fresh sea salt, aged sea salt, Asian dust, secondary nitrate, oil combustion, gasoline traffic, and diesel traffic.

Table 12. Summary statistics for the species used in this study of Point Reyes National Seashore ($\mu\text{g}/\text{m}^3$)

Species	Number of samples	Minimum	Maximum	Arithmetic mean	Arithmetic Std Deviation	Geometric Mean
PM _{2.5}	496	0.8239	27.6913	6.3436	3.9198	5.3165
OC1	496	0.0014	0.4344	0.0465	0.0583	0.0298
OC2	496	0.0015	1.3495	0.1061	0.1431	0.0592
OC3	496	0.0015	4.9718	0.3415	0.4868	0.1731
OC4	496	0.0090	2.5837	0.2173	0.2628	0.1404
OP	496	0.00065	0.64260	0.03661	0.05206	0.01861
EC1	496	0.0030	1.1987	0.0989	0.1384	0.0536
EC2	496	0.0028	0.1148	0.0202	0.0161	0.0153
Al	496	0.00103	0.42069	0.01079	0.03614	0.00399
As	496	0.00001	0.00104	0.00012	0.00015	0.00007
Br	496	0.00010	0.01893	0.00315	0.00225	0.00241
Ca	496	0.00043	0.22811	0.03781	0.03033	0.02752
Cl ⁻	496	0.0052	7.7361	1.1429	1.1993	0.5718
Cr	496	0.00001	0.37143	0.00117	0.01668	0.00014
Cu	496	0.00001	0.00322	0.00020	0.00035	0.00008
H	496	0.02768	0.91065	0.14963	0.11935	0.12242
Fe	496	0.0005	0.2924	0.0168	0.0304	0.0084
Pb	496	0.000015	0.006520	0.000494	0.000606	0.000264
Mn	496	0.000010	0.007090	0.000666	0.001008	0.000291
Ni	496	0.000015	0.002800	0.000405	0.000413	0.000229
NO ₃ ⁻	496	0.0076	22.9479	0.8684	1.7812	0.4423
K	496	0.00159	0.16901	0.04137	0.02811	0.03296
Se	496	0.00001	0.00143	0.00029	0.00023	0.00020
Si	496	0.00042	0.95305	0.04785	0.09419	0.01976
Sr	496	0.000025	0.003870	0.000681	0.000583	0.000449
S	496	0.0011	1.0127	0.3559	0.2016	0.2942
Ti	496	0.000015	0.027660	0.001652	0.002748	0.000750
V	496	0.00001	0.01000	0.00187	0.00187	0.00105
Zn	496	0.00002	0.04538	0.00162	0.00259	0.00095

Factor 1 correlates very strongly with Cl^- ($r = 0.97$), Sr ($r = 0.84$), Br ($r = 0.81$), Ca ($r = 0.74$), and is moderately correlated with K ($r = 0.54$). This factor can reasonably be interpreted as fresh sea salt emissions. The CPF plot indicates dominating directions pointing toward the Pacific Ocean (southwards). This directionality illustrates the strong dependence of this factor on the wind profile. It probably results from the sea breeze effect in which the temperature differential between sea and land leads to an on-shore breeze during the day and an off-shore breeze at night. Factor 2 where the latter has a strong correlation with S ($r = 0.88$). Thus, Factor 2 is identified as secondary sulfate. The CPF plot for Factor 2 points toward the ocean in an area where ships are converging as they move toward the entrance to San Francisco Bay..

The secondary nitrate source exhibits a diurnal pattern with high peaks in the colder months (January - March). This source shows a high positive correlation with NO_3^- ($r = 0.98$), EC1 ($r = 0.80$), and H ($r = 0.75$). It therefore seems reasonable to refer to this source as a secondary nitrate source. EC1 may be providing an active surface on which the nitrate particles nucleate. The CPF analysis suggests that this source is mainly associated with emissions from the eastern/northeastern directions of the site. This directionality might represent transport and processing of NO_x emissions from the several power plants and highways in these directions of the site.

Factor 4 has high positive correlations with EC, OC and H with the OC2, OC3, and OC4 fractions giving the highest correlations ($r = 0.89, 0.92, 0.92$, respectively). Using dynamometer tests, Watson et al (1994) reported high emissions of OC4 by gasoline vehicles (at least twice as much). The EC1 fraction was also reported to be generally more abundant in gasoline emissions than in diesel emissions. The presence of Si in the source profile and the moderate correlation with As suggests that it might be reasonable to report this factor as indicative of gasoline traffic emissions in which the As and Si are a result of re-suspended dust from traffic.

An oil combustion source was identified by the presence of Ni and V , species that have previously been associated with oil combustion (Lee et al, 1999). The CPF plot points to the SW suggesting ship impacts coming from vessels approaching the entrance to San Francisco Bay. There is a smaller probability to the southeast, potentially from ships already in the Bay. The origin of the small lobe to the NE is unknown.

Factor 6 does not have significant correlations with any specific chemical species used in this study. However, the presence of combustion species such as Pb , K , S , NO_3^- , EC and OC as well as Pb , S , and NO_3^- in the source profile (Figure 35) suggests that this source could reasonably be interpreted as a wood combustion or waste burning source. The source contribution series for this factor shows a sharp peak between 11th January and 26th January, 2002 (Figure 36) when the prevailing wind swept from 75° to 202° (average wind direction over this period was 127°). This direction would be from Marin County and the northern San Francisco Bay area where there could be considerable wood combustion for home heating. The CPF plot for this source (Figure 37) suggests that this source could be located in the directions of NE or WNW. The emissions from the WNW direction may be coming from camp fire activities or burning of wood products by the three saw mills that are situated in the directions of Latitude 38.83° , Longitude -123.01° ; Latitude 38.72° , Longitude -123.37° , and Latitude 38.80° , Longitude -123.01° . The U.S Department of Agriculture Forest Service and the Center for International Disaster Information (CIDI) report presence of wildfires in southern California during the week ending on 25th January, 2002 (<http://www.cidi.org/wildfire/0201/ix13.html>). It is therefore important to further explore the contribution of such wildfires to the observed $\text{PM}_{2.5}$ mass in this factor.

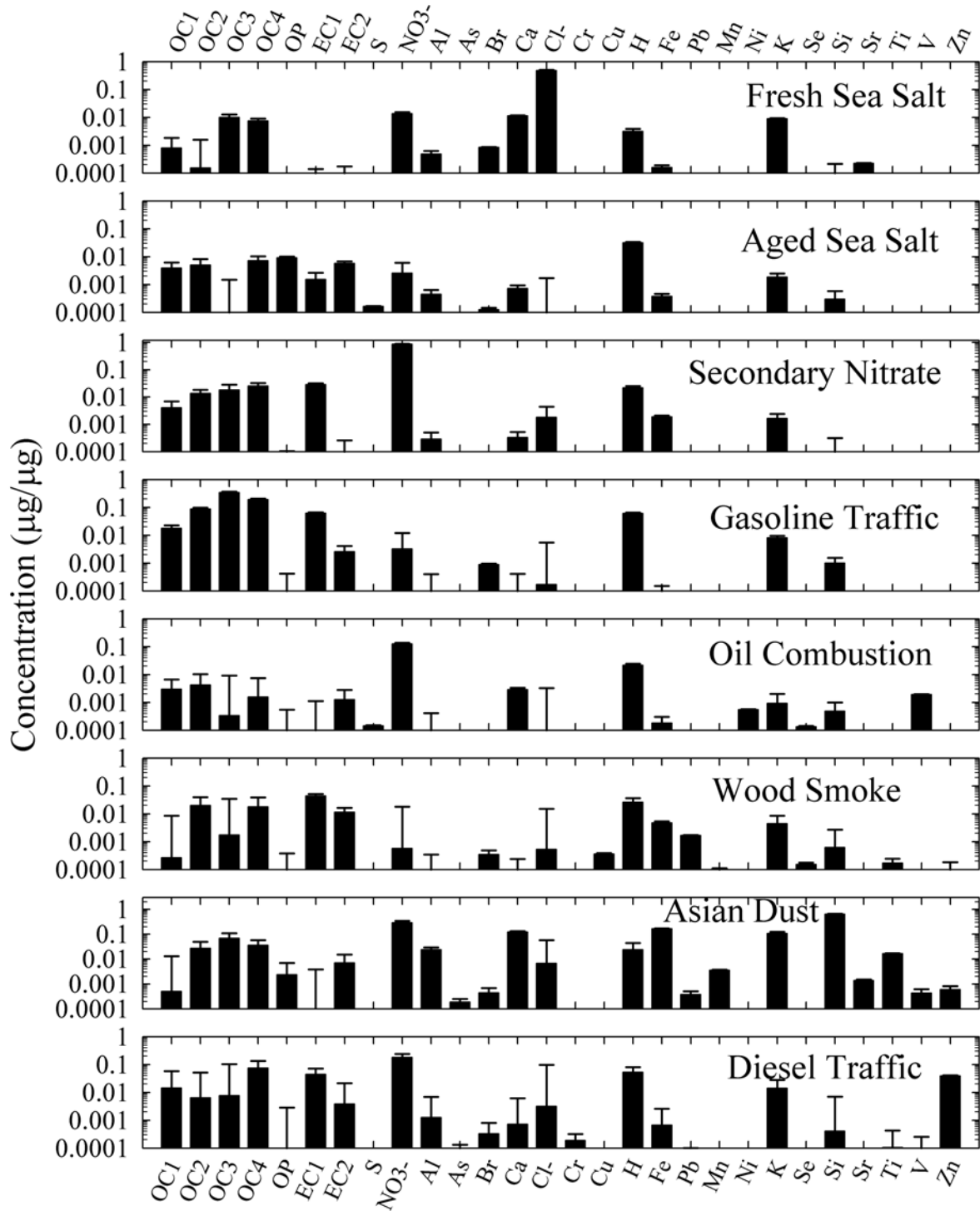


Figure 35 Source Profiles Derived from the Data from the Point Reyes National Seashore National Park IMPROVE Site

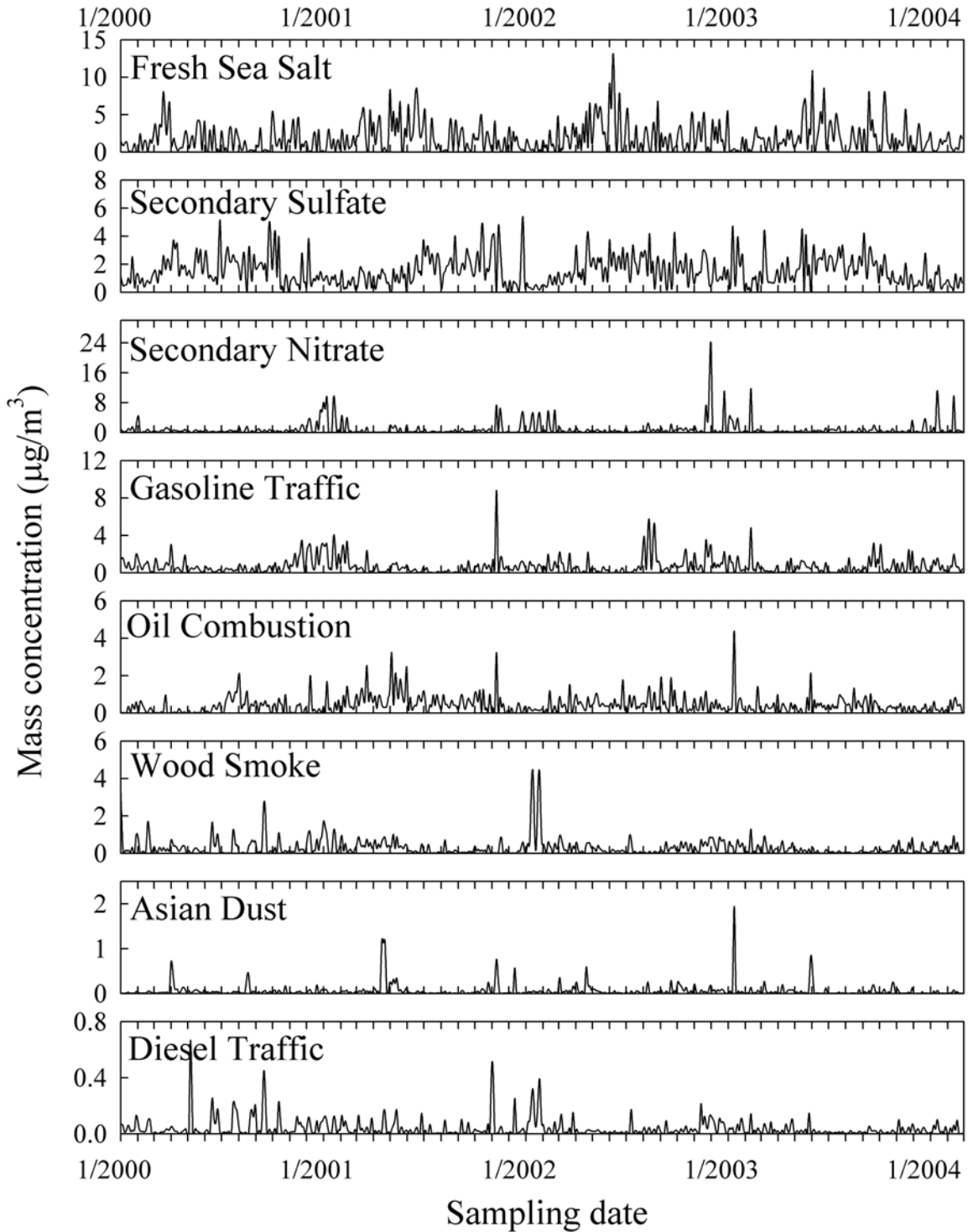


Figure 36 Source Contributions Derived from the Data from the Point Reyes National Seashore IMPROVE Site

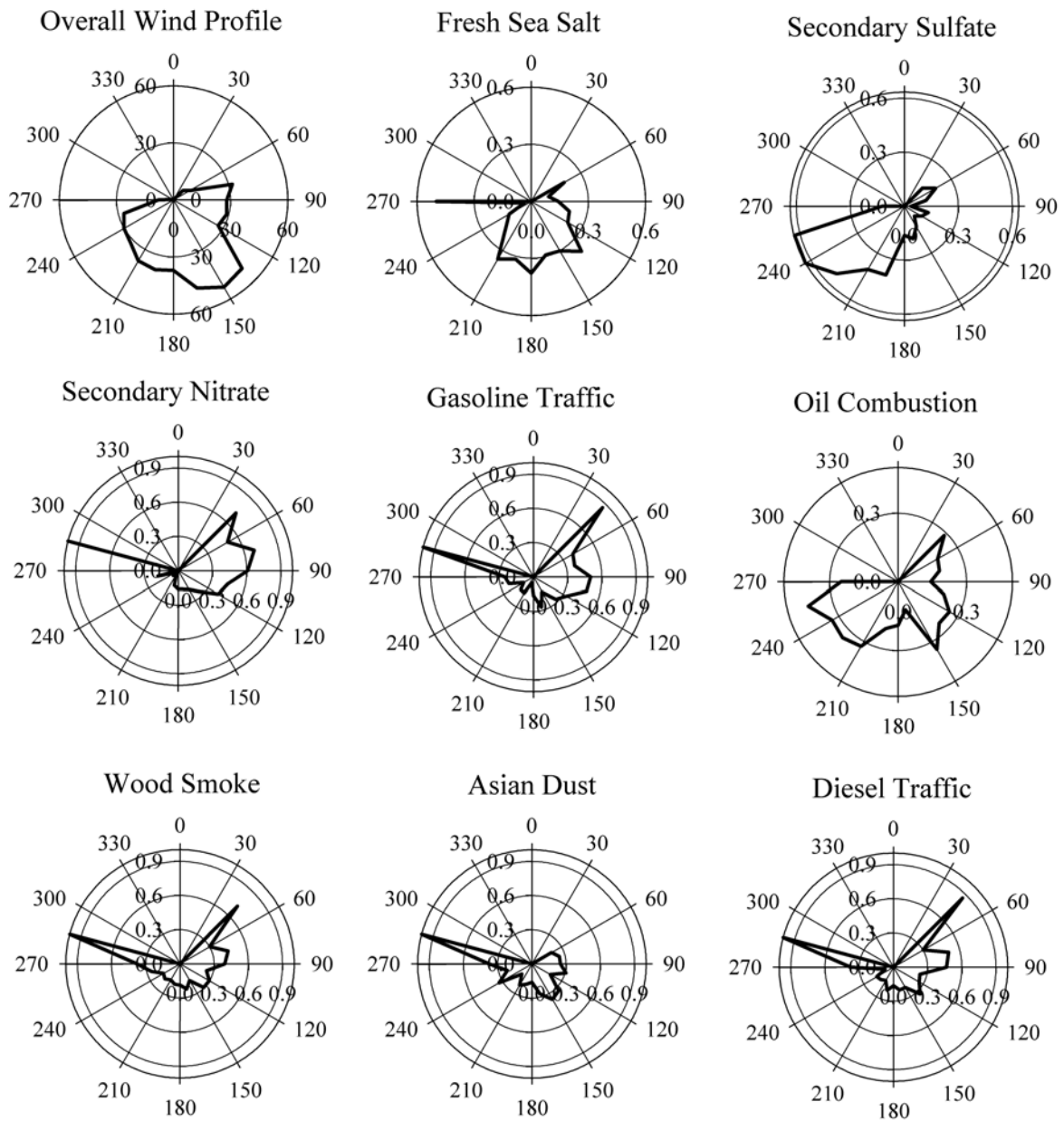


Figure 37 CPF Plots for the factor contributions derived from the Point Reyes National Seashore IMPROVE Site Data

Factor 7 has been identified as Asian desert dust. The temporal contribution shows high peaks every spring. Dust storms are reported to occur almost every spring in the deserts of Western China and have previously been found to be transported across the Pacific to the west coast of North America (Zhao and Hopke, 2004). This factor indicates a strong correlation with Si ($r = 0.76$), Fe ($r = 0.74$), Al ($r = 0.61$), and Ti ($r = 0.65$), which are all associated with dust particles (Seinfeld and Pandis, 1998). The temporal contribution (Figure 2) shows noticeable peaks on 1st April, 2000, 16th April, 2001, etc. In order to understand the origin of these dust particles, air parcel back trajectories ending at 12:00 AM UTC on 16th April, 2001 were constructed using NOAA HYSPLIT. The vertical velocity trajectories were constructed over a height of 500 meters above ground level. The trajectories crossed the Pacific Ocean and evidently passed through eastern Asia.

Factor 8 shows a moderate correlation with Zn ($r = 0.52$), which is a known oil additive element. The source profile also shows the presence of significant amounts of NO_3^- , EC, Ca, H, and Fe, which are characteristic of diesel emissions. The directionality of this factor suggests local emissions. This factor is suggested to represent diesel traffic emissions.

Figure 38 shows the relative contribution (percentage) of each of these sources to the apportioned mass. Given its close proximity to the ocean, the predominance of sea salt is reasonable.

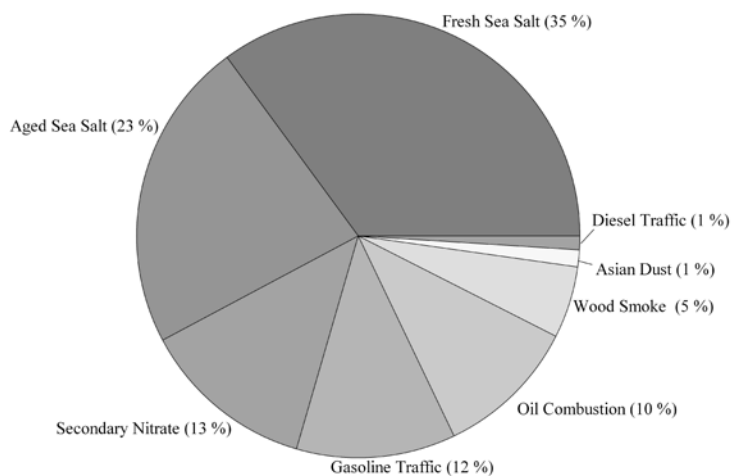


Figure 38 Apportionment of the $\text{PM}_{2.5}$ mass concentrations at the Point Reyes National Seashore IMPROVE Site

Redwood National Park

$\text{PM}_{2.5}$ samples were collected near Redwood National Park site in California (Figure 39). The location of the Redwood National Park site is latitude 41.5608, longitude -124.0839. The Redwood IMPROVE site is located 0.5 mile East of the Pacific Ocean. A total of 1640 samples were obtained from 3/2/1988 to 5/30/2004 for the Redwood National Park site. In the case of Redwood National Park site, 33 species (OC1, OC2, OC3, OC4, OP, EC1, EC2, EC3, SO_4^{2-} , NO_3^- , Al, As, Br, Ca, Cl, Cr, Cu, Fe, H, K, Mg, Mn, Na, Ni, Pb, Rb, Se, Si, Sr, Ti, V, Zn, Zr) were selected for PMF modeling and weak variables defined by the S/N ratio analyses (OC1, EC2, EC3, As, Cr, Mn, Rb, V, Zr) were down-weighted. Table 13 presents arithmetic mean, standard deviation, geometric mean, min. value, and max. value for individual species during the

sampling periods at the sampling site.

As the result of the PMF modeling, the optimal number of sources was determined to be 5 with an FPEAK equal to 0. This solution provided the most reasonable source profiles and source contributions for the Redwood National Park site data. The scaled F matrix (source profiles) are presented in Figure 40. The temporal variations of the quantitative mass contributions are shown in Figure 41. Figure 42 and Table 14 show the mean seasonal contributions for each particle source at the Redwood National Park site. The average source contributions for weekdays and weekend days are presented in Figure 43. The CPF plots are presented in Figure 44.

The species contributing to the first source as markers included OC3, OC4, EC1, NO₃⁻, Br, Ca, Fe, K, Mg, Na, and Zn. The first factor at Redwood National Park site was identified as motor vehicle emissions. For this data set, it was not possible to separate the motor vehicles into diesel and gasoline emissions as was the case with the other IMPROVE sites. The seasonal mean mass contributions for motor vehicle emissions were: fall (48.8%, 2.46 $\mu\text{g}/\text{m}^3$), winter (47.7%, 1.55 $\mu\text{g}/\text{m}^3$), spring (29.2%, 1.35 $\mu\text{g}/\text{m}^3$), and summer (21.4%, 0.98 $\mu\text{g}/\text{m}^3$). The mean weekend contribution of vehicle emissions was slightly higher than the mean weekday contribution (Figure 42). The CPF plot (Figure 43) indicates that the vehicle source is to the east of the site. This location is quite isolated from major highways. US highway 101 is located to the east of sampling site, and this result appears to correspond to the location of the vehicle emissions. It is likely that there are not sufficient differences in the relative amounts of diesel and gasoline vehicles between weekday and weekend to permit them to be separated.

The second source was identified as aged sea salt. The major marker species are Na, K, Ca, SO₄²⁻, NO₃⁻, OC3, OC4 and Fe. The mean aged sea salt seasonal contributions were: summer (29.3%, 1.35 $\mu\text{g}/\text{m}^3$), spring (26.0%, 1.20 $\mu\text{g}/\text{m}^3$), fall (19.1%, 0.96 $\mu\text{g}/\text{m}^3$), and winter (15.8%, 0.52 $\mu\text{g}/\text{m}^3$). This source showed no differences between the weekday contributions as compared to the weekend contributions. The CPF plot indicated that aged sea salt came mainly from the northwest.

The species contributing to the third source as markers included mainly Na, Cl, Mg, K, Ca, Br, SO₄²⁻, and NO₃⁻. This source was determined to be fresh sea salt. In this case, the mean spring contribution was higher than those for the other seasons (spring 1.17 $\mu\text{g}/\text{m}^3$ > summer 1.02 $\mu\text{g}/\text{m}^3$ > winter 0.78 $\mu\text{g}/\text{m}^3$ > fall 0.76 $\mu\text{g}/\text{m}^3$). The weekend contributions of fresh sea salt (1.02 $\mu\text{g}/\text{m}^3$) were a little higher than the weekday contribution (0.88 $\mu\text{g}/\text{m}^3$) although it is unclear why this difference would be observed. The CPF plot indicated the fresh sea salt source was mainly from the northeast and southwest. There are, thus, several apparent problems with these sea salt factors. The westerly direction for the aged sea salt is anomalous since that is the direction from which fresh sea salt might be expected. The northeasterly direction would have seemed more likely to be the direction for aged sea salt, but this location is very far from any large sources and recirculation patterns may result in the observed wind directional relationships.

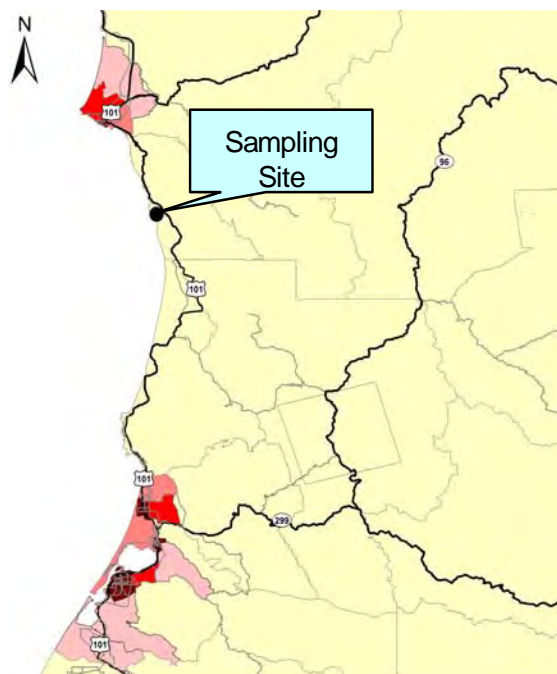


Figure 39. The location of the Redwood National Park sampling site.

Table 13. Summary statistics for the PM_{2.5} and species concentrations in the Redwood National Park site.

	Arithmetic Mean	Standard Deviation	Geometric Mean	Min.	Max.	NO. of BDL (%)
PM _{2.5} *	4.53	4.32	3.51	0.03	97.93	-
OC1	102.12	443.60	35.16	1.50	8803.90	1469(89.6)
OC2	166.72	427.80	94.83	1.50	12350.70	790(48.2)
OC3	387.36	594.37	224.62	3.00	9.446.40	398(24.3)
OC4	230.05	310.19	157.87	3.10	6.689.40	124(7.6)
OP	106.55	338.87	58.06	1.50	11192.20	686(41.8)
EC1	199.10	475.77	127.25	3.00	16037.10	121(7.4)
EC2	33.52	27.83	23.89	2.70	224.00	1222(74.5)
EC3	16.91	15.60	11.55	1.60	99.80	1516(92.4)
SO ₄ ²⁻	672.71	513.83	484.23	4.70	3042.90	50(3.0)
NO ₃ ⁻	259.84	242.45	172.84	0.40	2003.20	62(3.8)
Al	22.22	37.38	12.59	0.80	401.05	1207(73.6)
As	0.22	0.16	0.19	0.03	1.46	1204(73.4)
Br	2.28	1.62	1.76	0.05	11.42	19(1.2)
Ca	23.64	19.74	16.99	0.60	140.94	36(2.2)
Cl	544.67	593.38	269.11	0.40	3496.04	443(27.0)
Cr	0.93	0.81	0.55	0.02	5.77	1343(81.9)
Cu	0.42	0.53	0.29	0.04	8.34	770(47.0)
Fe	10.54	15.85	6.01	0.06	238.96	5(0.3)
H	140.07	166.20	110.38	10.67	4667.39	9(0.5)
K	36.50	27.55	28.66	1.68	266.97	1(0.1)
Mg	69.41	64.71	46.62	3.07	513.05	1100(67.1)
Mn	0.87	0.83	0.54	0.01	6.72	1233(75.2)
Na	503.81	552.96	303.05	7.64	4324.62	276(16.8)
Ni	0.34	0.36	0.25	0.03	4.71	1010(61.6)
Pb	0.93	1.78	0.60	0.05	45.85	431(26.3)
Rb	0.28	0.34	0.19	0.02	2.90	1371(83.6)
Se	0.22	0.17	0.17	0.02	1.58	903(55.1)
Si	34.48	49.74	21.00	1.00	778.02	186(11.3)
Sr	0.48	0.42	0.35	0.02	3.59	609(37.1)
Ti	1.94	1.93	1.30	0.02	22.28	887(54.1)
V	1.43	1.40	0.91	0.02	18.78	1110(67.7)
Zn	1.85	2.13	1.28	0.05	36.80	40(2.4)
Zr	0.31	0.37	0.19	0.03	2.41	1549(94.5)

* unit is µg/m³

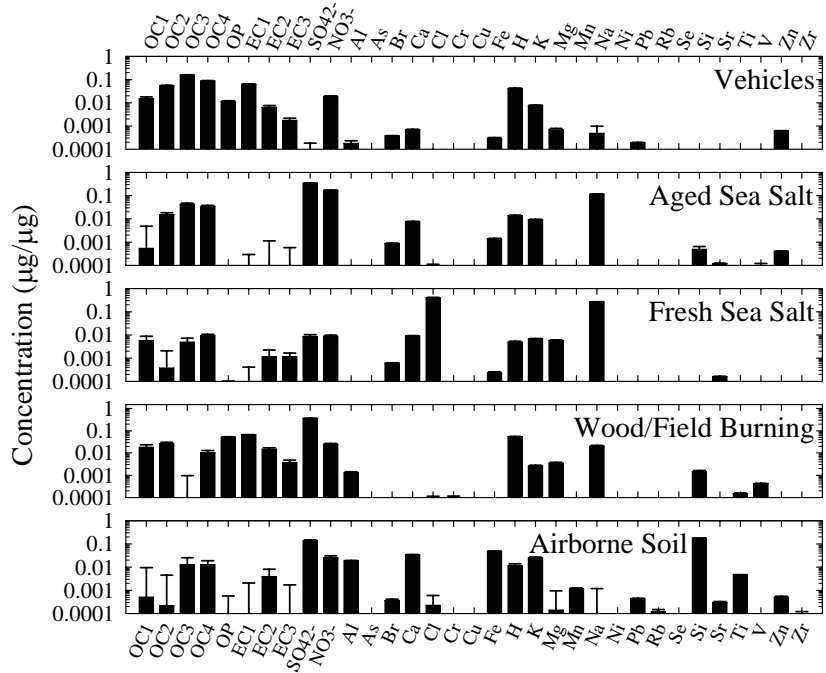


Figure 40. Source profiles for the Redwood National Park IMPROVE site constructed using the PMF model.

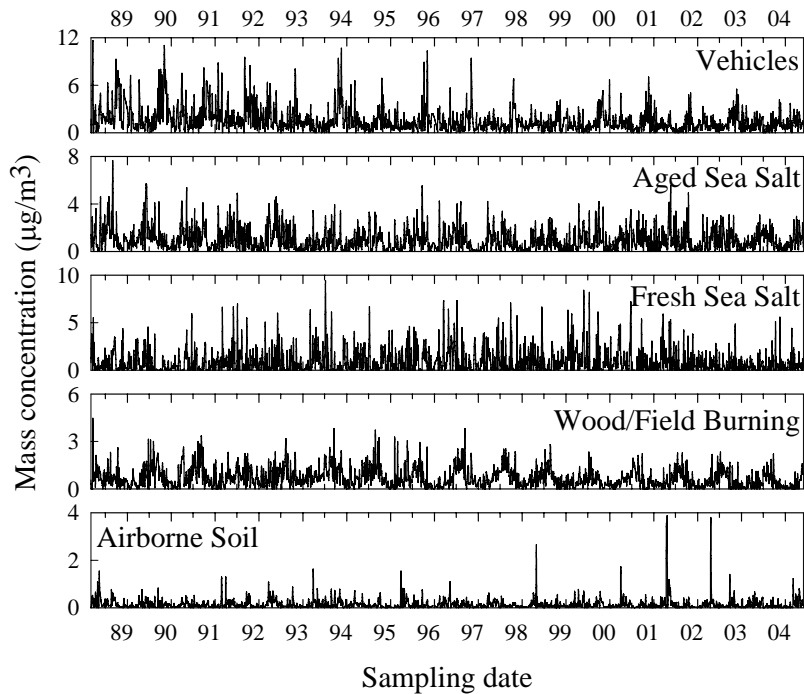


Figure 41. Temporal variation of source contribution for the Redwood National Park site constructed using the PMF2 model.

The fourth source was identified as the wood/field burning source. The major marker

species are OC1, OC2, OP, EC1, EC2, SO_4^{2-} , NO_3^- , K, Mg, Na, and Si. Wood/field burning mean seasonal source contributions were summer (24.7%, $1.13 \mu\text{g}/\text{m}^3$), fall (14.4%, $0.73 \mu\text{g}/\text{m}^3$), spring (13.5%, $0.62 \mu\text{g}/\text{m}^3$), and winter (10.4%, $0.34 \mu\text{g}/\text{m}^3$). The mean weekend contribution of wood/field burning was slightly higher than the weekday contribution.

Finally, the major species contributing to the fifth source included Si, K, Fe, Ca, Al, and Ti. This source was classified as airborne soil. Figure 41 shows that temporal variation of airborne soil shows very low, relatively uniform values over the sampling period except for April 22, 2001 ($3.86 \mu\text{g}/\text{m}^3$), April 20, 2002 ($3.76 \mu\text{g}/\text{m}^3$), and April 16, 2001 ($3.56 \mu\text{g}/\text{m}^3$). These high contributions are attributed to high contributions of long range transport soil from China during Asian dust storm periods (Figure 46). The mean seasonal mass contribution for soil were spring (6.0%, $0.28 \mu\text{g}/\text{m}^3$), fall (2.7%, $0.14 \mu\text{g}/\text{m}^3$), summer (2.4%, $0.11 \mu\text{g}/\text{m}^3$), and winter (2.1%, $0.07 \mu\text{g}/\text{m}^3$). There was no observable difference between the weekday ($0.16 \mu\text{g}/\text{m}^3$) and weekend ($0.15 \mu\text{g}/\text{m}^3$) concentrations. The CPF plot indicated airborne soil source comes mainly from the north.

Figure 46 presents the average contribution of all the sources identified during the sampling period. The average concentration of $\text{PM}_{2.5}$ for all the sources observed during the period was $4.53 \mu\text{g}/\text{m}^3$, whereas the concentration calculated through the PMF modeling was $4.41 \mu\text{g}/\text{m}^3$. The contribution of the vehicle source was 35.8% ($1.58 \mu\text{g}/\text{m}^3$). This source had the greatest effect on the local ambient air quality, followed by the aged sea salt source (23.2%, $1.02 \mu\text{g}/\text{m}^3$), fresh sea salt (21.4%, $0.94 \mu\text{g}/\text{m}^3$), wood/field burning (16.1%, $0.71 \mu\text{g}/\text{m}^3$), and airborne soil source (3.5%, $0.15 \mu\text{g}/\text{m}^3$), respectively. These results reflect the fact that sampling site is located near the coast (around 1 km) and far from any population centers or other anthropogenic sources.

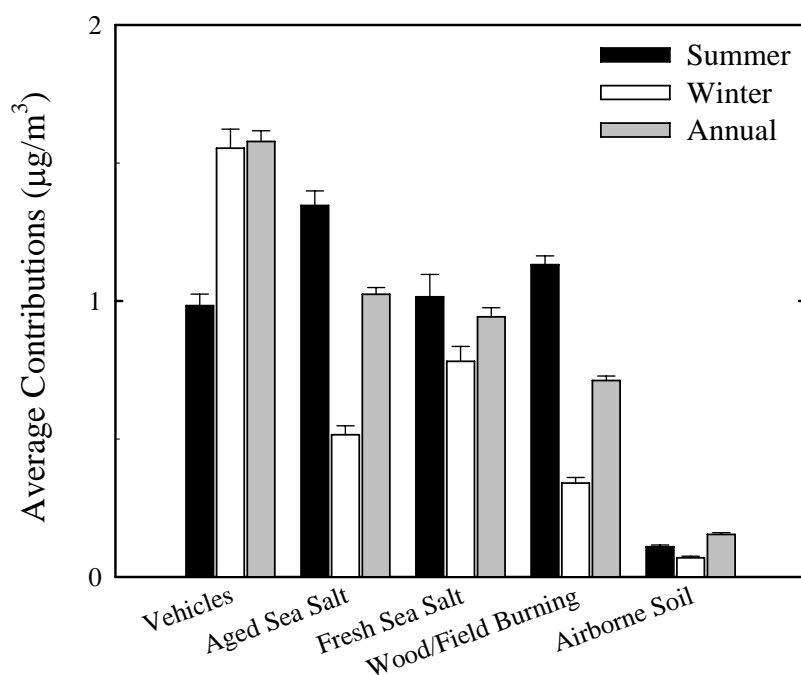


Figure 42. Comparison of the seasonal (summer: June to August, winter: December to February) contributions for each source in Redwood National Park site.

Table 14. Average seasonal source contributions for the Redwood National Park site.

	Winter		Spring		Summer		Fall		AVG.	
	$\mu\text{g}/\text{m}^3$	%								
Vehicle	1.55	47.7	1.35	29.2	0.98	21.4	2.46	48.8	1.58	35.8
Aged Sea Salt	0.52	15.8	1.20	26.0	1.35	29.3	0.96	19.1	1.02	23.2
Fresh Sea Salt	0.78	24.0	1.17	25.3	1.02	22.1	0.76	15.0	0.94	21.4
Wood/Field Burning	0.34	10.4	0.62	13.5	1.13	24.7	0.73	14.4	0.71	16.1
Airborne Soil	0.07	2.1	0.28	6.0	0.11	2.4	0.14	2.7	0.15	3.5
Sum	3.26	100.0	4.63	100.0	4.59	100.0	5.05	100.0	4.41	100.0

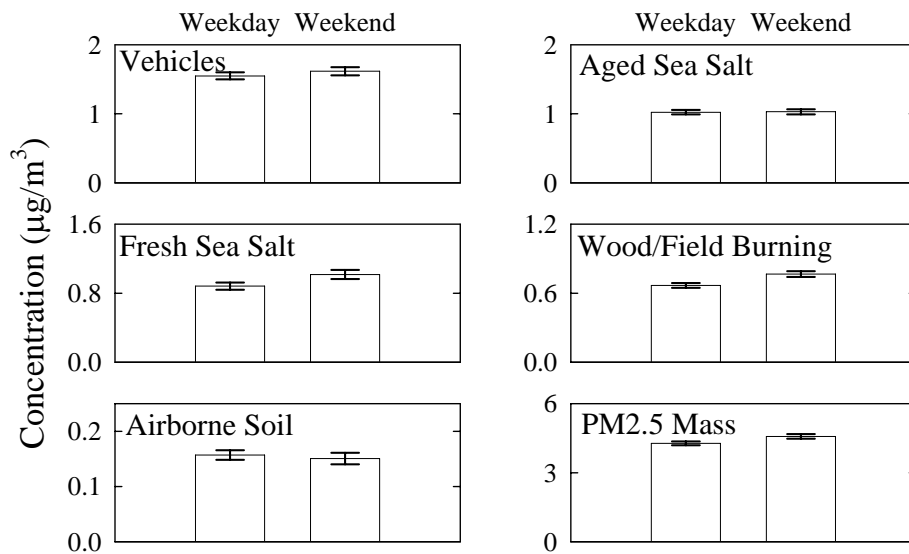


Figure 43. The average source contributions for weekdays and weekend days in Redwood National Park site.

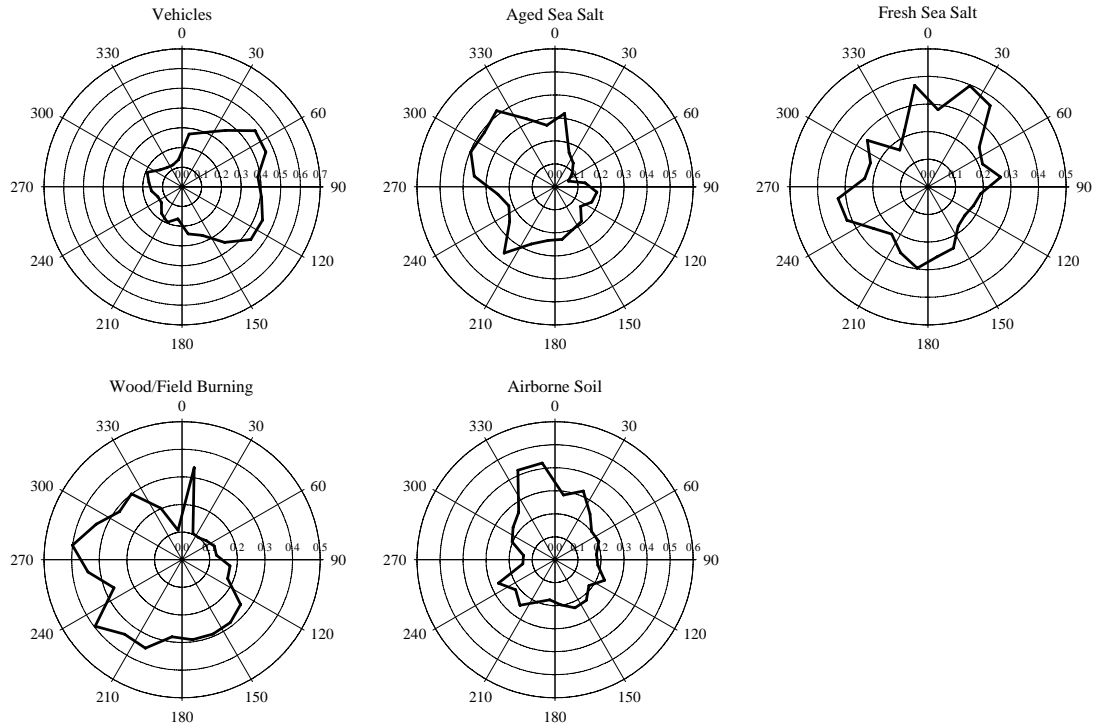


Figure 44. Conditional Probability Function (CPF) results based on source contributions obtained by the PMF analysis of the data from the Redwood National Park site.

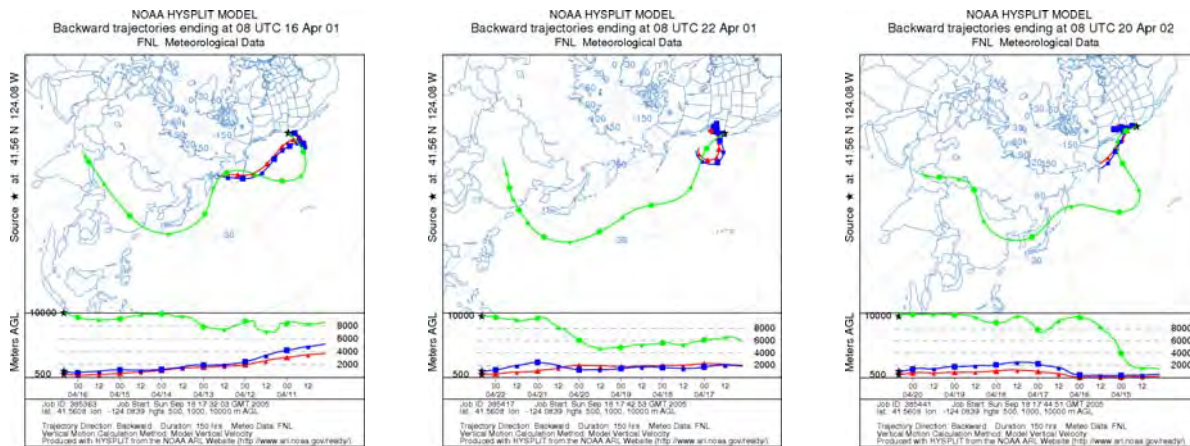


Figure 45. HYSPLIT back trajectories calculated for April 16, 2001, April 22, 2001, and April 20, 2002

Figure 47 shows the comparison of the predicted PM_{2.5} contributions from all sources with measured PM_{2.5} concentrations. The PMF resolved sources reproduced the measured mass values (slope = 0.891) and account for most of the variation in the PM_{2.5} concentrations ($R^2 = 0.92$).

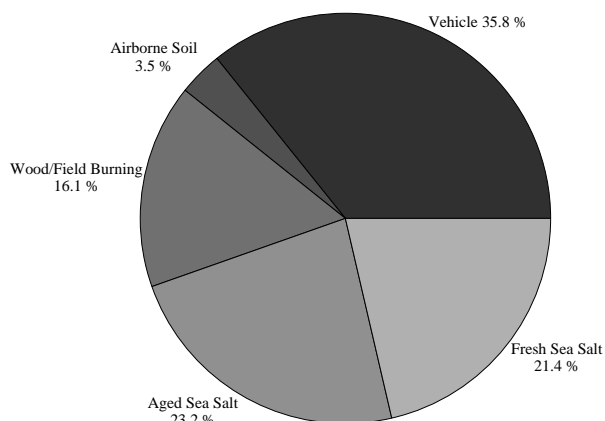


Figure 46. Average source contribution for the sampling period at Redwood National Park IMPROVE site.

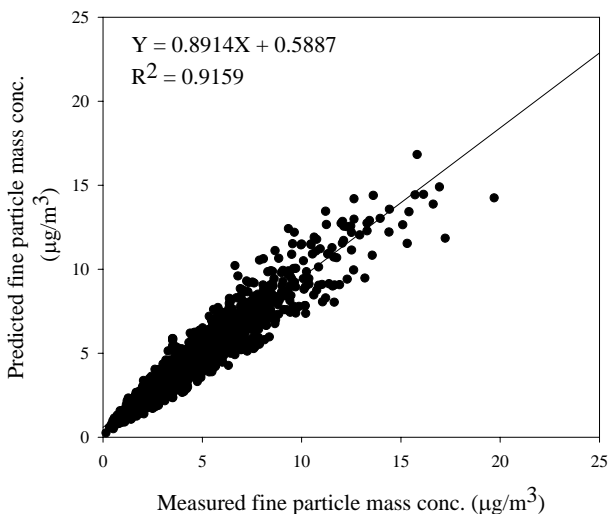


Figure 47. Comparison of the predicted PM_{2.5} mass concentrations with the measured PM_{2.5} mass concentrations for the Redwood National Park site.

Kalmiopsis

The Kalmiopsis site is surrounded by mountains (Figure 48) (latitude: 42.552, longitude -124.0589). A total of 493 samples were collected at this IMPROVE site from 3/11/2000 to 5/30/2004. The results of the analysis of the data from these samples have been reported by Hwang and Hopke (2006a). In the case of the Kalmiopsis data, 33 species (OC1, OC2, OC3, OC4, OP, EC1, EC2, EC3, SO₄²⁻, NO₃⁻, Al, As, Br, Ca, Cl, Cr, Cu, Fe, H, K, Mg, Mn, Na, Ni, P, Pb, Rb, Se, Si, Sr, Ti, V, Zn) were selected for the PMF modeling and weak variables defined by the S/N ratio analyses (EC3, Cr, Mg, P, V) were down-weighted. Table 15 present the summary statistics for individual species during this period at the Kalmiopsis site.

The optimal number of sources was determined as 7 with a value of FPEAK = 0. This combination provided good fits to the data and interpretable source profiles and source contributions for this site. Figure 49 shows the source profiles obtained for the Kalmiopsis site. The quantitative mass contributions of sources are presented in Figure 50. Figure 51 and Table 16 compare the seasonal contributions for each source at the Kalmiopsis site. The average source contributions for weekdays and weekend days at the sampling site are presented in Figure 52. In Figure 53, a comparison of the predicted PM_{2.5} contributions from all of the identified sources

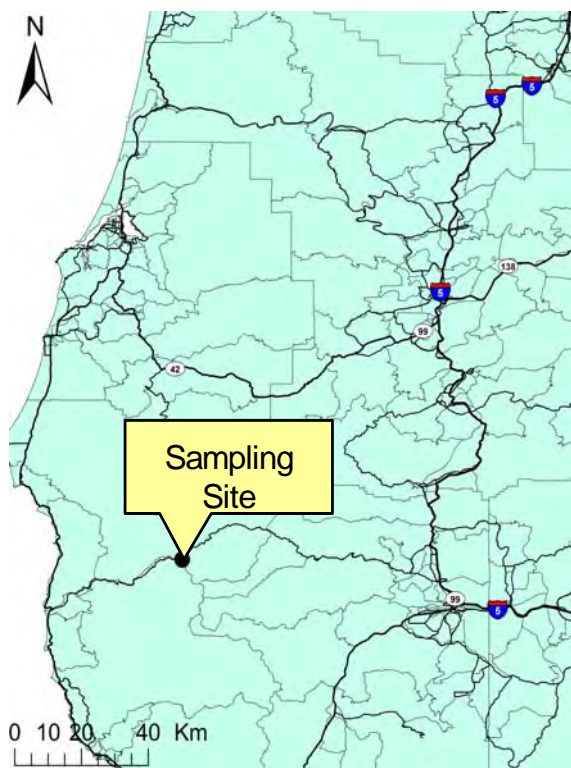


Figure 48. The location of the Kalmiopsis IMPROVE site.

with measured PM_{2.5} concentrations is presented. The PMF resolved sources effectively reproduced the measured values (slope = 0.898) and account for most of the variation in the PM_{2.5} concentrations (R² = 0.97).

Table 15. Summary statistics for the PM_{2.5} and species concentrations at the Kalmiopsis (ng/m³) site.

	Arithmetic Mean	Standard Deviation	Geometric Mean	Min.	Max.	NO. of BDL (%)
PM _{2.5} *	3.40	3.07	2.65	0.38	31.27	0
OC1	136.21	611.45	41.32	1.50	8419.3	385(77.8)
OC2	258.61	1,238.01	121.18	9.10	25,611.60	174(35.1)
OC3	671.44	1,100.09	431.90	45.70	18,198.90	30(6.0)
OC4	313.16	733.10	209.00	37.00	14,108.70	6(1.2)
OP	95.44	180.89	61.32	2.90	3,523.20	156(31.5)
EC1	216.29	485.79	150.04	14.70	9,996.20	8(1.6)
EC2	49.14	57.97	35.91	2.80	984.30	161(32.5)
EC3	16.02	31.52	10.98	2.80	344.00	414(83.5)
SO ₄ ²⁻	486.81	373.04	323.18	7.70	2,035.90	17(3.4)
NO ₃ ⁻	146.62	150.50	93.85	0.20	2,062.20	72(14.5)
Al	34.71	48.48	18.37	2.04	309.77	381(76.8)
As	0.31	0.63	0.21	0.03	8.32	239(48.2)
Br	1.23	1.90	0.90	0.05	39.77	0(0.0)
Ca	16.15	15.66	11.43	1.04	134.19	11(2.2)
Cl	111.37	169.96	35.99	0.28	1,041.94	228(46.0)
Cr	0.54	0.63	0.20	0.02	2.23	425(85.7)
Cu	0.25	0.41	0.18	0.03	4.95	199(40.1)
Fe	13.43	21.03	6.15	0.35	193.87	0(0.0)
H	155.01	181.21	118.45	30.29	1,98.32	0(0.0)
K	28.14	21.84	22.31	4.14	184.78	0(0.0)
Mg	26.59	16.30	22.08	5.96	75.93	424(85.5)
Mn	0.67	0.74	0.37	0.03	4.35	315(63.5)
Na	176.32	141.04	133.92	17.11	921.51	253(51.0)
Ni	0.21	0.43	0.15	0.03	5.99	301(60.7)
P	3.81	3.08	2.86	0.57	13.37	55(11.1)
Pb	0.64	1.08	0.45	0.05	20.08	472(95.2)
Rb	0.14	0.11	0.12	0.01	0.81	269(54.2)
Se	0.09	0.06	0.08	0.02	0.34	213(42.9)
Si	57.38	78.53	31.87	1.42	683.09	55(11.1)
Sr	0.25	0.22	0.17	0.02	2.02	139(28.0)
Ti	2.47	2.86	1.28	0.04	20.59	198(39.9)
V	0.75	0.89	0.38	0.02	7.13	329(66.3)
Zn	1.73	2.23	1.15	0.10	31.04	5(1.0)

* : unit is µg/m³

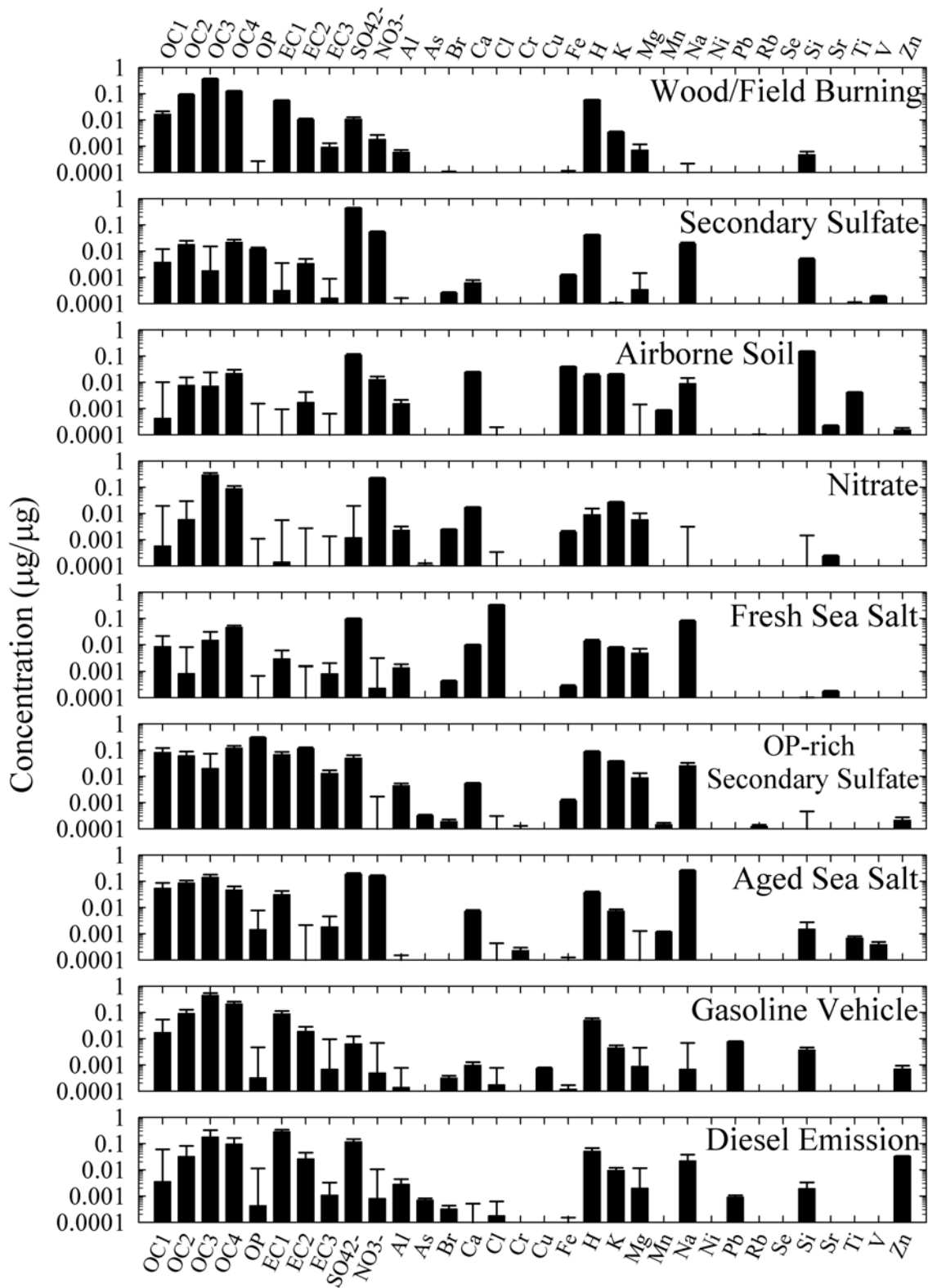


Figure 49. Source profiles for the Kalmiopsis IMPROVE site derived using the PMF2 model.

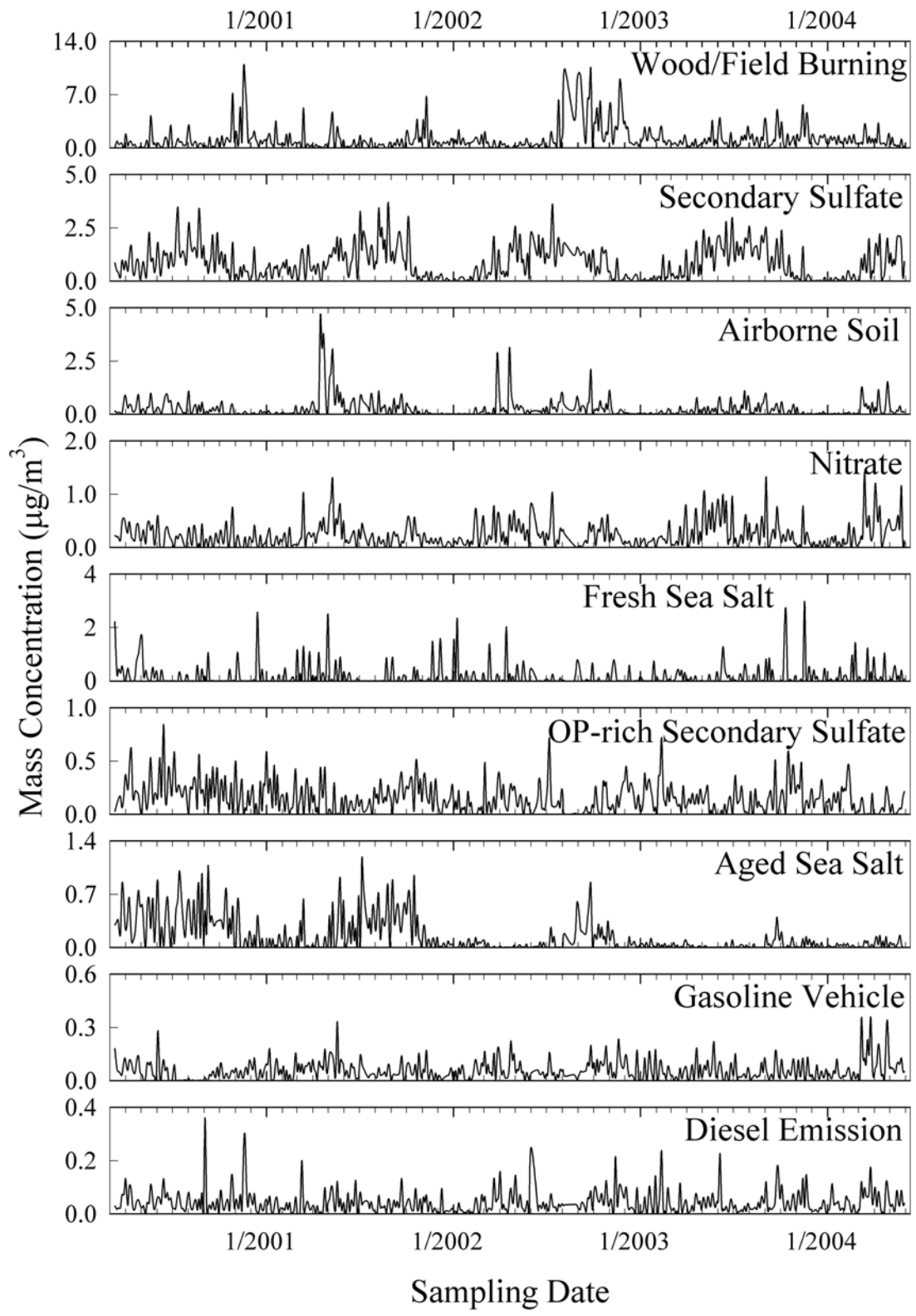


Figure 50. Temporal variation of source contributions for the Kalmiopsis site constructed using the PMF model.

The species contributing to the first source included OC2, OC3, OC4, EC1, EC2, SO₄²⁻, NO₃⁻, K, and Mg. This profile was identified as wood/field burning. Because Kalmiopsis is surrounded by a large forest, wildfires and wood/field burning are common. In the case of rural communities, wood is a common domestic heating fuel. The peak seasonal mass contribution of wood/field burning source was the fall (53.6 %, 2.16 µg/m³). Table 16 shows that the average contribution during the fall were about 3 times higher than the contribution during the spring and contributes 38.4 % (1.22 µg/m³) to the total PM_{2.5} mass concentration. Figure shows that weekday contributions (1.32 µg/m³) were somewhat higher than weekend contributions (1.00 µg/m³). In particular, wood/field burning source showed high contribution during July, 2002 ~ September, 2002 (Figure 50).

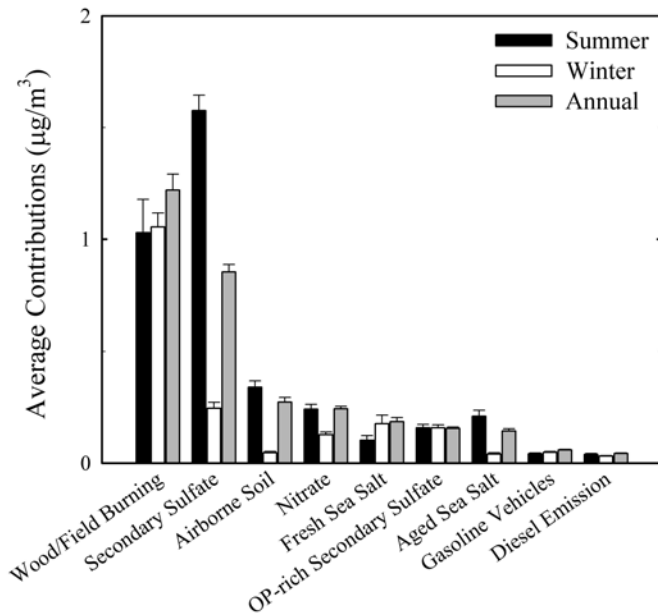


Figure 51. Seasonal and annual mean contributions of the various sources to the PM_{2.5} mass at Kalmiopsis.

Table 16. Average seasonal source contribution using the PMF model in Kalmiopsis IMPROVE site.

	Winter		Spring		Summer		Fall		AVG.	
	µg/m ³	%								
Wood/Field Burning	1.05	54.7	0.73	23.9	1.03	27.5	2.16	53.6	1.22	38.4
Secondary Sulfate	0.25	12.7	0.89	29.1	1.58	42.2	0.74	18.4	0.85	26.9
Airborne Soil	0.05	2.4	0.45	14.8	0.34	9.1	0.21	5.2	0.27	8.6
Nitrate	0.13	6.6	0.36	11.7	0.24	6.5	0.21	5.3	0.24	7.6
Fresh Sea Salt	0.18	9.1	0.26	8.3	0.10	2.7	0.18	4.6	0.19	5.8
OP + Sulfate	0.16	8.2	0.13	4.3	0.16	4.2	0.18	4.5	0.16	4.9
Aged Sea Salt	0.04	2.1	0.12	3.7	0.21	5.6	0.22	5.6	0.14	4.5
Gasoline Vehicle	0.05	2.5	0.08	2.7	0.04	1.1	0.06	1.5	0.06	1.9
Diesel Emission	0.03	1.6	0.05	1.5	0.04	1.0	0.06	1.4	0.04	1.4
Sum	1.93	100.0	3.07	100.0	3.74	100.0	4.03	100.0	3.18	100.0

On July 13, 2002, a wildfire began burning in the Biscuit Creek area (in the south Kalmiopsis roadless area) and continued to spread as far as the Rogue River on September 5, 2002. More than 180,000 acres of the Kalmiopsis wilderness burned and the total area of fire was 500,000 acres (Harma and Morrison, 2003).

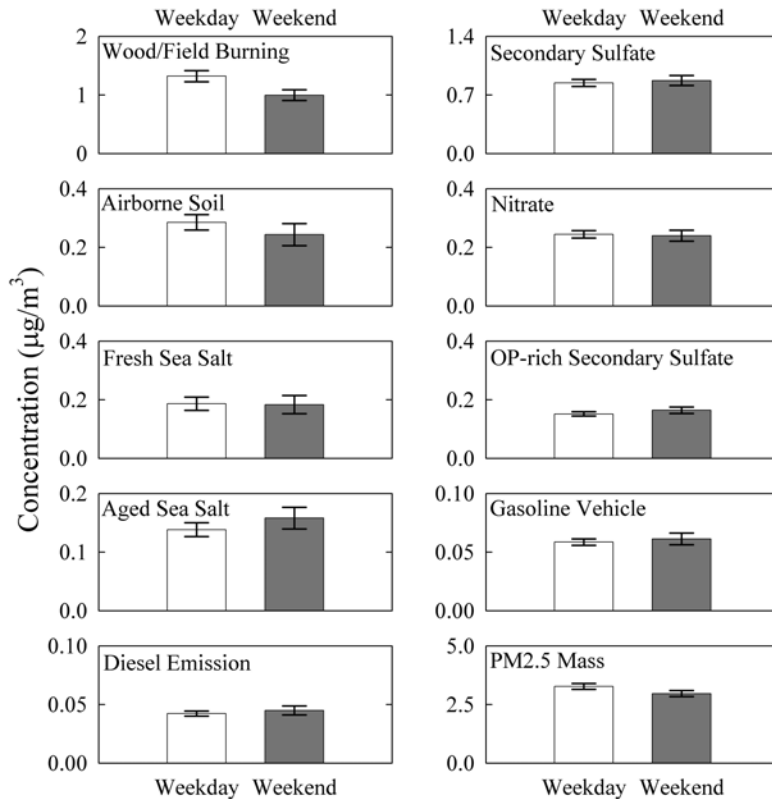


Figure 52. The average source contributions for weekdays and weekend days at the Kalmiopsis site.

The wood/field burning source contributions, total carbon, K and SO_4^{2-} concentrations for during sampling periods are shown in Figure 54 (the box denotes the Biscuit wildfire period). This figure shows that there were high wood/field burning contributions in good agreement with high TC and K concentration during the Biscuit wildfire period. Also, the carbon/sulfate ratios during the non smoke typically show an average ratio value of 2.6 ± 2.0 . During strong smoke events, this ratio ranged from 12 to 60 (VanCuren, 2003). For the Kalmiopsis site, the carbon/sulfate ratio was 11.6 during Biscuit wildfire periods (while non-wildfire samples ratio was 4.1). Although the wild fire would not be a source of sulfate, it does produce significant quantities of reactive organic compounds and thus, increased oxidant concentrations. Thus, some increase in sulfate production might be correlated with the fire episode leading to the apparent sulfate concentration.

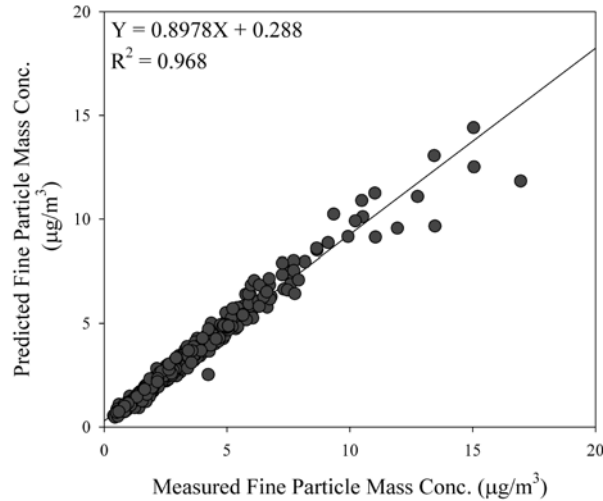


Figure 53. Comparison of the predicted total PM_{2.5} mass concentrations from the PMF analysis with the measured PM_{2.5} mass concentrations for the Kalmiopsis IMPROVE site.

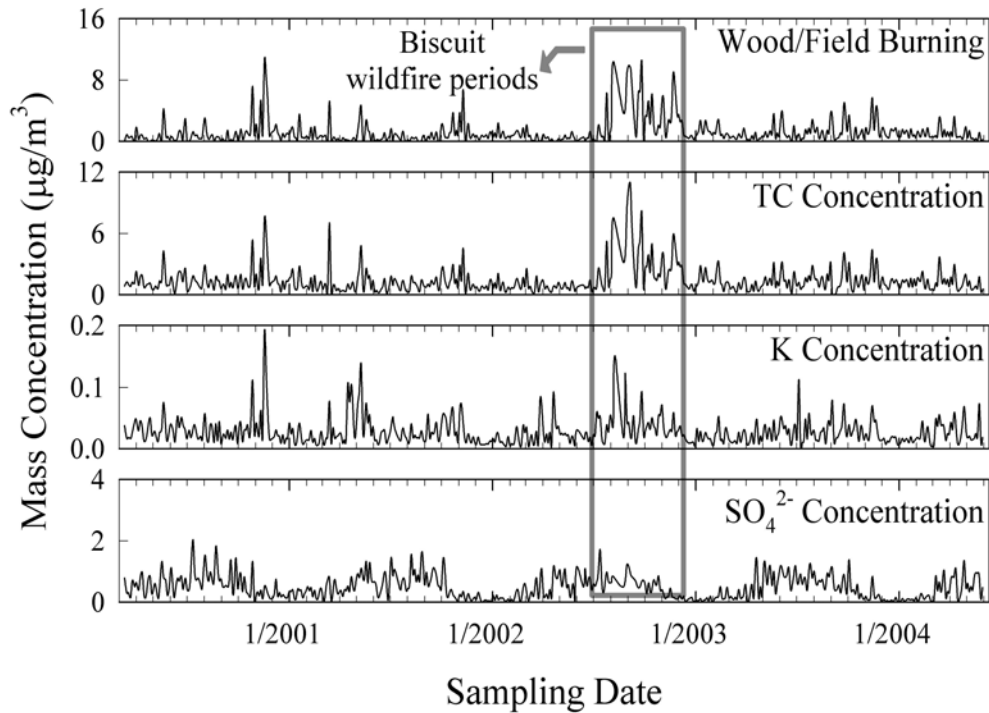


Figure 54. Comparison of wood/field burning source contributions and TC, K, SO₄²⁻ concentrations during the Biscuit wildfire period.

For this site, the potential source contribution function (PSCF) was calculated for each source. This analysis uses air parcel back trajectories to create a conditional probability field around the receptor site that can assist in identifying the likely locations of the sources identified at the site. A complete description of the technique is given by Begum et al. (2005). The PSCF

plot for the wood/field burning source in Kalmiopsis site is presented in Figure 55. This plot shows a major source area in the Siskiyou County and another is eastern Oregon. These results are in good agreement with the Biscuit wildfire site.

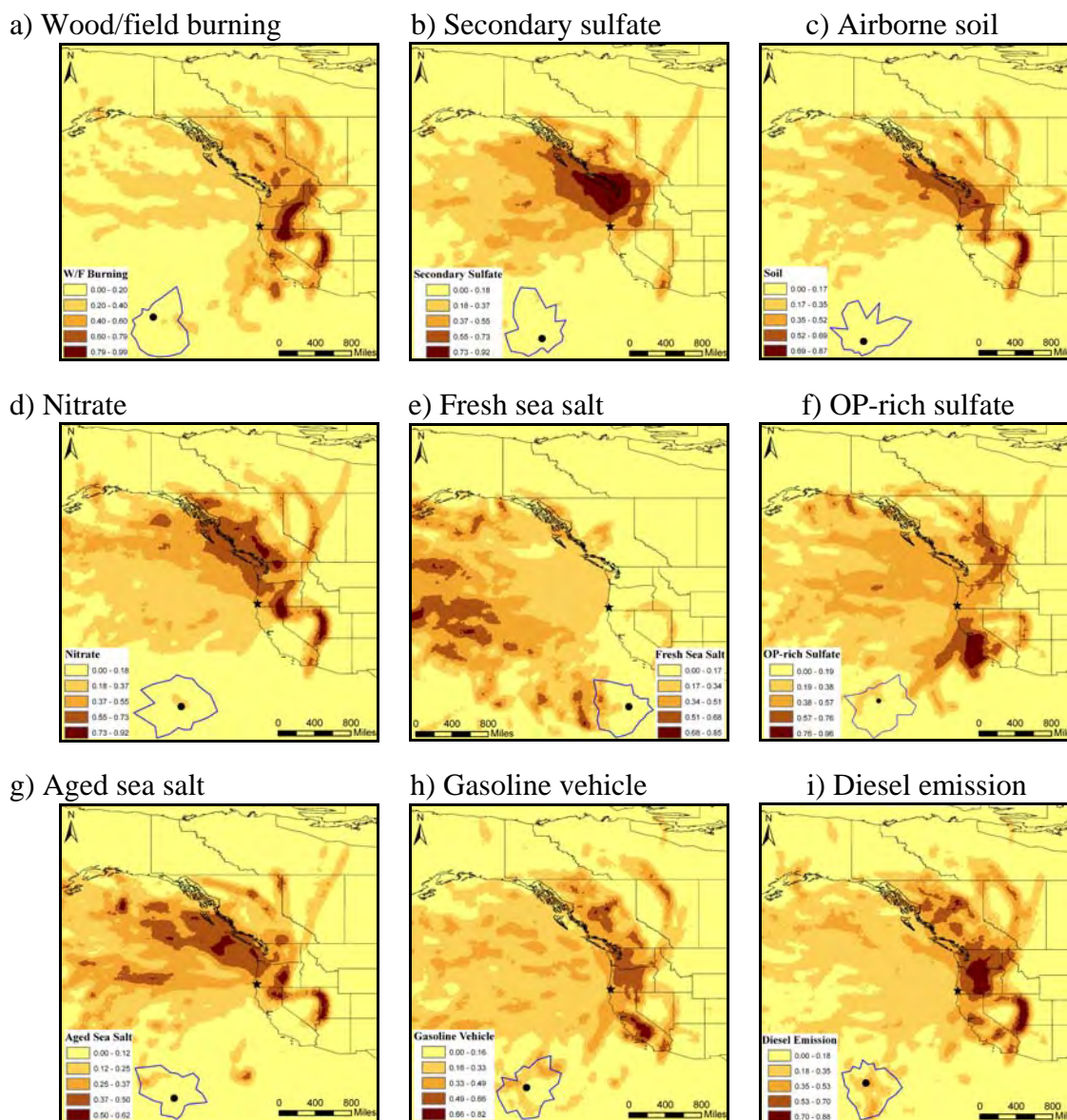


Figure 55. PSCF plots for the source contributions resolved from the $PM_{2.5}$ composition data obtained at the Kalmiopsis IMPROVE site.

The species associated with the second source included SO_4^{2-} and NO_3^- , and these were classified as secondary sulfate and contributed 26.9 % ($0.85 \mu g/m^3$) to the total $PM_{2.5}$ mass concentration. The average seasonal mass contributions show its peak contribution to be in the summer (Table 16). Although NH_4^+ was not available to include in the PMF modeling, SO_4^{2-} and NH_4^+ would presumably exist as secondary sulfate such as $(NH_4)_2SO_4$. Figure 5 shows there is no significant difference between the weekdays versus the weekend concentrations. As

shown in Figure 55, the PSCF plot of secondary sulfate shows major potential source areas in western Washington, northwestern Oregon, and the near shore Pacific Ocean area where there are active shipping lanes.

Washington and Oregon have only one coal-fired power plant in each state. In the case of Washington, the Centralia Power Plant, with a production capacity of 1,404 MW, is located in the southwest Washington. This plant emitted 83,600 tons of SO₂ in 2000. For Oregon, the Boardman power plant, with a production capacity of 600 MW, situated in the north central Oregon. This plant emitted 14,374 tons of SO₂ in 2000 (Peele, 2003; US EPA, 2005). The high PSCF values that lie in these area could be related to SO₂ emissions from coal-fired power plants. Moreover, the pulp mills and petroleum refineries in these areas could contribute to the secondary sulfate concentrations. In the case of the Pacific Ocean, there are many ships burning high sulfur residual oil such that this area can contribute secondary sulfate source.

The third source was determined to be airborne soil. The major species contributing to the this source included Si, Al, Ca, Fe, Ca, K, and Ti. The temporal variation of the source contribution plot shows very strong contributions in March and April 2001. The peak seasonal mass contribution of airborne soil source was in the spring (14.8 %, 0.45 µg/m³). Figure 5 showed that the average weekday contribution of airborne soil source (0.29 µg/m³) was somewhat higher than the weekend contribution (0.24 µg/m³). This source accounts for 8.6 % (0.27 µg/m³) of the PM_{2.5} concentration. This seasonal patterns suggests the influence of intercontinental transport of Asian dust. Asian dust episodes have been observed at a number of sites in the western United States (VanCuren and Cahill, 2002, Liu et al., 2003a, Vancuren, 2003, Zhao and Hopke, 2004). The major intercontinental dust episodes are in March and April. At higher altitudes, the impact of transported dust can also be observed at other times during the year (Liu et al., 2003). Thus, the observed soil contributions during the remainder of the year are likely to be locally disturbed soils.

The fourth source profile includes a high concentration NO₃⁻ and this source accounts for 7.6 % (0.24 µg/m³) of the total PM_{2.5} mass concentration. In general, secondary nitrate is known to be seasonal with high contributions in winter because lower temperature and higher humidity help the formation of secondary nitrate particles (Seinfeld and Pandis, 1998). However, the seasonal average mass contributions of secondary nitrate show a peak in spring in this study. The reason for this behavior is not known.

The species contributing to the fifth source include Cl, Na, SO₄²⁻, Mg, K, and Ca. So, this source is assigned to be fresh sea salt and contributed 5.8 % (0.19 µg/m³) to the total PM_{2.5} mass concentration. In the case of this source, the spring contribution was higher than other season contributions (spring 0.26 µg/m³ > fall and winter 0.18 µg/m³ > summer 0.10 µg/m³). The fresh sea salt source showed no significant differences in the mean contributions between the weekdays versus weekends (Figure 5).

The sixth source was classified as an OP-rich secondary sulfate with high abundances of OP and sulfate. A profile with high abundances of OP and sulfate has been reported in previous IMPROVE studies such as the Mammoth Cave National Park (Zhao and Hopke, 2006), Great Smoky Mountains National Park (Kim and Hopke, 2006), Bondville, IL (Kim et al., 2005), and Washington, DC (Begum et al., 2005; Kim and Hopke, 2004a) studies. It accounts for 4.9 % (0.16 µg/m³) of the PM_{2.5} mass concentration (Table 2). Yu et al. (2002) showed that an association between the water soluble organic carbon and OP formation in the thermal analysis of Hong Kong and China aerosols. It is suggested that the OP-rich secondary sulfate aerosols may be in part the result of heterogeneous acidic catalyzed reactions between the acidic sulfate and gaseous organic compounds that leads to additional secondary organic aerosol formation (Jang et al., 2003). The average mass contributions of OP-rich secondary sulfate shows a peak in fall (Table 2). Similar to the secondary sulfate contributions, OP-rich secondary sulfate showed no difference between weekdays and weekend days (Figure 5). In Figure 7, the PSCF plot of OP-rich sulfate showed high potential areas in the forested regions of the western-central California, eastern Washington, and southern British Columbia in Canada. These areas are

likely to be related to the organic carbon emissions from biogenic sources. The PSCF plot of OP-rich sulfate indicates regional influences of the biogenic as well as anthropogenic secondary aerosol. Further study is needed to understand the nature of OP-rich sulfate source that has been found at most IMPROVE sites.

The major species contributing to the seventh source included Na, SO_4^{2-} , NO_3^- , and Ca. These species suggest that this material is aged sea salt. The aged sea salt source peaked in the fall (fall $0.22 \mu\text{g}/\text{m}^3 >$ summer $0.21 \mu\text{g}/\text{m}^3 >$ spring $0.12 \mu\text{g}/\text{m}^3 >$ winter $0.04 \mu\text{g}/\text{m}^3$). The aged sea salt source showed no significant difference between weekdays and weekend days (Figure 5).

The eighth source profile was assigned to gasoline vehicle emissions. The OC3, OC4, and EC1 were major species contributing to the eighth source along with minor species such as Pb, Si, K, Ca, Mg, and Zn. This source was identified on the basis of high levels of OC, with a lower value of EC. The spring contributions ($0.08 \mu\text{g}/\text{m}^3$, 2.7 %) were higher than for the other seasons (fall $0.06 \mu\text{g}/\text{m}^3$, winter $0.05 \mu\text{g}/\text{m}^3$, and summer $0.04 \mu\text{g}/\text{m}^3$). Gasoline vehicle emissions showed no significant difference between the weekend and weekday contributions (Figure 5). As shown in Figure 7, the PSCF plot of gasoline vehicle emissions shows major potential source areas in central California including Bakersfield, Fresno, and Sacramento. These areas are located between the Coastal Range and the Sierra Nevada Mountains. Interstate Highway 5 and California Highway 99 pass through these areas.

The species contributing to the ninth source profile are EC1, OC3, OC4, SO_4^{2-} , Na, K, Mg, Pb, Si, and Zn. The final source was identified as diesel emissions. The Si in the gasoline vehicle and diesel emissions profiles may be from associated road dust. The seasonal average mass contributions of diesel emission show a peak in fall ($0.06 \mu\text{g}/\text{m}^3$, 1.4 %). Similar to the gasoline vehicle contributions, the diesel emissions showed no differences between weekdays and weekend days (Figure 5).

It was not possible to resolve a residual oil profile from these data and thus, there is no evidence of a direct impact of ship emissions on this site. The profiles for aged sea salt and secondary sulfate contain the highest concentrations of vanadium and nickel. Thus, the direct emissions from the residual oil combustion in the ship engines has become fully admixed with the sources related to the sulfate and sea salt that has interacted with the sulfuric and nitric acid produced from the oxidation of the SO_2 and NO_x emitted from the ships.

Olympic National Park

$\text{PM}_{2.5}$ samples collected on every third day at the IMPROVE monitoring site located near the Olympic National Park, WA were analyzed in this study (latitude: 48.0065N; longitude: 122.9727W; elevation: 600 m). As shown in Figure 56, the monitoring site is located adjacent to the northeastern edge of the Olympic National Park. The site is situated 63 km northwest of Seattle and 50 km southeast of Victoria, Canada. Strait of Juan De Fuca that is a major channel used for ferries, boats, and container ships is located north of the site. Port Townsend and Sequim are located 16 km northeast and 12 km northwest of the monitoring site, respectively. Highway 101 is closely situated about 2.5 km north of the site. Wind data measured at Port

Angeles located 25 km west of the site were used in this study.

Samples for which $PM_{2.5}$ were not available or below aero, or for which $PM_{2.5}$ had error flag were excluded from data set. Samples for which eight carbon fractions were not available were also excluded. To obtain reasonable model fit, the fireworks sample collected on July 5, 2003 was excluded in this study. Overall, 11.4 % of the original data were not included in this study. SO_4^{2-} was not included and only S was used in this study because they showed good correlations ($slope = 2.9 \pm 0.02$, $r^2 = 0.97$). The OP was subtracted from EC1 and utilized as an independent variable.

Thus, EC1 in this study did not include OP. Chemical species that have missing values more than 80 % or below MDL values more than 90 % were excluded. The chemical species that have S/N ratio below 0.2 (defined as bad variables) were not included in this study. A total of 293 samples collected between August 2001 and May 2004 and 33 species including $PM_{2.5}$ were used in this study. The estimated uncertainties of species that have S/N ratio between 0.2 and 2 (weak variable) and species that have below MDL values more than 50 % were increased by a factor of five and a factor of three, respectively, to reduce their weight in the solution. The estimated uncertainties of OC1 were increased by a factor of three to reduce the influence of the positive artifact from the adsorption of gaseous OC. The estimated uncertainties of EC1 were increased by a factor of three to account for the additional uncertainty from the subtraction of OP. Table 17 provides a summary of $PM_{2.5}$ speciation data and S/N ratios.

An eight-source model with $FPEAK = 0$ and a $FKEY$ matrix provided the most interpretable solution. For the $FKEY$ matrix, values of all elements were set to zero, except for a value of 1 for NO_3^- in wood smoke. The average source contributions of each source to the $PM_{2.5}$ mass concentrations are provided in Table 18. The resolved sources effectively reproduce the measured values and account for most of the variation in the $PM_{2.5}$ mass concentrations as shown in the comparisons of the daily reconstructed $PM_{2.5}$ mass contributions from all sources with measured $PM_{2.5}$ mass concentrations ($slope = 0.86 \pm 0.02$ and $r^2 = 0.91$ in Figure 57). The averaged seasonal contributions are compared (summer: April - September; winter: October - March) in Figure 58. Source profiles, source contributions, weekday/weekend variations, and CPF plots are presented in Figures 59, 60, 61, and 62.

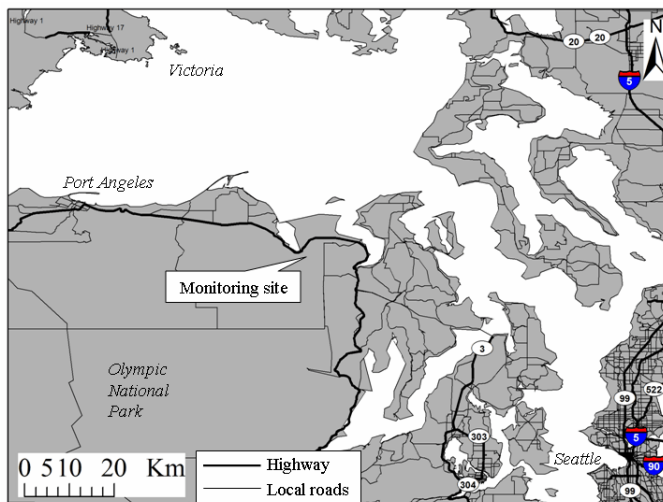


Figure 56. Map showing the location of the Olympic National Park IMPROVE sampling site.

Table 17. Summary of PM_{2.5} species mass concentrations at the Olympic National Park site.

Species	Arithmetic mean (µg/m ³)	Geometric mean (µg/m ³)	Minimum (µg/m ³)	Maximum (µg/m ³)	Number of below MDL values (%)	S/N ratio
PM _{2.5}	2.7795	2.2987	0.3426	7.7906	0	NA ¹
OC1	0.0522	0.0414	0.0015	0.5532	62.2	0.9
OC2	0.1172	0.0879	0.0015	0.5988	31.3	5.0
OC3	0.3780	0.2754	0.0151	1.8620	18.4	15.2
OC4	0.2141	0.1765	0.0357	0.8734	4.1	107.1
OP	0.0812	0.0594	0.0030	0.3180	26.2	7.1
EC1	0.0984	0.0744	0.0061	0.3774	17.0	14.3
EC2	0.0409	0.0325	0.0030	0.1203	27.9	6.8
EC3	0.0107	0.0082	0.0030	0.0398	75.5	0.4
S	0.2204	0.1640	0.0155	0.7787	0	NA ¹
NO ₃ ⁻	0.2746	0.2018	0.0006	1.9144	3.1	331.7
Al	0.0237	0.0140	0.0018	0.3040	73.5	2.4
As	0.0002	0.0002	0.0001	0.0007	36.4	3.5
Br	0.0012	0.0009	0.0001	0.0043	0	NA ¹
Ca	0.0110	0.0081	0.0006	0.0850	3.1	1846.7
Cl	0.1066	0.0288	0.0004	0.8302	70.1	83.3
Cr	0.0002	0.0001	0.0000	0.0038	52.7	1.1
Cu	0.0003	0.0002	0.0000	0.0017	15.3	37.6
Fe	0.0082	0.0049	0.0003	0.1504	0	NA ¹
H	0.1238	0.1053	0.0160	0.4091	0	NA ¹
K	0.0196	0.0165	0.0028	0.1105	0.3	16764.9
Mg	0.0255	0.0211	0.0081	0.0845	79.3	0.4
Mn	0.0004	0.0002	0.0000	0.0031	19.0	8.1
Na	0.1633	0.1212	0.0113	0.9798	63.6	2.1
Ni	0.0004	0.0003	0.0000	0.0017	11.2	84.6
Pb	0.0008	0.0006	0.0001	0.0065	3.1	592.2
Rb	0.0001	0.0001	0.0001	0.0005	46.6	2.3
Se	0.0001	0.0001	0.0000	0.0006	23.5	13.6
Si	0.0375	0.0263	0.0021	0.6097	23.5	75.9
Sr	0.0002	0.0001	0.0000	0.0010	29.6	7.8
Ti	0.0011	0.0007	0.0000	0.0150	20.7	23.1
V	0.0013	0.0009	0.0000	0.0058	12.6	58.2
Zn	0.0027	0.0021	0.0002	0.0128	0	NA ¹

¹ not available(infinite S/N ratio caused by no below MDL value)

Secondary sulfate has a high concentration of S and NH_4^+ accounts for 21 % of the $\text{PM}_{2.5}$ mass concentration. It contributed the most at this northwestern rural area. It also has relatively high OC4 and OP concentrations. Secondary sulfate aerosols typically become associated with secondary OC and tracer elements and this is consistent with observations (Liu et al., 2003). Secondary sulfate shows a strong seasonal variation with higher concentrations in summer when the photochemical activity is highest as shown in Figure 58, 68, 108.

Oil combustion is characterized by high concentrations of OC carbon fractions and S, and tracer elements Ni, and V reflecting residual oil combustion for the utilities and industries. This source contributed 19 % to the $\text{PM}_{2.5}$ mass concentrations. Oil combustion shows a strong summer-high seasonal variation and weekend-high variation. As shown in Figure 62, 72, 112, the CPF plot points to northwest and north suggesting the sources of the oil combustion are likely residual oil burning ships and ferries that show increased activities on weekend in summer.

Motor vehicle emissions were identified by higher concentrations of OC and EC (Watson et al., 1994). It contributed 18 % of the $\text{PM}_{2.5}$ mass concentrations. In Figures 58, 68, 108 and 61, 71, 111, motor vehicle emissions show weak summer-high seasonal variation and weekend-high variation also indicating increased activities in this area on weekend in summer.

Wood smoke is characterized by has large amount of lower temperature carbon fractions, especially OC3 and OC4, and K contributing 13 % to the $\text{PM}_{2.5}$ mass concentration. Wood smoke has a winter-high seasonal trend shown in Figure 58, 68, 108. In Figure 60, 70, 110, there are continuous wood smoke contributions between October 2002 and January 2003 that is consistent with the results from the analysis of the Beacon Hill IMPROVE data presented later in this report. Wood smoke does not show any weekday/weekend variation. The CPF plot for wood smoke points to the northeast and southeast as major source directions.

Sea salt is identified by its high concentration of Na^+ and Cl^- , accounting for 10% of the $\text{PM}_{2.5}$ mass concentration. This source shows a strong summer-high seasonal pattern, and does not show weekday/weekend variation. The CPF plot shows the contributions from the Strait of Juan De Fuca.

Secondary nitrate is separated by its high concentration of NO_3^- and NH_4^+ . It accounts for 10 % of the $\text{PM}_{2.5}$ mass concentration. The secondary nitrate aerosol has weak summer-high seasonal variation and does not show weekday/weekend variation. The CPF plot points the major contributions from north and east of the site.

Airborne soil is identified by Si, Fe, Al and Ca contributing 7 % to the $\text{PM}_{2.5}$ mass concentration. Crustal particles could be contributed by wind-blown soil dust and re-suspended by road traffic. In Figure 60, 70, 110, the elevated contribution at Olympic National Park on April 20, 2002 is consistent with the results from the STN data studies for Seattle and vicinity area and it was likely caused by Asian dust storm. Airborne soil has a strong seasonal variation with summer-high. This source does not show weekday/weekend variation. The CPF plot of airborne soil points to the northeast where Port Townsend is located.

In this study, it was possible to separate boat emissions. Boat emissions are identified by high carbon fractions, S, NO_3^- , K, Ca, and Zn. As shown in Figures 61, 71, 111 and 62, 72, 112, the strong weekend-high variation and the major source direction of northeast suggest that this is the emissions from two-stroke engine used for the commercial and recreational boats. Ca and Zn might come from the engine lubricant oil and have been seen in other studies (Kim and Hopke, 2005).

Table 18. Average source contributions ($\mu\text{g}/\text{m}^3$) to $\text{PM}_{2.5}$ mas concentration at the Olympic National Park site.

Sources	Average source contribution (%)
Secondary sulfate	0.54 (20.7)
Oil combustion	0.50 (19.3)
Motor vehicle	0.47 (18.0)
Wood smoke	0.33 (12.9)
Sea salt	0.25 (9.7)
Secondary nitrate	0.25 (9.5)
Airborne soil	0.18 (6.8)
Boat	0.08 (3.2)

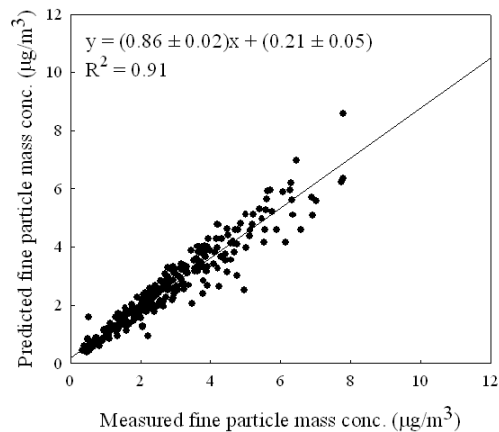


Figure 57. Measured versus PMF predicted $\text{PM}_{2.5}$ mass concentrations at the Olympic National Park site.

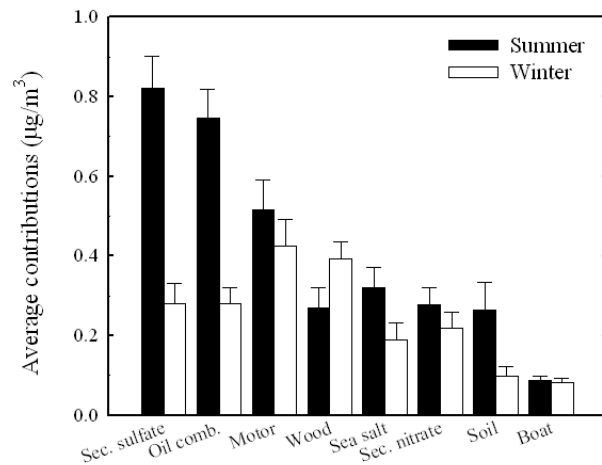


Figure 58. The seasonal comparison of source contributions to $\text{PM}_{2.5}$ mass concentration at the Olympic National Park site (mean \pm 95 % distribution).

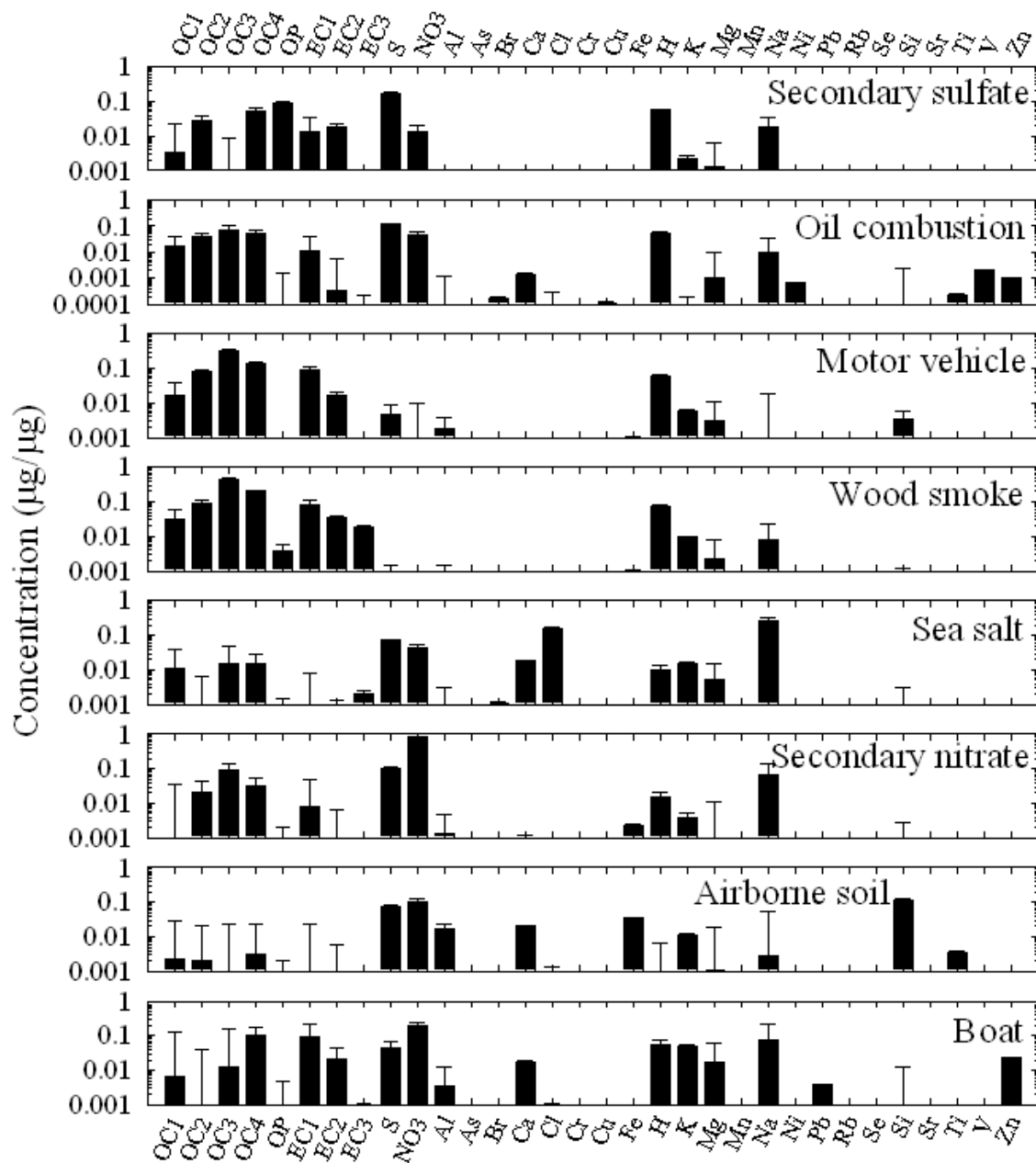


Figure 59. Source profiles deduced from PM_{2.5} samples measured at the Olympic National Park site (prediction \pm standard deviation).

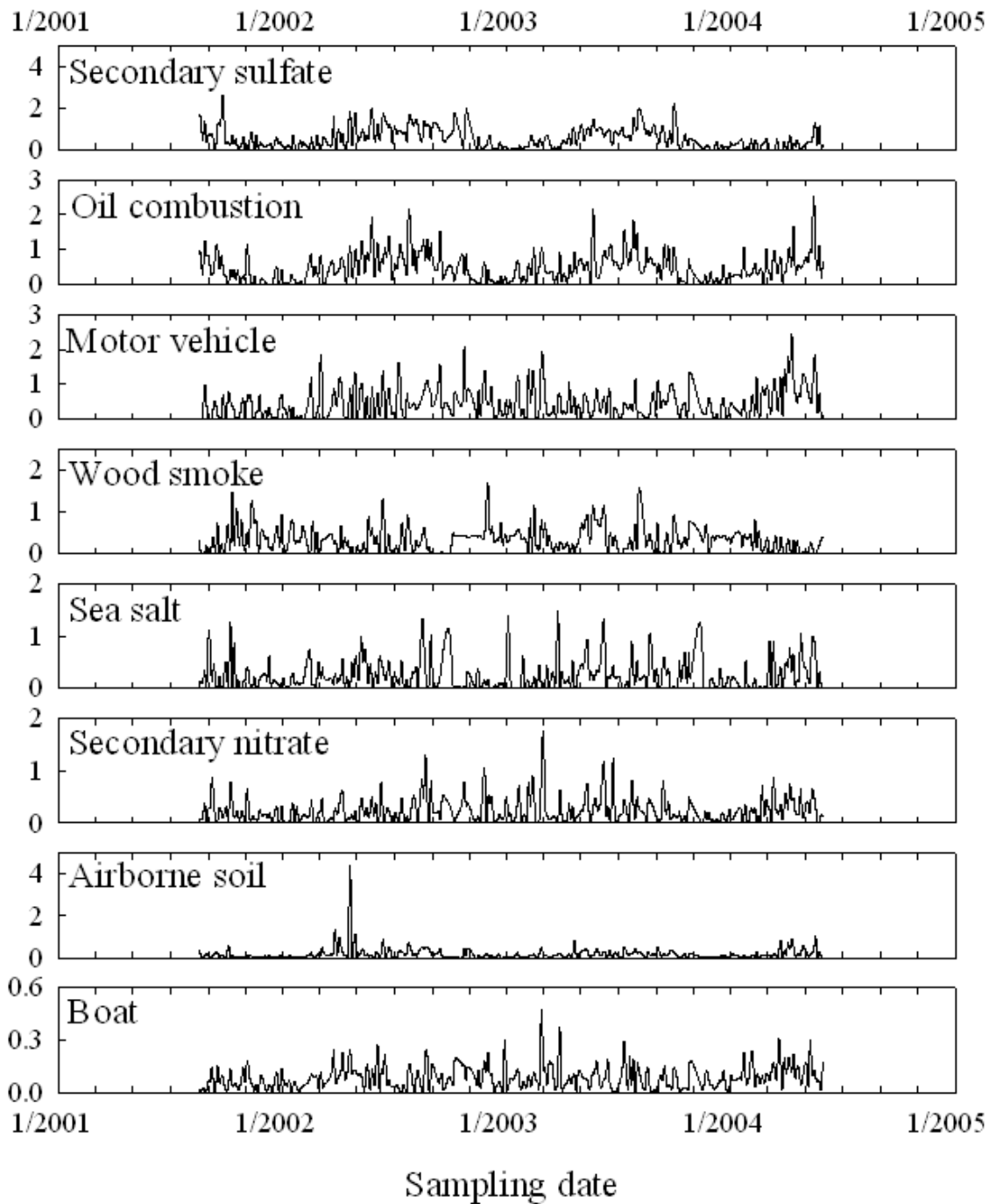


Figure 60. Time series plot of source contributions at the Olympic National Park site.

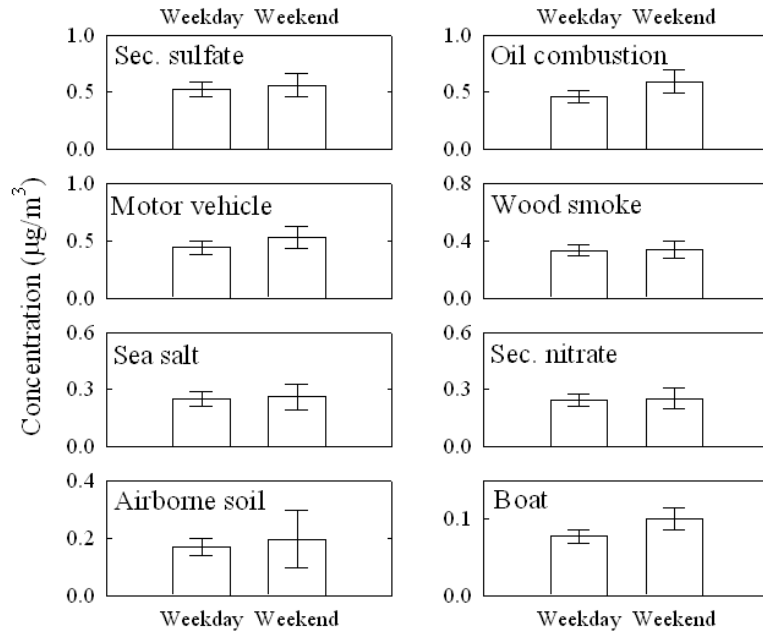


Figure 61. Weekday/weekend variations at the Olympic National Park site (mean \pm 95 % distribution).

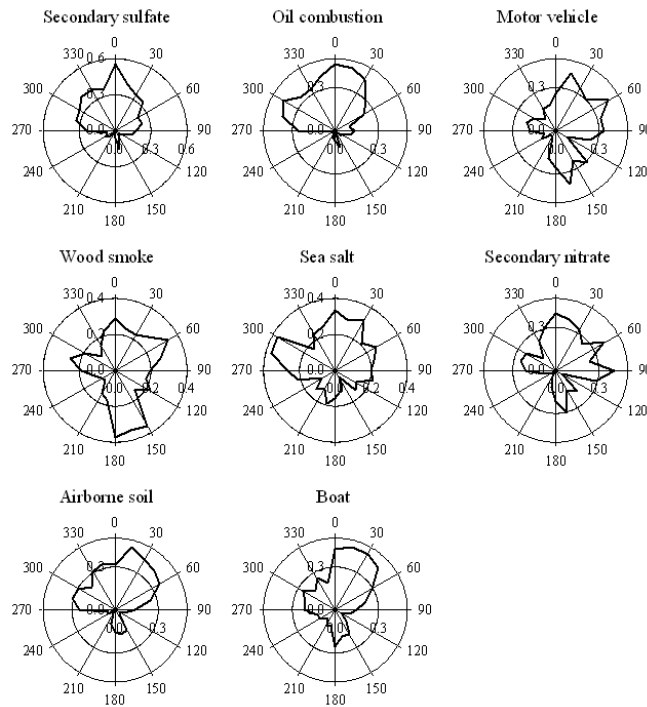


Figure 62. CPF plots for the highest 25 % of the mass contributions at the Olympic National Park site.

Effect of Changing Analytical Methodology on Ship Emissions Apportionment

On December 1, 2002, the IMPROVE network changed analytical methods from PIXE for elements with atomic numbers less than that of iron to Cu-anode XRF and eliminated the measurement of sodium by particle-induced gamma emission. This change substantially improved the sensitivity of the elemental analysis for many light elements, particularly those with atomic numbers around vanadium. To illustrate the effect of this change, Figure 63 shows a plot of the vanadium errors at Point Reyes National Seashore over the time frame of the analysis presented earlier in this report. The sharp decrease in these uncertainties following the change in analysis method can be clearly observed.

Since PMF weights the data points by a measure of the data point uncertainty, a study was made to examine the impact of this change in analysis method on the identification and apportionment of the residual oil combustion source. To explore the influence of this change, data from two IMPROVE sites, Point Reyes National Seashore and Aqua Tibia, have been reanalyzed in several different ways.

The following cases have been examined relative to the base case that was previously presented in this report.

Case 1: PIXE V and XRF V without down-weighting.

Case 2: PIXE V and XRF V with 2 times down-weighting of PIXE V.

Case 3-1: Data until Nov 30, 2001 with PIXE V.

Case 3-2: Data from Dec. 1, 2001 with XRF V.

Case 4. V uncertainties prior to Dec. 1, 2001 were increased by a factor of 2.

In Case 1, the V values were divided into two variables, PIXE V prior to 12/1/2001 with missing values for the rest of the samples and XRF V with missing values up to 12/1/2001 and actual values after that date. In case 2, the PIXE V uncertainties were doubled to give them less influence in the analysis. Case 3 separates the data set into two portions with separate analyses while Case 4 uses the same data as the base case (original analyses), but with the V uncertainties prior to 12/1/2001 doubled. The results for these two sites are as follows.

Aqua Tibia

Table 19 compares the vanadium concentrations in the source profiles derived from cases 1 and 2. It can be seen that essentially the same values were determined for both the PIXE and XRF V values both with and without additional downweighting of the PIXE V values. There is extremely good correlation between the resulting contribution values for Cases 1 and 2 with the base case, but surprisingly the contributions are only about 2/3 of the base case values.

Figure 64 shows the pairwise comparisons of the resolved contributions for each of the cases considered. .

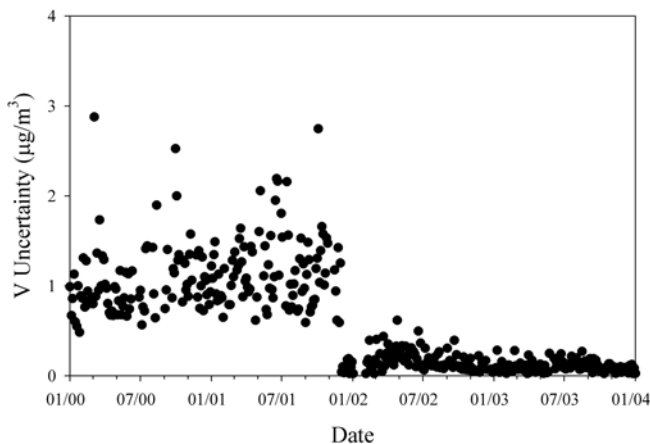


Figure 63. Uncertainties in the V concentrations measured at Point Reyes National Seashore as a function of the date on which the sample was collected.

Table 19. Comparison of the PIXE and XRF V values from the Case 1 and 2 analyses.

	PIXE_V		XRF_V	
	Concentration	Std Error	Concentration	Std Error
Aqua Tibia				
Case 1	0.0094	0.0014	0.0102	0.0005
Case 2	0.0089	0.0025	0.0110	0.0005
Point Reyes				
Case 1	0.0016	0.0002	0.0029	0.0001
Case 2	0.0019	0.0004	0.0035	0.0001

For Case 3, the data prior to the change in analytical method agree fairly well with the base case with a slope of 0.90, but with a much greater spread in the values ($r^2 = 0.66$). However, the data with the XRF vanadium produced much higher contributions (slope of 3.85 and an $r^2 = 0.91$). Although the mean V value was lower with the XRF values, more mass appears to correlate with this factor than with the presence of the PIXE values. This behavior is also seen in Case 4 where downweighting the PIXE V permits the XRF V to dominate sufficiently to push the slope up to 4.72 with an r^2 of 0.81. This results is quite surprising as it is difficult to understand how there can be this large a shift from the base case by this limited downweighting of the PIXE V values particularly in light of the Case 1 and 2 results.

Point Reyes

The same case designations have been used for the Point Reyes data. The concentrations of V in the profiles for cases 1 and 2 are also presented in Table 19. However, in this case, there is less variation in the results. Again Cases 1 and 2 are reduced from the base case although in this case to values more of the order of 3/4 of the original values rather than the 2/3 values in the prior case. In this case there is much more variability among the V concentrations in the profiles as compared to Aqua Tibia.

Figure 65 provides the pairwise comparisons of the contributions derived from the analyses of the data for the various cases with the base case contributions. Splitting the data set produced reduced contributions based on the PIXE V values and with more spread in the results. For Case 3-1, the slope is 0.79 with an $r^2 = 0.74$. The XRF V values produced a slope of 0.90 and an $r^2 = 0.92$. Thus, the elevated contributions observed for Aqua Tibia were not observed at Point Reyes. Case 4 also produce a slope of 0.69 similar to Cases 1 and 2 and an r^2 of 0.92.

Thus, in general, the intermixing of the PIXE and XRF vanadium values appear to overpredict the contribution of ship diesels with two anomalous cases for Aqua Tibia that need to be further explored.

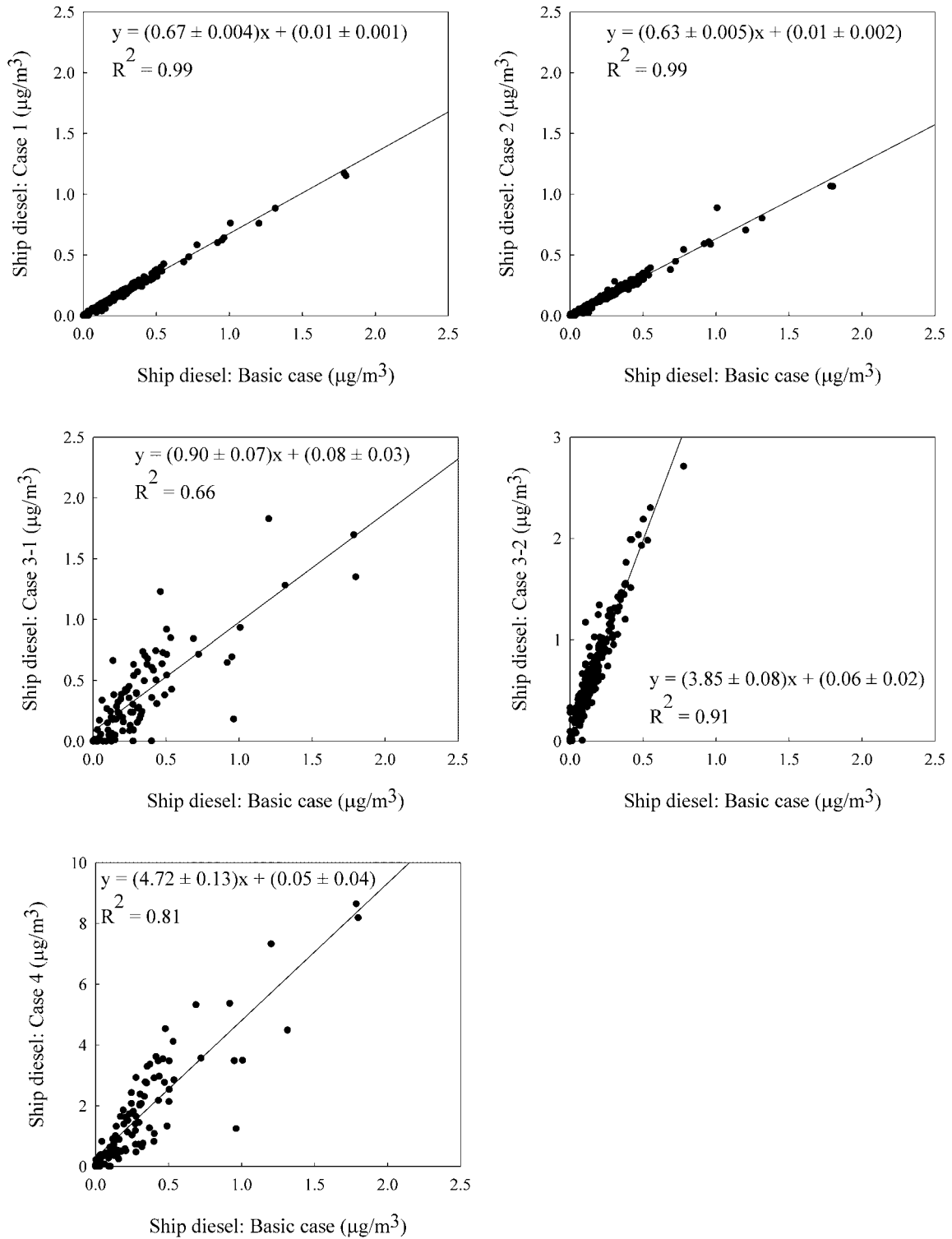


Figure 64. The pairwise comparisons of the contribution values derived from the Aqua Tibia data for the four defined cases.

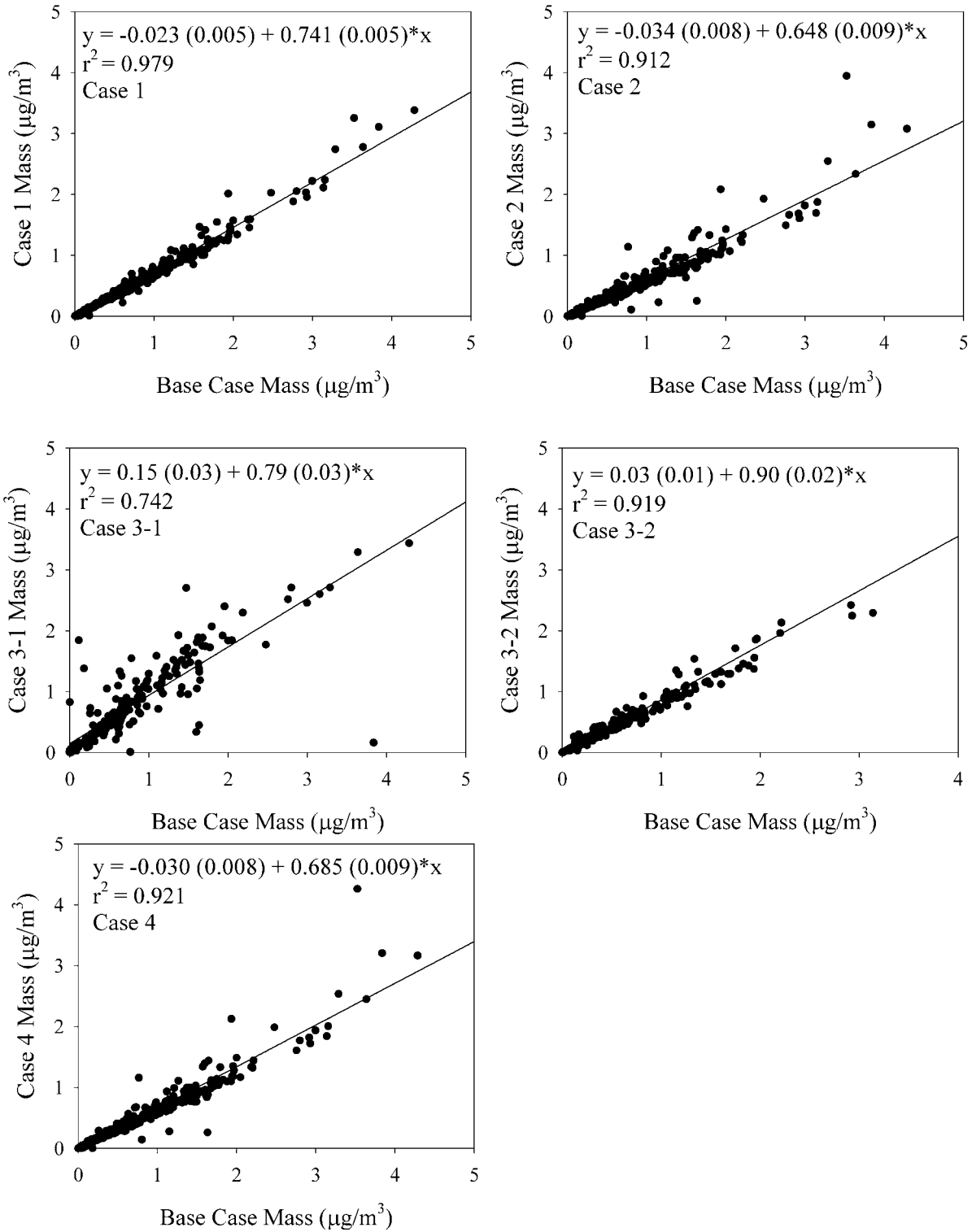


Figure 65. The pairwise comparisons of the contribution values derived from the Point Reyes data for the four defined cases.

STN Data

There are STN sites in Anchorage, Seattle, Portland, San Jose, Los Angeles, and San Diego. The data from the EPA's Speciation Trends Network (STN) presents some major challenges because of the way the sample analyses have been performed. We have been analyzing a number of STN data sets from samples collected in the eastern and mid-western US using PMF2 and ME2. This extensive experience with OC blank correction, error estimations, and source apportionment provided us with unique experience with respect to handling the STN data.

Concentrations of EC (element carbon), OC (organic carbon) and OCX were reported for the PM_{2.5} samples before July 2003. EC, OC and temperature-resolved carbon fractions, OC peak 1 (maximum temperature 310°C), OC peak 2 (480°C), OC peak 3 (615°C), OC peak 4 (900°C) and pyrolyzed carbon have been reporting since July 2003. Total EC and OC were selected here for analysis. Sampled nylon filters were analyzed for three cations (NH₄⁺, K⁺ and Na⁺) and two anions (NO₃⁻ and SO₄²⁻) analysis using Ion Chromatography (IC). The Teflon filters are analyzed for mass loading and elemental analysis. The mass concentrations are determined using gravimetry. Concentrations of 48 elements are analyzed using X-ray fluorescence (XRF). Blank values and error estimations were estimated using the procedures outlined in Kim *et al.* (2005).

Anchorage, AK

The analyzed PM_{2.5} samples were collected on a one-in-three day schedule at Garden monitoring site located in Anchorage, AK. The site is located at 61.2067N latitude and 149.8208W longitude with sampling occurring from February 2002 to November 2003. The site location is shown in Figure 66. The Garden monitoring site is located at the church parking lot within residential area about 9 km northeast of the Anchorage International Airport. Highway AK-1 is situated west and north of the site. The Port of Anchorage and an Air Force Base are situated 5 km northwest and 4 km north of the site, respectively. Wind data measured at the Merrill Municipal Airport located about 200 m northwest of the site were used in this study.

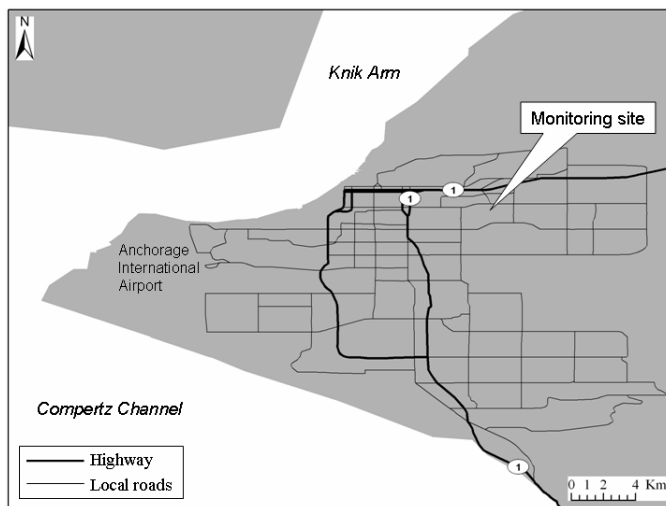


Figure 66. Location of the three STN monitoring sites.

The estimated OC blank value, 0.87 µg/m³ was estimated utilizing the intercept of the regression of OC concentrations against PM_{2.5} mass concentrations and the STN OC concentrations in this report were blank corrected by subtracting the estimated OC blank concentration. A comprehensive set of error structures estimated by Kim *et al.* (2005) was used for this source apportionment study. Samples for which PM_{2.5} or OC data were not available or below detection limits, or for which PM_{2.5} or OC mass concentration had error flag were excluded from data set. The samples collected on July 4, 2002, December 31, 2002, and July 5, 2003 were highly influenced by fireworks and were excluded from this study. Overall, 26.8% of the data were not included in this study.

IC SO₄⁻ was excluded from the analyses to prevent double counting of mass concentrations since XRF S and IC SO₄²⁻ showed a good correlation (*slope* = 2.7, *r*² = 0.73). Because of the higher analytical precision of IC Na⁺ and IC K⁺ compared to XRF Na and XRF K, the IC variables were included in the analyses. Chemical species that have below MDL

values for more than 90% of the samples were excluded. Thus, a total of 150 samples and 25 species including PM_{2.5} mass concentrations in samples collected between 2002 and 2003 were used. A summary of PM_{2.5} speciation data and S/N ratios are provided in Table 20.

A seven-source model with a value of FPEAK = 0.1 provided the most physically reasonable source profiles at the Garden monitoring site. In addition, it was found necessary to increase the estimated uncertainties of NH₄⁺ and Cu by a factor of 3. The average source contributions of each source to the PM_{2.5} mass concentrations are provided in Table 21. Comparisons of the daily reconstructed PM_{2.5} mass contributions from all sources with measured PM_{2.5} mass concentrations shows that the resolved sources effectively reproduce the measured values and account for most of the variation in the PM_{2.5} mass concentrations in Figure 67. In Figure 68, the averaged seasonal contributions from each source are compared (summer: April - September; winter: October - March). The source profiles, corresponding source contributions, weekday/weekend variations, and CPF plots are presented in Figures 69, 70, 71, and 72, respectively.

Table 20. Summary of PM_{2.5} species mass concentrations at Garden site.

Species	Arithmetic mean (µg/m ³)	Geometric mean (µg/m ³)	Minimum (µg/m ³)	Maximum (µg/m ³)	Number of below MDL values (%)	S/N ratio
PM _{2.5}	6.3807	5.8538	2.9000	18.9000	0	NA [†]
OC	2.7502	2.2430	0.2109	11.0309	0.7	1691.4
EC	0.6826	0.5936	0.0237	2.3500	2.7	104.5
S	0.2011	0.1751	0.0335	0.6980	0	NA
NO ₃ ⁻	0.4894	0.3840	0.0388	2.3900	0	8374.7
NH ₄ ⁺	0.2100	0.1473	0.0064	0.8800	10.0	108.3
Al	0.0433	0.0266	0.0013	0.2020	58.7	2.5
Ba	0.0241	0.0230	0.0002	0.0851	79.3	0.3
Br	0.0024	0.0018	0.0001	0.0164	51.3	1.7
Ca	0.0261	0.0208	0.0005	0.1250	4.7	106.7
Cl	0.0250	0.0113	0.0001	0.1850	68.7	2.5
Cr	0.0018	0.0013	0.0001	0.0272	74.0	0.7
Cu	0.0066	0.0045	0.0001	0.0207	28.7	10.7
Fe	0.0623	0.0510	0.0081	0.2920	0.7	4640.8
K ⁺	0.0844	0.0813	0.0484	0.1150	94.7	0.3
Mn	0.0017	0.0015	2.0·10 ⁻⁵	0.0054	72.7	0.6
Na ⁺	0.1368	0.0861	0.0044	0.7650	24.7	15.6
Ni	0.0010	0.0009	1.0·10 ⁻⁵	0.0098	86.7	0.3
Pb	0.0056	0.0042	0.0001	0.0365	60.7	1.2
Si	0.1177	0.0808	0.0074	0.6730	2.0	706.4
Sn	0.0135	0.0119	0.0006	0.0489	86.0	0.3
Ta	0.0099	0.0099	0.0002	0.0416	84.0	0.4
Ti	0.0058	0.0045	0.0004	0.0194	36.0	4.0
V	0.0012	0.0013	0.0001	0.0046	92.7	0.1
Zn	0.0087	0.0062	0.0002	0.0372	20.7	19.1

¹ not available(infinite S/N ratio caused by no below MDL value)

Gasoline vehicle and diesel emissions were separated by different abundances of OC and EC (Watson et al., 1994). Gasoline vehicles emissions have high concentration of the OC. In contrast, diesel emissions were tentatively identified on the basis of the high concentration of EC. Gasoline vehicle contributed the most accounting for 44% of the PM_{2.5} mass concentrations at Garden site. The average contributions from diesel emissions to PM_{2.5} mass concentration were 5%. Gasoline vehicle and diesel emissions show weak winter-high seasonal variations (Figure 58, 68, 108). As shown in Figure 61, 71, 111, gasoline vehicle and diesel emissions show weak weekend-high variations that can be explained by the elevated impacts on weekends from the vehicle emissions from the church parking lot. As a main source direction, the CPF plots point east for the gasoline vehicle and southeast and southwest for the diesel emissions. Diesel emissions extracted by PMF may represent only diesel vehicle emissions moving at reasonable speed in fluid traffic. Diesel emissions operating at very slow speeds and in stop and go traffic are likely to be apportioned into the gasoline emission category (Shah *et al.*, 2004).

Table 21. Average source contributions ($\mu\text{g}/\text{m}^3$) to PM_{2.5} mas concentration.

Sources	Average source contribution (%)
Gasoline vehicle	2.66 (43.5)
Secondary nitrate	0.91 (14.9)
Secondary sulfate	0.89 (14.6)
Unknown	0.67 (11.0)
Sea salt	0.33 (5.4)
Diesel emissions	0.33 (5.3)
Airborne soil	0.32 (5.2)

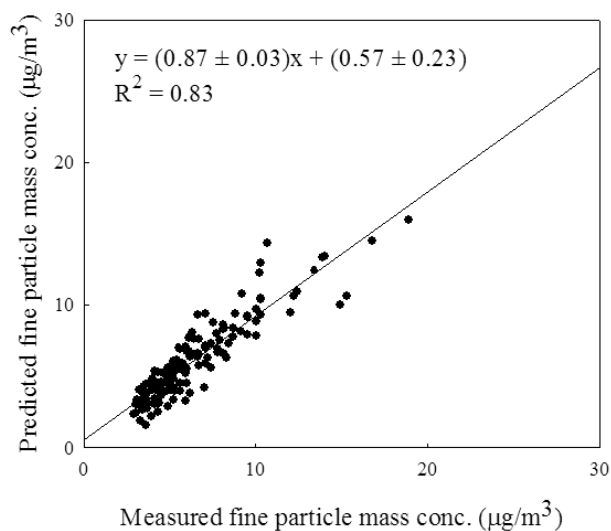


Figure 67. Measured versus PMF predicted PM_{2.5} mass concentrations.

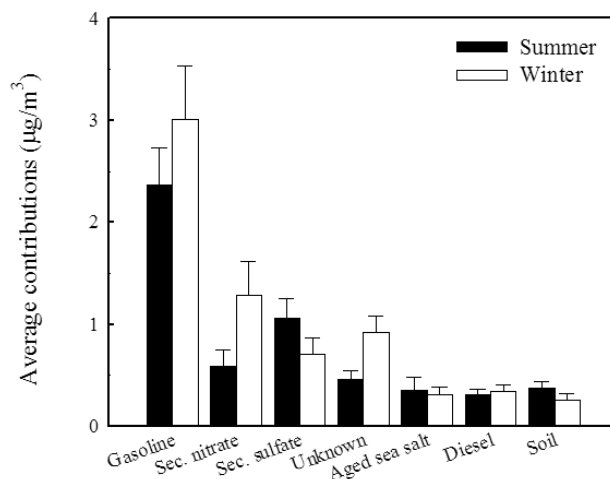


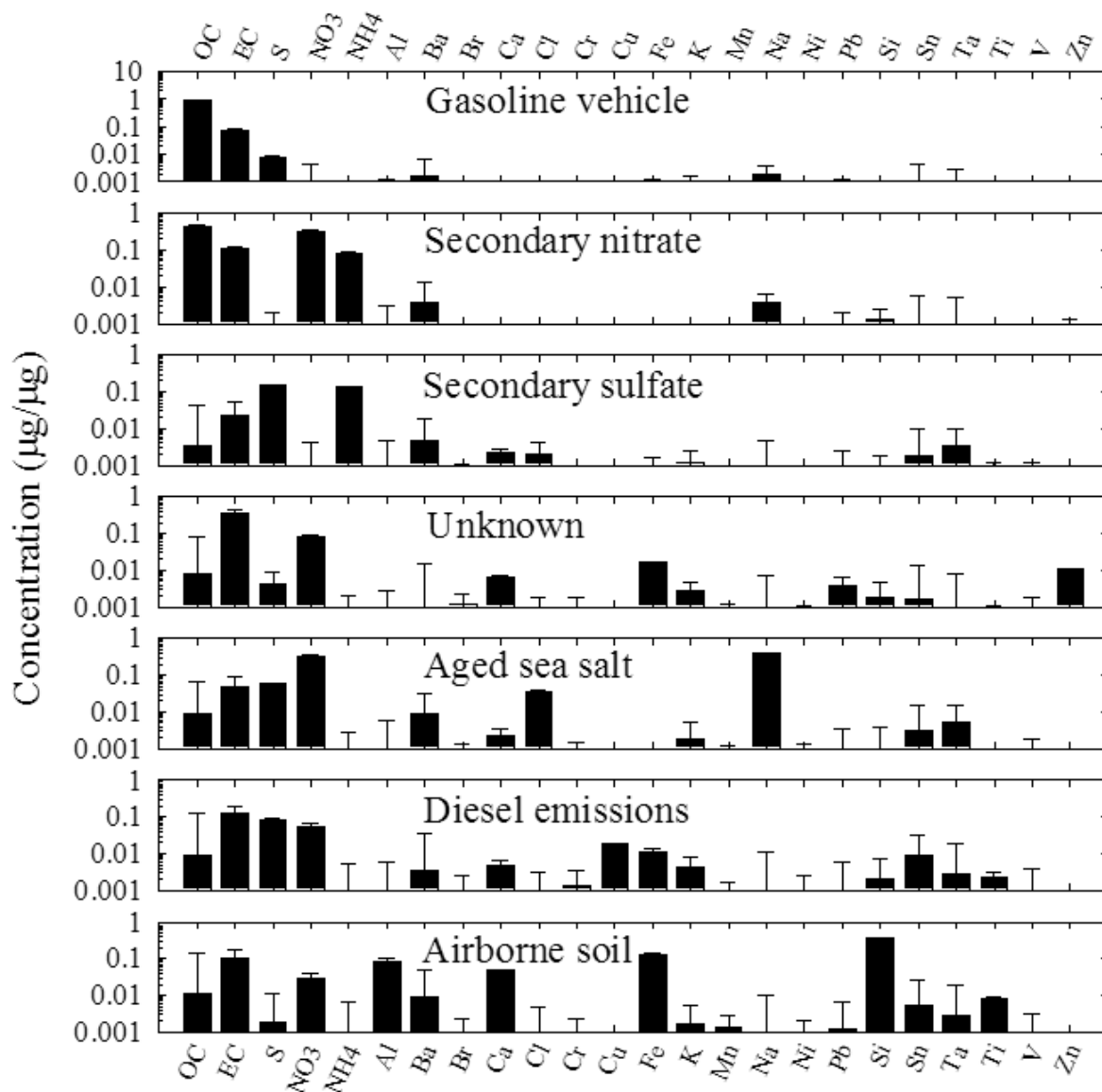
Figure 68. The seasonal comparison of source contributions to PM_{2.5} mass concentration (mean \pm 95% distribution).

Secondary nitrate aerosol is represented by its high concentration of NO₃⁻ and NH₄⁺. It accounts for 15% of the PM_{2.5} mass concentration. The secondary nitrate aerosol has seasonal

variation with maxima in winter as shown in Figure 72. These peaks in winter indicate that low temperature and high relative humidity help the formation of secondary nitrate particles. In Figure 76, the CPF plot for the secondary nitrate aerosol points east as a main source direction that is consistent with the main source direction of the gasoline vehicle.

Secondary sulfate aerosol has a high concentration of S and NH_4^+ account for 15% of the $\text{PM}_{2.5}$ mass concentration at Garden site. Secondary sulfate shows seasonal variation with higher concentrations in summer when the photochemical activity is highest.

The unknown source has high EC, NO_3^- , Fe, Zn, Ca, and Pb concentrations accounting for 1% of the $\text{PM}_{2.5}$ mass concentration. This source shows strong winter-high variation and has high impacts from northwest. This source is likely to include contributions from metal processing or incinerator. However, such sources were not identified in Anchorage area and it requires additional investigation.



1

Figure 69. Source profiles deduced from PM_{2.5} samples measured at Garden monitoring site (prediction ± standard deviation).

Sea salt is characterized by its high concentration of Na⁺ and NO₃⁻. Since there is a significant Cl⁻ concentration in the profile, it appears that this profile represents an admixture of fresh sea salt with aged marine aerosol. The reduction of Cl⁻ from the value it would have in fresh sea salt is caused by Cl⁻ displacement by acidic gases during the transport. Sea salt accounts for 5% of the PM_{2.5} mass concentrations.

Airborne soil is identified by Si, Fe, Al and Ca contributing 5% to the PM_{2.5} mass concentration. Airborne soil has a summer-high seasonal variation. The weekday-high variation in Figure 75 suggests that airborne soil identified at Garden site could be mainly re-suspended crustal materials by road traffic. It does not appear that there was significant influence of Asian dust events that were seen at more southerly sites.

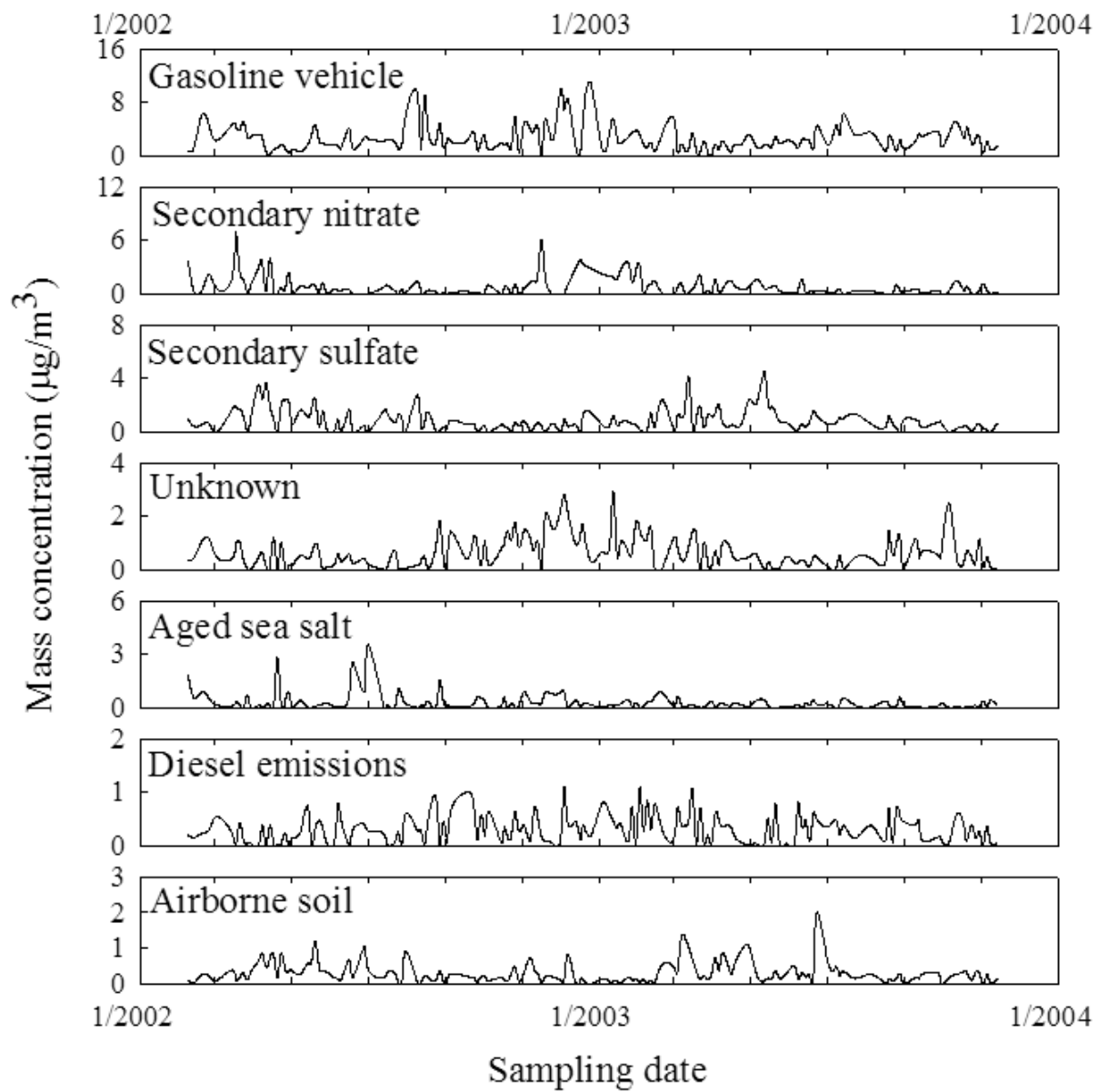


Figure 70. Time series plot of source contributions at Garden monitoring site.

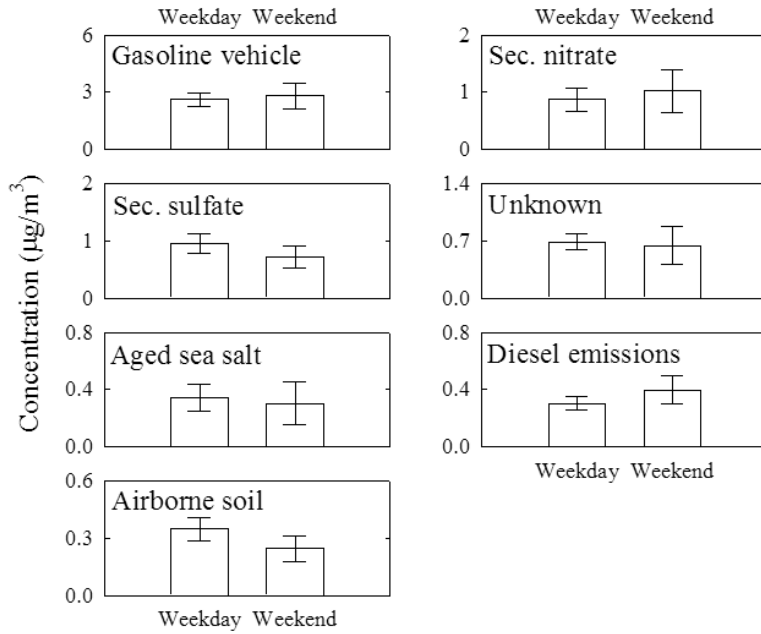


Figure 71. Weekday/weekend variations at Garden monitoring site (mean \pm 95% distribution).

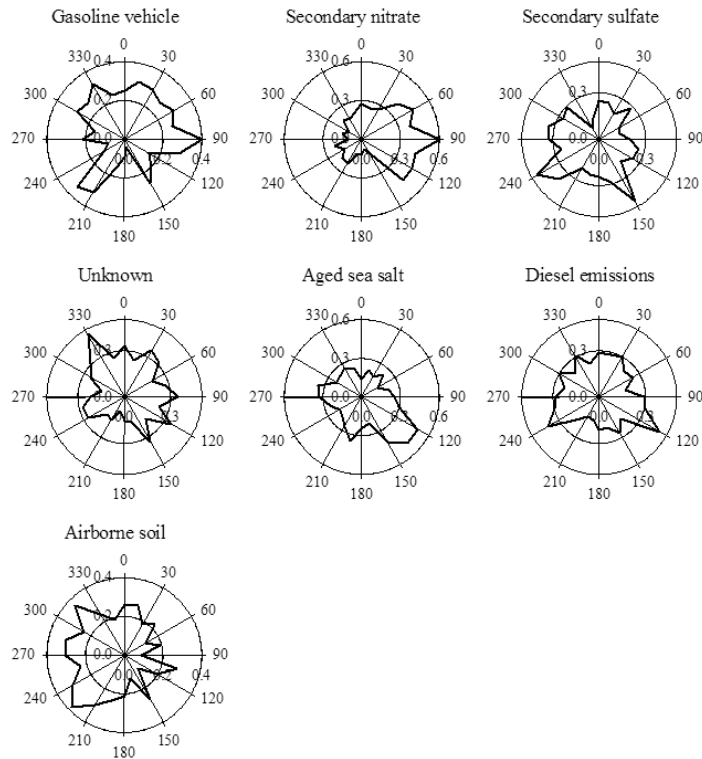


Figure 72. CPF plots for the highest 25% of the mass contributions at Garden monitoring site.

Seattle, WA

The analyzed PM_{2.5} samples were collected on a one-in-six day schedule at the four STN monitoring sites (Lake Forest, Olive St., Duwamish, Georgetown) and a one-in-three day schedule at Beacon Hill monitoring sites located in Seattle, WA and vicinity area as shown in Figure 73. The Lake Forest monitoring site is located 20 km north of the downtown Seattle. The area to the north and west of the site is residential. Local roads are closely situated to the southeast and northeast of the site. Olive St. monitoring site is located at downtown Seattle. Highway 5 is situated close to the east of the site. Beacon Hill monitoring site is located on a hilltop, 99 m above sea level. The monitoring site is located 5 km southeast of the downtown Seattle. The area to the immediate north and east is residential. The hill is part of a larger ridge defining the eastern edge of an industrialized valley. Highways 90 and 5 are situated about 2 km north and 1 km west of the site, respectively. Duwamish and Georgetown monitoring sites are located within the industrial area 6 km and 8 km south of the downtown Seattle, respectively. The Port of Seattle, container shipping, and warehousing areas are located north, northwest, and west of the sites. Highways 5 and 99 are situated close of the sites. Wind data measured at the each site were used except for the Olive St. and Georgetown sites. For the Olive St. and Georgetown sites, wind data measured at the Beacon Hill and Duwamish sites were used in this study, respectively. The summary of five monitoring sites and sampling periods used in the analyses are shown in Table 22. The intercepts in PM_{2.5} regression against OC concentration are considered to be integrated OC blank concentrations as shown in Table 23. The STN OC concentrations in this report were blank corrected by subtracting the estimated OC blank concentrations. Errors for the source apportionment was estimated by procedure proposed by Kim *et al.* (2005).

For the PMF analysis, samples for which PM_{2.5} or OC data were not available or below zero, or for which PM_{2.5} or OC mass concentration had error flag were excluded from data set. To obtain a reasonable fit, the fireworks samples collected at Beacon Hill site on July 5, 2000, January 1, 2001, July 4, 2002, and July 5, 2003 in which K, Ba, Ca, Cu, Pb, and Sr concentrations were unusually high were excluded in this study. For the Georgetown data, the fireworks sample on January 1, 2001 in which K and Sr mass concentrations were high was excluded. Overall, 11.1% of the original Lake Forest data, 4.5% of the Olive St. data, 9.4% of the Beacon Hill data, 9.4% of the Duwamish data, and 20.3% of the Georgetown data were excluded from this study.

Since XRF S and IC SO₄²⁻ showed good correlations (*slope* = 2.5, *r*² = 0.93 for Lake Forest data; *slope* = 2.5, *r*² = 0.97 for Olive St. data; *slope* = 2.7, *r*² = 0.96 for Beacon Hill data; *slope* = 2.5, *r*² = 0.95 for Duwamish data; *slope* = 2.7, *r*² = 0.97 for Georgetown data), IC SO₄²⁻ was excluded from the analysis to prevent double counting of mass concentrations. Also, IC Na⁺ and IC K⁺ having higher analytical precision were chosen over XRF Na and XRF K. Chemical species that have >90% below MDL values were excluded. For Beacon Hill, the mass concentrations of Ba, Ce, Cu, Eu, Ga, and La show step changes on March 2002 caused by a change of the analytical lab. Those chemical species were excluded from the analysis for the Beacon Hill data. Thus, a total of 185 samples and 30 species, 128 samples and 35 species, 546

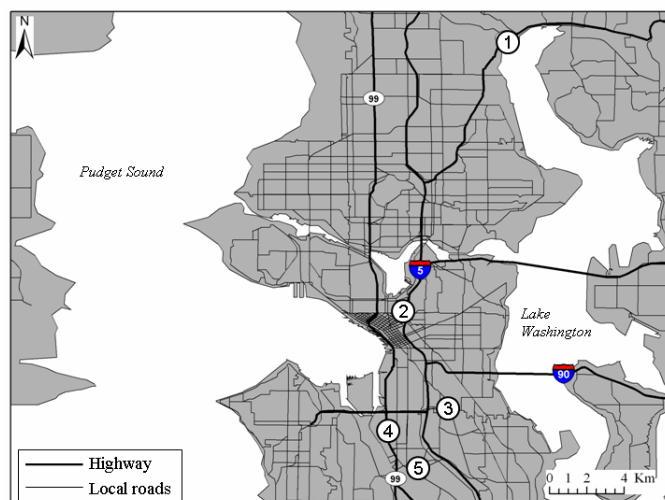


Figure 73. Location of the STN monitoring sites: 1. Lake Forest, 2. Olive St., 3. Beacon Hill, 4. Duwamish, and 5. Georgetown.

samples and 28 species, 154 samples and 35 species, and 235 samples and 32 species including PM_{2.5} mass concentrations collected between 2000 and 2005 were used for the Lake Forest, Olive St., Beacon Hill, Duwamish, and Georgetown, respectively.

Table 22. Summary of STN sites in Seattle, Washington

AIRS code	Monitoring site	Sampler	Latitude	Longitude	sampling period
530330024	Lake Forest	RASS ¹	47.7533	-122.2772	Oct. 2001 - Mar. 2005
530330048	Olive St	RASS	47.3699	-122.1978	Jan. 2003 - Mar. 2005
530330080	Beacon Hill	MASS ²	47.5697	-122.3125	Feb. 2000 - Mar. 2005
530330057	Duwamish	RASS	47.5633	-122.3383	Jun. 2002 - Mar. 2005
530330032	Georgetown	RASS	47.5456	-122.3222	May 2000 - Oct. 2004

¹ Reference Ambient Air Sampler (Andersen Instruments, Smyrna, GA)

² Mass Aerosol Speciation Sampler (URG, Chapel Hill, NC)

Table 23. Summary of OC blank concentrations estimated from regression of PM_{2.5} mass concentrations against OC concentrations.

Monitoring site	OC blank (µg/m ³)
Lake Forest	0.51
Olive St	1.51
Beacon Hill	0.33
Duwamish	0.27
Georgetown	0.08

As recommended by Paatero and Hopke (2003), the estimated uncertainties of species that have *S/N* ratio between 0.2 and 2 (weak variable) and species that have below MDL values more than 50% were increased by a factor of five and a factor of three, respectively, to reduce their weight in the solution. The estimated uncertainties were increased by a factor of thirty for the samples for which mass concentration had error flags. In addition, to obtain physically reasonable PMF solution, it was found necessary to increase three times the estimated uncertainties of OC, EC, and NH₄⁺ (Lake Forest); OC, EC, and Zn (Olive St); OC and Zn (Georgetown).

The measured PM_{2.5} mass concentration was included as an independent variable in the PMF modeling to directly obtain the mass apportionment without the usual multiple regression. The utilization of PM_{2.5} mass concentration as a variable is specified in detail in Kim et al (2003). A summary of PM_{2.5} speciation data and *S/N* ratios are provided in Tables 24 to 28.

Table 24. Summary of PM_{2.5} species mass concentrations at Lake Forest.

Species	Arithmetic mean (µg/m ³)	Geometric mean (µg/m ³)	Minimum (µg/m ³)	Maximum (µg/m ³)	Number of below MDL values (%)	S/N ratio
PM _{2.5}	11.0336	8.9271	3.2512	45.2234	0	NA ¹
OC	4.4696	3.3972	0.0071	20.1851	1.6	1231.6
EC	0.9597	0.6623	0.0161	4.9700	8.6	49.0
S	0.4449	0.3785	0.0687	1.5397	0	NA
NO ³⁻	0.8395	0.6755	0.1660	4.4500	0	NA
NH ₄ ⁺	0.4231	0.2871	0.0015	2.1000	7.6	347.3
Al	0.0183	0.0101	0.0001	0.3140	65.4	2.0
As	0.0017	0.0013	1.7·10 ⁻⁵	0.0075	40.0	3.8
Ba	0.0125	0.0103	0.0005	0.0654	76.2	0.6
Br	0.0033	0.0022	3.3·10 ⁻⁵	0.0280	16.8	28.5
Ca	0.0247	0.0214	0.0027	0.1280	0	NA
Cl	0.1053	0.0392	0.0002	0.8840	22.7	117.4
Cr	0.0008	0.0006	4.6·10 ⁻⁵	0.0066	71.9	0.8
Cu	0.0034	0.0025	0.0001	0.0123	13.0	32.4
Fe	0.0531	0.0440	0.0086	0.2090	0	NA
Hh	0.0012	0.0011	0.0001	0.0055	87.6	0.2
K ⁺	0.1109	0.1007	0.0412	0.2700	54.1	7.4
Mg	0.0173	0.0112	0.0012	0.1180	75.1	1.0
Mn	0.0016	0.0011	0.0001	0.0108	43.2	3.4
Na ⁺	0.2592	0.1695	0.0166	1.6500	5.4	169.5
Ni	0.0009	0.0007	2.0·10 ⁻⁵	0.0047	50.3	2.3
Pb	0.0035	0.0026	4.7·10 ⁻⁵	0.0151	36.8	4.0
Se	0.0007	0.0006	4.6·10 ⁻⁵	0.0064	88.1	0.3
Si	0.0460	0.0326	0.0024	0.6990	2.7	332.2
Sn	0.0046	0.0046	3.0·10 ⁻⁵	0.0243	85.9	0.2
Sr	0.0008	0.0007	4.0·10 ⁻⁵	0.0068	81.1	0.4
Ta	0.0038	0.0039	3.4·10 ⁻⁵	0.0216	88.1	0.2
Ti	0.0036	0.0027	0.0002	0.0234	31.4	6.5
V	0.0023	0.0024	0.0001	0.0103	83.2	0.1
Zn	0.0095	0.0069	0.0006	0.0543	0.5	2212.7

¹ not available(infinite S/N ratio caused by no below MDL value)

Table 25. Summary of PM_{2.5} species mass concentrations at Olive St.

Species	Arithmetic mean (µg/m ³)	Geometric mean (µg/m ³)	Minimum (µg/m ³)	Maximum (µg/m ³)	Number of below MDL values (%)	S/N ratio
PM _{2.5}	10.6638	9.6537	4.1185	37.0663	0	NA ¹
OC	3.1958	2.7672	0.6451	12.7124	0	NA
EC	1.4178	1.2709	0.3380	3.6125	0	NA
S	0.4653	0.3945	0.1027	1.9244	0	NA
NO ³⁻	1.1966	0.9207	0.2020	5.2800	0	NA
NH ₄ ⁺	0.5785	0.4053	0.0253	2.5878	0	NA
Al	0.0152	0.0104	0.0001	0.0992	61.7	1.9
As	0.0013	0.0010	0.0001	0.0065	48.4	2.1
Ba	0.0149	0.0121	0.0002	0.0499	59.4	1.0
Br	0.0026	0.0021	0.0003	0.0123	13.3	27.1
Ca	0.0483	0.0437	0.0116	0.1414	0	NA
Cl	0.1468	0.0447	0.0003	2.4400	17.2	217.5
Cr	0.0014	0.0010	0.0001	0.0067	44.5	3.3
Cu	0.0066	0.0058	0.0013	0.0165	5.5	148.0
Eu	0.0051	0.0039	0.0001	0.0182	76.6	0.8
Fe	0.1355	0.1226	0.0368	0.3647	0	NA
Hg	0.0012	0.0011	0.0001	0.0054	85.9	0.2
K ⁺	0.0836	0.0772	0.0362	0.2309	66.4	3.3
Mg	0.0190	0.0132	0.0010	0.0932	70.3	1.2
Mn	0.0035	0.0024	4.0·10 ⁻⁵	0.0149	25.0	15.1
Na ⁺	0.2219	0.1545	0.0115	1.6500	4.7	169.7
Ni	0.0018	0.0013	4.6·10 ⁻⁵	0.0092	22.7	13.2
P	0.0035	0.0026	0.0001	0.0152	83.6	0.4
Pb	0.0036	0.0027	0.0002	0.0228	32.8	5.1
Sc	0.0004	0.0003	2.7·10 ⁻⁵	0.0024	89.8	0.0
Se	0.0008	0.0006	2.8·10 ⁻⁵	0.0120	87.5	0.4
Si	0.0511	0.0431	0.0045	0.2808	3.1	428.7
Sm	0.0028	0.0019	4.6·10 ⁻⁵	0.0101	86.7	0.4
Sn	0.0047	0.0047	2.0·10 ⁻⁵	0.0246	88.3	0.2
Sr	0.0013	0.0008	1.9·10 ⁻⁵	0.0320	61.7	1.4
Tb	0.0050	0.0032	0.0001	0.0184	89.8	0.4
Ti	0.0055	0.0043	0.0001	0.0219	14.1	27.0
V	0.0049	0.0037	0.0009	0.0271	55.5	1.1
Zn	0.0197	0.0168	0.0032	0.0575	0	NA
Zr	0.0018	0.0012	0.0002	0.0231	78.9	0.6

¹ not available(infinite S/N ratio caused by no below MDL value)

Table 26. Summary of PM_{2.5} species mass concentrations at Beacon Hill.

Species	Arithmetic mean (µg/m ³)	Geometric mean (µg/m ³)	Minimum (µg/m ³)	Maximum (µg/m ³)	Number of below MDL values (%)	S/N ratio
PM _{2.5}	8.8270	7.5664	1.5000	38.9400	0	NA ¹
OC	2.6760	2.1442	0.2075	10.9689	0.4	3001.4
EC	0.6541	0.5324	0.0002	2.7200	0.5	1218.9
S	0.4450	0.3712	0.0185	1.9100	0	NA
NO ₃ ⁻	0.7628	0.6126	0.1261	4.8200	0	119236.0
NH ₄ ⁺	0.4965	0.3764	0.0161	3.3200	0.2	40746.6
Al	0.0233	0.0110	3.8·10 ⁻⁵	0.2390	75.9	1.7
Br	0.0022	0.0018	3.0·10 ⁻⁵	0.0143	8.2	34.8
Ca	0.0280	0.0241	0.0047	0.1985	0	NA
Cl	0.0722	0.0225	4.3·10 ⁻⁵	1.7300	36.4	42.9
Cr	0.0018	0.0013	0.0001	0.0190	31.8	6.7
Fe	0.0553	0.0434	0.0013	0.3162	0	NA
K ⁺	0.0536	0.0436	0.0026	1.2844	37.8	15.5
Mg	0.0263	0.0139	0.0002	0.1680	79.3	1.2
Mn	0.0037	0.0021	2.0·10 ⁻⁵	0.0303	27.6	14.3
Mo	0.0021	0.0019	2.5·10 ⁻⁵	0.0114	85.9	0.3
Na ⁺	0.1470	0.1067	0.0048	1.1200	1.5	832.6
Ni	0.0024	0.0014	1.3·10 ⁻⁵	0.0323	24.7	15.9
Pb	0.0041	0.0031	3.4·10 ⁻⁵	0.0407	19.6	9.7
Sb	0.0061	0.0059	0.0001	0.0306	88.5	0.2
Se	0.0007	0.0006	7.4·10 ⁻⁶	0.0085	89.0	0.3
Si	0.0442	0.0319	0.0009	0.5220	5.7	155.5
Sn	0.0069	0.0058	1.3·10 ⁻⁶	0.0271	68.2	0.7
Sr	0.0010	0.0007	3.7·10 ⁻⁶	0.0397	69.3	0.7
Ta	0.0048	0.0045	4.8·10 ⁻⁵	0.0193	70.2	0.6
Ti	0.0032	0.0024	0.0001	0.0255	32.2	5.6
V	0.0042	0.0024	0.0001	0.0469	27.2	14.8
Zn	0.0097	0.0076	0.0008	0.0510	0.2	6672.3

¹ not available(infinite S/N ratio caused by no below MDL value)

Table 27. Summary of PM_{2.5} species mass concentrations at Duwamish.

Species	Arithmetic mean (µg/m ³)	Geometric mean (µg/m ³)	Minimum (µg/m ³)	Maximum (µg/m ³)	Number of below MDL values (%)	S/N ratio
PM _{2.5}	12.5112	10.8551	3.9000	45.6402	0	NA ¹
OC	5.0187	4.3018	1.3128	19.1842	0	NA
EC	1.4994	1.2105	0.1190	5.3800	0.6	1031.5
S	0.6092	0.5371	0.1630	2.2966	0	NA
NO ³⁻	1.1017	0.8258	0.1445	5.6600	0	5170.2
NH ₄ ⁺	0.5840	0.3948	0.0084	2.5607	1.9	816.5
Al	0.0273	0.0182	0.0002	0.2619	40.3	7.1
As	0.0021	0.0014	0.0001	0.0111	32.5	6.3
Ba	0.0142	0.0117	0.0002	0.0720	68.2	0.7
Br	0.0032	0.0024	4.6·10 ⁻⁵	0.0137	9.7	44.1
Ca	0.1760	0.1355	0.0265	0.8011	0	NA
Cl	0.1698	0.0650	0.0014	2.6200	14.3	307.1
Co	0.0006	0.0005	4.6·10 ⁻⁵	0.0031	87.7	0.3
Cr	0.0034	0.0021	4.6·10 ⁻⁵	0.0303	22.1	19.6
Cu	0.0079	0.0055	0.0004	0.0554	3.9	256.2
Eu	0.0069	0.0040	0.0001	0.0479	83.8	0.8
Fe	0.1690	0.1278	0.0084	0.7006	0	NA
Hg	0.0015	0.0012	4.6·10 ⁻⁵	0.0101	85.1	0.4
K ⁺	0.0931	0.0849	0.0368	0.2897	55.2	5.3
Mg	0.0202	0.0150	0.0009	0.0707	64.3	1.5
Mn	0.0108	0.0057	0.0001	0.1190	9.7	130.3
Mo	0.0037	0.0024	4.3·10 ⁻⁵	0.0256	80.5	0.7
Na ⁺	0.2903	0.2227	0.0144	1.6500	0.6	315.6
Ni	0.0038	0.0024	0.0002	0.0363	15.6	38.8
P	0.0068	0.0038	0.0001	0.0623	77.9	1.0
Pb	0.0074	0.0053	4.6·10 ⁻⁵	0.0352	13.0	34.1
Sb	0.0055	0.0056	4.6·10 ⁻⁵	0.0273	89.0	0.2
Se	0.0015	0.0009	4.6·10 ⁻⁵	0.0165	71.4	1.2
Si	0.0993	0.0803	0.0074	0.6156	0	NA
Sn	0.0086	0.0064	0.0004	0.1060	66.9	1.0
Sr	0.0015	0.0011	2.7·10 ⁻⁵	0.0071	40.3	2.9
Tb	0.0054	0.0029	4.6·10 ⁻⁵	0.0273	89.6	0.5
Ti	0.0064	0.0052	0.0002	0.0281	13.0	31.5
V	0.0073	0.0048	0.0002	0.0389	50.6	2.6
Zn	0.0254	0.0174	0.0022	0.1260	0	NA

¹ not available(infinite S/N ratio caused by no below MDL value)

Table 28. Summary of PM_{2.5} species mass concentrations at Georgetown.

Species	Arithmetic mean (µg/m ³)	Geometric mean (µg/m ³)	Minimum (µg/m ³)	Maximum (µg/m ³)	Number of below MDL values (%)	S/N ratio
PM _{2.5}	10.0479	8.5710	2.5000	43.7000	0	NA [†]
OC	4.1248	3.4768	0.8268	16.6218	0	NA
EC	1.0141	0.7608	0.0183	5.5500	4.3	105.9
S	0.4956	0.4118	0.0568	1.4500	0	NA
NO ³⁻	0.8507	0.6558	0.1308	5.2100	0	24911.7
NH ₄ ⁺	0.4873	0.3485	0.0021	2.2900	2.6	1047.3
Al	0.0257	0.0138	0.0002	0.3537	46.0	6.0
As	0.0018	0.0014	4.6·10 ⁻⁵	0.0088	37.0	4.4
Ba	0.0174	0.0144	0.0007	0.0527	54.5	1.4
Br	0.0034	0.0025	0.0001	0.0158	10.2	46.3
Ca	0.0527	0.0427	0.0079	0.5784	0	NA
Cl	0.1251	0.0361	0.0008	2.4000	20.9	151.8
Cr	0.0045	0.0022	0.0001	0.1186	20.0	29.3
Cu	0.0071	0.0038	0.0002	0.1800	8.9	100.3
Eu	0.0078	0.0043	0.0002	0.0754	85.1	0.7
Fe	0.1609	0.1082	0.0048	2.1300	0	NA
K ⁺	0.0649	0.0561	0.0166	0.2390	48.1	5.3
Mg	0.0217	0.0133	0.0001	0.1863	62.6	2.1
Mn	0.0133	0.0064	0.0001	0.2240	11.5	140.2
Mo	0.0043	0.0026	0.0001	0.0822	72.3	1.2
Na ⁺	0.2257	0.1687	0.0039	1.4600	2.6	270.9
Ni	0.0062	0.0026	0.0001	0.2852	14.0	72.8
P	0.0062	0.0039	0.0001	0.0747	81.3	0.7
Pb	0.0086	0.0058	0.0001	0.0559	10.2	45.2
Se	0.0007	0.0006	4.7·10 ⁻⁵	0.0035	88.5	0.2
Si	0.0720	0.0530	0.0044	0.9437	1.7	833.4
Sn	0.0066	0.0059	0.0001	0.0175	62.1	0.8
Sr	0.0009	0.0008	3.0·10 ⁻⁵	0.0042	69.4	0.8
Ta	0.0053	0.0045	9.3·10 ⁻⁶	0.0227	77.9	0.5
Ti	0.0054	0.0039	0.0006	0.0531	12.3	30.5
V	0.0053	0.0039	0.0001	0.0292	61.3	1.4
Zn	0.0226	0.0155	0.0011	0.1607	0	NA

[†] not available(infinite S/N ratio caused by no below MDL value)

Seven, ten, eleven, and nine-source models with values of FPEAK = 0 provided the most physically reasonable source profiles for the Lake Forest, Olive St., Beacon Hill, and Georgetown data, respectively. For the Duwamish data, a eleven-source model with a value of

FPEAK = -0.2 provided the most reasonable source profiles. The average source contributions of each source to the PM_{2.5} mass concentrations are provided in Table 29.

Comparisons of the daily reconstructed PM_{2.5} mass contributions from all sources with measured PM_{2.5} mass concentrations shows that the resolved sources effectively reproduce the measured values and account for most of the variation in the PM_{2.5} mass concentrations in Figure 74. In Figure 75, the averaged seasonal contributions from each source are compared (summer: April - September; winter: October - March). The source profiles, corresponding source contributions, weekday/weekend variations, and CPF plots are presented in Figures 76 - 95. The average source contributions to PM_{2.5} mass concentrations were compared in Figure 96.

It was possible to separate gasoline vehicle emissions from diesel emissions in Olive St., Beacon Hill, Duwamish, and Georgetown data. In Lake Forest data, gasoline vehicle and diesel emissions were not separated and identified as a motor vehicle emissions. Gasoline vehicle and diesel emissions are represented by high OC and EC, whose abundances differ between these sources (Watson *et al.*, 1994). Gasoline vehicles emissions have high concentration of the OC. In contrast, diesel emissions were tentatively identified on the basis of the high concentration of EC. The average contributions from gasoline vehicles to PM_{2.5} mass concentration were 13 - 30% and diesel emissions were 2 - 9%. Motor vehicle contributed 27% to PM_{2.5} concentration measured at Lake Forest. The contributions from gasoline vehicle were higher at Beacon Hill than those at other sites. Diesel emissions contributed more at Olive St. and Duwamish sites as shown in Figure 96.

As shown in Figures 86 to 90, gasoline vehicle emissions identified at Beacon Hill do not show a strong weekday/weekend variation. In contrast, diesel emissions show high contributions on week days. However, both gasoline and diesel emissions identified at Olive St. do not show clear weekday/weekend variations. Both gasoline and diesel emissions identified at Duwamish and Georgetown located in industrial area show clear weekday/weekend variations.

The CPF plot for motor vehicle identified in Lake Forest shown in Figure 91 likely points to local roads located northwest and southeast of the site. For the Olive St., CPF plots pointing southeast suggest that gasoline and diesel emissions appear to have high contributions from interstate Highway 5. The CPF plots for the Beacon Hill data indicate the gasoline emission impacts from mostly residential area (northeast, east, and southeast) and the diesel emission impacts from the Highway 5 (west). The CPF plots for the gasoline and diesel emissions at Duwamish and Georgetown similarly point to Port of Seattle (north) and Highway 5 (southeast).

Shah *et al.* (2004) reported that diesel engines operating at very slow speeds and in stop and go traffic produce OC/EC ratios that are similar to typical gasoline vehicle emissions. There is significantly more EC than OC in the emissions only under more continuous motion at higher speeds (transient and cruise). Therefore, the diesel emissions profile that was extracted by PMF may represent only diesel vehicles moving at reasonable speed in fluid traffic conditions. Diesel emissions in stop and go traffic are likely to be apportioned into the gasoline emission category.

The secondary nitrate aerosol is represented by its high concentration of NO₃⁻ and NH₄⁺. It accounts for 12% - 26% of the PM_{2.5} mass concentration at all five monitoring sites. The secondary nitrate aerosol has seasonal variation with maxima in winter as shown in Figures 75 and 81 - 85. These peaks in winter indicate that low temperature and high relative humidity help the formation of secondary nitrate particles.

Secondary sulfate aerosol has a high concentration of SO₄²⁻ and NH₄⁺ account for 17% - 20% of the PM_{2.5} mass concentration at all five monitoring sites. Secondary sulfate profiles typically include carbons that become associated with the secondary sulfate (Liu *et al.*, 2003). As shown in Figure 75, the secondary sulfate shows seasonal variation with higher concentrations in summer at all monitoring sites when the photochemical activity is highest except Duwamish site. Secondary sulfate shows relatively constant contributions to the PM_{2.5} mass concentrations in Figure 96 except Duwamish site. The winter-high seasonal variation at

Duwamish site and the higher values of the averaged contribution of secondary sulfate than other sites shown in Table 29 and Figure 96 suggest the existence of the local sulfate sources near Duwamish site.

Table 29. Average source contributions ($\mu\text{g}/\text{m}^3$) to $\text{PM}_{2.5}$ mass concentration.

Sources	Average source contribution (%)				
	Lake Forest	Olive St	Beacon Hill	Duwamish	Georgetown
Secondary nitrate	1.19 (11.8)	2.70 (25.9)	1.50 (17.9)	2.87 (23.5)	2.00 (20.8)
Secondary sulfate	1.70 (16.9)	1.84 (17.6)	1.51 (18.0)	2.48 (20.3)	1.77 (18.4)
Wood smoke	3.07 (30.5)	0.75 (7.2)	0.65 (7.8)	1.21 (9.9)	1.86 (19.3)
Motor vehicle	2.67 (26.6)				
Gasoline vehicle		1.38 (13.2)	2.51 (30.0)	1.59 (13.0)	1.80 (18.7)
Diesel emissions		0.91 (8.7)	0.21 (2.6)	0.65 (5.3)	0.18 (1.9)
Airborne soil	0.23 (2.3)	0.99 (9.4)	0.22 (2.7)	0.70 (5.7)	0.49 (5.1)
Oil combustion		0.39 (3.7)	0.43 (5.1)	0.44 (3.6)	
Aged sea salt	0.93 (9.3)	0.59 (5.6)	0.53 (6.4)	0.48 (3.9)	1.15 (11.9)
Sea salt	0.27 (2.7)	0.40 (3.8)	0.17 (2.0)	0.44 (3.6)	0.24 (2.5)
Metal processing		0.50 (4.8)	0.65 (7.7)	0.78 (6.4)	0.14 (1.5)
Cement kiln				0.57 (4.7)	

Wood smoke is characterized by OC, EC, and K (Watson *et al.*, 2001) contributing 7 - 31% to the $\text{PM}_{2.5}$ mass concentration. Wood smoke contributed the most at residential Lake Forest site. This source has a winter-high seasonal trend shown in Figure 81. There are not clear weekday/weekend variations in the wood smoke contributions.

Airborne soil is represented by Si, Fe, Al and Ca contributing 2 - 9% to the $\text{PM}_{2.5}$ mass concentration. Crustal particles could be contributed by wind-blown soil dust and re-suspended by road traffic. Airborne soil contributed the most at Olive St. and Duwamish sites. Airborne soil does not show clear seasonal variation. At Olive St., Beacon Hill, and Duwamish sites, this source shows clear weekday-high variation. The elevated airborne soil contributions on April 20, 2002 were identified at Lake Forest, Beacon Hill, and Georgetown sites. The backward trajectories in Figure 97 showed that the elevated airborne soil contribution on April 20, 2002 and two other peaks identified at Beacon Hill (April 12, 2000 and April 22, 2001) were likely caused by Asian dust storms.

Oil combustion is characterized by high concentrations of carbon fractions, S, V, and Ni reflecting residual oil combustion for the utilities and industries. This source was identified at Olive St., Beacon Hill, and Duwamish sites and contributed 4 - 5% to the $\text{PM}_{2.5}$ mass concentrations. As shown in Figure 98, the CPF plots of this source point to the Port of Seattle suggesting the sources of the oil combustion are likely cargo ships, tugs, commercial harbor craft, ferries, cargo-handling machines, and trains. Oil combustion does not show strong seasonal variations. There is not clear weekday/weekend variations in this source at Beacon Hill and Duwamish sites. At Olive St. site, oil combustion shows weekend-high variation.

Sea salt is represented by its high concentration of Na^+ and Cl^- , accounting for 2 - 4% of the $\text{PM}_{2.5}$ mass concentration. This source shows a winter-high seasonal pattern, and does not show clear weekday/weekend variation. The CPF plot shows the contributions from the southwest, which is consistent at all five sites.

Aged sea salt is characterized by its high concentration of Na^+ , SO_4^{2-} , and NO_3^- . The lack of Cl^- in the profile is caused by Cl^- displacement by acidic gases. Aged sea salt accounts for 4 - 12% of the $\text{PM}_{2.5}$ mass concentrations at all monitoring sites. This particle shows a

summer-high seasonal pattern. Aged sea salt identified at Duwamish only shows a weekend-high variation.

Metal processing source that are characterized by carbons, Fe, and Zn were identified at Olive St., Beacon Hill, Duwamish, and Georgetown data. This source accounts for 2 - 8% of the PM_{2.5} mass concentration. This source has a strong winter-high seasonal pattern at Olive St. and Duwamish.

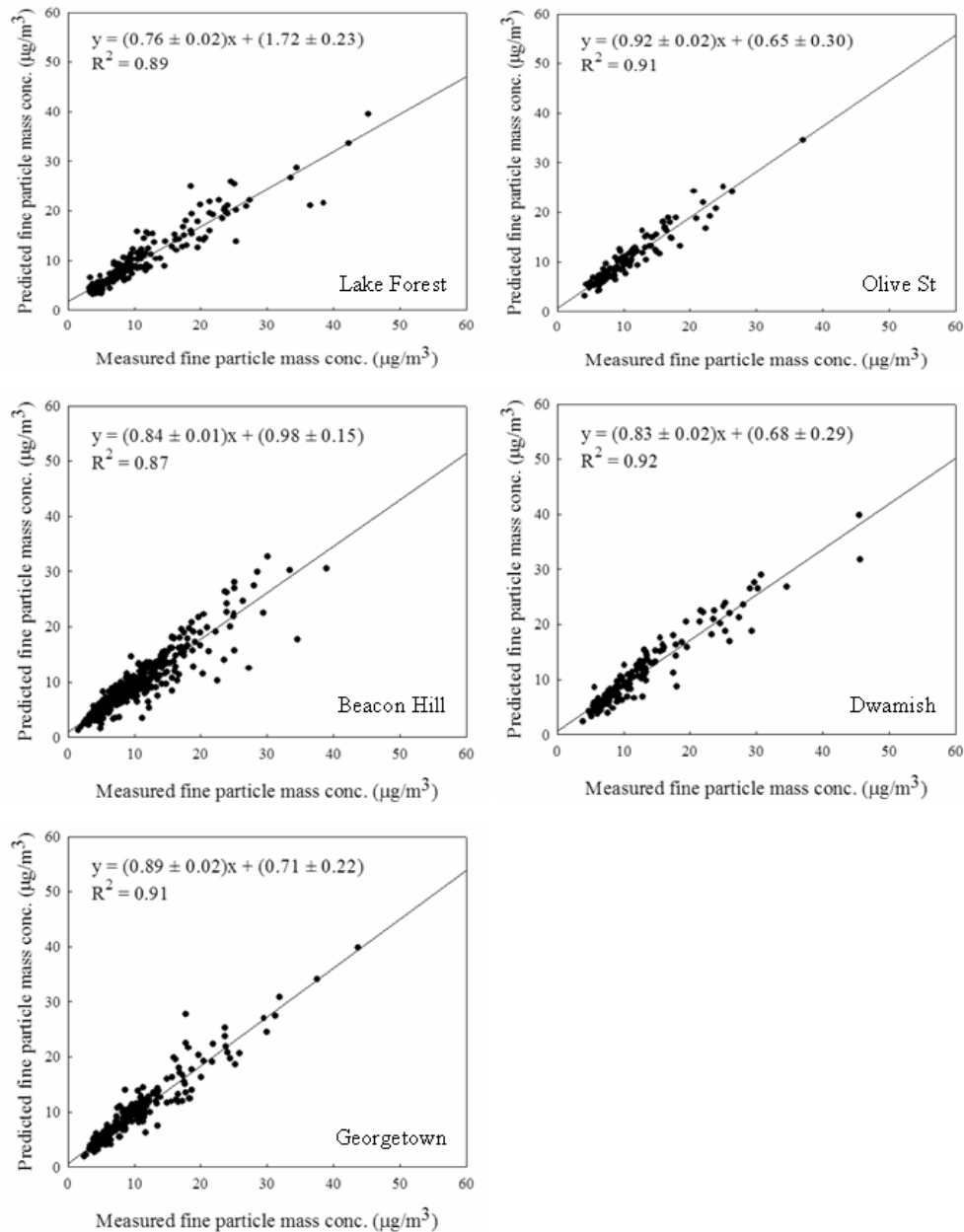


Figure 74. Measured versus PMF predicted PM_{2.5} mass concentrations.

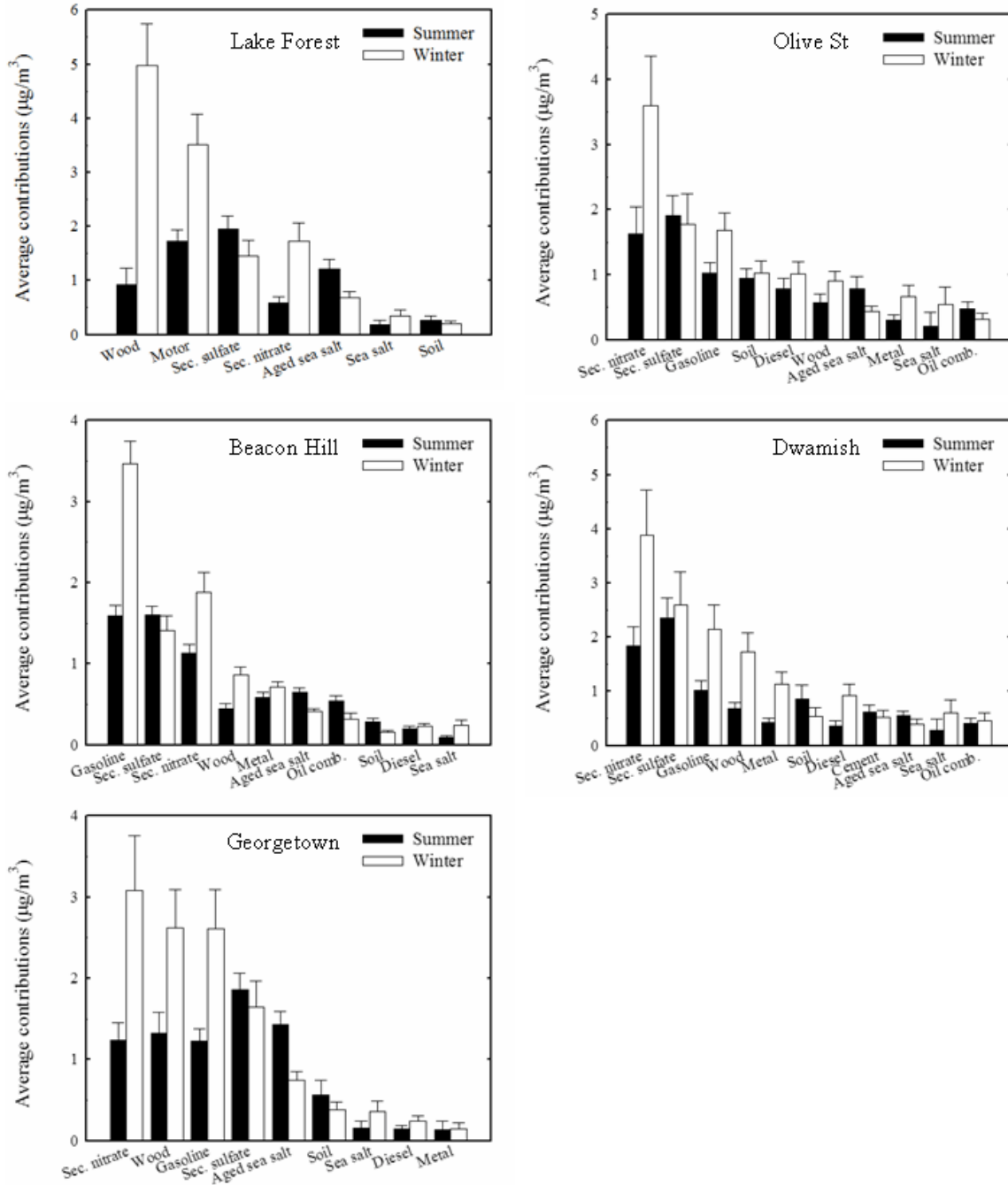


Figure 75. The seasonal comparison of source contributions to PM_{2.5} mass concentration (mean \pm 95% distribution)

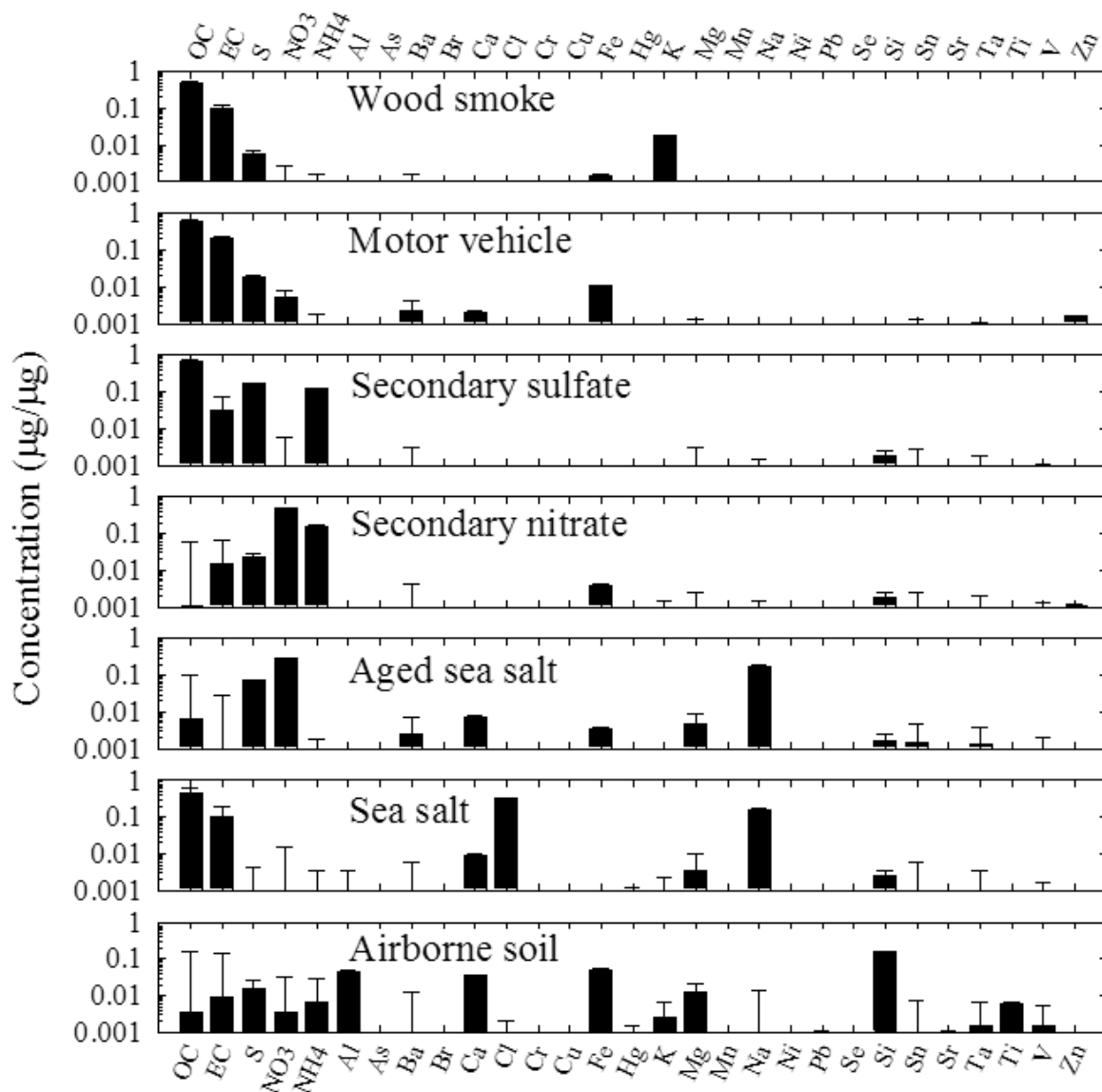


Figure 76. Source profiles deduced from PM_{2.5} samples measured at Lake Forest (prediction ± standard deviation).

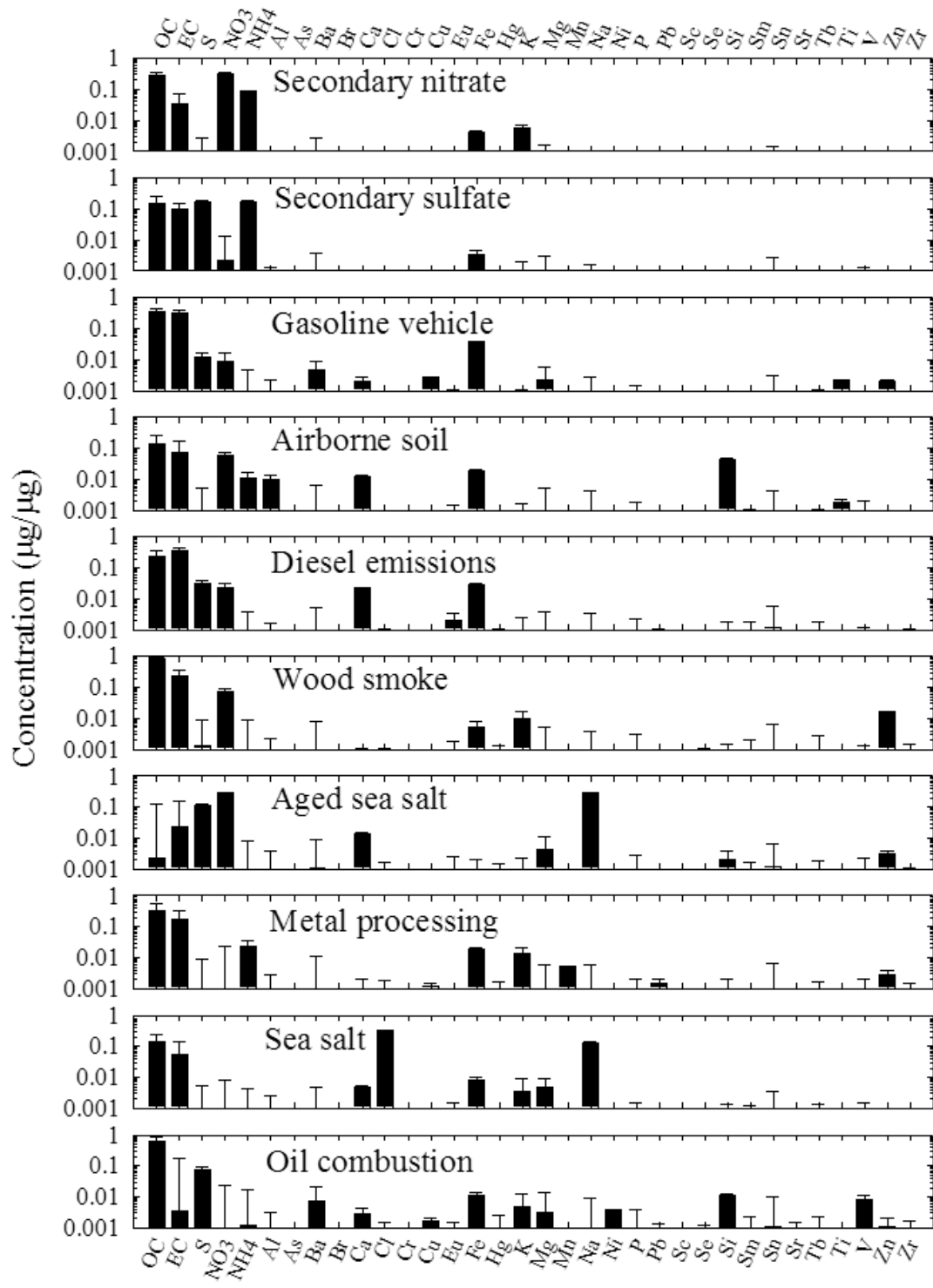


Figure 77. Source profiles deduced from PM_{2.5} samples measured at Olive St. (prediction ± standard deviation).

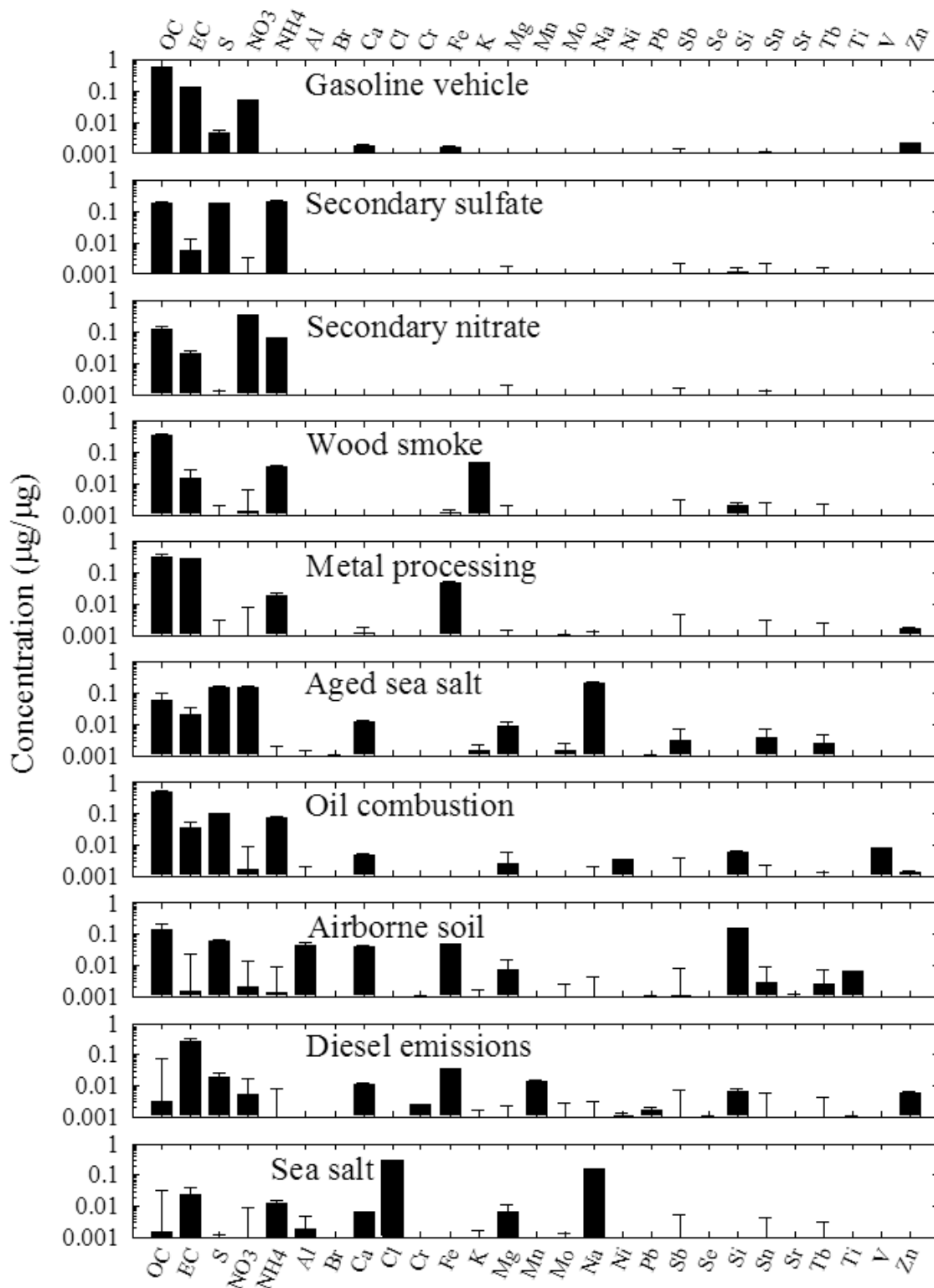


Figure 78. Source profiles deduced from $PM_{2.5}$ samples measured at Beacon Hill (prediction \pm standard deviation).

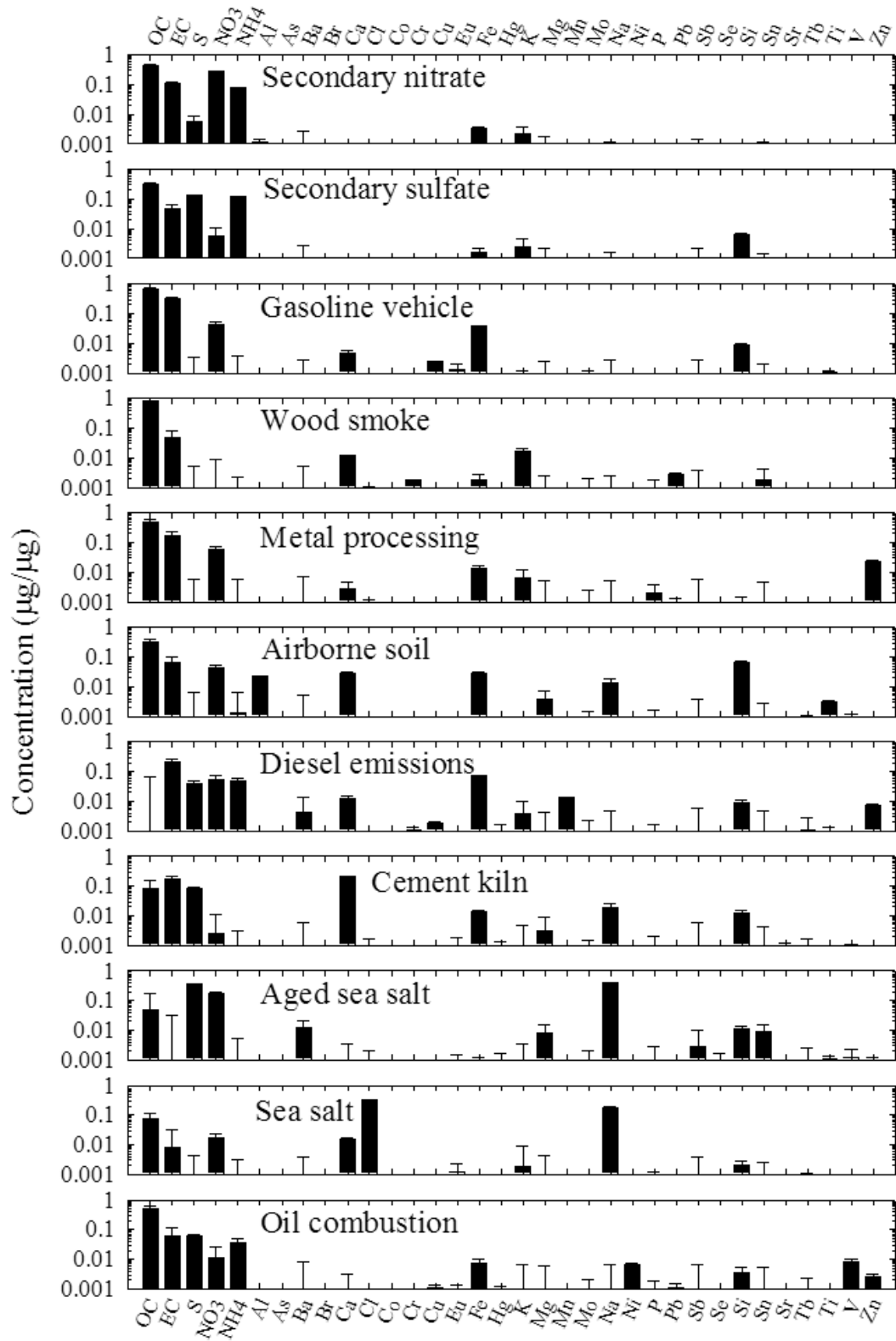


Figure 79. Source profiles deduced from PM_{2.5} samples measured at Duwamish (prediction ± standard deviation).

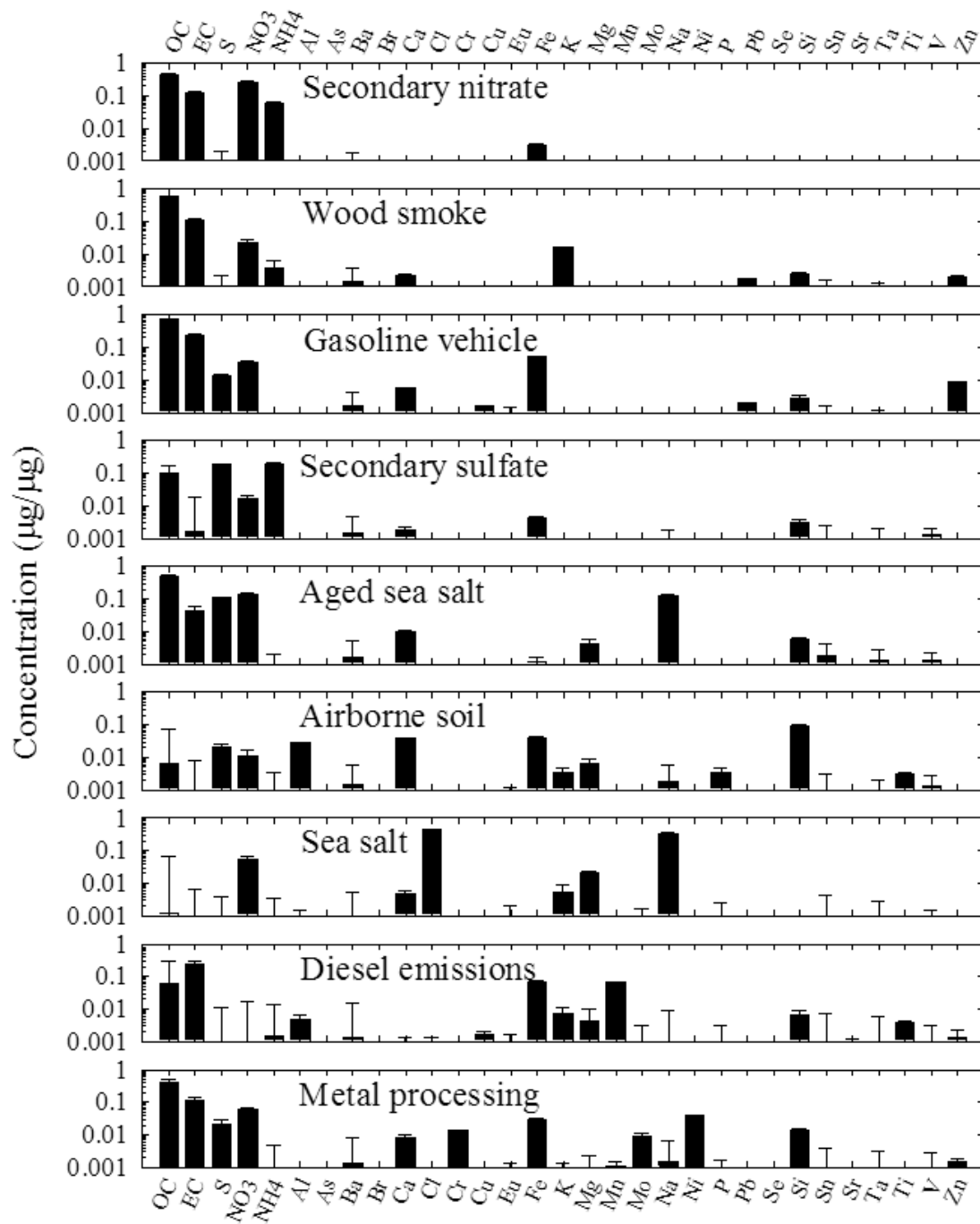


Figure 80. Source profiles deduced from $PM_{2.5}$ samples measured at Georgetown (prediction \pm standard deviation).

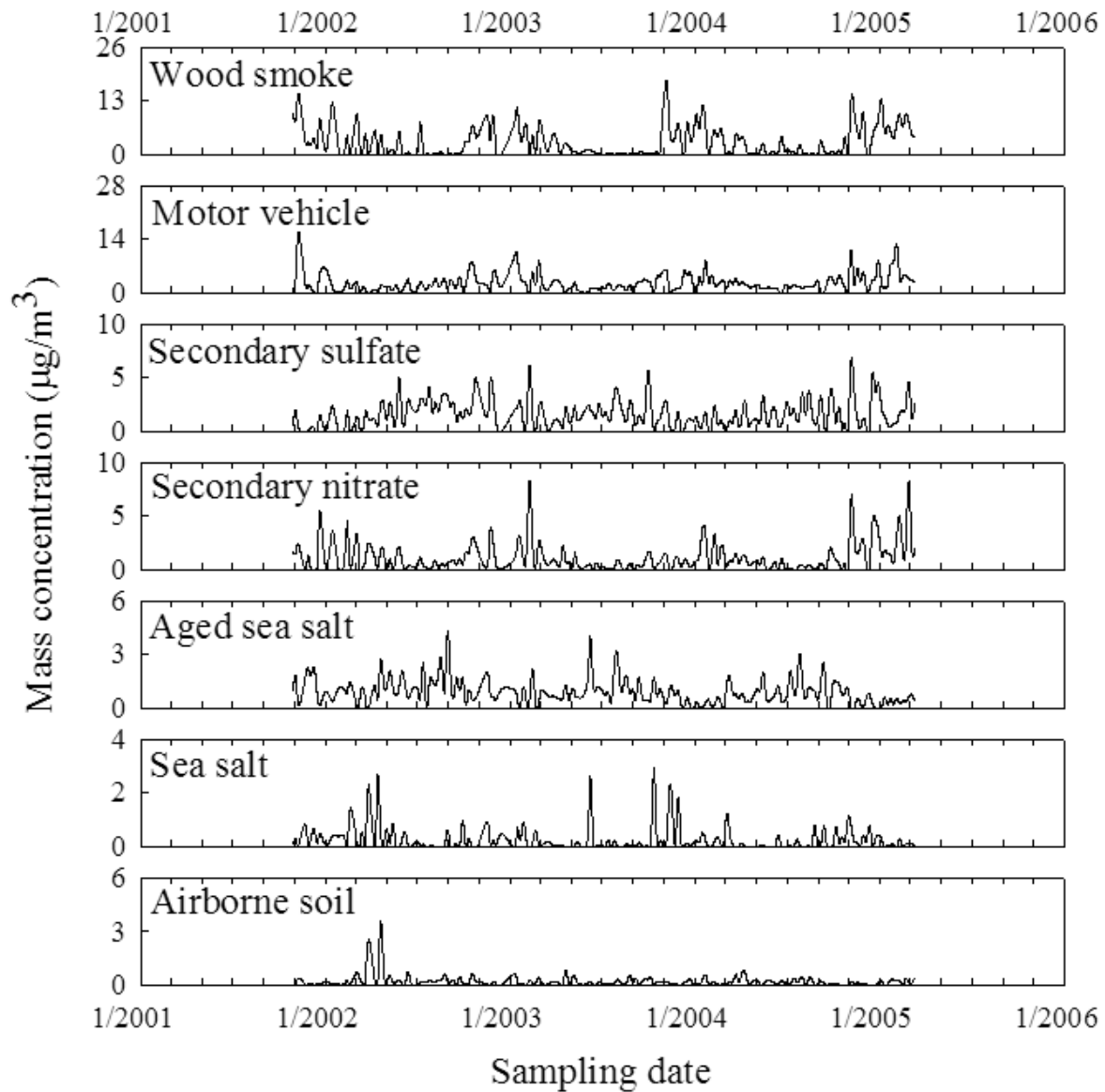


Figure 81. Time series plot of source contributions at Lake Forest.

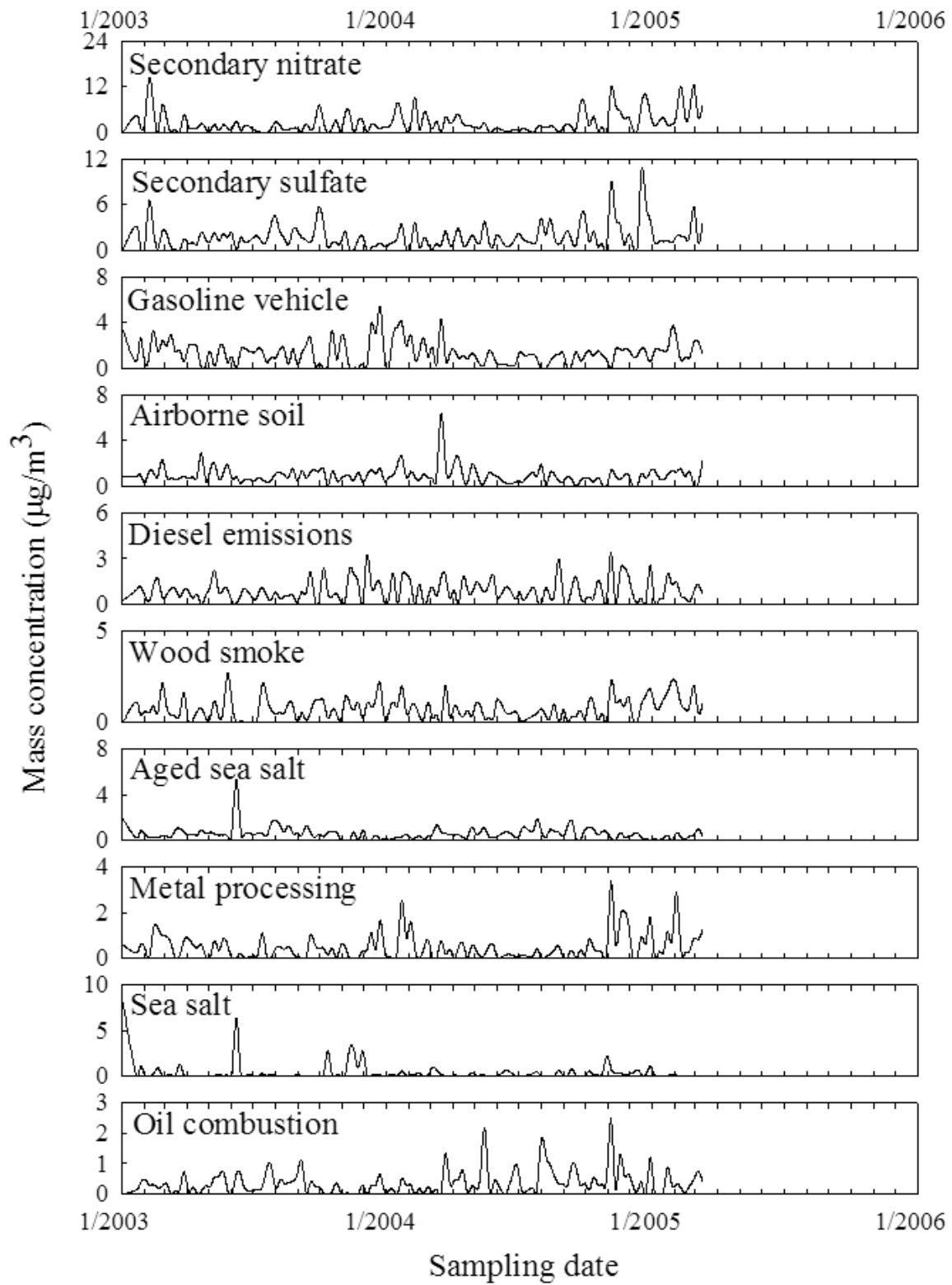


Figure 82. Time series plot of source contributions at Olive St.

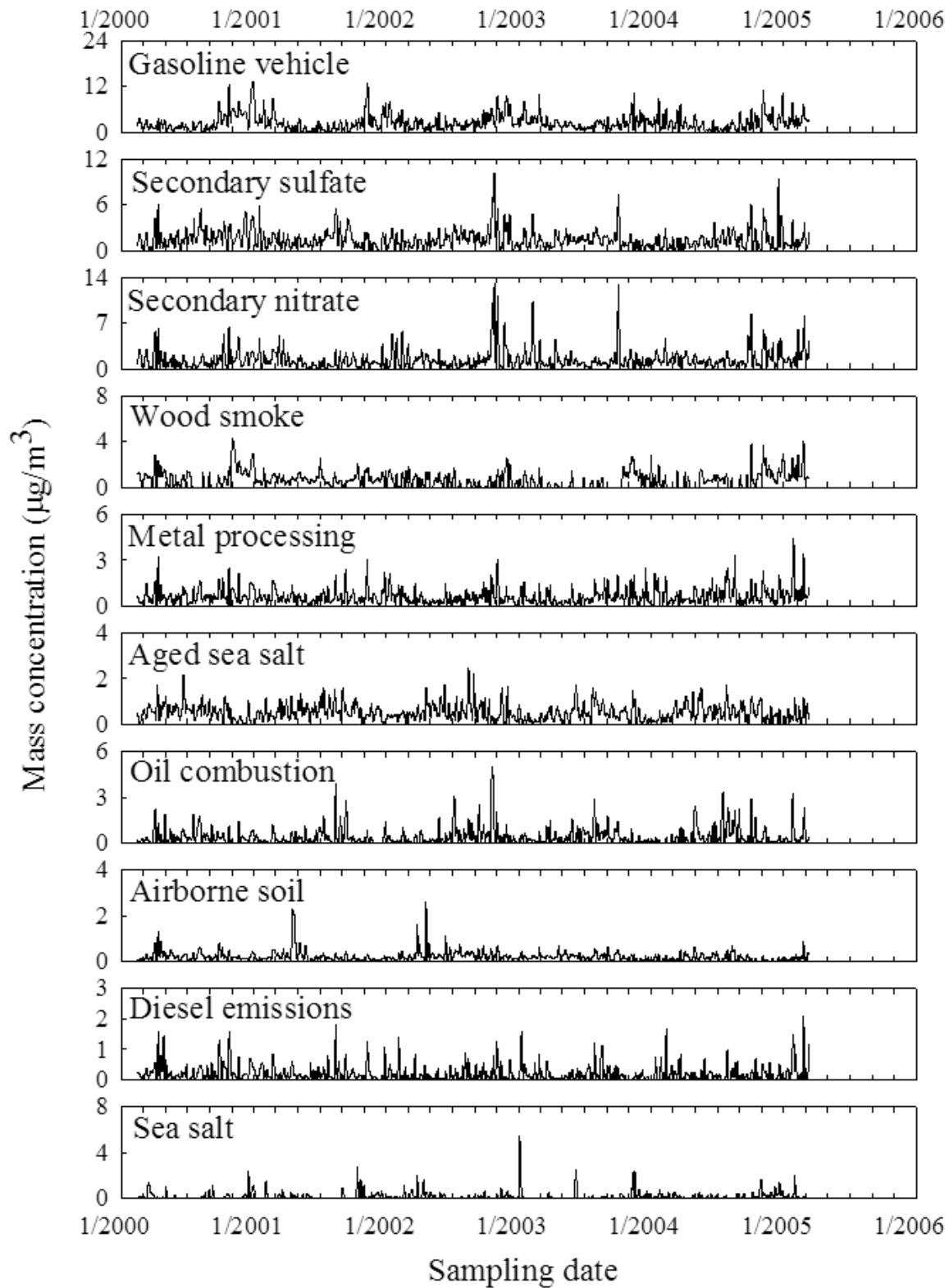


Figure 83. Time series plot of source contributions at Beacon Hill.

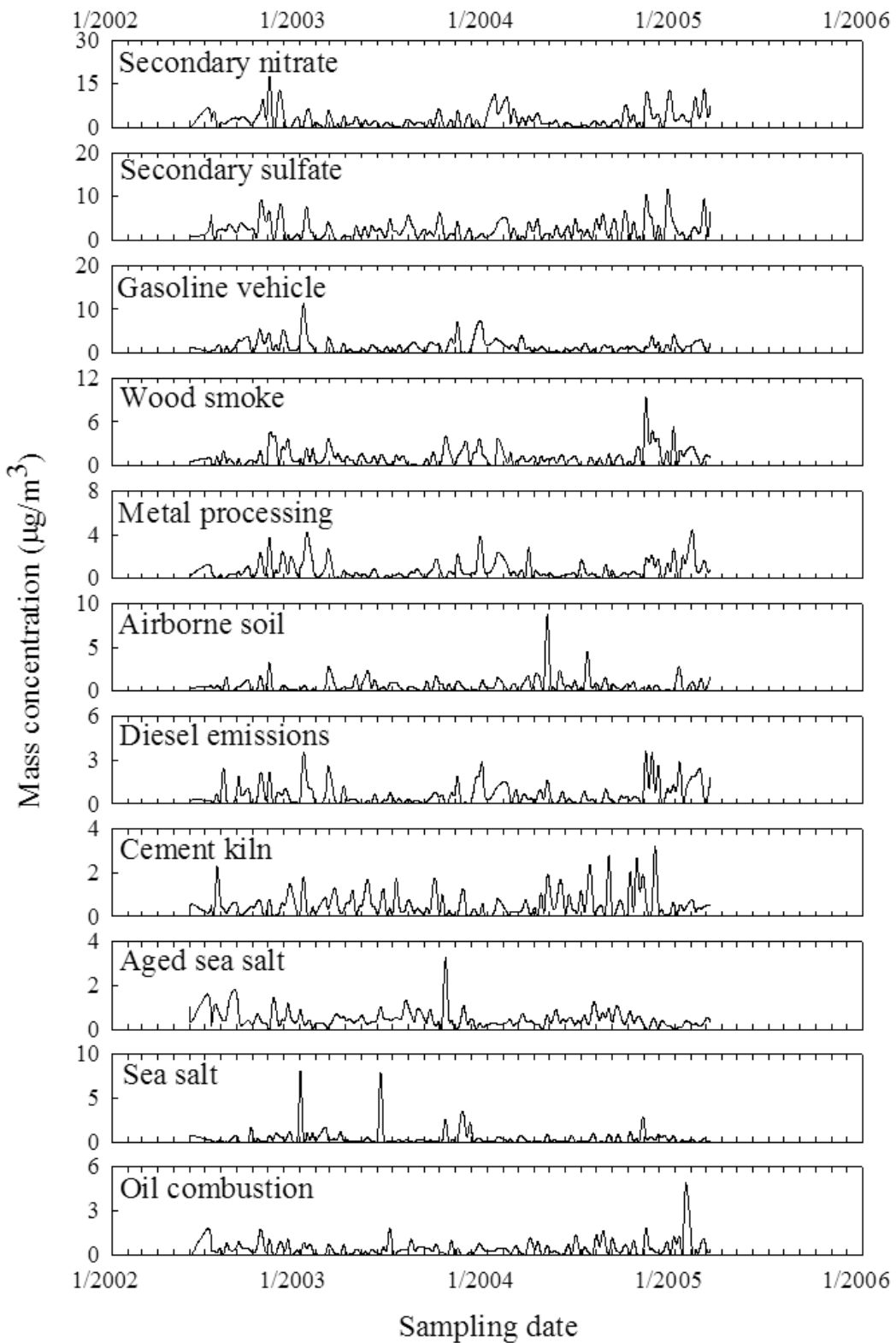


Figure 84. Time series plot of source contributions at Duwamish.

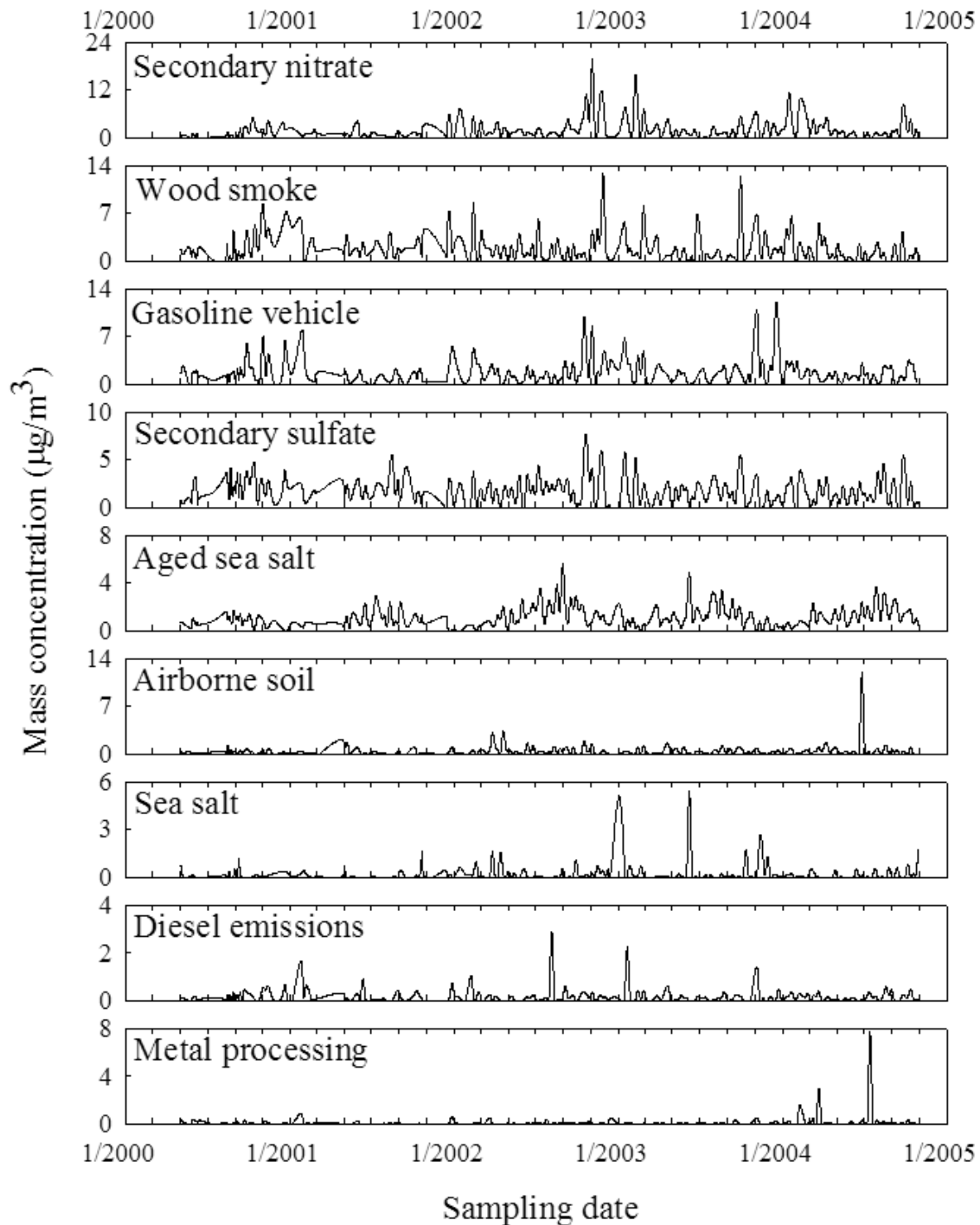


Figure 85. Time series plot of source contributions at Georgetown.

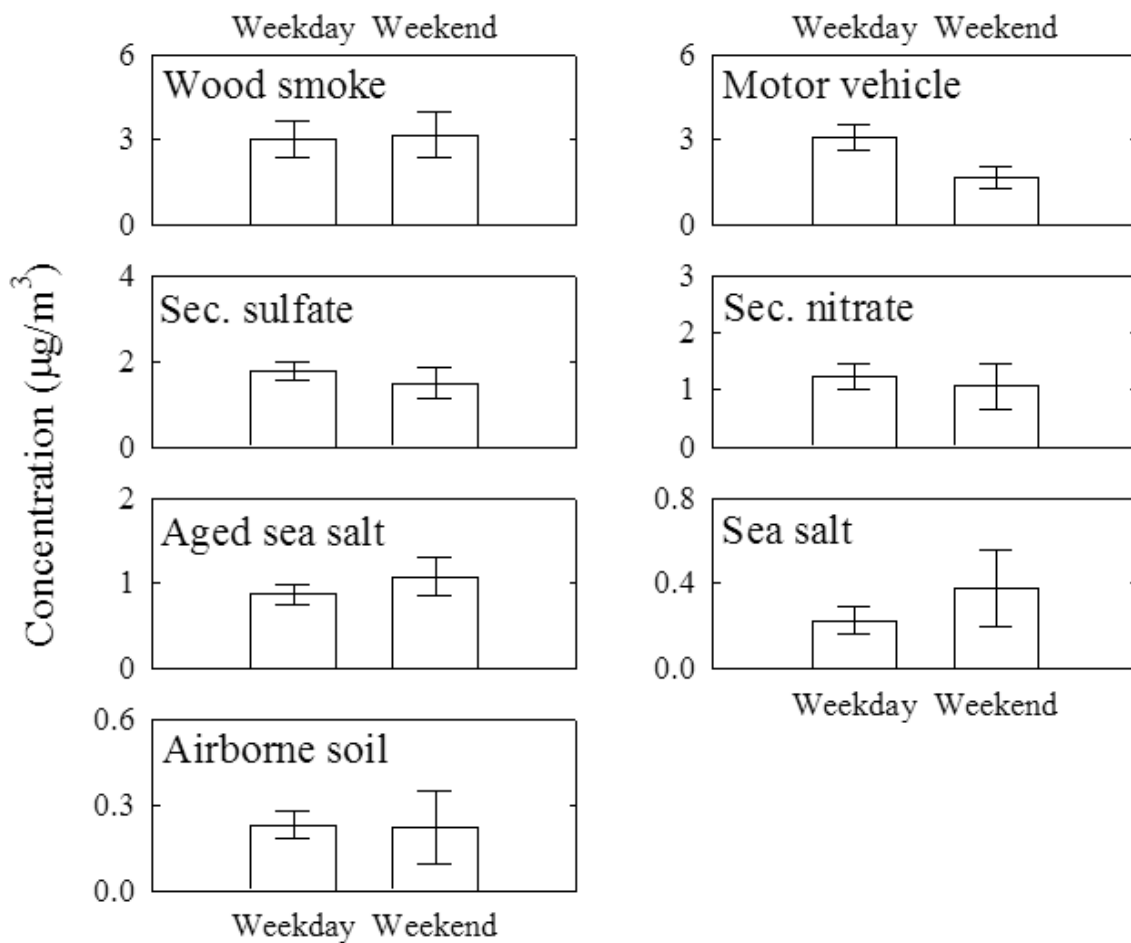


Figure 86. Weekday/weekend variations at Lake Forest (mean \pm 95% distribution).

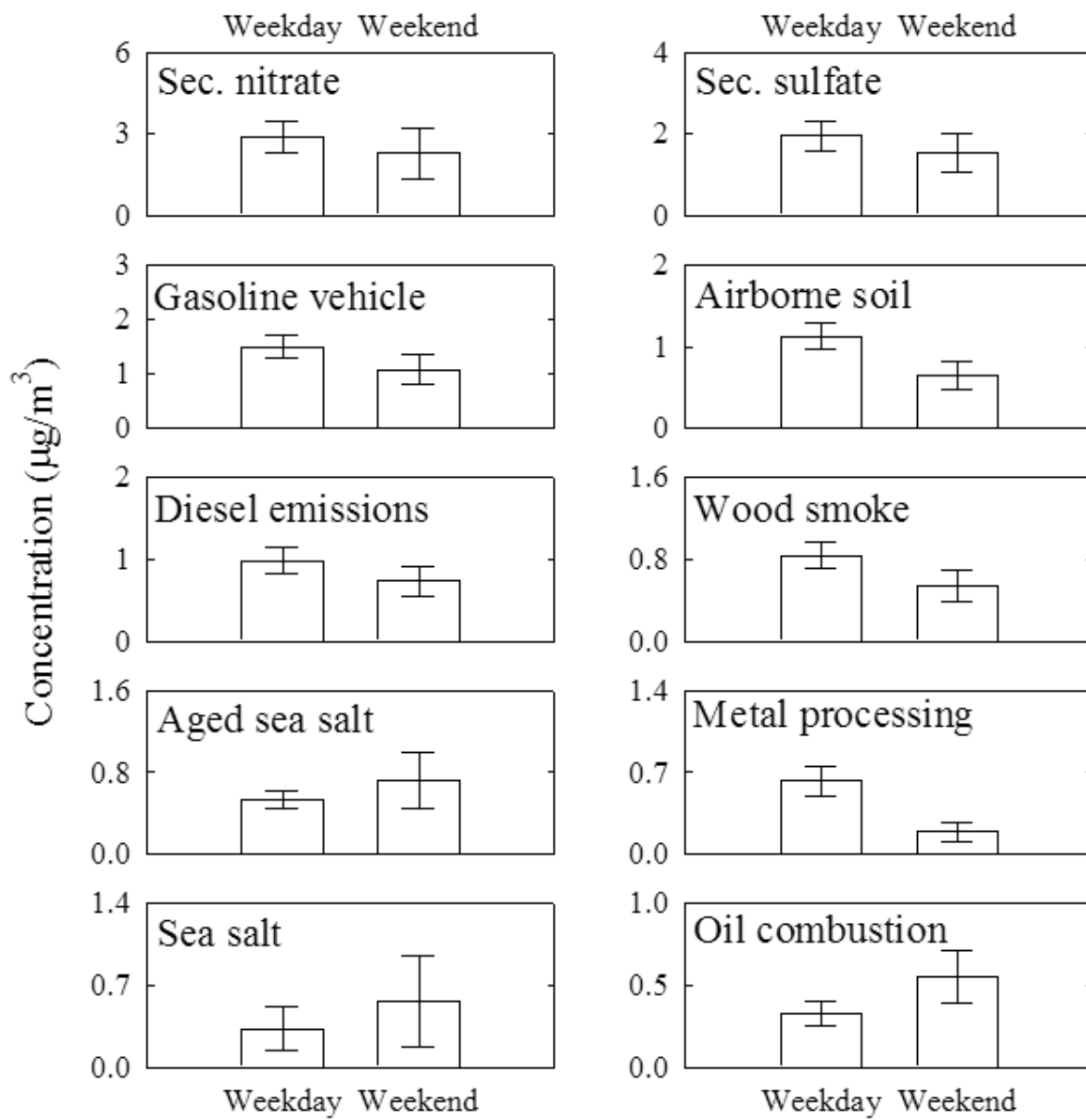


Figure 87. Weekday/weekend variations at Olive St. (mean \pm 95% distribution).

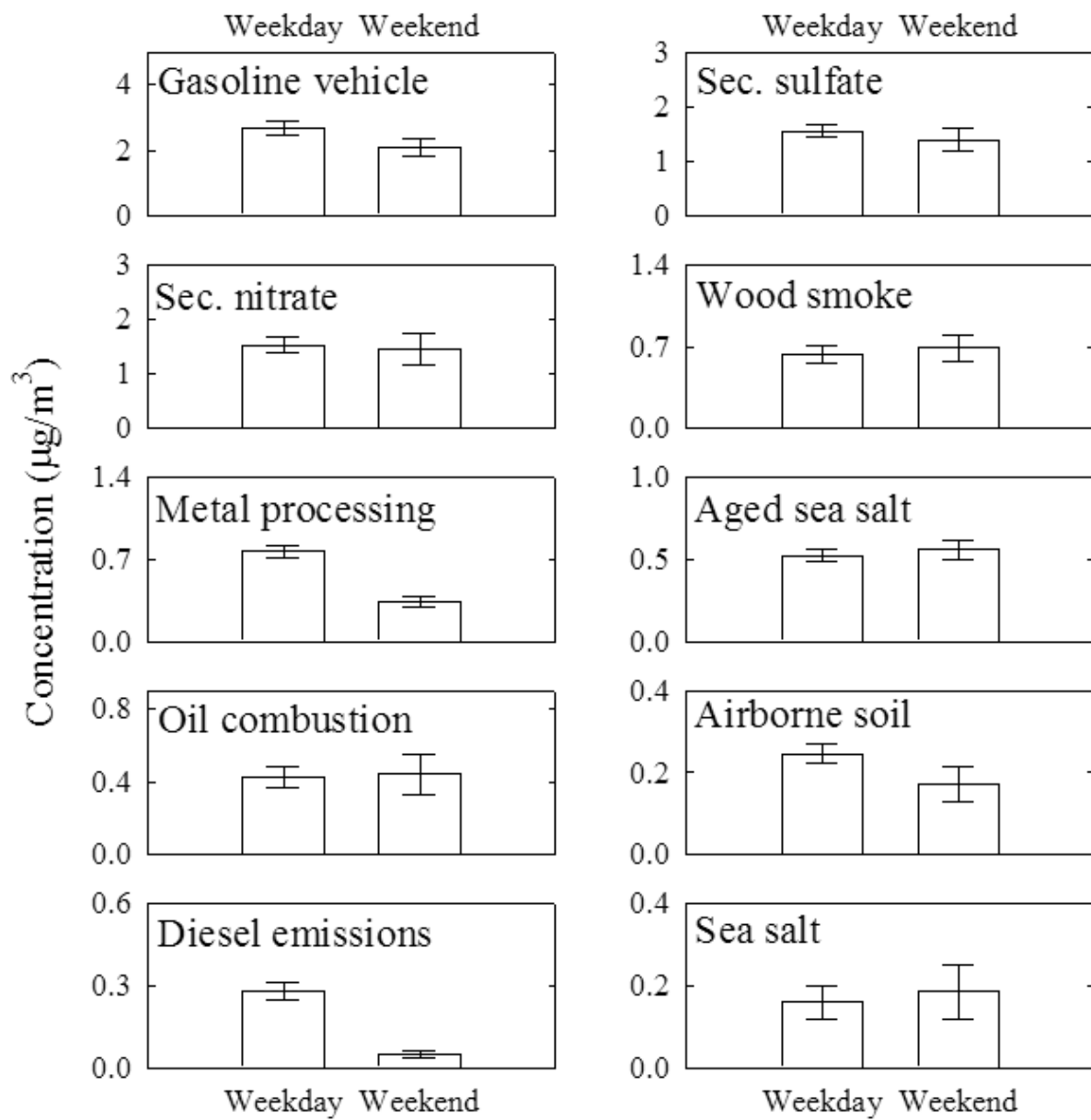


Figure 88. Weekday/weekend variations at Beacon Hill (mean \pm 95% distribution).

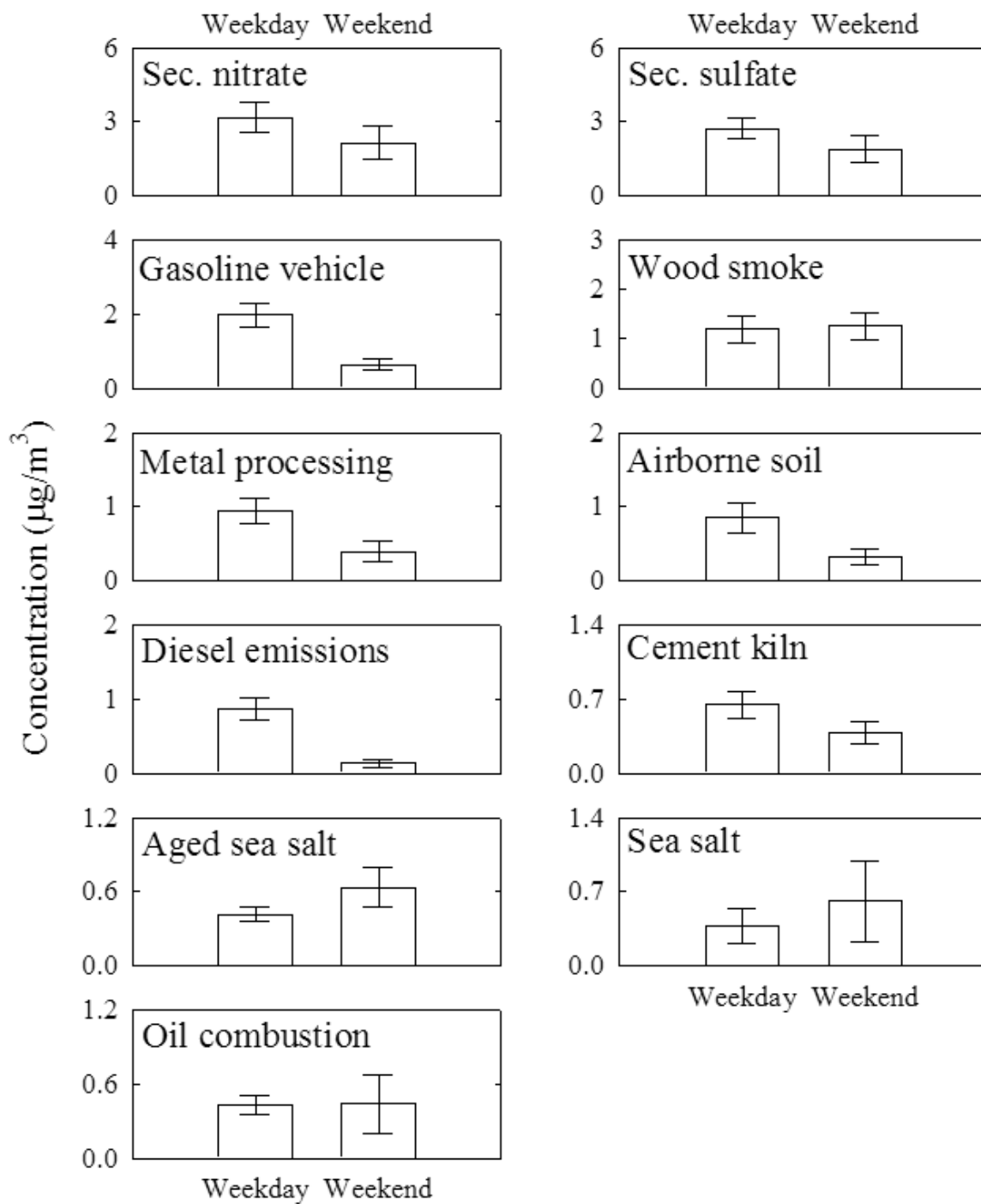


Figure 89. Weekday/weekend variations at Duwamish (mean ± 95% distribution).

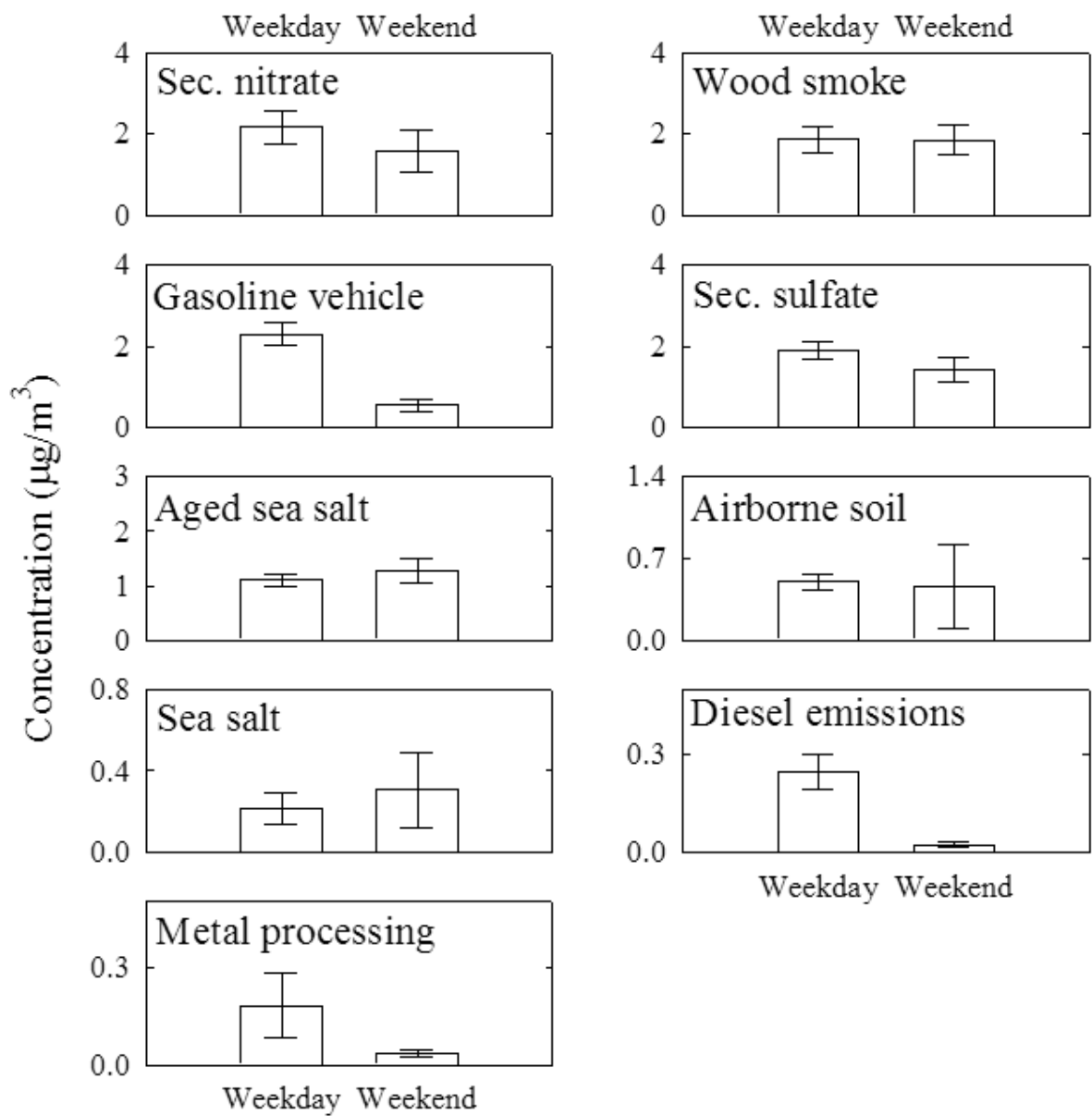


Figure 90. Weekday/weekend variations at Georgetown (mean \pm 95% distribution).

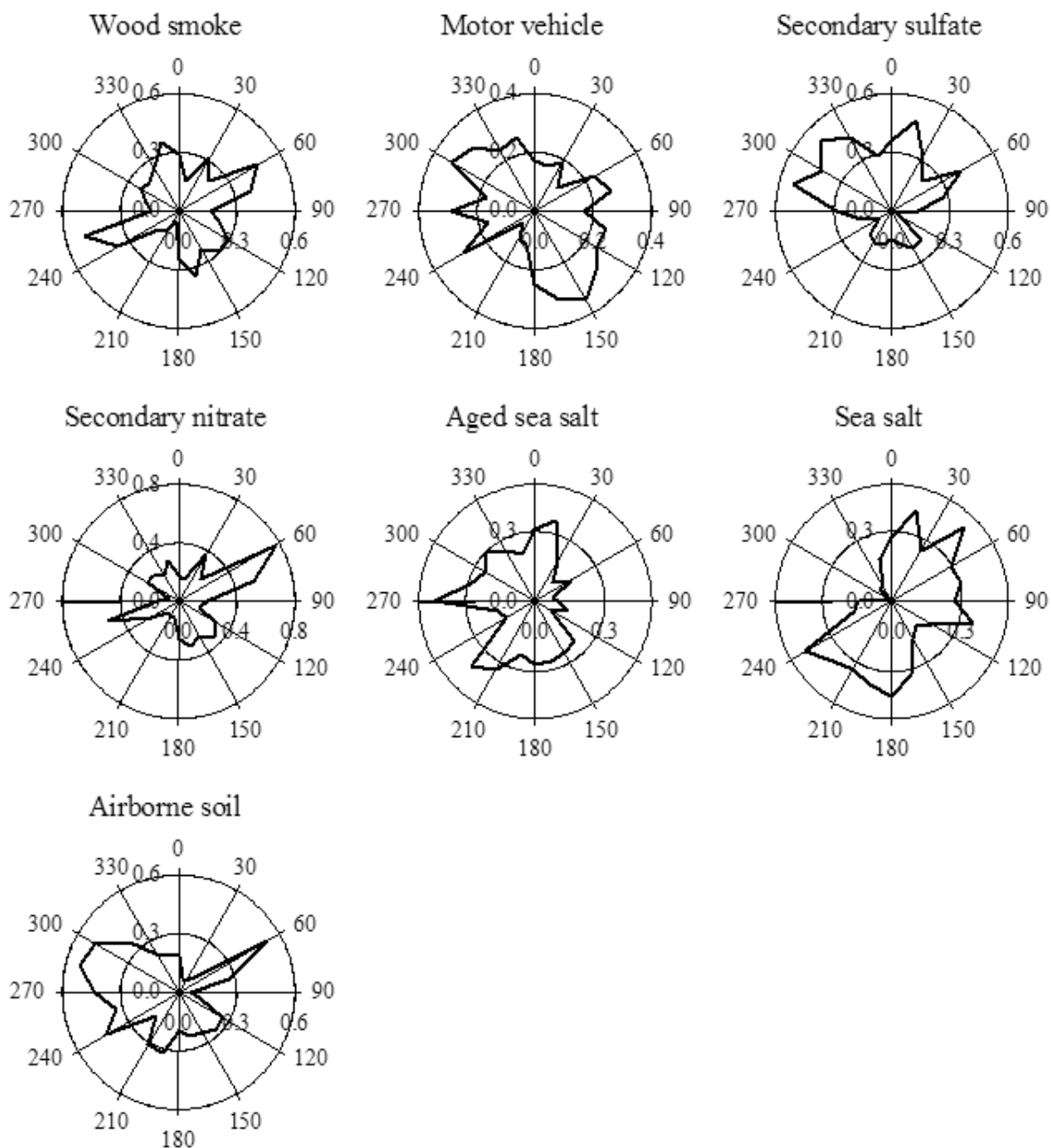


Figure 91. CPF plots for the highest 25% of the mass contributions at Lake Forest.

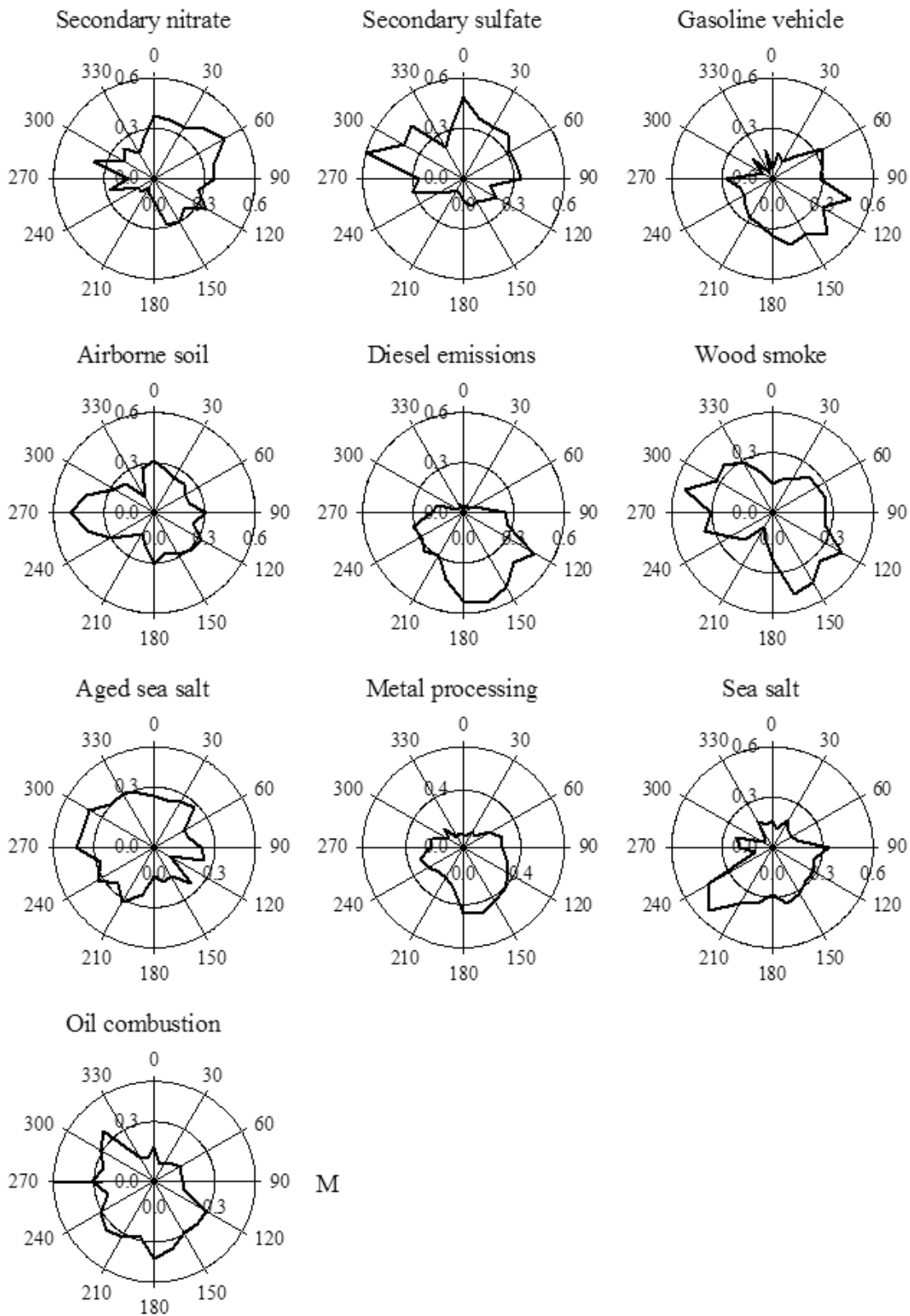


Figure 92. CPF plots for the highest 25% of the mass contributions at Olive St.

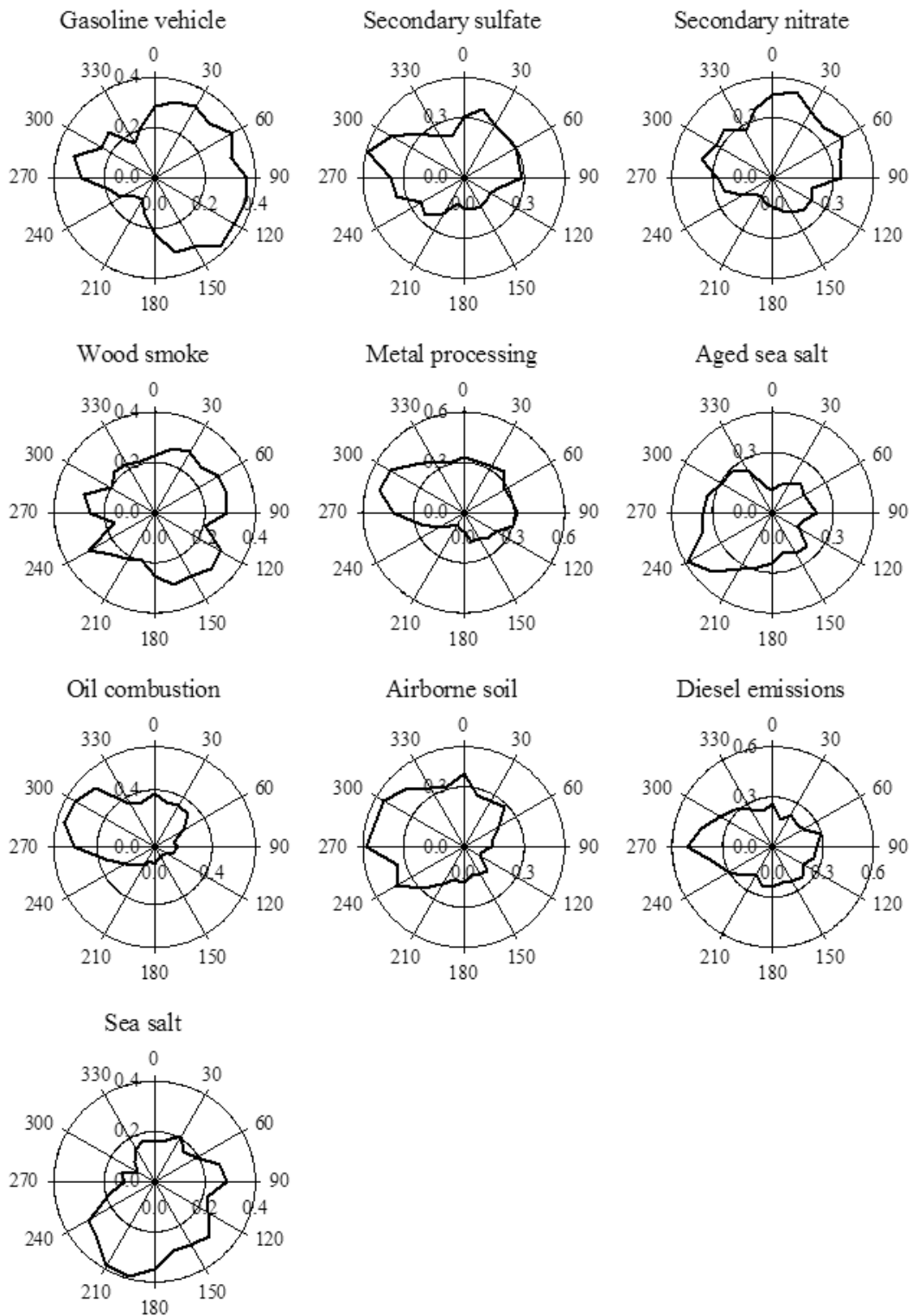


Figure 93. CPF plots for the highest 25% of the mass contributions at Beacon Hill.

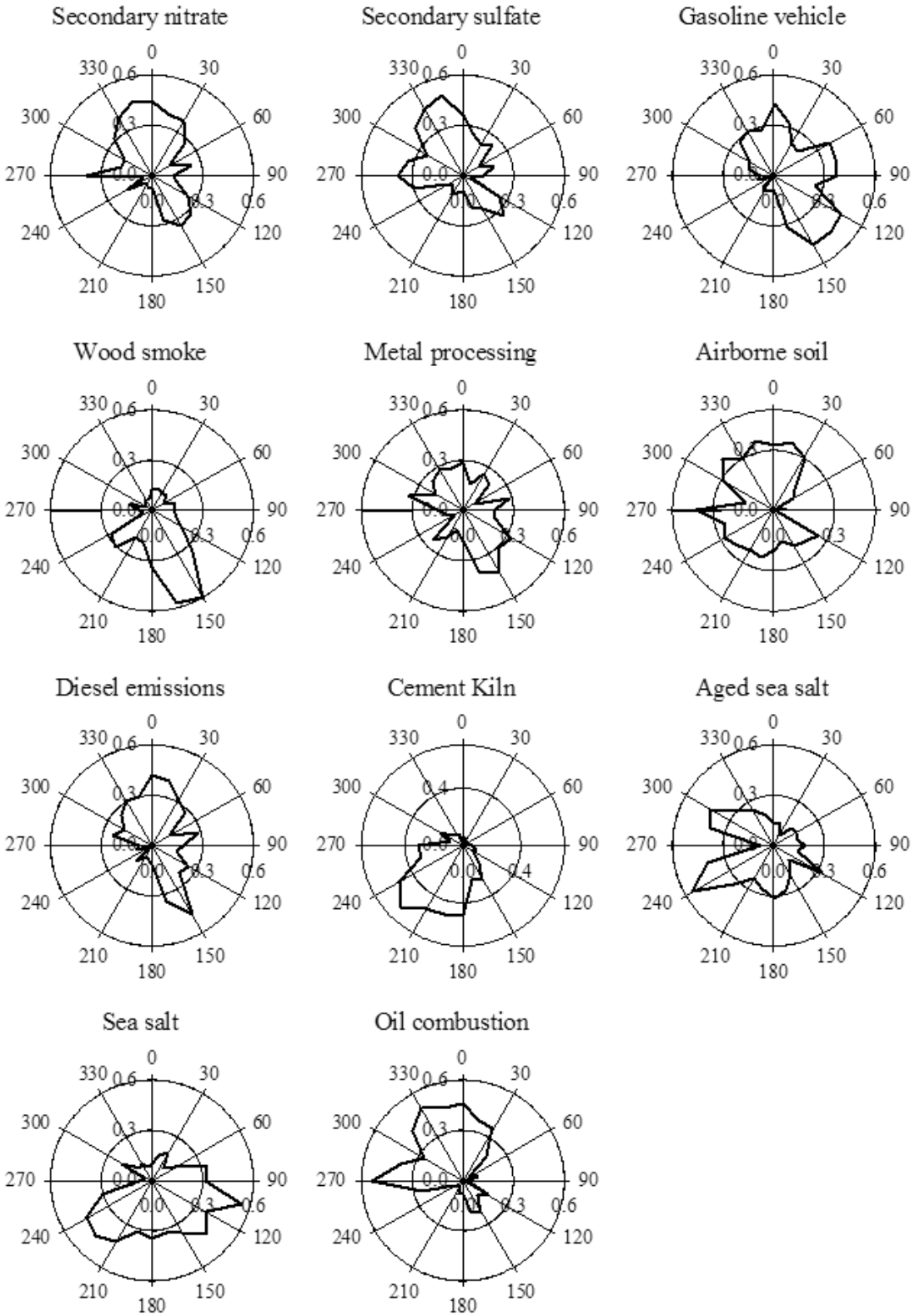


Figure 94. CPF plots for the highest 25% of the mass contributions at Duwamish.

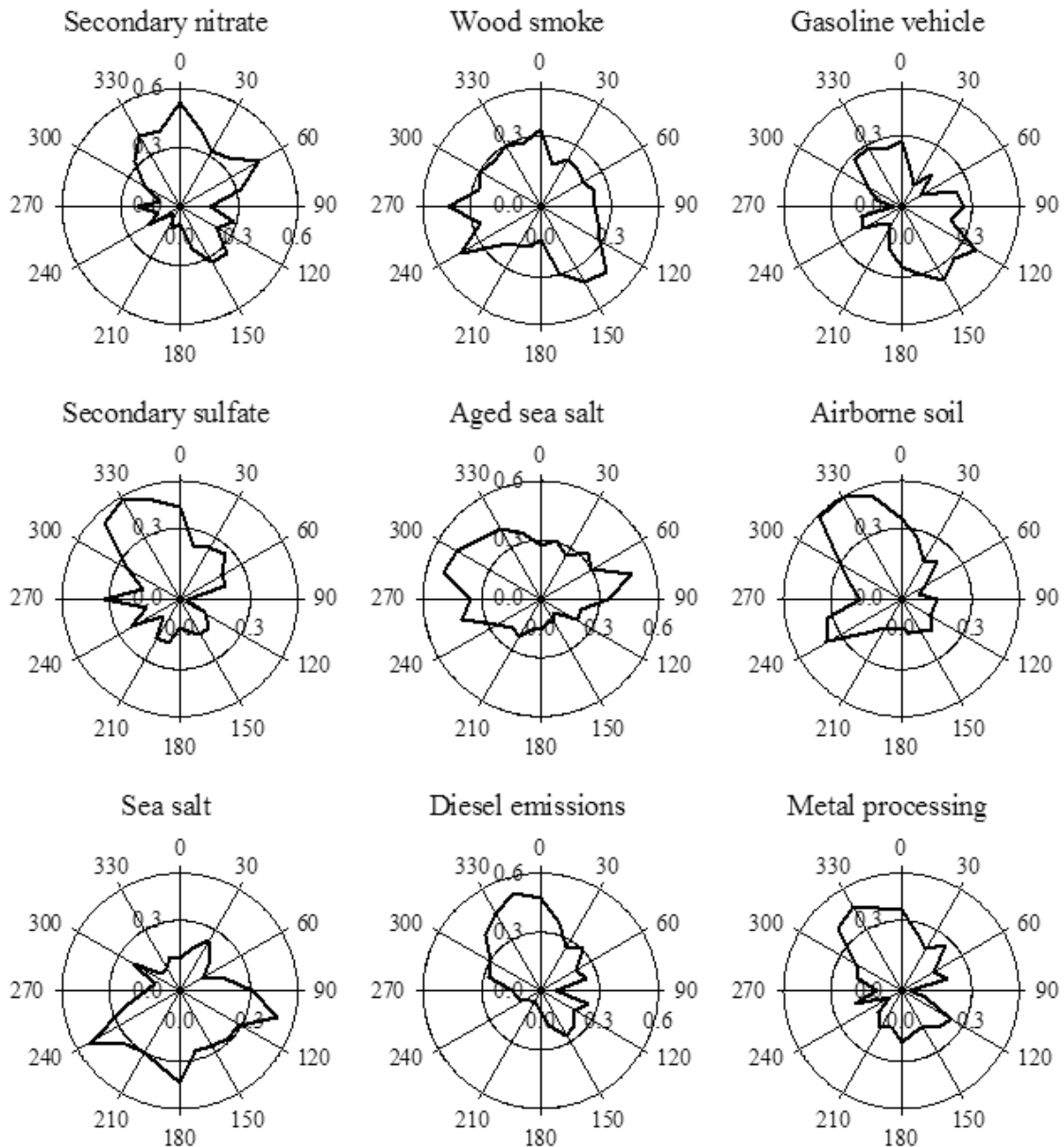


Figure 95. CPF plots for the highest 25% of the mass contributions at Georgetown.

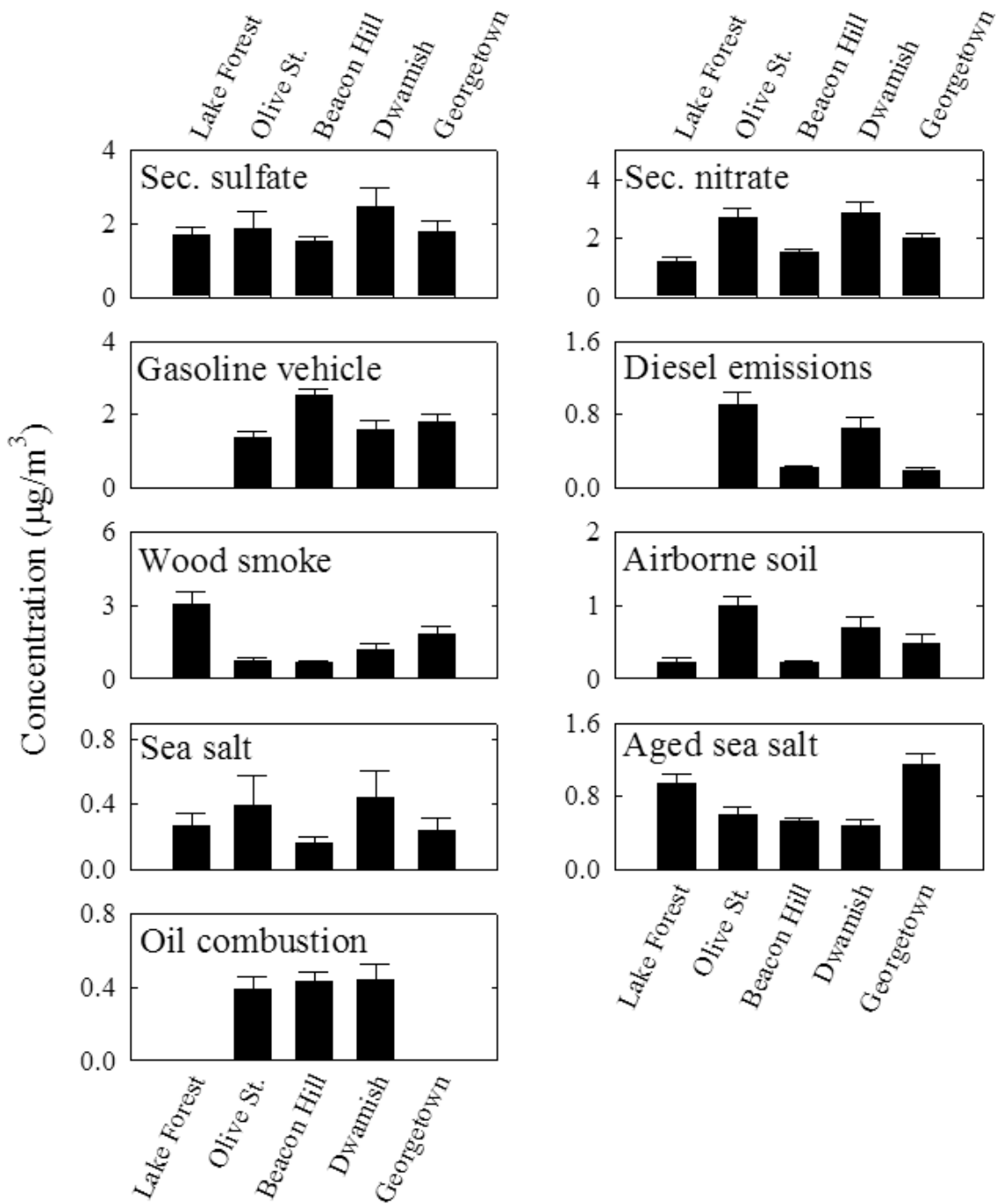
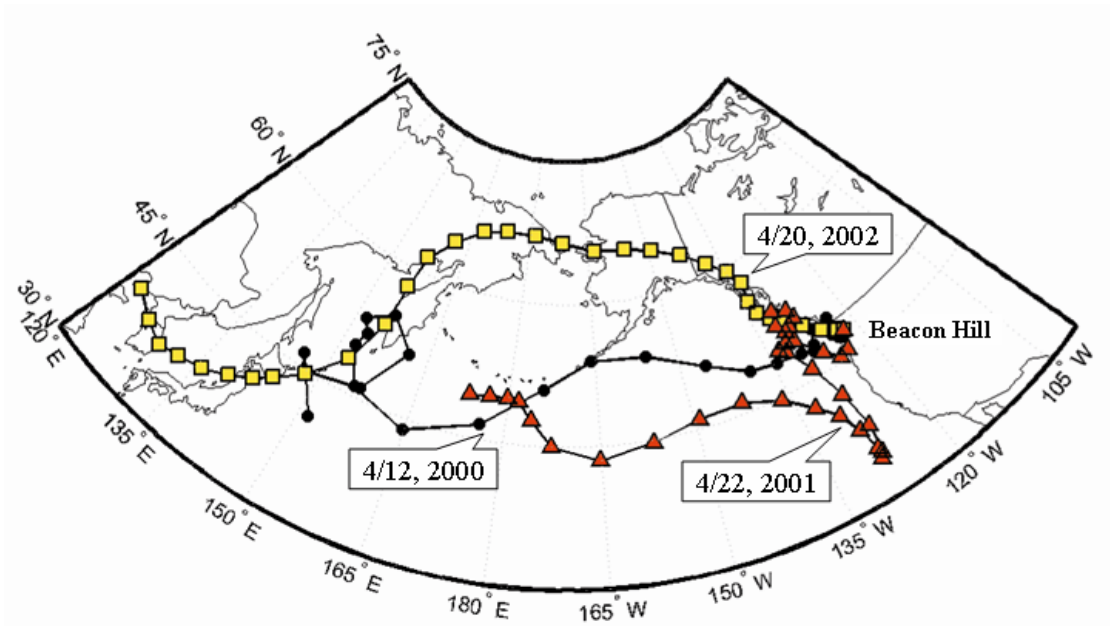


Figure 96. The comparison of average source contributions to PM_{2.5} mass concentrations (mean ± 95% distribution).



. Backward trajectories for days with high impacts of airborne soil arriving at Beacon Hill on Apr. 12, 2000 (circle), Apr. 22, 2001 (triangle), and Apr. 20, 2002 (square) calculated from NOAA Air Resource Laboratory.

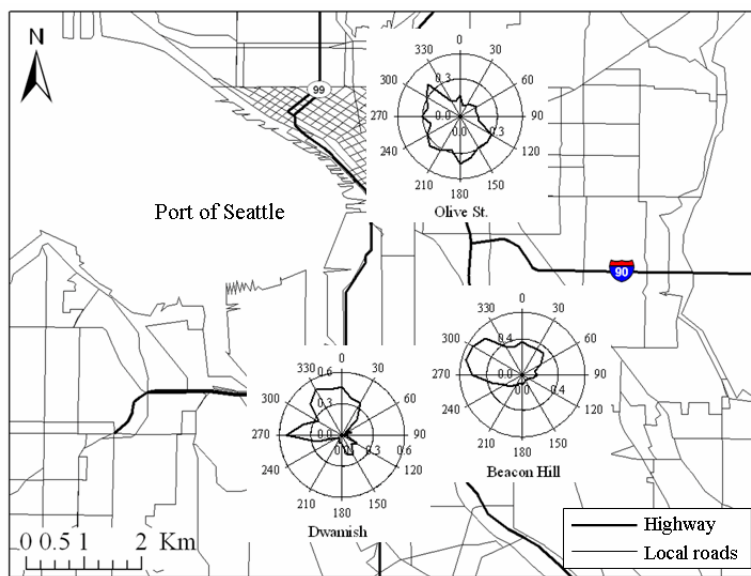


Figure 98. Source directions of oil combustion identified by PMF and CPF analyses.

Beacon Hill IMPROVE The analyzed $PM_{2.5}$ samples were collected on every third day at the IMPROVE monitoring site located at Beacon Hill, Seattle, WA (latitude: 47.5696N; longitude: 122.3119W; elevation: 97.7 m). This site is co-located with STN Beacon Hill monitoring site (See Figure 77). The Beacon Hill monitoring site is located within the urban area and 5 km southeast of the downtown business district as shown in Figure 99. The monitoring site is located inside a water reservoir impoundment. There is residential area immediate north and east of the reservoir. The Port of Seattle and container shipping/warehousing areas are located northwest and west of the site. Highways I-90 and I-5 are closely situated about 2 km north and 1 km west of the site. Wind data measured at the monitoring site were used.

For the source apportionment study, samples for which $PM_{2.5}$ were not available or below aero, or for which the $PM_{2.5}$ value had an error flag were excluded from data set. Samples for which the eight carbon fractions were not available were also excluded. The fireworks samples collected at Beacon Hill site on July 4, 2002, July 5, 2003, and January 1, 2005 were excluded in this study. Overall, 10.2 % of the original data were not included.

SO_4^{2-} was not included and only S was used in this study because they showed good correlations ($slope = 3.0 \pm 0.04$, $r^2 = 0.94$). The reported EC1 concentration in IMPROVE/TOR method includes the OP concentration. In this study, the OP was subtracted from EC1 and utilized as an independent variable. Thus, EC1 in this study did not include OP. Chemical species that have missing values more than 80 % or below MDL values more than 90 % were excluded. As recommended by Paatero and Hopke (2003), the chemical species that have S/N ratio below 0.2 (defined as bad variables) were not included in this study. A total of 316 samples collected between July 2001 and May 2004 and 34 species including $PM_{2.5}$ were used in this study. Table 30 shows a summary of $PM_{2.5}$ species analyzed in this study.

The estimated uncertainties of species that have S/N ratio between 0.2 and 2 (weak variable) and species that have below MDL values more than 50 % were increased by a factor of five and a factor of three, respectively, to reduce their weight in the solution. In addition, to obtain physically reasonable PMF solution, it was found necessary to increase three times the estimated uncertainties of K. The estimated uncertainties of OC1 were increased by a factor of three to reduce the influence of the positive artifact from the adsorption of gaseous OC. Table 30 provides a summary of $PM_{2.5}$ speciation data and S/N ratios. In this study, the measured $PM_{2.5}$ mass concentration was included as an independent variable in the PMF modeling to directly obtain the mass apportionment without the usual multiple regression (Kim et al., 2003).



Figure 99. Location of the IMPROVE monitoring sites at Beacon Hill, Seattle.

A ten-source model with FPEAK = 0 and a FKEY matrix provided the most interpretable solution. For the FKEY matrix, values of all elements were set to zero, except for a value of 5 for NO₃⁻ in airborne soil and a value of 7 for EC1 in sea salt. The average source contributions of each source to the PM_{2.5} mass concentrations are provided in Table 31.

Table 30. Summary of PM_{2.5} species mass concentrations at Beacon Hill, Seattle.

Species	Arithmetic mean (µg/m ³)	Geometric mean (µg/m ³)	Minimum (µg/m ³)	Maximum (µg/m ³)	Number of below MDL values (%)	S/N ratio
PM _{2.5}	7.4299	6.4294	1.7287	24.7531	0	NA ¹
OC1	0.2577	0.1697	0.0031	1.5751	14.9	30.2
OC2	0.4556	0.3604	0.0749	1.9753	4.1	NA ¹
OC3	1.1241	0.8697	0.0801	3.8194	0.9	1311.6
OC4	0.8806	0.6798	0.0701	3.8575	0	NA ¹
OP	0.0258	0.0186	0.0030	0.2503	88.0	0.3
EC1	0.5526	0.4614	0.0305	3.3555	0	4515.3
EC2	0.0562	0.0440	0.0062	0.2170	16.8	11.4
EC3	0.0186	0.0134	0.0030	0.0729	69.0	1.0
S	0.4225	0.3545	0.0657	1.5694	0	NA ¹
NO ₃ ⁻	0.8999	0.6925	0.0992	4.6723	0.3	9624.0
Al	0.0478	0.0350	0.0032	0.2895	69.6	3.1
As	0.0009	0.0007	0.0001	0.0036	7.9	32.0
Br	0.0024	0.0021	0.0006	0.0064	0	NA ¹
Ca	0.0338	0.0294	0.0079	0.2017	1.6	5464.2
Cl	0.0870	0.0246	0.0006	0.6720	70.9	35.8
Cr	0.0014	0.0009	0.0001	0.0125	12.3	27.7
Cu	0.0027	0.0022	0.0004	0.0136	0	NA ¹
Fe	0.0682	0.0540	0.0065	0.2574	0	NA ¹
H	0.3341	0.2833	0.0691	1.2287	0	NA ¹
K	0.0465	0.0407	0.0131	0.1677	0	NA ¹
Mg	0.0432	0.0342	0.0094	0.1107	84.8	0.4
Mn	0.0038	0.0022	0.0001	0.0254	6.6	194.4
Na	0.2543	0.2045	0.0336	0.8455	61.7	2.1
Ni	0.0017	0.0010	0.0001	0.0157	4.7	431.8
Pb	0.0034	0.0029	0.0006	0.0142	0	NA ¹
Rb	0.0002	0.0002	0.0000	0.0007	44.9	2.7
Se	0.0005	0.0003	0.0000	0.0034	7.3	122.4
Si	0.0752	0.0580	0.0079	0.6575	4.7	516.9
Sr	0.0005	0.0004	0.0001	0.0056	4.1	93.4
Ti	0.0039	0.0030	0.0002	0.0327	4.4	246.6
V	0.0050	0.0029	0.0001	0.0348	11.1	138.7
Zn	0.0107	0.0089	0.0013	0.0522	0	NA ¹
Zr	0.0003	0.0003	0.0001	0.0007	80.7	0.5

¹ not available(infinite S/N ratio caused by no below MDL value)

Comparisons of the daily reconstructed PM_{2.5} mass contributions from all sources with measured PM_{2.5} mass concentrations shows that the resolved sources effectively reproduce the measured values and account for most of the variation in the PM_{2.5} mass concentrations in Figure 100. In Figure 101, the averaged seasonal contributions from each source are compared (summer: April - September; winter: October - March). The source profiles, corresponding source contributions, weekday/weekend variations, and CPF plots are presented in Figures 102, 103, 104, and 105, respectively.

Secondary nitrate is represented by its high concentration of NO₃ and NH₄⁺. It accounts for 23 % of the PM_{2.5} mass concentration at Beacon Hill site. The secondary nitrate aerosol has seasonal variation with the highest in winter. These peaks in winter indicate that low temperature and high relative humidity help the formation of secondary nitrate particles.

Wood smoke is characterized by OC3, OC4, and K contributing 20 % to the PM_{2.5} mass concentration. This source profile has large amount of lower temperature carbon fractions (OC1–OC4). Wood smoke has a strong winter-high seasonal trend. The elevated wood smoke contributions between October 2002 and January 2003 are consistent with the results from the analysis of the Olympic National Park data. There are not clear weekday/weekend variations in the wood smoke contributions. The CPF plot for wood smoke points to the northeast and east, where the residential areas are located.

Secondary sulfate has a high concentration of S and NH₄⁺ account for 13 % of the PM_{2.5} mass concentration. As shown in the seasonal mean source contributions plot, secondary sulfate shows a strong seasonal variation with higher concentrations in summer when the photochemical activity is highest.

Table 31. Average source contributions (µg/m³) to PM_{2.5} mas concentration at Beacon Hill, Seattle..

Sources	Average source contribution (%)
Secondary nitrate	1.66 (23.3)
Wood smoke	1.40 (19.6)
Secondary sulfate	1.92 (12.9)
Gasoline vehicle	0.85 (11.9)
Aged sea salt	0.79 (11.1)
Oil combustion	0.60 (8.4)
Airborne soil	0.32 (4.5)
Sea salt	0.26 (3.7)
Metal processing	0.19 (2.6)
Diesel emissions	0.14 (2.0)

Gasoline vehicle and diesel emissions were separated by different abundances of OC and EC (Watson et al., 1994). Gasoline vehicle and diesel have high concentrations of the OC fractions and EC fractions, respectively. Specifically, gasoline vehicle emissions has large amounts of OC3 and OC4. Diesel emissions contain high concentrations of EC1. Gasoline vehicle contributed 12 % of the PM_{2.5} mass concentrations. The average contributions from diesel emissions to PM_{2.5} mass concentration were 2 %. Gasoline vehicle emissions show strong winter-high seasonal variations. Diesel emissions do not have strong seasonal variations. Gasoline vehicle and diesel emissions do not show a strong weekday/weekend variation. The CPF plots for the Beacon Hill data indicate the gasoline emission impacts from mostly residential area (northeast, east, and southeast) and the diesel emission impacts from the highway I-5 (west). As reported by Shah *et al.* (2004), diesel emissions operating at very slow speeds and

in stop and go traffic are likely to be shown as gasoline vehicle emissions. Diesel emissions extracted by PMF may represent only diesel vehicle emissions moving at reasonable speed in fluid traffic.

Aged sea salt is characterized by its high concentration of NO_3^- and Na^+ . The lack of Cl^- in the profile is caused by Cl^- displacement by acidic gases. Aged sea salt accounts for 11 % of the $\text{PM}_{2.5}$ mass concentrations. This particle shows a weak summer-high seasonal pattern. Aged sea salt does not show a weekday/weekend variation.

Oil combustion is characterized by high concentrations of OC carbon fractions, S, Ni, and V reflecting residual oil combustion for the utilities and industries. This source contributed 8 % to the $\text{PM}_{2.5}$ mass concentrations. The elevated oil combustion contributions on October 17 and 23, 2002 are consistent with the results from the analysis of the STN Beacon Hill data. Oil combustion shows a strong summer-high seasonal variations. There is not clear weekday/weekend variations in this source at Beacon Hill. The CPF plot of this source points to the Port of Seattle suggesting the sources of the oil combustion are likely cargo ships, tugs, commercial harbor craft, ferries, cargo-handling machines, and trains.

Airborne soil is represented by Si, Fe, Al and Ca contributing 5 % to the $\text{PM}_{2.5}$ mass concentration. Crustal particles could be contributed by wind-blown soil dust and re-suspended by road traffic. Airborne soil does not show clear seasonal variation. This source shows clear weekday-high variation. The CPF plot of airborne soil points to the west where highway I-5 is situated.

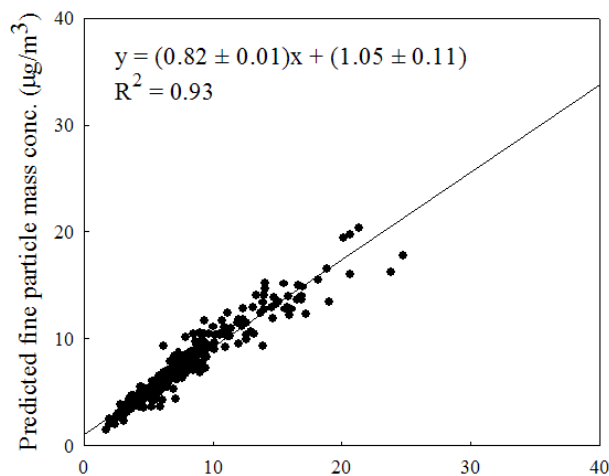


Figure 100. Measured versus PMF predicted $\text{PM}_{2.5}$ mass concentrations at Beacon Hill, Seattle.

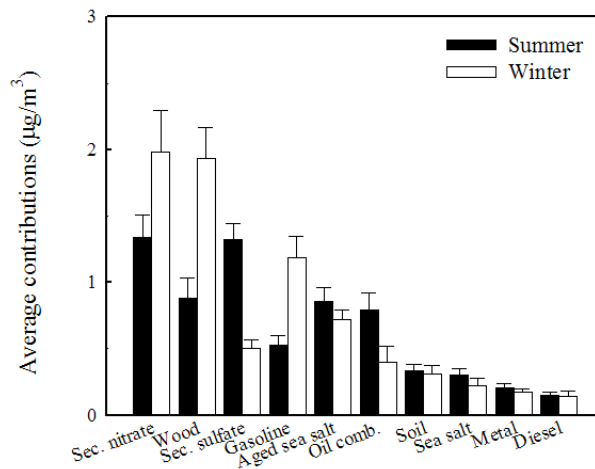


Figure 101. The seasonal comparison of source contributions to $\text{PM}_{2.5}$ mass concentration at Beacon Hill, Seattle (mean \pm 95 % distribution).

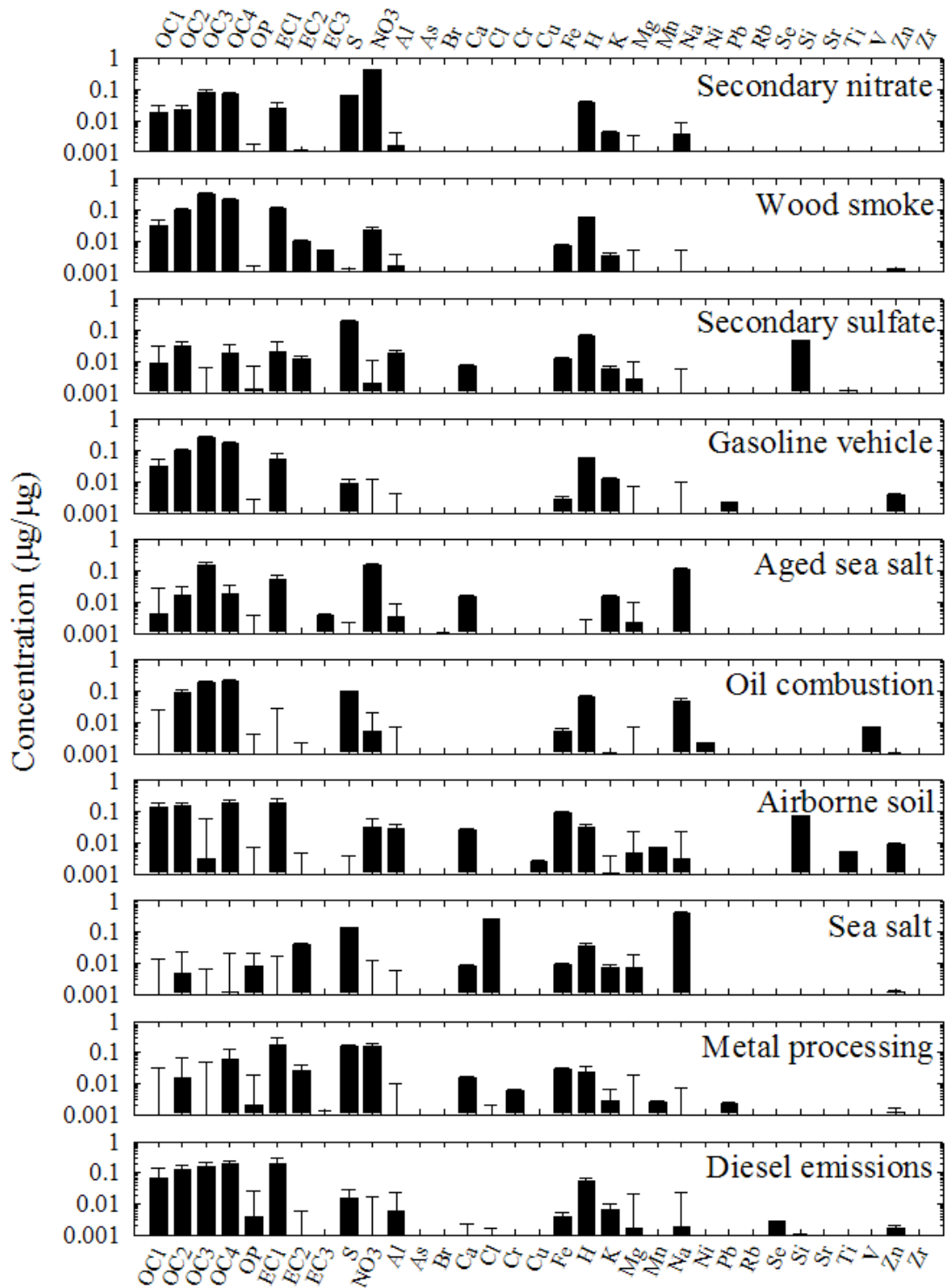


Figure 102. Source profiles deduced from PM_{2.5} samples measured at Beacon Hill, Seattle (prediction ± standard deviation).

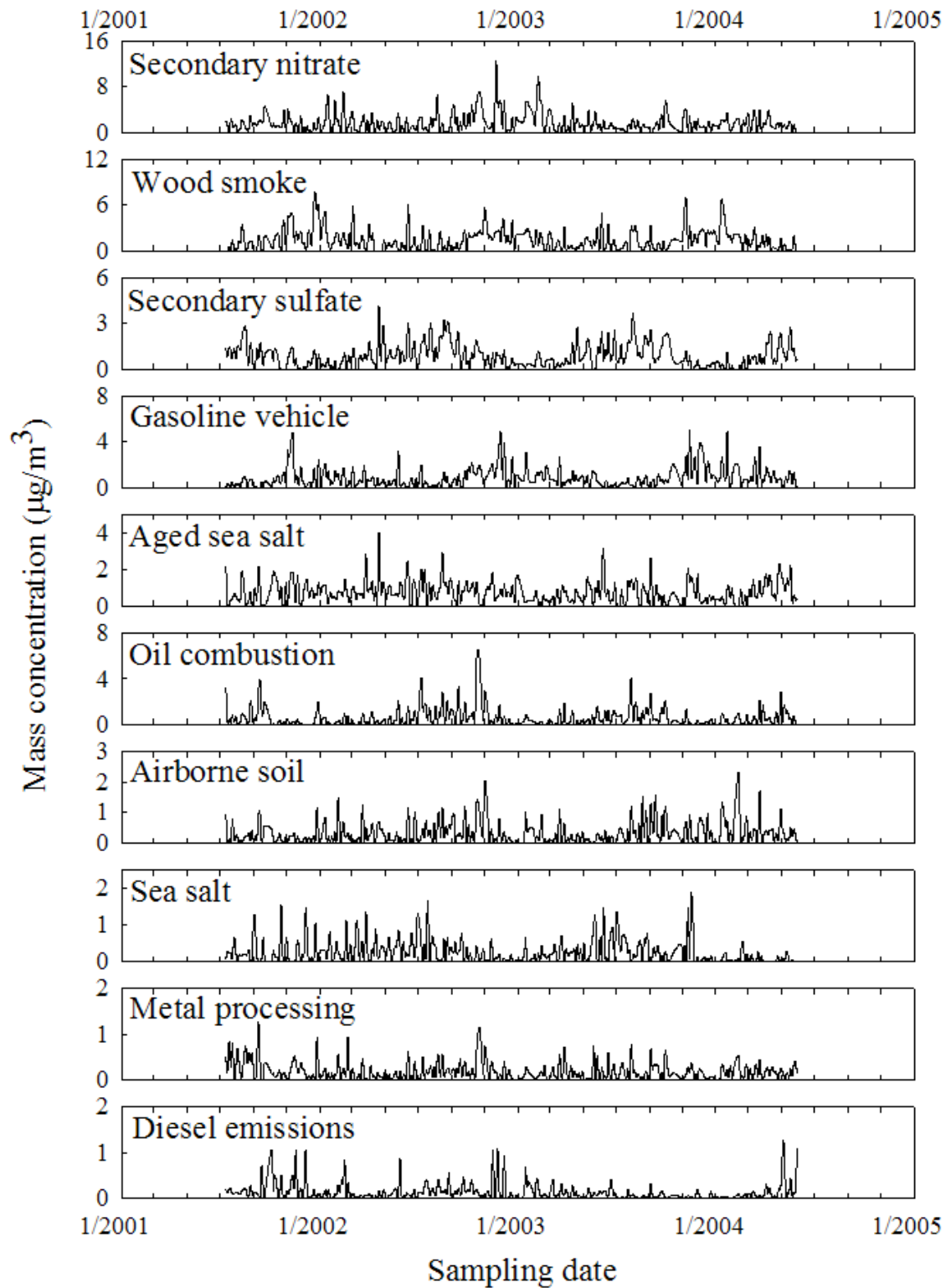


Figure 103. Time series plot of source contributions at Beacon Hill, Seattle.

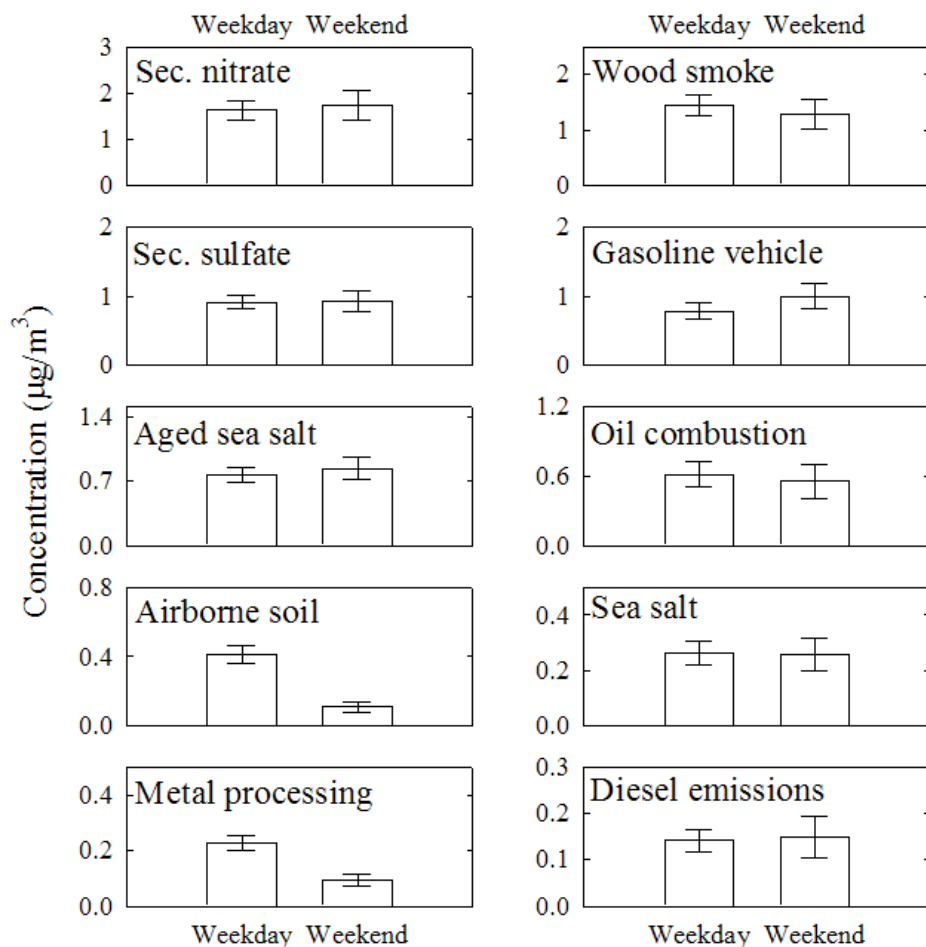


Figure 104. Weekday/weekend variations at Beacon Hill, Seattle (mean ± 95% distribution).

Sea salt is represented by its high concentration of Na^+ and Cl^- , accounting for 4% of the $\text{PM}_{2.5}$ mass concentration. This source shows a weak winter-high seasonal pattern, and does not show weekday/weekend variation. The CPF plot shows the contributions from the southwest.

Metal processing is characterized by its high concentration of OC carbon fractions, EC1, Fe, Se, and Zn. This source accounts for 3% of the $\text{PM}_{2.5}$ mass concentration. This source has a strong weekday-high variation. There are ferrous-metal processing plant located about 5 km west of the site, as well as several facilities located southwest of the site. In Figure 7, the CPF plot of metal processing points to northwest and southwest is consistent with the direction of the known industries near the Beacon Hill monitoring site.

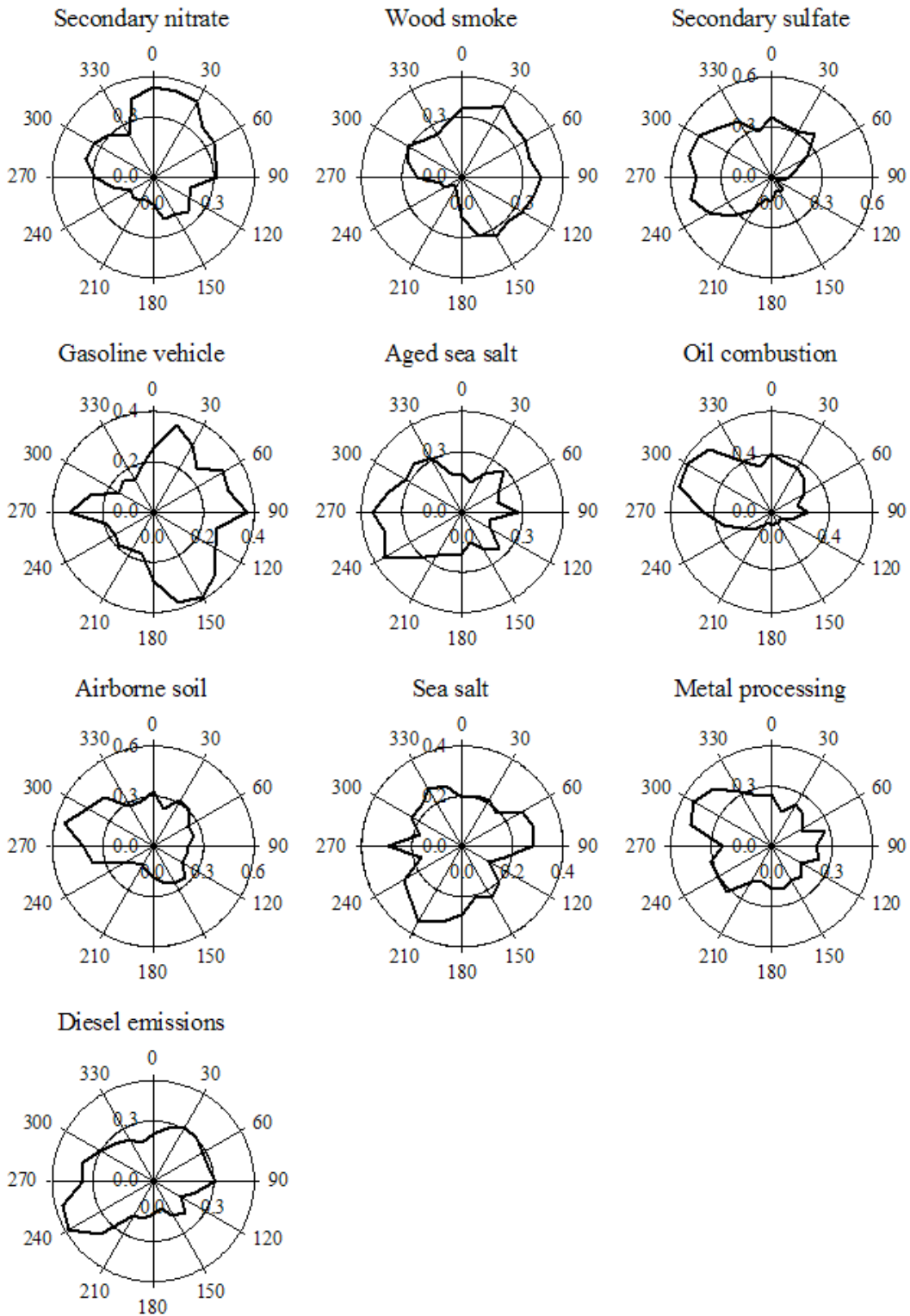


Figure 105. CPF plots for the highest 25 % of the mass contributions at Beacon Hill, Seattle.

Comparison of Beacon Hill Site Results Results were obtained from two collocated sampling systems at Beacon Hill with one in the STN network and one in the IMPROVE network. Table 32 provides a comparison of the resulting source apportionments. There are some small differences in the sampling periods between the two networks resulting in some differences in the measured concentrations as reflected in Tables 22 and 26. The apportionment results primarily reflect the differences in the organic and elemental carbon data that go into the analyses. In the STN analysis, only OC and EC are available while the 8 IMPROVE carbon fractions are included. These extra variables provide more weight to the carbon data in the fitting process. It can be seen that the sources with only limited involvement of OC or EC (sulfate, nitrate, soil, etc.) are reasonably similar and reflect the differences in the average concentrations. The major discrepancies arise in the “Gasoline vehicle” emissions and “Wood smoke” where the relative intensities are reversed between the two network data sets. There is no way to determine if one set of results is “better” than the other. However, in a city known for its wood smoke, the higher woodsmoke and lower gasoline vehicle emissions in the IMPROVE solution appear to be more reasonable. The IMPROVE data also tend to apportion somewhat more mass to the oil combustion and again the wind directional data supported an attribution of that source to the Port of Seattle.

Table 32. Comparison of the source apportionments from samples collected at the Beacon Hill Site in both the STN and IMPROVE networks.

Sources	Average Source Contributions (%)	
	Beacon Hill STN	Beacon Hill IMPROVE
Secondary nitrate	1.50 (17.9)	1.66 (23.3)
Secondary sulfate	1.51 (18.0)	1.92 (12.9)
Wood smoke	0.65 (7.8)	1.40 (19.6)
Gasoline vehicle	2.51 (30.0)	0.85 (11.9)
Diesel emissions	0.21 (2.6)	0.14 (2.0)
Airborne soil	0.22 (2.7)	0.32 (4.5)
Oil combustion	0.43 (5.1)	0.60 (8.4)
Aged sea salt	0.53 (6.4)	0.79 (11.1)
Sea salt	0.17 (2.0)	0.26 (3.7)
Metal processing	0.65 (7.7)	0.19 (2.6)

Portland, OR

PMF was applied to a $PM_{2.5}$ compositional data set of 24-hr integrated samples collected on a one-in-three day schedule at the STN Roselawn monitoring site located in Portland, OR (Figure 106). The site is at 45.5613N latitude and 122.6679W longitude. The Roselawn monitoring site is located at the urban residential area about 5 km southwest of the Portland International Airport. Highway I-5 is located 750 m west of the site. In 2004, Portland Community College situated about 500 m northwest of the site was under massive construction. Meteorological measurements at the Portland International Airport were used in this study. The sampling period analyzed in this study was October 2002 - April 2005.

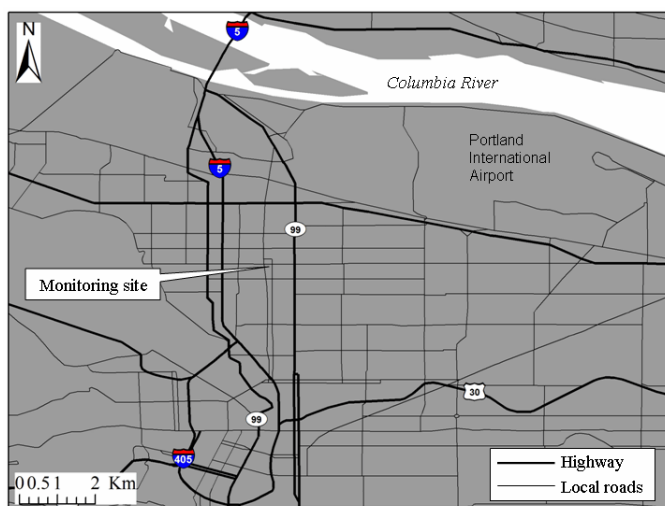


Figure 106. Location of the Roselawn monitoring site in Portland, OR..

An integrated OC blank concentration $0.87 \mu\text{g}/\text{m}^3$ was estimated utilizing the intercept of the regression of OC concentrations against $PM_{2.5}$ mass concentrations (Tolocka *et al.*, 2001). Samples for which $PM_{2.5}$ or OC data were not available were excluded before the regression between $PM_{2.5}$ and OC concentration. Comparing co-located $PM_{2.5}$ data measured by STN and Federal Reference Method (FRM), two outliers were excluded from the data set. OC concentrations in this report were blank corrected by subtracting the estimated OC blank concentration. A comprehensive set of error structures estimated by Kim *et al.* (2005) was used for this source apportionment study.

For the PMF analysis, samples for which $PM_{2.5}$ or OC data were not available or below aero, or for which $PM_{2.5}$ or OC mass concentration had error flag were excluded from data set. The fireworks samples collected on July 5, 2004 was excluded in this study. Overall, 8 % of the data were not included in this study. IC SO_4^{2-} was excluded from the analyses to prevent double counting of mass concentrations since XRF S and IC SO_4^{2-} showed good correlations ($\text{slope} = 2.6$, $r^2 = 0.95$). IC Na^+ and IC K^+ were included instead of XRF Na and XRF K in the analyses due to the higher analytical precision. Chemical species that have below MDL values more than 90 % were excluded. As recommended by Paatero and Hopke (2003), the chemical species that have S/N ratio below 0.2 (defined as bad variables) were not included. Thus, a total of 269 samples and 26 species including $PM_{2.5}$ mass concentrations collected between 2002 and 2005 were analyzed.

The estimated uncertainties of species that have S/N ratio between 0.2 and 2 (defined as weak variables) and species that have below MDL values more than 50 % were increased by a factor of five and a factor of three, respectively, to reduce their weight in the solution. The estimated uncertainties were increased by a factor of thirty for the samples for which mass concentration had error flags. Table 33 provides a summary of $PM_{2.5}$ speciation data and S/N ratios. In this study, the measured $PM_{2.5}$ mass concentration was included as an independent variable in the PMF modeling to directly obtain the mass apportionment without the usual multiple regression (Kim *et al.*, 2003).

Table 33. Summary of PM_{2.5} species mass concentrations at Roselawn site.

Species	Arithmetic mean (µg/m ³)	Geometric mean (µg/m ³)	Minimum (µg/m ³)	Maximum (µg/m ³)	Number of below MDL values (%)	S/N ratio
PM _{2.5}	10.5717	9.1869	2.9000	38.5000	0	NA [†]
OC	3.8464	3.1612	0.5942	15.5242	0	NA [†]
EC	0.8112	0.6584	0.0834	2.8700	6.3	48.9
S	0.5042	0.4201	0.0085	1.7600	0.4	13537.4
NO ₃ ⁻	1.1155	0.8431	0.0524	5.6300	0	17104.7
NH ₄ ⁺	0.6126	0.4224	0.0042	2.6900	1.9	1387.9
Al	0.0338	0.0211	0.0011	0.2430	72.1	1.2
Ba	0.0022	0.0018	0.0000	0.0079	51.3	1.5
Ca	0.0395	0.0299	0.0006	0.1890	3.3	291.0
Cl	0.0685	0.0265	0.0002	0.9440	42.8	14.4
Cr	0.0025	0.0019	0.0000	0.0318	60.6	1.6
Cu	0.0096	0.0062	0.0002	0.0523	21.9	22.0
Fe	0.0922	0.0677	0.0091	0.4920	0.7	6153.8
K ⁺	0.1061	0.0964	0.0237	0.2840	54.3	6.2
Mg	0.0270	0.0208	0.0007	0.1900	88.8	0.3
Mn	0.0109	0.0049	0.0001	0.1180	36.8	13.7
Na ⁺	0.1887	0.1451	0.0042	1.4200	5.9	91.6
Ni	0.0022	0.0017	0.0000	0.0096	48.0	2.7
P	0.0072	0.0059	0.0002	0.0456	90.0	0.2
Pb	0.0081	0.0056	0.0001	0.0698	47.2	2.9
Se	0.0022	0.0017	0.0000	0.0525	89.2	0.4
Si	0.0802	0.0537	0.0015	0.6000	14.1	46.6
Sr	0.0016	0.0015	0.0000	0.0055	84.0	0.2
Ti	0.0064	0.0041	0.0003	0.1700	50.9	2.9
V	0.0037	0.0027	0.0001	0.0199	49.8	2.4
Zn	0.0155	0.0103	0.0001	0.0836	8.6	92.7

[†] not available(infinite S/N ratio caused by no below MDL value)

In this study, ten-source model with FPEAK = 0 provided the most physically reasonable source profiles. The average source contributions of each source to the PM_{2.5} mass concentrations are provided in Table 34. Comparisons of the daily reconstructed PM_{2.5} mass contributions from all sources with measured PM_{2.5} mass concentrations shows that the resolved sources effectively reproduce the measured values and account for most of the variation in the PM_{2.5} mass concentrations in Figure 107. In Figure 108, the averaged seasonal contributions from each source are compared (summer: April - September; winter: October - March). The source profiles, corresponding source contributions, weekday/weekend variations, and CPF plots are presented in Figures 109, 110, 111, and 112, respectively.

Wood smoke is characterized by OC, EC, and K (Watson et al., 2001) contributing 27 % to the PM_{2.5} mass concentration. Wood smoke has a winter-high seasonal trend indicating residential wood burning. There are not clear weekday/weekend variations in the wood smoke contributions.

Secondary sulfate aerosol has a high concentration of S and NH₄⁺ account for 18 % of the PM_{2.5} mass concentration at Roselawn site. Secondary sulfate shows weak seasonal variation with higher concentrations in winter.

Secondary nitrate aerosol is represented by its high concentration of NO₃⁻ and NH₄⁺. It accounts for 16 % of the PM_{2.5} mass concentration. The secondary nitrate aerosol has strong seasonal variation with higher in winter. The CPF plot for the secondary nitrate aerosol points west as one of the main source directions where major highway is situated.

Aged sea salt is characterized by its high concentration of Na⁺ and NO₃⁻. The lack of Cl⁻ in the profile is caused by Cl⁻ displacement by acidic gases during the transport. Aged sea salt accounts for 10 % of the PM_{2.5} mass concentrations. The CPF plot points northwest as a main source direction of the aged sea salt.

Gasoline vehicle and diesel emissions were separated by different abundances of OC and EC (Watson et al., 1994). Gasoline vehicle and diesel have high concentration of the OC and EC, respectively. Gasoline vehicle contributed 9 % of the PM_{2.5} mass concentrations. The average contributions from diesel emissions to PM_{2.5} mass concentration were 4 %. Gasoline vehicle and diesel emissions show winter-high seasonal variations. Gasoline vehicle emissions do not show a strong weekday/weekend variation. In contrast, diesel emissions show high contributions on week days indicating that the diesel emissions are mostly from vehicles operating on weekdays. As a main source direction, the CPF plot points west and northeast for the diesel emissions. For the gasoline vehicle, the CPF plot does not clearly show specific direction. As reported by Shah *et al.* (2004), diesel emissions operating at very slow speeds and in stop and go traffic are likely to be shown as gasoline vehicle emissions. Diesel emissions extracted by PMF may represent only diesel vehicle emissions moving at reasonable speed in fluid traffic.

Table 34. Average source contributions (μg/m³) to PM_{2.5} mas concentration at Roselawn site.

Sources	Average source contribution (%)
Wood smoke	2.82 (27.4)
Secondary sulfate	1.84 (17.9)
Secondary nitrate	1.62 (15.7)
Aged sea salt	1.00 (9.7)
Gasoline vehicle	0.97 (9.4)
Airborne soil	0.58 (5.7)
Construction	0.58 (5.6)
Diesel emissions	0.41 (3.9)
Sea salt	0.25 (2.4)
Metal processing	0.23 (2.2)

Airborne soil is identified by Si, Fe, Al and Ca contributing 6 % to the PM_{2.5} mass concentration. Airborne soil has a strong summer-high seasonal variation. The weekday-high variation suggests that airborne soil may be mainly re-suspended crustal materials by road traffic.

Construction has high OC, EC, S, Ca, Cu, and Fe concentrations accounting for 6 % of the PM_{2.5} mass concentration. There was massive construction of new facilities at the Portland Community College located about 500 m northwest of the Roselawn monitoring site in 2004. Also, there was parking lot paving and building construction south and southeast of the site in summer 2004. Thus, PM_{2.5} originating from construction contributed significantly in 2004. In Figure 62, 72, 112, one of the major source directions identified by the CPF plot is northwest that is consistent with the direction of the massive construction.

Sea salt is represented by its high concentration of Na⁺ and Cl⁻, accounting for 2 % of the PM_{2.5} mass concentration. This source does not show either seasonal variation or weekday/weekend variation. The CPF plot points southwest as a source direction.

Metal processing is characterized by EC, Fe, and Mn. This source accounts for 2 % of the PM_{2.5} mass concentration. This source has a strong weekday-high variation. The CPF plot shows that this source contributed from west and northeast of the Roselawn site.

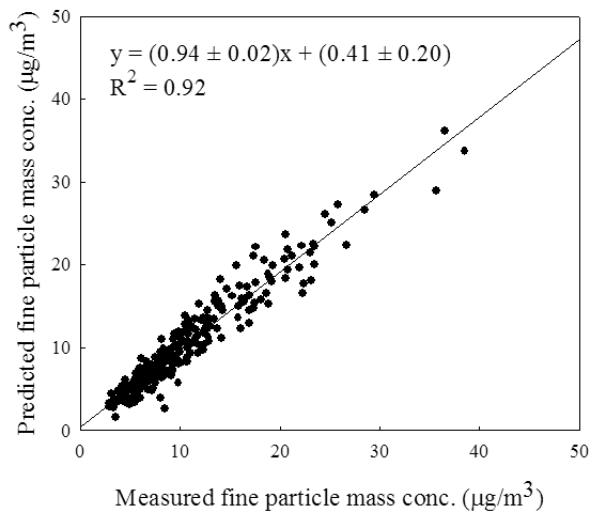


Figure 107. Measured versus PMF predicted PM_{2.5} mass concentrations at the Roselawn site in Portland, OR.

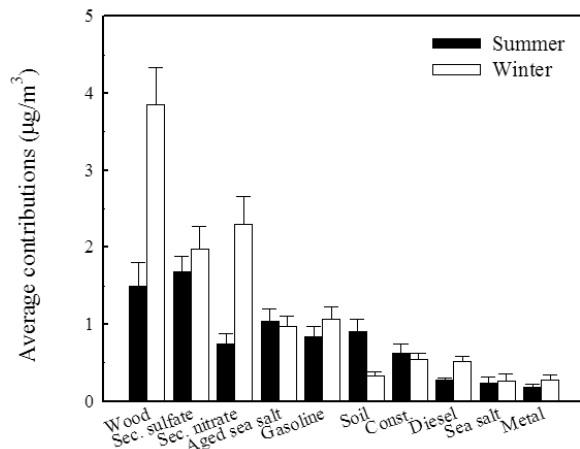


Figure 108. The seasonal comparison of source contributions to PM_{2.5} mass concentration at the Roselawn site in Portland, OR (mean ± 95 % distribution).

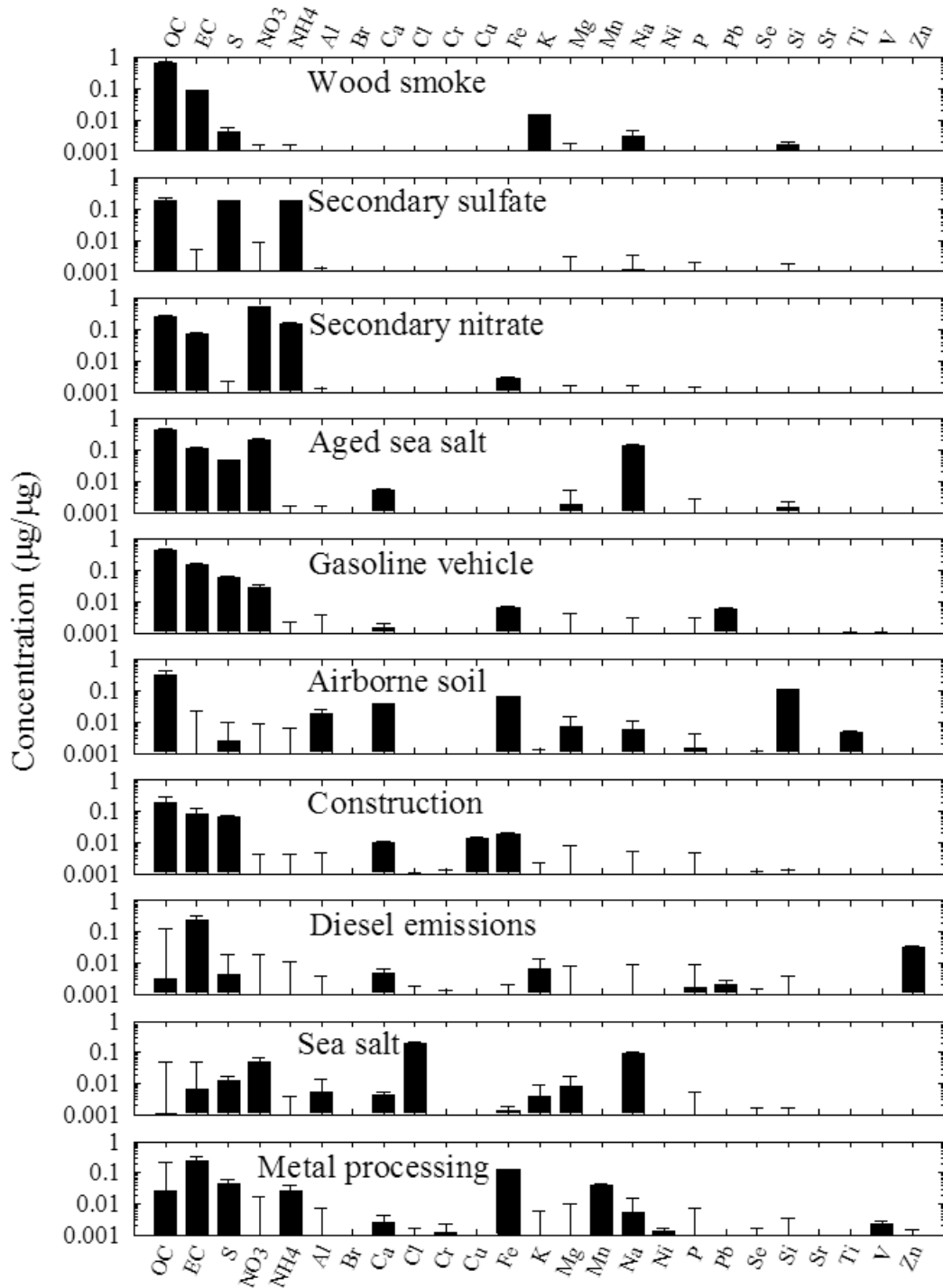


Figure 109. Source profiles deduced from PM_{2.5} samples measured at the Roselawn site in Portland, OR (prediction ± standard deviation).

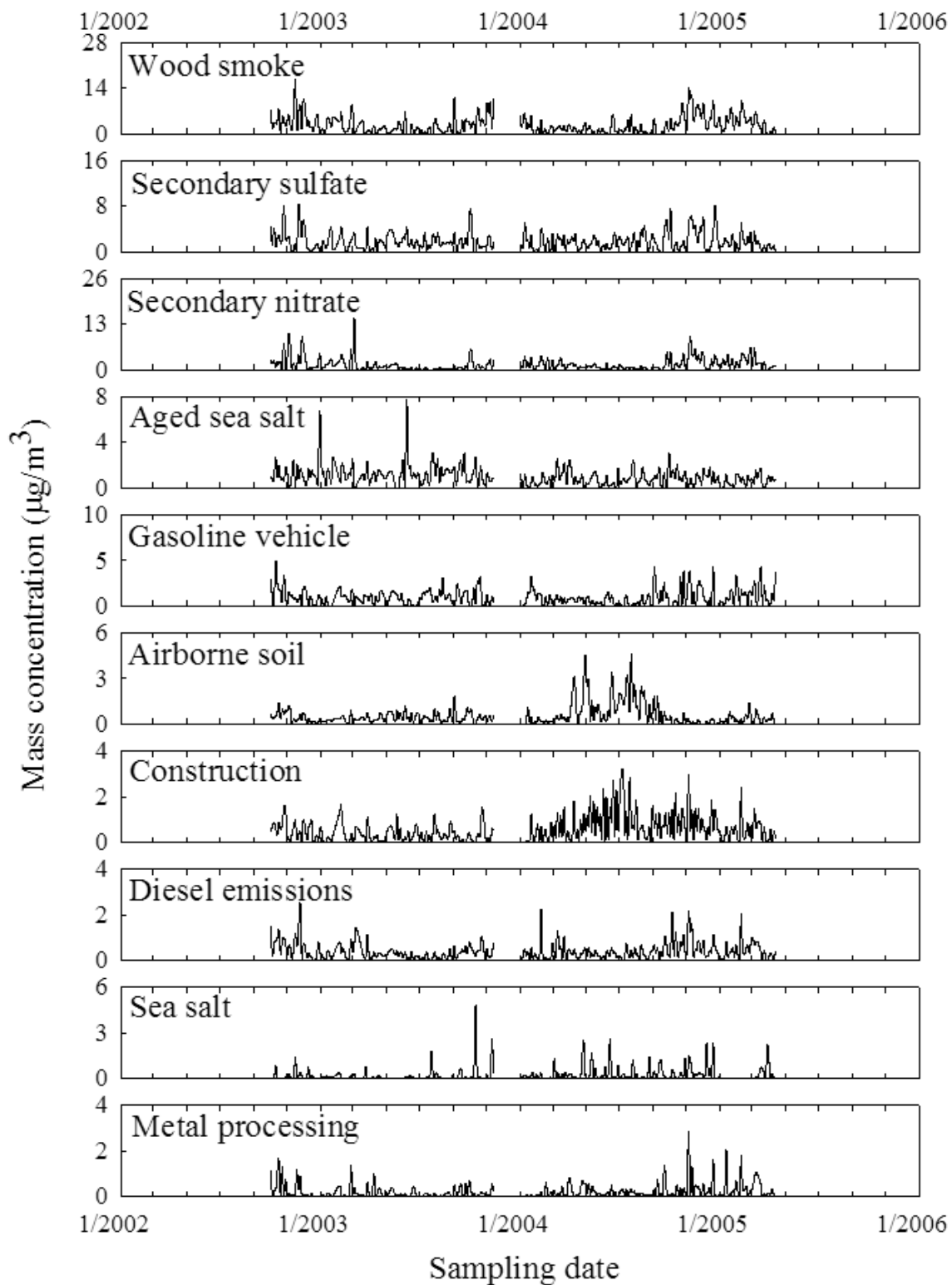


Figure 110. Time series plot of source contributions at the Roselawn site in Portland, OR.

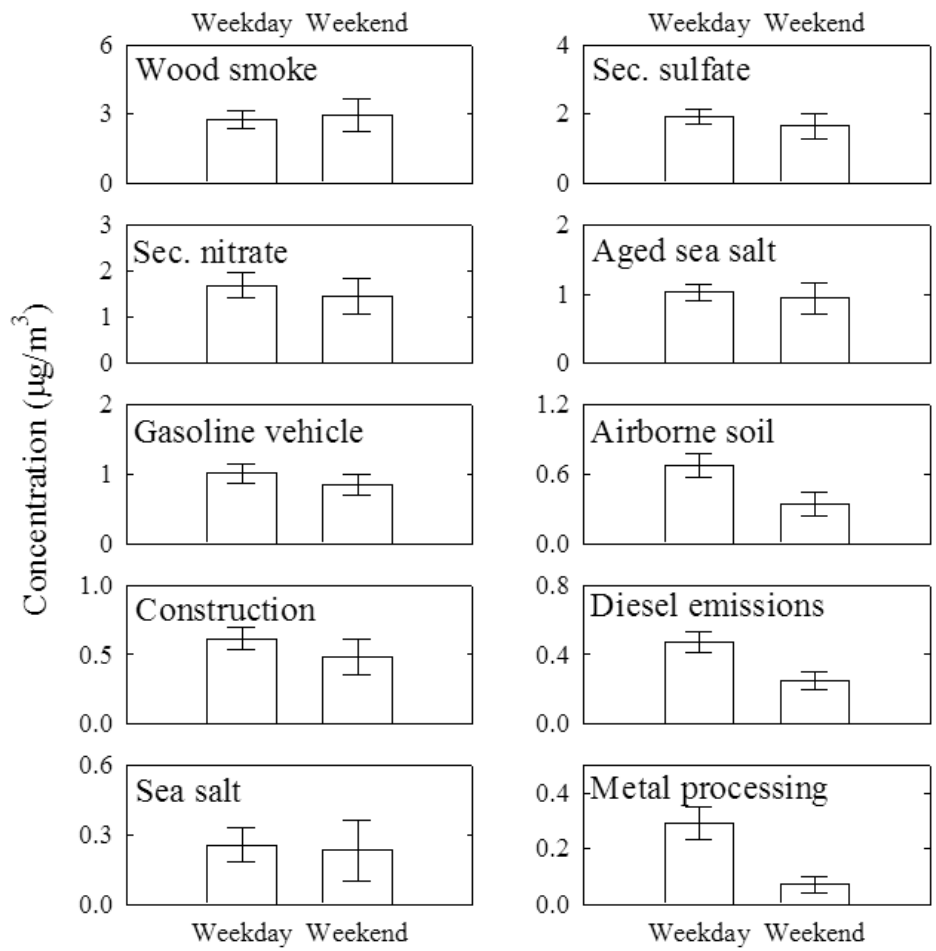


Figure 111. Weekday/weekend variations at the Roselawn site in Portland, OR (mean \pm 95 % distribution).

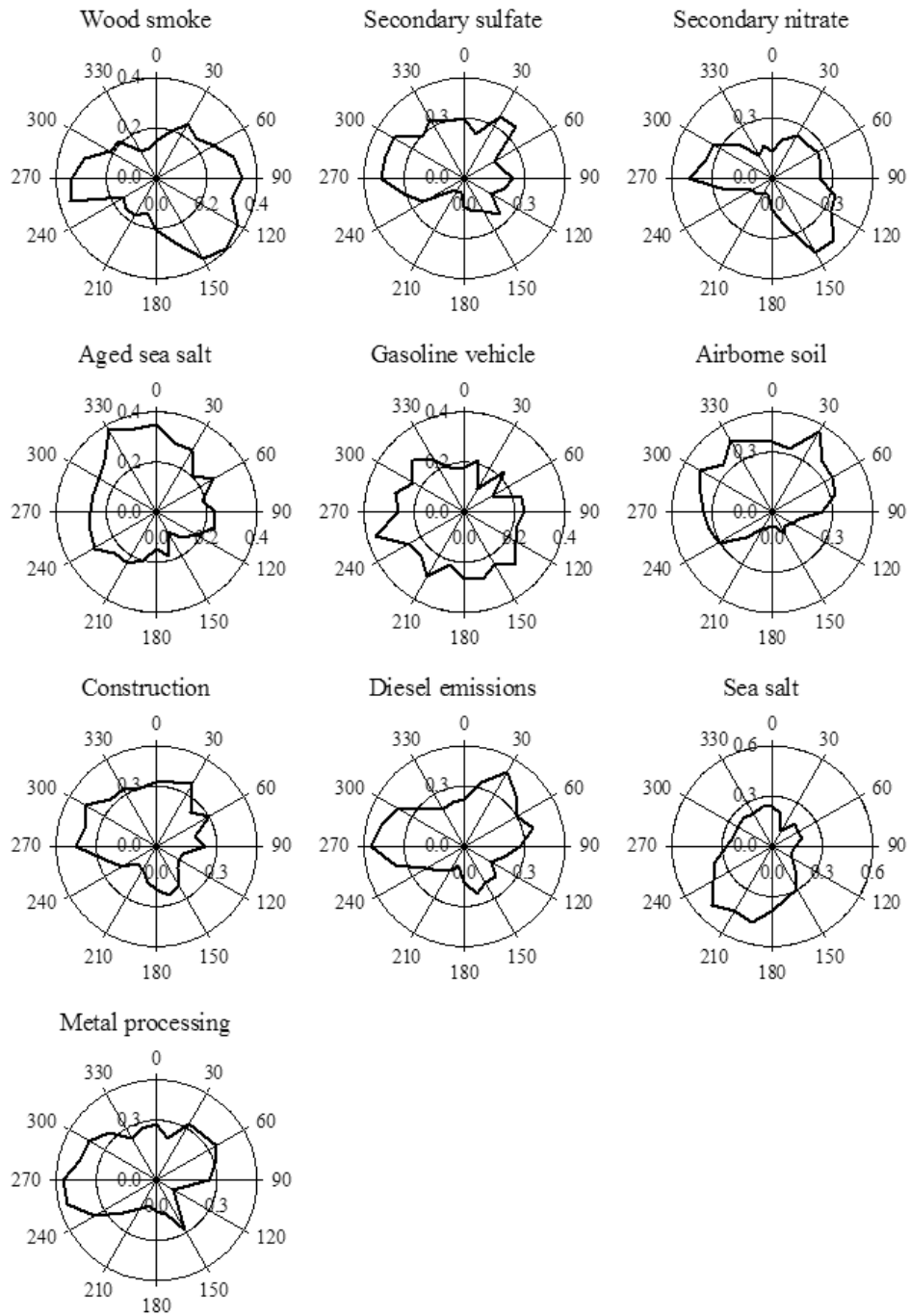


Figure 112. CPF plots for the highest 25 % of the mass contributions at the Roselawn site in Portland, OR.

San Jose, CA

PM_{2.5} samples were collected at two sites in San Jose, CA. (Figure 113). The location of the 4th Street site (site ID: 60850004) is latitude 37.34, longitude -121.89 and the location of the Jackson Street site (site ID: 60850005) is latitude 37.35, longitude -121.895. The 4th Street site was located east of San Jose International Airport and the distance between the 4th Street site and the Jackson Street site is around 8 km.

Samples were collected every 3 or 6 days and a total of 221 samples were obtained from 2/10/2000 to 5/2/2002 for the 4th Street site and a total of 230 samples were obtained from 10/20/2002 to 2/12/2005 for the Jackson Street site.

Data screening and sample selection were done in a similar manner. OC blanks were estimated and subtracted from the data (Kim *et al.*, 2005). Then, both sites' data were organized into data sets for the PMF modeling. In order to analyze point-source impacts from various wind directions, the CPF was calculated using source contribution estimates from PMF coupled with the wind direction values measured at the site (Kim *et al.*, 2003).

In the case of 4th Street site, 25 species (OC, EC, S, NO₃⁻, NH₄⁺, Al, Ba, Br, Ca, Cl, Cr, Cu, Fe, K, Mg, Mn, Na⁺, Ni, Pb, Si, Sn, Sr, Ti, V, Zn) were selected for PMF modeling and weak variables defined by the S/N ratio analyses (Cr, Mg, Pb, Sr, Sn, V) were downweighted. Also in the case of Jackson Street site, 27 species (OC, EC, S, NO₃⁻, NH₄⁺, Al, As, Ba, Br, Ca, Cd, Cl, Cr, Cu, Fe, K, Mg, Mn, Na⁺, Ni, Pb, Si, Sn, Sr, Ti, V, Zn) were selected for PMF modeling and weak variables defined by the S/N ratio analyses (As, Ba, Cd, Cr, Mg, Mn, Pb, Sr, Sn, V) were downweighted. Tables 35 and 36 present summary statistics for the individual species during the sampling periods at two sampling sites. The results of the analyses of the data from these two sites have been presented by Hwang and Hopke (2006b)

4th Street. The optimal number of sources was determined to be 9 based on examination of the scaled residuals and the Q value. The examination of the Q value a function of FPEAK was performed. To estimate source contributions and source profiles in actual units for these matrices, scaling coefficients were obtained using a multiple linear regression (Hopke *et al.*, 1980). Figure 114 shows the source profiles obtained for the 9 factor PMF solution at 4th Street, San Jose. Figure 115 presents time series of contributions from each source. Table 37 provides a comparison of seasonal contributions for each source and shows the average source contribution for the whole period of sampling using the PMF model in 4th Street, San Jose. The results of average source contributions for weekdays and weekend days at the sampling site are presented in Figure 116.

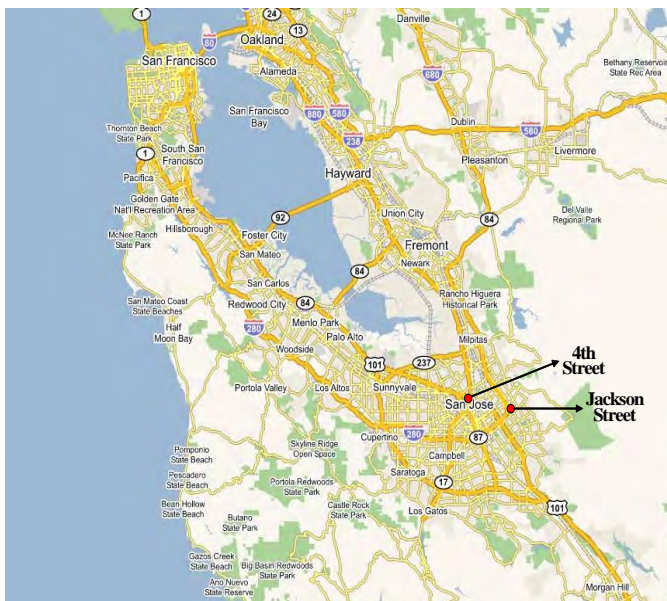


Figure 113. The location of the sampling site.

Table 35. Summary statistics for the PM_{2.5} and species concentrations in the 4th Street, San Jose.

	Arithmetic Mean (ng/m ³)	Standard Deviation (ng/m ³)	Geometric Mean (ng/m ³)	Minimum	Maximum (ng/m ³)	NO. Of BDL (%)
PM _{2.5} *	15.02	10.06	12.67	3.19	61.99	-
OC	5604.65	4345.91	4642.99	1582.20	27992.20	1(0.5)
EC	1063.73	911.35	815.39	114.20	5740.00	9(4.1)
S	472.86	266.57	402.16	63.79	1780.00	0(0.0)
NO ₃ ⁻	2908.01	2901.10	1969.91	265.00	15100.00	0(0.0)
NH ₄ ⁺	878.76	989.42	480.02	6.53	4780.00	11(5.0)
Al	47.68	72.68	23.40	0.18	601.00	103(46.6)
Ba	55.69	28.23	46.83	1.83	145.00	62(28.1)
Br	3.48	2.33	2.69	0.23	11.70	71(32.1)
Ca	99.49	86.89	77.94	17.43	813.00	0(0.0)
Cl	251.78	385.33	74.67	0.69	2370.00	41(18.6)
Cr	1.87	1.80	1.31	0.11	17.21	155(70.1)
Cu	4.26	3.58	3.00	0.11	21.20	60(27.1)
Fe	144.87	123.66	110.13	19.7	949.00	0(0.0)
K	80.17	65.65	59.20	6.88	338.00	1(0.5)
Mg	41.99	45.90	26.81	0.23	338.00	131(59.3)
Mn	3.59	3.18	2.48	0.11	19.80	100(45.2)
Na ⁺	633.01	489.09	479.44	43.20	2490.00	2(0.9)
Ni	16.35	36.66	6.35	0.11	426.00	29(13.1)
Pb	5.51	10.51	3.64	0.11	143.70	138(62.4)
Si	163.22	196.66	111.53	18.04	1960.00	0(0.0)
Sn	17.75	6.96	16.22	1.93	35.60	126(57.0)
Sr	3.20	4.34	1.89	0.11	28.50	162.(73.3)
Ti	9.13	7.20	7.07	0.45	56.40	38(17.2)
V	2.02	1.62	1.39	0.06	8.99	168(76.0)
Zn	9.93	11.35	5.67	0.11	64.20	61(27.6)

* : unit is µg/m³

Table 36. Summary statistics for the PM_{2.5} and species concentrations at the Jackson Street, San Jose.

	Arithmetic Mean (ng/m ³)	Standard Deviation (ng/m ³)	Geometric Mean (ng/m ³)	Minimum (ng/m ³)	Maximum (ng/m ³)	NO. of BDL (%)
PM _{2.5} *	14.35	10.11	11.79	2.28	55.89	-
OC	5312.07	3869.68	4267.57	663.10	19476.90	1(0.4)
EC	973.98	860.58	720.44	65.80	4950.00	10(4.3)
S	455.39	323.14	373.78	57.10	2360.00	0(0.0)
NO ₃ ⁻	2968.64	3160.12	1886.81	228.00	19600.00	15(6.5)
NH ₄ ⁺	1017.92	1167.03	564.65	9.70	6130.00	21(9.1)
Al	47.19	53.23	27.66	0.12	370.00	131(57.0)
As	1.70	1.34	1.14	0.01	8.00	188(81.7)
Ba	24.44	19.95	17.93	0.24	124.00	194(84.3)
Br	3.54	2.51	2.55	0.02	11.50	69(30.0)
Ca	78.11	59.81	62.00	8.87	399.00	0(0.0)
Cd	6.40	6.72	3.65	0.08	42.30	209(90.9)
Cl	267.97	367.62	91.62	0.12	2220.00	58(25.2)
Cr	2.88	4.87	1.58	0.08	45.20	137(59.6)
Cu	6.73	7.32	4.48	0.12	69.60	46(20.0)
Fe	138.80	112.86	107.79	16.90	727.00	0(0.0)
K	100.84	148.25	69.48	2.67	1640.00	1(0.4)
Mg	53.54	45.95	34.93	0.93	212.00	158(68.7)
Mn	2.46	2.17	1.66	0.02	13.80	153(66.5)
Na ⁺	480.91	407.32	340.36	23.00	1900.00	18(7.8)
Ni	8.01	13.10	4.02	0.04	132.00	46(20.0)
Pb	3.87	4.55	2.28	0.08	45.20	178(77.4)
Si	129.40	122.39	91.38	4.64	990.00	11(4.8)
Sn	11.47	8.98	7.31	0.12	36.60	206(89.6)
Sr	3.25	4.68	1.93	0.10	31.30	165(71.7)
Ti	8.41	6.57	6.31	0.24	47.00	61(26.5)
V	2.46	2.39	1.78	0.12	22.90	159(69.1)
Zn	8.15	8.51	5.05	0.12	59.80	57(24.8)

* : unit is µg/m³

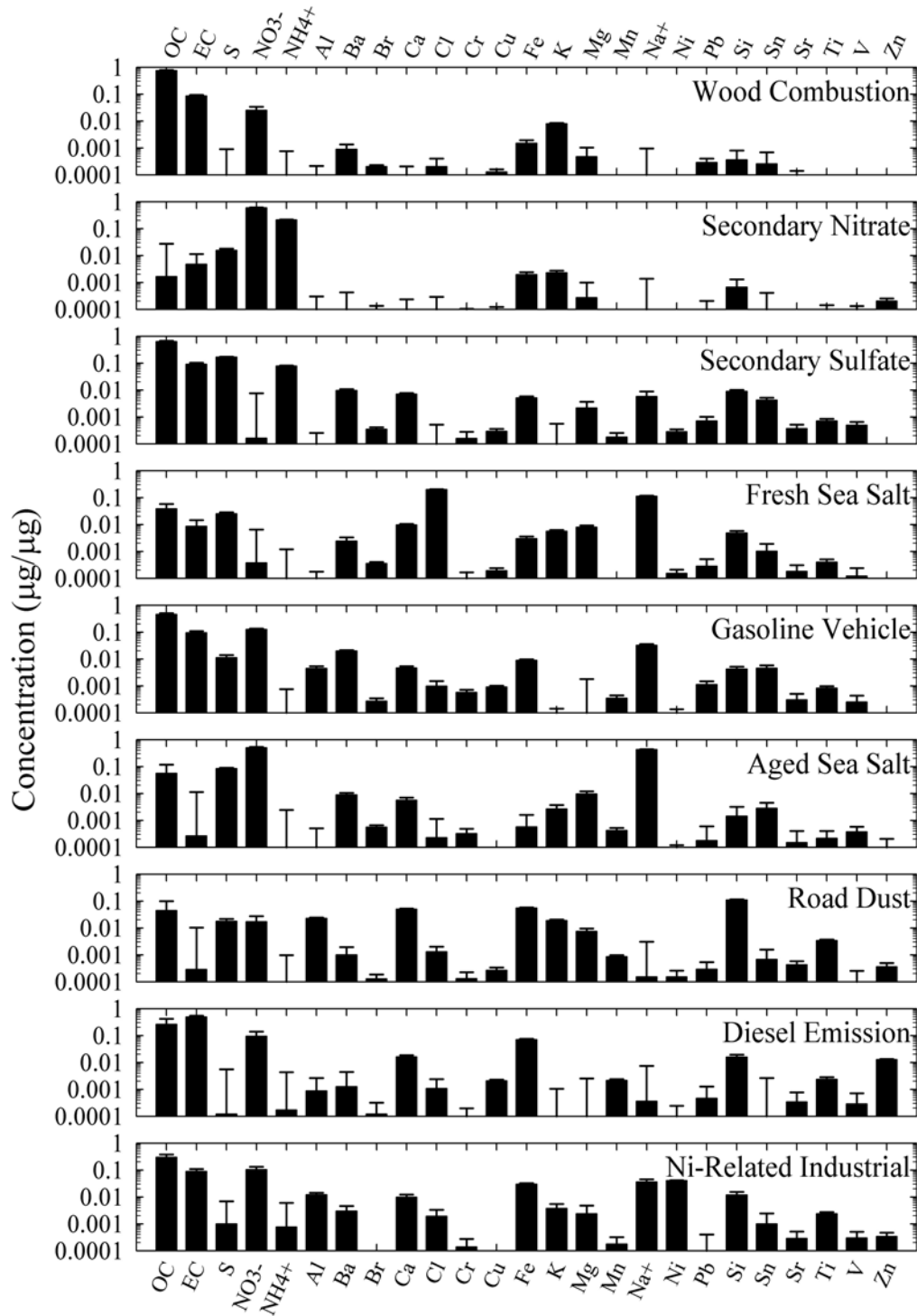


Figure 114. Source profile for the 4th Street STN site.

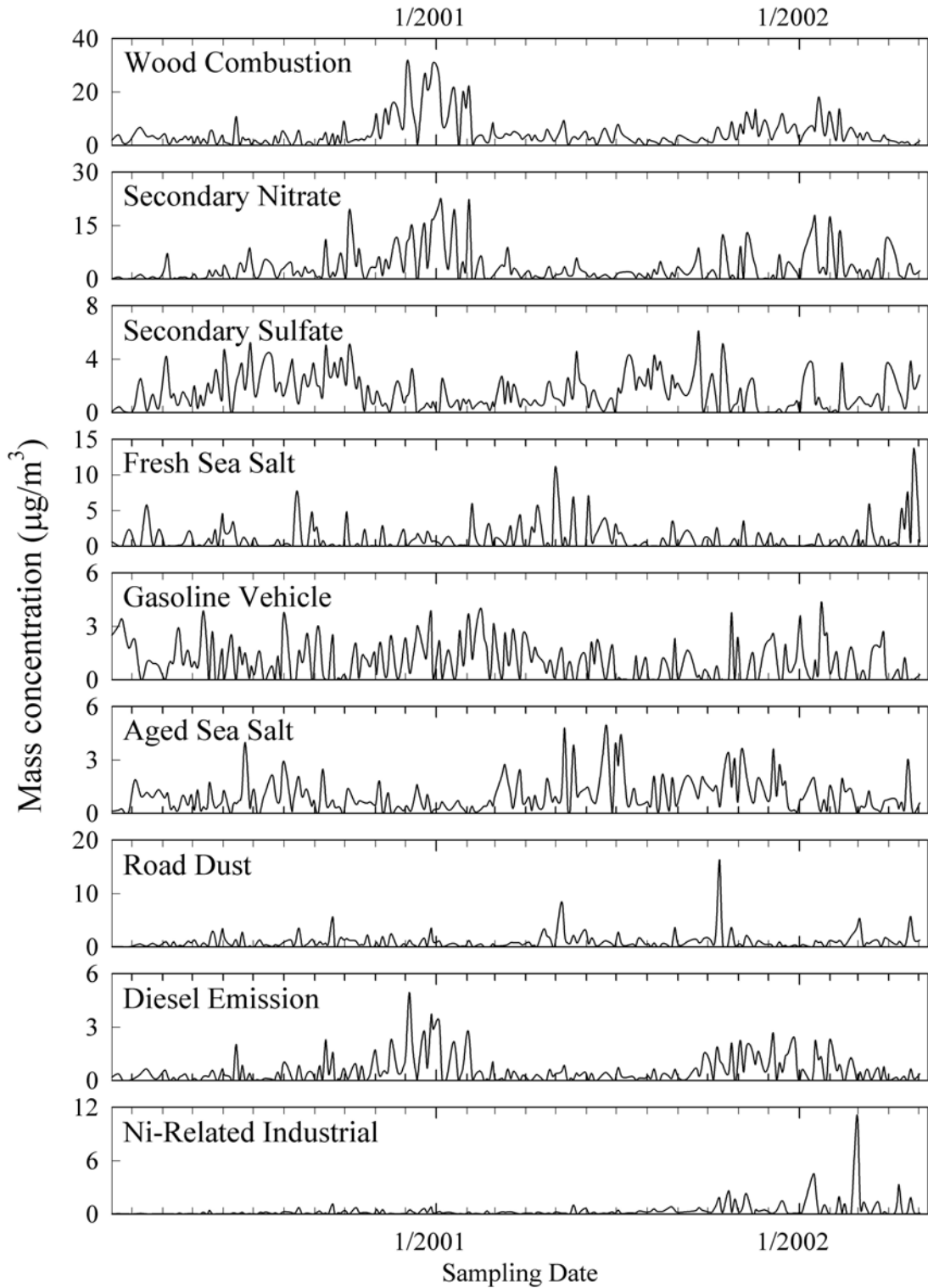


Figure 115. Temporal variation of source contribution for the 4th Street STN site.

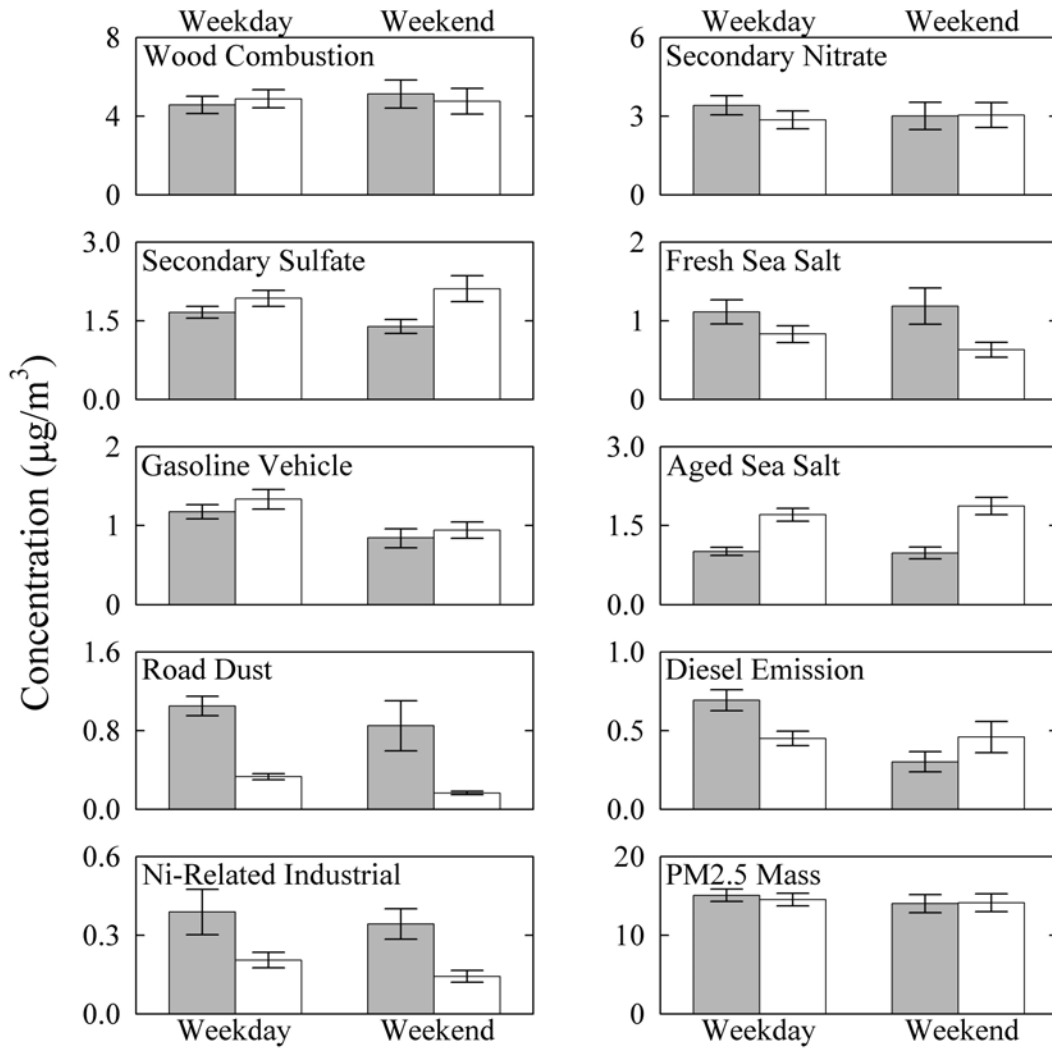


Figure 116. The average source contributions for weekdays and weekend days in 4th Street (gray bar) and Jackson Street (white bar).

The species contributing to the first source included OC, EC, NO₃⁻, K, Fe, and Mg. This profile was identified as the wood combustion source. As shown in the time series plot for this source, the highest level of wood combustion occurred in the winter. With particularly high contributions in winter 2001. Table 4 shows that the contributions during the winter were about 2.3 times higher than the contribution during the summer, and that weekend contributions were somewhat higher than weekday contributions (Figure 116).

Table 37. Average seasonal source contribution using the PMF model in 4th Street, San Jose.

	Winter		Spring		Summer		Fall		AVG.	
	µg/m ³	%								
Wood Combustion	9.5	44.4	2.88	24.8	2.1	19.1	4.9	31	4.73	32.1
Secondary Nitrate	5.79	27	1.91	16.5	1.99	18	3.86	24.4	3.29	22.3
Secondary Sulfate	0.73	3.4	1.47	12.7	2.34	21.2	1.84	11.6	1.58	10.7
Fresh Sea Salt	0.76	3.6	1.65	14.2	1.3	11.8	0.66	4.2	1.13	7.7
Gasoline Vehicle	1.64	7.7	1.04	9	0.79	7.1	0.79	5	1.07	7.3
Aged Sea Salt	0.7	3.2	0.97	8.4	1.27	11.6	1.11	7	1.01	6.8
Road Dust	0.58	2.7	1.17	10.1	0.79	7.1	1.41	8.9	0.99	6.7
Diesel Emission	1.09	5.1	0.25	2.2	0.27	2.4	0.79	5	0.57	3.9
Ni-Related Industrial	0.63	3	0.27	2.3	0.18	1.6	0.45	2.8	0.37	2.5
Sum	21.42	100	11.62	100	11.01	100	15.81	100	14.75	100

The major marker species contributing to the second source included NO₃⁻ and NH₄⁺, and this was classified as secondary nitrate. The average mass contributions of secondary nitrate show a peak in winter. Weekday contributions were somewhat higher than weekend contributions (Figure 116).

The species associated with the third source included S and NH₄⁺, and these were classified as secondary sulfate. The average seasonal mass contributions show its peak contribution to be in the summer. Figure 116 shows that no significant difference between the concentrations measured on weekdays versus those measured on weekend days. Since NOx emissions (559.9 tons/day) in the San Francisco Bay area were greater than SOx emissions (71.6 tons/day), it can be expected that the secondary nitrate contributions should be greater than the secondary sulfate contributions.

The species contributing to the fourth source included Cl, Na⁺, S, Ca, Mg, K, and Si. This source was identified as fresh sea salt. The peak seasonal mass contributions of fresh sea salt source was in the spring. There was no difference between the concentrations measured on weekdays versus those measured on weekends (Figure 116).

The fifth source was assigned the gasoline vehicle emissions. OC, EC, and NO₃⁻ were major species contributing to the third source along with minor species such as Ba, Fe, Sn, Al, Ca, and Pb. This source was identified on the basis of high levels of OC and EC, with a higher proportion of OC. However, Shah et al. (2004) have shown that very slow moving and stop and go diesel vehicle emissions have OC/EC ratios that are very similar to those of gasoline vehicles. Thus, it is likely that this is a mixed source including gasoline and slow moving diesel vehicle emissions. The gasoline vehicle emission contributions showed no difference among the seasons

(Table 37). Weekday contributions of gasoline vehicle emissions were higher than the weekend contributions (Figure 116).

The sixth source was classified as the aged sea salt source. Although the main species in sea salt are known to be Na^+ , Cl , SO_4^{2-} , K , and Ca , only Na^+ showed a high concentration in the source profile. Cl was again depleted so this is aged sea salt. Aged sea salt source showed relatively low contributions in all seasons (winter $0.70 \mu\text{g}/\text{m}^3$, spring $0.97 \mu\text{g}/\text{m}^3$, summer $1.27 \mu\text{g}/\text{m}^3$, and fall $1.11 \mu\text{g}/\text{m}^3$, respectively). Similar to the fresh sea salt contributions, the aged sea salt source showed no significant difference between weekdays and weekend days (Figure 116).

The major species contributing to the seventh source included Si , Fe , Ca , Al , K , and Mg and this factor was assigned to be soil and road dust. The temporal variation of source contribution plot shows very strong contributions in October 2001. It is not known why such high values were observed during this period. During the fall, there can be strong Santa Ana winds from the east and soil could be carried to the site from the Central Valley. The weekday contribution of soil/road dust source was higher than the weekend contribution (Figure 116) that is similar to the increased contribution of gasoline vehicles to the weekday samples.

The major species contributing to the eighth source included OC , EC , NO_3^- , Fe , Na^+ , Si , Zn , Ca , and Cu . This source was assigned to diesel emissions. For diesel emissions, EC was higher relative to OC than was seen in the gasoline vehicle source profile. Zn and Ca are additives in motor oil and Si , Cu and Fe are released from brake pads. The Fe can also be from muffler ablation. For diesel emissions, the winter ($1.09 \text{ mg}/\text{m}^3$) and fall ($0.79 \text{ mg}/\text{m}^3$) contributions were higher than the spring ($0.25 \text{ mg}/\text{m}^3$) and summer contributions ($0.27 \text{ mg}/\text{m}^3$). The weekday contribution of diesel emission was higher than the weekend contribution (Figure 116).

The final source was an unknown Ni-related industrial source. The species contributing to this source as markers included OC , EC , NO_3^- , Fe , Na^+ , and Ni . Ni is generally associated with oil combustion, but there was no V in this source profile. The average concentration of Ni over the sampling period ($16.35 \text{ ng}/\text{m}^3$) is much higher than the average concentration of V ($2.02 \text{ ng}/\text{m}^3$). Also, Ni had little correlation with V ($r = 0.2$). This source was assigned to be some type of Ni-related industrial source. The contribution temporal variation plot shows very high values in February 2002. There is no significant difference between the concentrations measured on weekdays versus weekend days (Figure 116).

Jackson Street. The optimal number of sources in Jackson Street was also determined to be 9. Figure 117 shows the source profiles for the Jackson Street, San Jose site. Figure 118 presents the contributions of each source that to the $\text{PM}_{2.5}$ mass. Table 38 presents a comparison of seasonal contributions for each source and the average source contribution for the whole period of sampling using the PMF model at the Jackson Street site in San Jose.

The species contributing to the first source as markers included OC , EC , NO_3^- , K , Fe , and Ba and this profile was again assigned to wood combustion. Again the winter contributions were higher than the other seasonal contributions (winter $8.92 \mu\text{g}/\text{m}^3 > \text{fall } 5.68 \mu\text{g}/\text{m}^3 > \text{spring } 2.04 \mu\text{g}/\text{m}^3 > \text{summer } 1.11 \mu\text{g}/\text{m}^3$). At Jackson Street, there were no differences between the weekdays contributions versus those for weekend days (Figure 116).

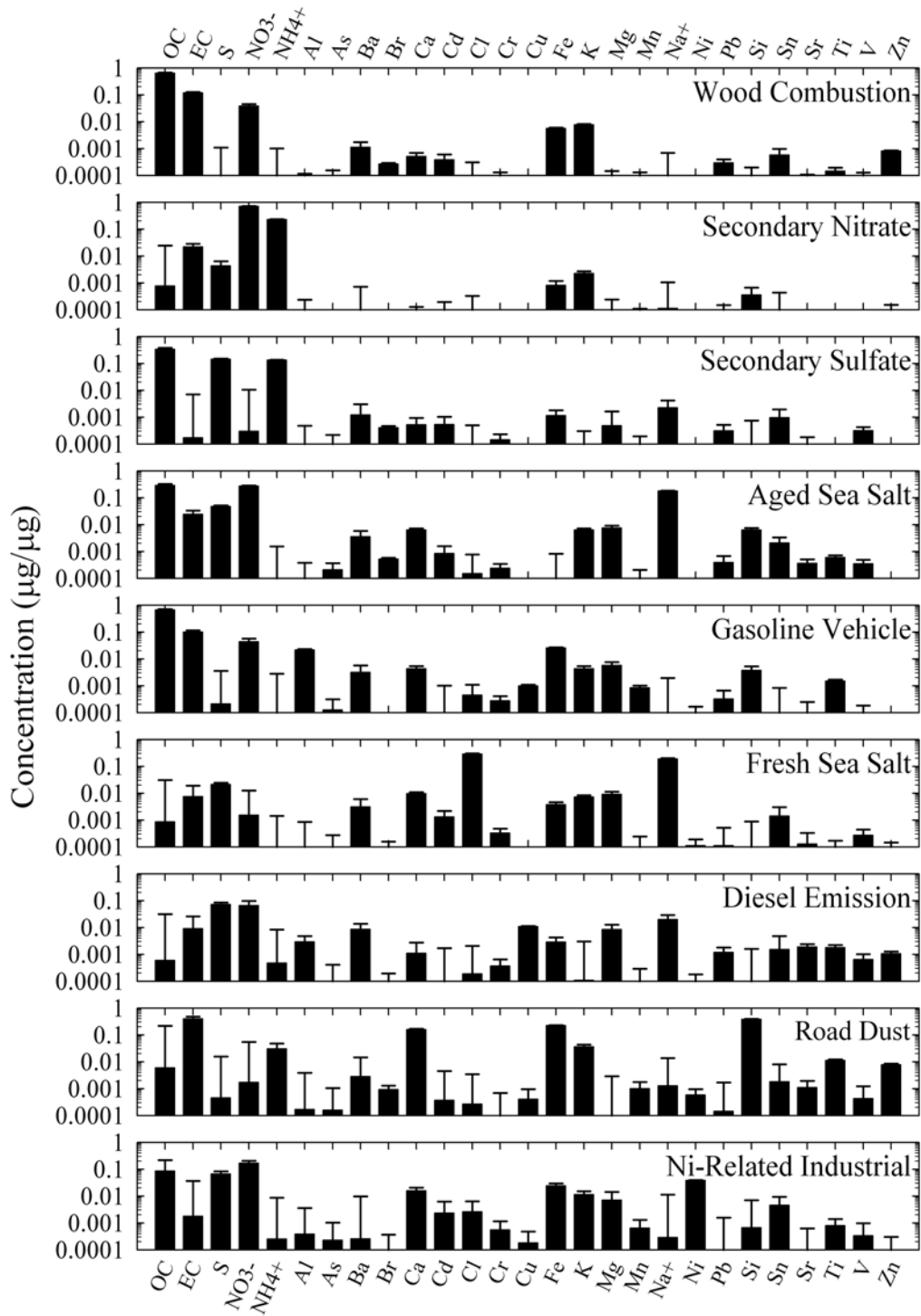


Figure 117. Source profiles for the Jackson Street STN site.

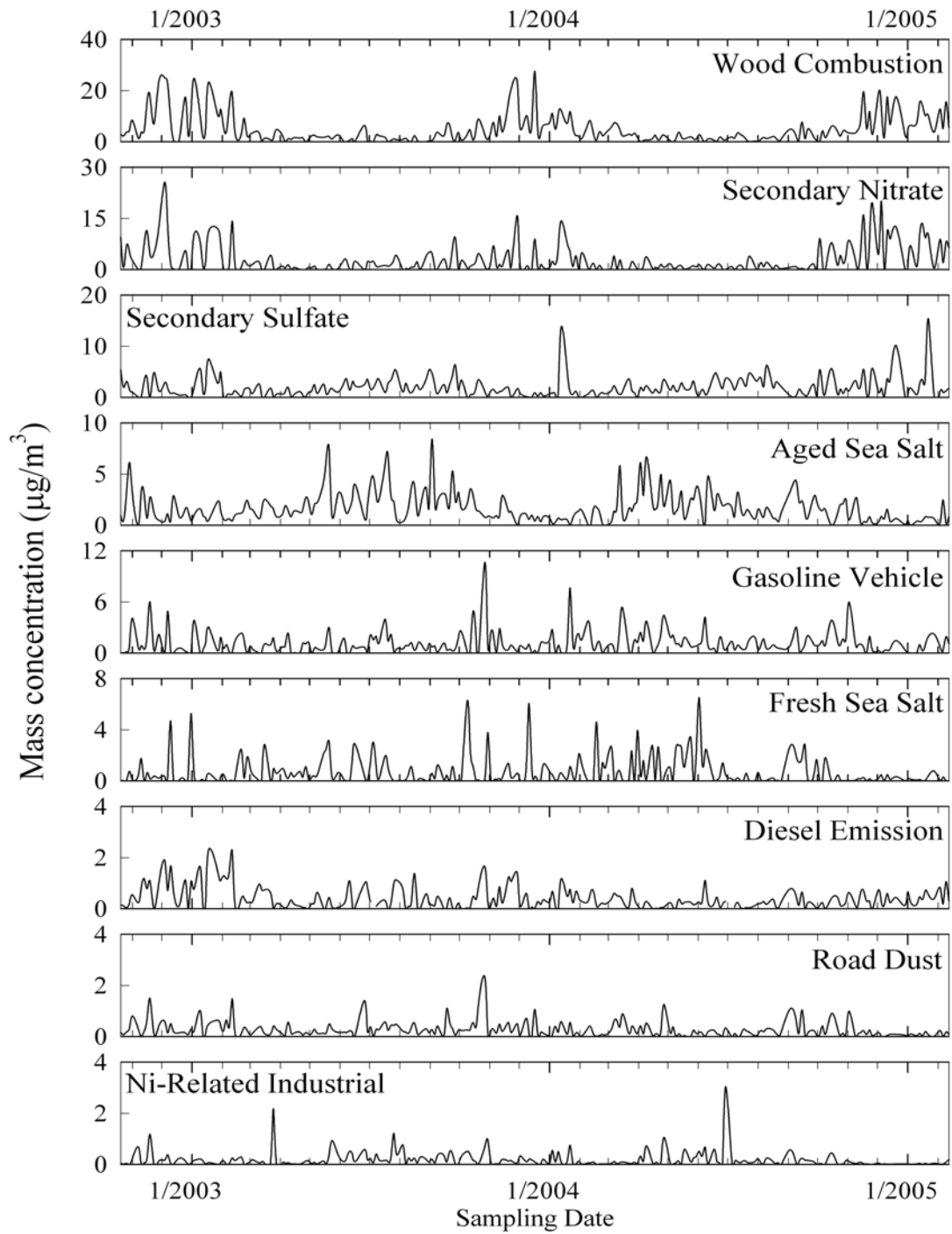


Figure 118. Temporal variation of source contribution for the Jackson Street STN site.

Table 38. Average seasonal source contributions in Jackson Street, San Jose.

	Winter		Spring		Summer		Fall		AVG.	
	$\mu\text{g}/\text{m}^3$	%								
Wood Combustion	8.92	46.8	2.04	21.1	1.11	11.1	5.68	34.1	4.84	33.6
Secondary Nitrate	4.77	25	0.9	9.3	1.27	12.7	3.89	23.4	2.92	20.3
Secondary Sulfate	1.89	9.9	1.38	14.3	2.75	27.4	1.99	12	1.99	13.9
Fresh Sea Salt	0.67	3.5	1.07	11.1	0.66	6.6	0.68	4.1	0.76	5.3
Gasoline Vehicle	1.06	5.6	1.17	12.2	1.04	10.4	1.49	9	1.2	8.3
Aged Sea Salt	0.84	4.4	2.4	24.9	2.13	21.2	1.95	11.7	1.76	12.4
Road Dust	0.23	1.2	0.25	2.6	0.23	2.3	0.38	2.3	0.27	1.9
Diesel Emission	0.59	3.1	0.24	2.5	0.56	5.6	0.39	2.4	0.45	3.2
Ni-Related Industrial	0.1	0.5	0.19	2	0.29	2.9	0.18	1.1	0.18	1.3
Sum	19.08	100	9.65	100	10.04	100	16.65	100	14.38	100

The species contributing to the second source are NO_3^- , NH_4^+ , and EC and was identified as secondary nitrate with its peak contributions again in the winter. This source showed no weekend/weekday differences (Figure 116). The third source profile included S, NH_4^+ , and OC and was assigned to be secondary sulfate. In the case of this average source contributions (1.99 $\mu\text{g}/\text{m}^3$, 13.9%) were about 1.3 times higher than the secondary sulfate at the 4th Street site (1.58 $\mu\text{g}/\text{m}^3$, 10.7%).

The fourth source was identified as the aged sea salt source. The major marker species is Na^+ , OC, NO_3^- , S, EC, Ca, and K. The average aged sea salt source contributions were highest in the spring and lowest in winter (Table 38) with no differences between the weekday and weekend contributions (Figure 116).

The fifth source was assigned to gasoline vehicle emissions. OC and EC were the major species contributing to this profile along with NO_3^- , Al, Fe, Ba, Ca, K, and Mg. Gasoline vehicle emissions contributions showed higher weekday values than those on the weekends (Figure 116).

The species contributing to the sixth source included Na^+ , Cl, Ca, Mg, K, and Fe. This factor was identified as fresh sea salt. The average seasonal mass contributions of fresh sea salt were similar to those of aged sea salt with a maximum in the spring and a minimum in the winter and no weekend/weekday difference.

The major species contributing to the seventh source included EC, OC, NO_3^- , S, Ba, Cu, Mg, Na^+ , and Zn. This profile was classified as diesel emissions although with somewhat different proportions of EC and OC as compared to the 4th Street site diesel emission source. EC is the primary pollutant emitted by diesel combustion. The temporal variation of diesel emissions showed fairly uniformly values over the sampling period with no seasonal differences (Table 38).

The major species contributing to the eighth source included Si, Fe, Ca, K, EC, and Ti. This source was classified as road dust source. Temporal variation of road dust source shows uniformly trends during the sampling period except Oct. 27, 2003 contribution. This source showed only small differences among the seasons with a small increase in the fall during the period of the easterly Santa Ana winds. The weekday contributions of soil source were higher

than the weekend contributions (Figure 116) probably as a result of the higher traffic levels on weekdays.

Finally, the ninth source was again an unknown Ni-related industrial source. The species contributing to this source as markers included NO_3^- , OC, S, Ni, Fe, Ca, and Sn. The mass contribution of Ni-related industrial source showed a weak peak in the summer. Weekday contribution was higher than the weekend contribution (Figure 116). The weekday pattern suggests activities of this facility on weekdays.

Comparison of the 4th Street and Jackson Street Results. This study applied PMF to data from two sampling sites (former site and relocated site). Nine sources were found at both sites: wood combustion, secondary nitrate, secondary sulfate, fresh sea salt, gasoline vehicle, aged sea salt, road dust, diesel emission, and Ni-related industrial source, respectively. The CPF plots in the 4th Street (black line) and Jackson Street (gray line) are presented in Figure 119. In this figure, the gray areas denote the area of overlap between the 4th Street and the Jackson Street results. The CPF plot indicated wood combustion source located to the east, south, west-southwest, and north (weak). In the case of $\text{PM}_{2.5}$ emission inventory in this area, residential wood combustion is the highest source of $\text{PM}_{2.5}$, especially in the winter (CARB, 2005). Since the residential areas are located to the east, south, and west-southwest of the sampling site, this CPF result supports the assignment of wood combustion.

The CPF plot indicated secondary nitrate, gasoline vehicle, and diesel emission sources to the north, northeast, west, and south as shown in Figure 119. These sources are related to on-road and off-road vehicle emissions. Since highways and local roads are adjacent to each of the sites, it can be anticipated that they would affect the apparent directions from which the emissions come to the site.

The CPF plot indicated secondary sulfate source to the north, northeast, and northwest as shown in Figure 119. The SO_2 emitted various sources was converted into H_2SO_4 to from SO_4^{2-} . In this area, the largest sources of SO_2 were ships and petroleum refineries.¹⁸ Since the six petroleum refineries are located to the north of the sampling site and ships are frequently operating in northern areas of San Francisco Bay, this result supports the assignment of secondary sulfate.

The CPF plots indicated that sea salt (fresh and aged) originated to the west and northeast. Since the Pacific Ocean is located to the west of the sampling site and the San Francisco Bay is to the northeast, this result supports the sea salt assignments.

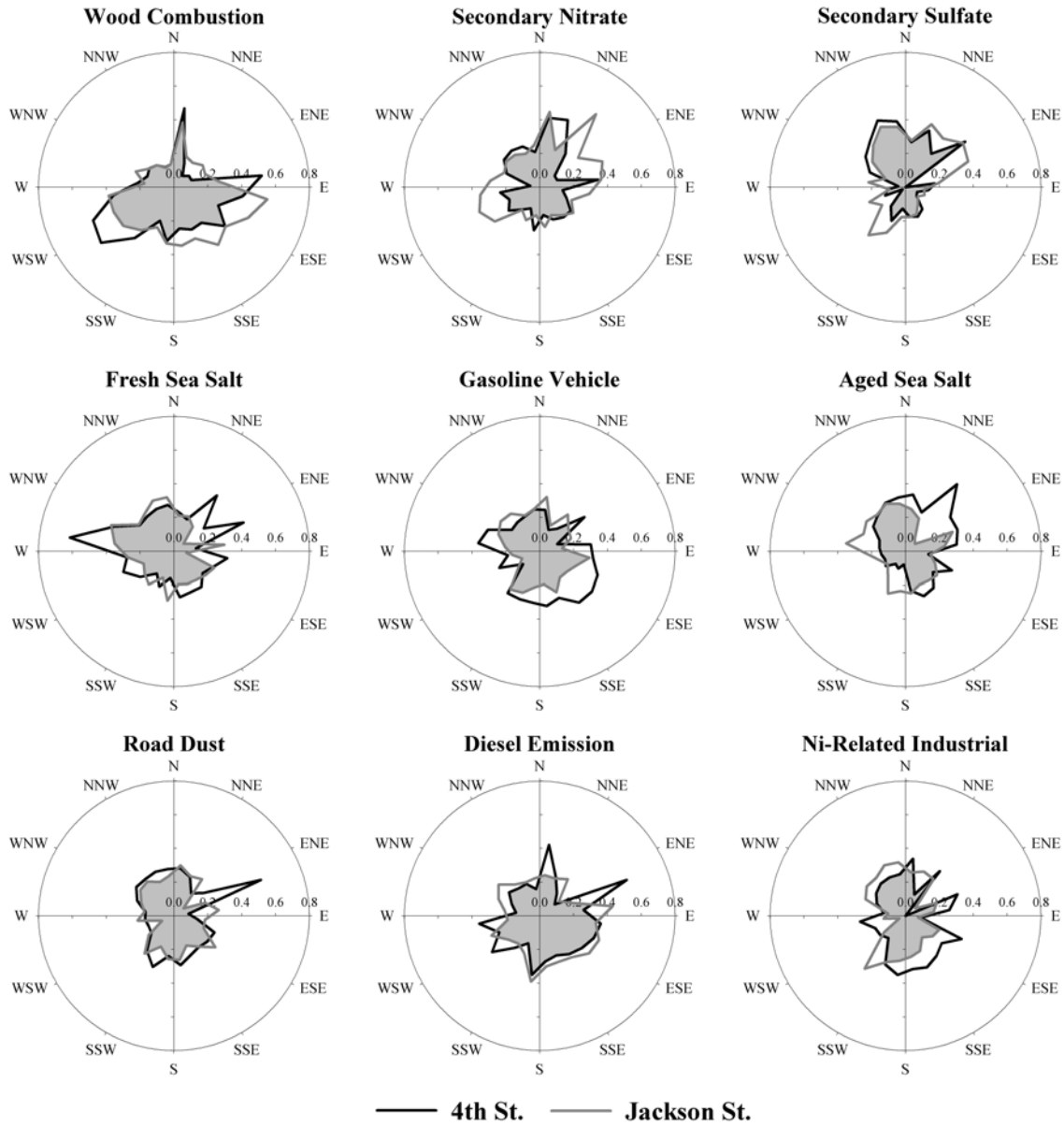


Figure 119. Conditional Probability Function (CPF) results based on source contributions obtained by the PMF analysis of the data from the 4th Street (dark line) and Jackson Street (gray line) in San Jose (gray area denote overlap area between the 4th Street and Jackson Street).

In Figure 120, a comparison of the predicted $PM_{2.5}$ contributions from all sources with measured $PM_{2.5}$ concentrations shows that the PMF resolved sources effectively reproduce the measured values and account for most of the variation in the $PM_{2.5}$ concentrations (4th Street: $R^2 = 0.955$; Jackson Street: $R^2 = 0.953$).

Table 39 presents the average source contributions of all the sources identified during the sampling period in two sampling sites. The average concentration of $PM_{2.5}$ calculated using the PMF modeling at the 4th Street and Jackson Street was $14.75 \mu\text{g}/\text{m}^3$ and $14.38 \mu\text{g}/\text{m}^3$ (the average $PM_{2.5}$ concentration observed $14.73 \mu\text{g}/\text{m}^3$ and $14.35 \mu\text{g}/\text{m}^3$). For 4th Street, the largest source was wood combustion accounting for 32.1% ($4.73 \mu\text{g}/\text{m}^3$) of the $PM_{2.5}$ mass. Secondary nitrate and secondary sulfate were the other large anthropogenic contributions to the fine particle mass. At Jackson Street, the contribution of the wood combustion source was 33.6% ($4.84 \mu\text{g}/\text{m}^3$). This source had also the largest effect on the local ambient air quality, followed by secondary nitrate (20.3%, $2.92 \mu\text{g}/\text{m}^3$), secondary sulfate (13.9%, $1.99 \mu\text{g}/\text{m}^3$), aged sea salt (12.4%, $1.76 \mu\text{g}/\text{m}^3$), gasoline vehicle source (8.3%, $1.20 \mu\text{g}/\text{m}^3$), respectively.

Contribution of wood combustion, secondary nitrate, secondary sulfate, fresh sea salt, gasoline vehicle, and diesel emission source showed similar results between the 4th Street and Jackson Street. The road dust source and Ni-related industrial source contributions at 4th Street ($0.99 \mu\text{g}/\text{m}^3$ and $0.37 \mu\text{g}/\text{m}^3$) were about 3.7 times and 2.1 times higher than at Jackson Street ($0.27 \mu\text{g}/\text{m}^3$, $0.18 \mu\text{g}/\text{m}^3$). By comparison, the average Ni concentration at the 4th Street ($16.4 \text{ ng}/\text{m}^3$) was about 2 times higher than the average Ni concentration at the Jackson Street ($8.0 \text{ ng}/\text{m}^3$). On the other hand, the mean aged sea salt contribution at Jackson Street ($1.76 \mu\text{g}/\text{m}^3$) was about 1.7 times higher than 4th Street ($1.01 \mu\text{g}/\text{m}^3$).

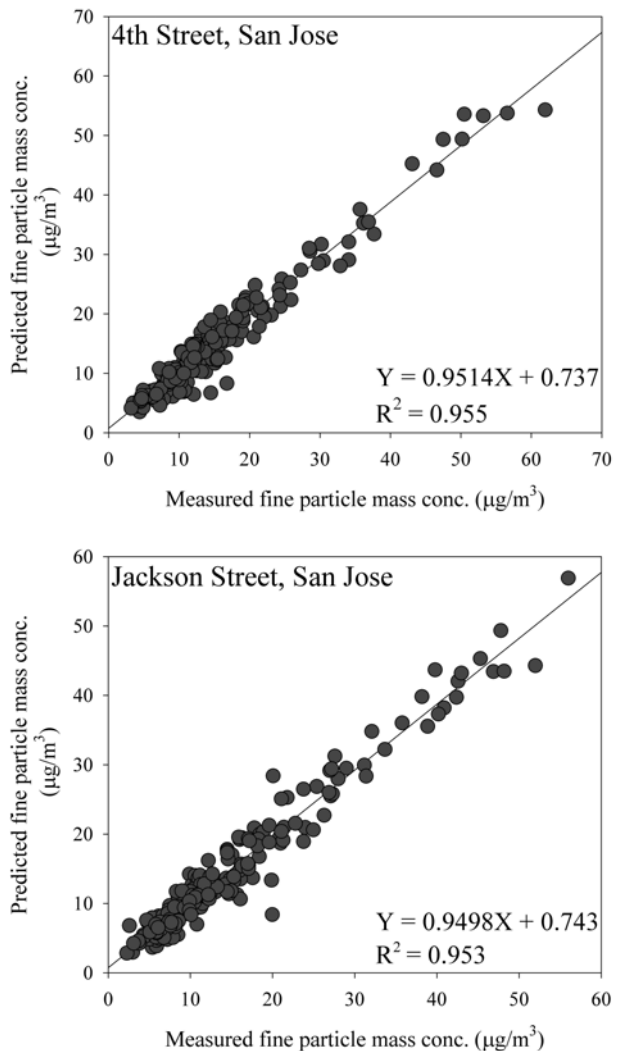


Figure 120. Comparison of the predicted total $PM_{2.5}$ mass concentrations from the PMF analysis with measured $PM_{2.5}$ mass concentrations for the 4th Street and Jackson Street sites.

Table 39. Average source contributions to PM_{2.5} mass concentration in 4th Street and Jackson Street.

	Average Source Contribution			
	4th Street		Jackson Street	
	µg/m ³ (S.E*)	%	µg/m ³ (S.E*)	%
Wood Combustion	4.73 (0.38)	32.1	4.84 (0.37)	33.6
Secondary Nitrate	3.29 (0.30)	22.3	2.92 (0.28)	20.3
Secondary Sulfate	1.58 (0.09)	10.7	1.99 (0.13)	13.9
Fresh Sea Salt	1.13 (0.13)	7.7	0.76 (0.08)	5.3
Gasoline Vehicle	1.07 (0.07)	7.3	1.20 (0.09)	8.3
Aged Sea Salt	1.01 (0.06)	6.8	1.76 (0.10)	12.4
Road Dust	0.99 (0.10)	6.7	0.27 (0.02)	1.9
Diesel Emission	0.57 (0.05)	3.9	0.45 (0.05)	3.2
Ni-Related Industrial	0.37 (0.06)	2.5	0.18 (0.02)	1.3

*: Standard error

Figure 121 shows the comparison of the average source contributions during the summer and winter. Contributions of wood combustion and secondary nitrate at the two sampling sites in winter were much higher than in summer. On the other hand, contribution of secondary sulfate and aged sea salt source were higher in summer than in the winter at each site. Gasoline vehicle emissions and road dust do not show strong seasonal tendencies. The average contributions of emitting natural sources in 4th Street and Jackson Street (fresh sea salt + aged sea salt) was 2.14 µg/m³ (14.5%) and 2.52 µg/m³ (17.5%), respectively. The average contributions of anthropogenic sources at 4th Street and at Jackson Street were 12.6 µg/m³ (85.5%) and 11.86 µg/m³ (82.5%), respectively. Given the interyear variability in meteorology and source emissions, the results from the two sites are quite comparable to one another and could probably be combined in a single analysis.

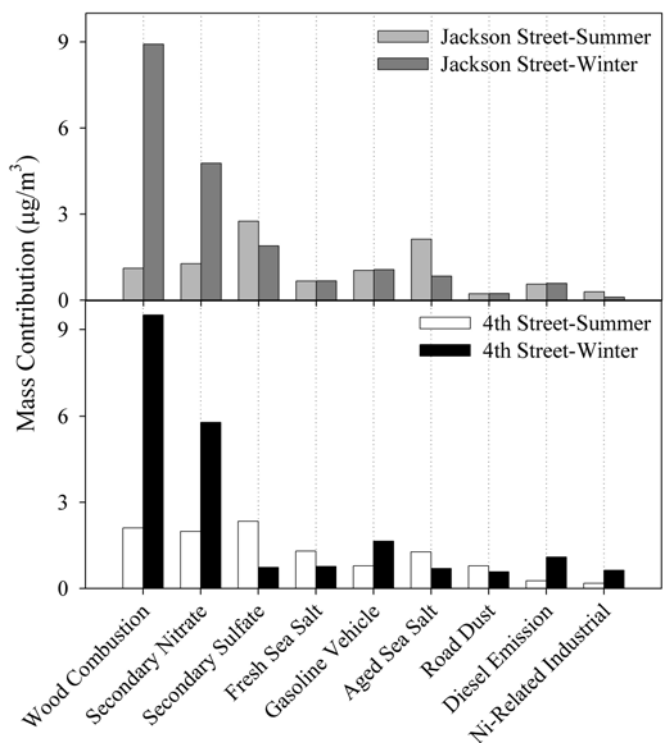


Figure 121. Comparison of average source contributions for the each sampling site during summer and winter periods.

Los Angeles, CA

The analyzed PM_{2.5} samples were collected on a one-in-six day schedule at Simi Valley and Los Angeles (LA) monitoring sites and a one-in-three day schedule at Rubidoux monitoring sites. The analysis results for the data from these sites is presented by Kim and Hopke (2007). The site locations are shown in Figure 122. The Simi Valley monitoring site is located about 50 km northwest of the downtown LA. The surrounding area is residential. Highway 118 is situated about 500 m north of the site. LA monitoring site is located about 100 m southeast of the Dodger Stadium. Local roads are closely situated, and Interstate Highways 5, 110, and 101 are situated close to the east, west, and south of the site, respectively. Rubidoux is located about 60 km east of the downtown LA. Highway 60 is located 500 m north of the site, and Highway 215 is situated about 5 km west of the monitoring site. Wind data measured at the Los Angeles International Airport (LAX) were used for Simi Valley and LA sites. Burbank Airport wind data were used for Rubidoux site. The summary of three monitoring sites and sampling periods used in the analyses are shown in Table 40.

The OC blank concentration was estimated utilizing the intercept of the regression of OC concentrations against PM_{2.5} mass concentrations suggested by Tolocka *et al.* (2001). Samples for which PM_{2.5} or OC data were not available were excluded before the regression between PM_{2.5} and OC concentration. Comparing co-located PM_{2.5} data measured by STN and Federal Reference Method (FRM), outliers were censored for the all three data sets. The intercepts in PM_{2.5} regression against OC concentration are considered to be integrated OC blank concentrations as shown in Table 41. The STN OC concentrations in this report were blank corrected by subtracting the estimated OC blank concentrations.

Table 40. Summary of STN sites in South Coast Air Basin.

AIRS code	Monitoring site	Sampler	Latitude	Longitude	sampling period
061112002	Simi Valley	SASS ¹	34.2775	-118.6847	Oct. 2001 - Dec. 2004
060371103	Los Angeles	SASS	34.0672	-118.2419	Jun. 2002 - Dec. 2004
060658001	Rubidoux	SASS	34.0103	-117.4261	May 2001 - Dec. 2004

¹ Spiral Aerosol Speciation Samplers (Met One Instruments, Grants Pass, OR)

Table 41. Summary of OC blank concentrations estimated from regression of PM_{2.5} mass concentrations against OC concentrations.

Monitoring site	OC blank (µg/m ³)
Simi Valley	2.94
Los Angeles	2.88
Rubidoux	3.93

A comprehensive set of error structures for the source apportionment was estimated by procedure proposed by Kim *et al.* (2005). For the XRF MDL values, the average MDL values among five MDL values from five XRF were used in this study (Kim *et al.*,2005).

For the PMF analysis, samples for which PM_{2.5} or OC data were not available or below detection limits, or for which PM_{2.5} or OC mass concentration had error flags were excluded from the data set. To obtain reasonable model fit, the fireworks samples collected at LA site on January 1, 2004 and at Rubidoux site on July 6, 2001, July 4, 2002, July 5, 2003, and January 1, 2004 in which OC, K, As, Ba, Cu, and Pb mass concentrations were unusually high were

excluded in this study. Overall, 34.7% of the Simi Valley data, 21.7% of the LA data, and 25.5% of the Rubidoux data were not included in this study.

In this source apportionment study, IC SO_4^{2-} was excluded from the analyses to prevent double counting of mass concentrations since XRF S and IC SO_4^{2-} showed good correlations ($\text{slope} = 3.1$, $r^2 = 0.98$ for Simi Valley data; $\text{slope} = 3.0$, $r^2 = 0.91$ for LA data; $\text{slope} = 3.1$, $r^2 = 0.96$ for Rubidoux data). Due to the higher analytical precision compared to XRF Na and XRF K, IC Na^+ and IC K^+ were included in the analyses. Chemical species that have below MDL values more than 90% were excluded. Thus, a total of 111 samples and 27 species, 100 samples and 30 species, and 280 samples and 29 species including $\text{PM}_{2.5}$ mass concentrations collected between 2001 and 2004 were used for the Simi Valley, LA, and Rubidoux sites, respectively.

As recommended by Paatero and Hopke (2003), the estimated uncertainties of species that have S/N ratio between 0.2 and 2 (weak variable) and species that have below MDL values more than 50% were increased by a factor of five and a factor of three, respectively, to reduce their weight in the solution. The estimated uncertainties were increased by a factor of thirty for the samples for which mass concentration had error flags. In addition, to obtain physically reasonable PMF solution, it was found necessary to increase three times the estimated uncertainties of Zn (Simi Valley and LA,); Al, Na, Cl, and NH_4^+ (Rubidoux).

In this study, the measured $\text{PM}_{2.5}$ mass concentration was included as an independent variable in the PMF modeling to directly obtain the mass apportionment without a multiple regression. The utilization of $\text{PM}_{2.5}$ mass concentration as a variable is specified in detail in Kim et al (2003). A summary of $\text{PM}_{2.5}$ speciation data and S/N ratios are provided in Tables 42 to 44.

Seven-source model with values of $\text{FPEAK} = -0.2$, seven-source model with values of $\text{FPEAK} = 0$, and nine-source models with values of $\text{FPEAK} = -0.2$ provided the most physically reasonable source profiles for the Simi Valley, LA, and Rubidoux sites, respectively. The average source contributions of each source to the $\text{PM}_{2.5}$ mass concentrations are provided in Table 45.

Comparisons of the daily reconstructed $\text{PM}_{2.5}$ mass contributions from all of the sources with the measured $\text{PM}_{2.5}$ mass concentrations shows that the resolved sources effectively reproduce the measured values and account for most of the variation in the $\text{PM}_{2.5}$ mass concentrations in Figure 122. In Figure 123, the averaged seasonal contributions from each source are compared (summer: April - September; winter: October - March). The source profiles, corresponding source contributions, weekday/weekend variations, and CPF plots are presented in Figures 124 to 135.

Gasoline vehicle emissions identified at three sites do not show a strong weekday/weekend variation in Figures 130 to 132. In contrast, diesel emissions show high contributions on week days at Simi Valley and LA indicating that the diesel emissions are mostly from vehicles operating on weekdays. Diesel emissions identified at Rubidoux show weak weekday-high variations.

The CPF plots for the gasoline and diesel emissions identified at Simi Valley likely point toward local roads located northeast and south of the site (Figure 133). At LA site, CPF plots pointing northeast suggest that gasoline and diesel emissions have high contributions from Interstate Highway 5. The CPF plots for the gasoline and diesel emissions at Rubidoux do not show specific source directions. Diesel emissions extracted by PMF may represent only diesel vehicle emissions moving at reasonable speed in fluid traffic. Diesel emissions operating at very slow speeds and in stop and go traffic are likely to be apportioned into the gasoline emission category (Shah *et al.*, 2004).

Table 42. Summary of PM_{2.5} species mass concentrations at Simi Valley.

Species	Arithmetic mean ($\mu\text{g}/\text{m}^3$)	Geometric mean ($\mu\text{g}/\text{m}^3$)	Minimum ($\mu\text{g}/\text{m}^3$)	Maximum ($\mu\text{g}/\text{m}^3$)	Number of below MDL values (%)	S/N ratio
PM _{2.5}	16.0117	14.3665	4.3000	47.4000	0	NA ¹
OC	2.5888	1.8804	0.0241	8.6641	4.5	235.2
EC	0.8235	0.7512	0.2990	2.0700	0	NA
S	0.9446	0.6846	0.0455	2.5000	0	NA
NO ³⁻	4.3793	2.9126	0.1540	20.2000	0	55329.0
NH ₄ ⁺	1.9688	1.2228	0.0205	8.5300	0	13058.8
Al	0.0337	0.0230	0.0004	0.2190	53.2	2.4
Ba	0.0309	0.0267	0.0003	0.1080	71.2	0.6
Br	0.0049	0.0041	0.0001	0.0164	10.8	23.8
Ca	0.0491	0.0411	0.0039	0.1910	1.8	520.6
Cl	0.0298	0.0175	0.0001	0.3800	38.7	6.8
Cr	0.0021	0.0014	0.0002	0.0200	71.2	0.9
Cu	0.0050	0.0042	0.0005	0.0150	15.3	15.4
Fe	0.0911	0.0822	0.0300	0.2600	0	NA
Hg	0.0032	0.0028	0.0005	0.0100	86.5	0.2
K ⁺	0.0883	0.0805	0.0293	0.2060	65.8	3.2
Mg	0.0438	0.0267	0.0005	0.3310	75.7	1.0
Mn	0.0020	0.0017	0.0001	0.0053	67.6	0.8
Na ⁺	0.3521	0.2507	0.0100	1.3100	4.5	212.4
Ni	0.0024	0.0019	0.0002	0.0075	34.2	4.1
Pb	0.0033	0.0030	0.0001	0.0164	81.1	0.3
Si	0.1098	0.0887	0.0029	0.3300	3.6	243.5
Sr	0.0017	0.0016	0.0001	0.0062	81.1	0.3
Ta	0.0119	0.0104	0.0005	0.0658	82.0	0.4
Ti	0.0069	0.0058	0.0001	0.0192	19.8	9.1
V	0.0051	0.0040	0.0001	0.0145	27.9	6.8
Zn	0.0052	0.0039	0.0001	0.0191	23.4	10.0

¹ not available(infinite S/N ratio caused by no below MDL value)

Table 43. Summary of PM_{2.5} species mass concentrations at Los Angeles.

Species	Arithmetic mean (µg/m ³)	Geometric mean (µg/m ³)	Minimum (µg/m ³)	Maximum (µg/m ³)	Number of below MDL values (%)	S/N ratio
PM _{2.5}	21.0710	19.0031	7.0000	66.2000	0	NA ¹
OC	3.8265	3.2121	0.5510	16.0210	0	NA
EC	1.4846	1.3229	0.3390	3.9200	0	NA
S	1.1980	0.8259	0.1100	4.1200	0	NA
NO ³⁻	6.6503	5.0165	0.6290	22.5000	0	NA
NH ₄ ⁺	2.9761	2.0201	0.1180	11.4000	0	NA
Al	0.0453	0.0321	0.0030	0.2660	56.0	2.5
Ba	0.0330	0.0264	0.0005	0.1320	72.0	0.7
Br	0.0054	0.0046	0.0004	0.0111	8.0	36.4
Ca	0.0863	0.0622	0.0024	0.4100	1.0	1665.7
Cl	0.0604	0.0298	0.0026	0.5240	30.0	19.1
Cr	0.0037	0.0022	0.0001	0.0600	48.0	3.3
Cu	0.0116	0.0087	0.0006	0.0469	9.0	63.7
Eu	0.0124	0.0073	0.0001	0.0723	88.0	0.5
Fe	0.2506	0.1907	0.0100	1.0300	0	NA
K ⁺	0.0909	0.0863	0.0500	0.1850	63.0	3.8
Mg	0.0272	0.0209	0.0004	0.0800	80.0	0.5
Mn	0.0059	0.0047	0.0001	0.0167	25.0	9.9
Na ⁺	0.3673	0.2747	0.0009	1.4200	2.0	604.9
Ni	0.0032	0.0025	0.0002	0.0135	31.0	6.2
P	0.0082	0.0062	0.0005	0.0202	88.0	0.3
Pb	0.0061	0.0048	0.0003	0.0221	50.0	1.9
Si	0.1691	0.1188	0.0100	1.1200	3.0	446.6
Sn	0.0112	0.0112	0.0001	0.0500	87.0	0.2
Sr	0.0032	0.0024	0.0001	0.0118	59.0	1.4
Ta	0.0095	0.0099	0.0001	0.0334	83.0	0.3
Ti	0.0138	0.0109	0.0016	0.0574	8.0	46.8
V	0.0066	0.0054	0.0004	0.0184	18.0	15.1
Zn	0.0188	0.0145	0.0011	0.0843	2.0	472.1
Zr	0.0029	0.0026	0.0001	0.0100	81.0	0.3

¹ not available(infinite S/N ratio caused by no below MDL value)

Table 44. Summary of PM_{2.5} species mass concentrations at Rubidoux.

Species	Arithmetic mean (µg/m ³)	Geometric mean (µg/m ³)	Minimum (µg/m ³)	Maximum (µg/m ³)	Number of below MDL values (%)	S/N ratio
PM _{2.5}	31.0136	27.5269	5.1000	79.2000	0	NA ¹
OC	3.6531	2.7877	0.0370	12.6670	2.5	598.8
EC	1.4671	1.2611	0.3300	4.4800	0	NA
S	1.1667	0.8850	0.0883	3.2000	0	NA
NO ³⁻	12.2449	9.1534	0.3140	40.5000	0	NA
NH ₄ ⁺	4.7433	3.3661	0.0959	16.9000	0	NA
Al	0.0646	0.0440	0.0008	0.3240	38.2	7.3
Ba	0.0344	0.0282	0.0004	0.1350	67.1	0.8
Br	0.0065	0.0058	0.0003	0.0167	3.6	111.1
Ca	0.1683	0.1289	0.0070	0.9180	0	NA
Cl	0.1142	0.0530	0.0013	0.8950	22.5	50.6
Cr	0.0027	0.0018	0.0001	0.0246	58.6	1.9
Cu	0.0073	0.0060	0.0004	0.0400	9.3	38.5
Eu	0.0095	0.0074	0.0000	0.0356	85.4	0.4
Fe	0.1796	0.1568	0.0346	0.5830	0	NA
K ⁺	0.1014	0.0939	0.0402	0.2730	47.1	8.2
Mg	0.0402	0.0269	0.0002	0.3090	72.5	1.1
Mn	0.0043	0.0033	0.0000	0.0145	33.2	5.4
Na ⁺	0.3231	0.2114	0.0050	1.8100	6.8	157.1
Ni	0.0026	0.0020	1.0·10 ⁻⁵	0.0144	32.9	4.9
P	0.0108	0.0077	0.0001	0.0670	83.9	0.5
Pb	0.0069	0.0052	0.0002	0.0400	47.1	2.3
Si	0.2007	0.1674	0.0036	0.8750	1.1	1495.1
Sn	0.0126	0.0116	0.0001	0.0700	84.6	0.3
Sr	0.0022	0.0019	0.0001	0.0074	66.8	0.8
Ta	0.0122	0.0107	0.0002	0.0673	82.1	0.4
Ti	0.0113	0.0094	0.0002	0.0411	10.7	28.8
V	0.0059	0.0047	0.0001	0.0200	20.0	11.8
Zn	0.0271	0.0164	0.0006	0.2130	0.7	1901.0

¹ not available(infinite S/N ratio caused by no below MDL value)

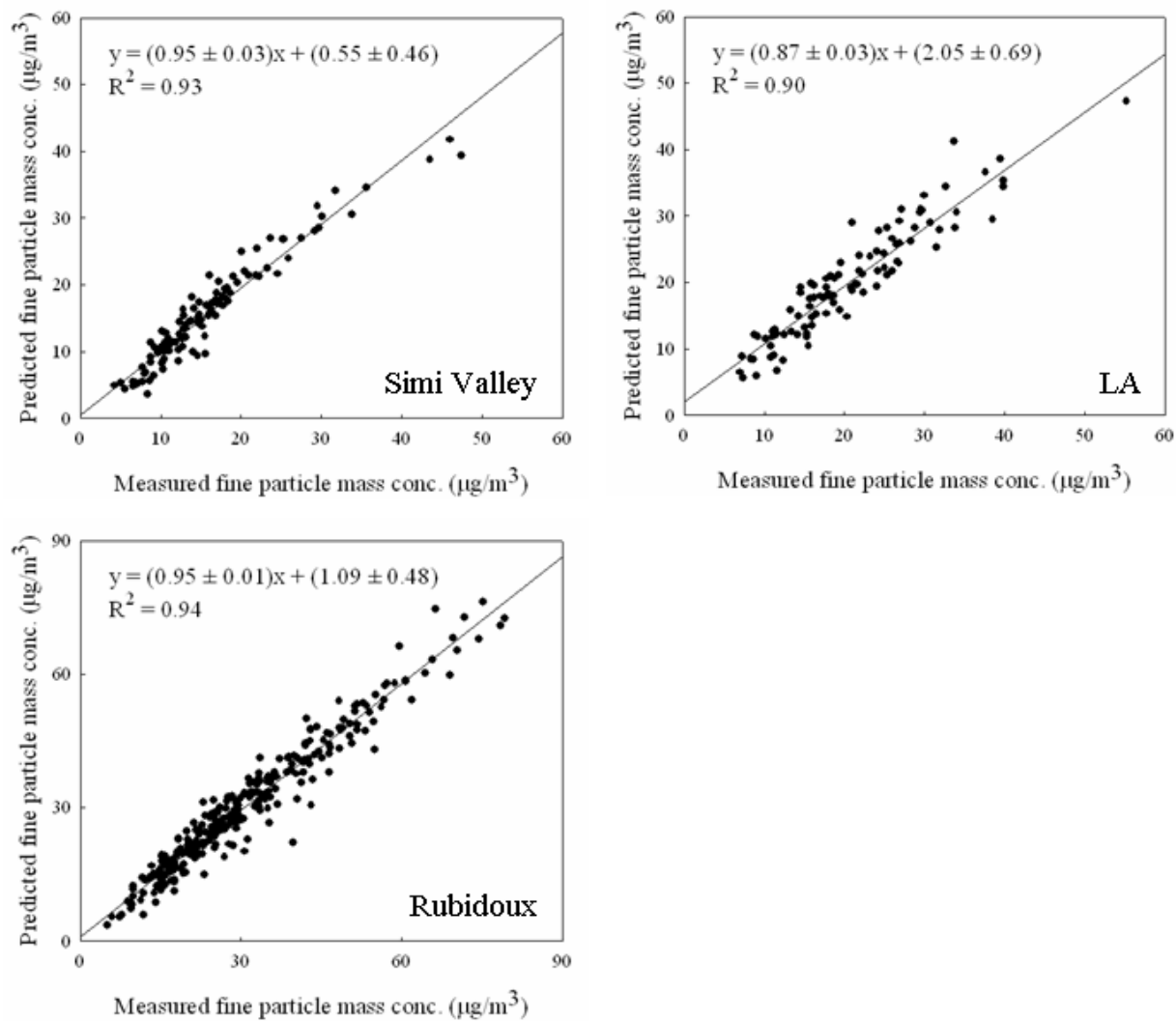


Figure 122. Measured versus PMF predicted PM_{2.5} mass concentrations.

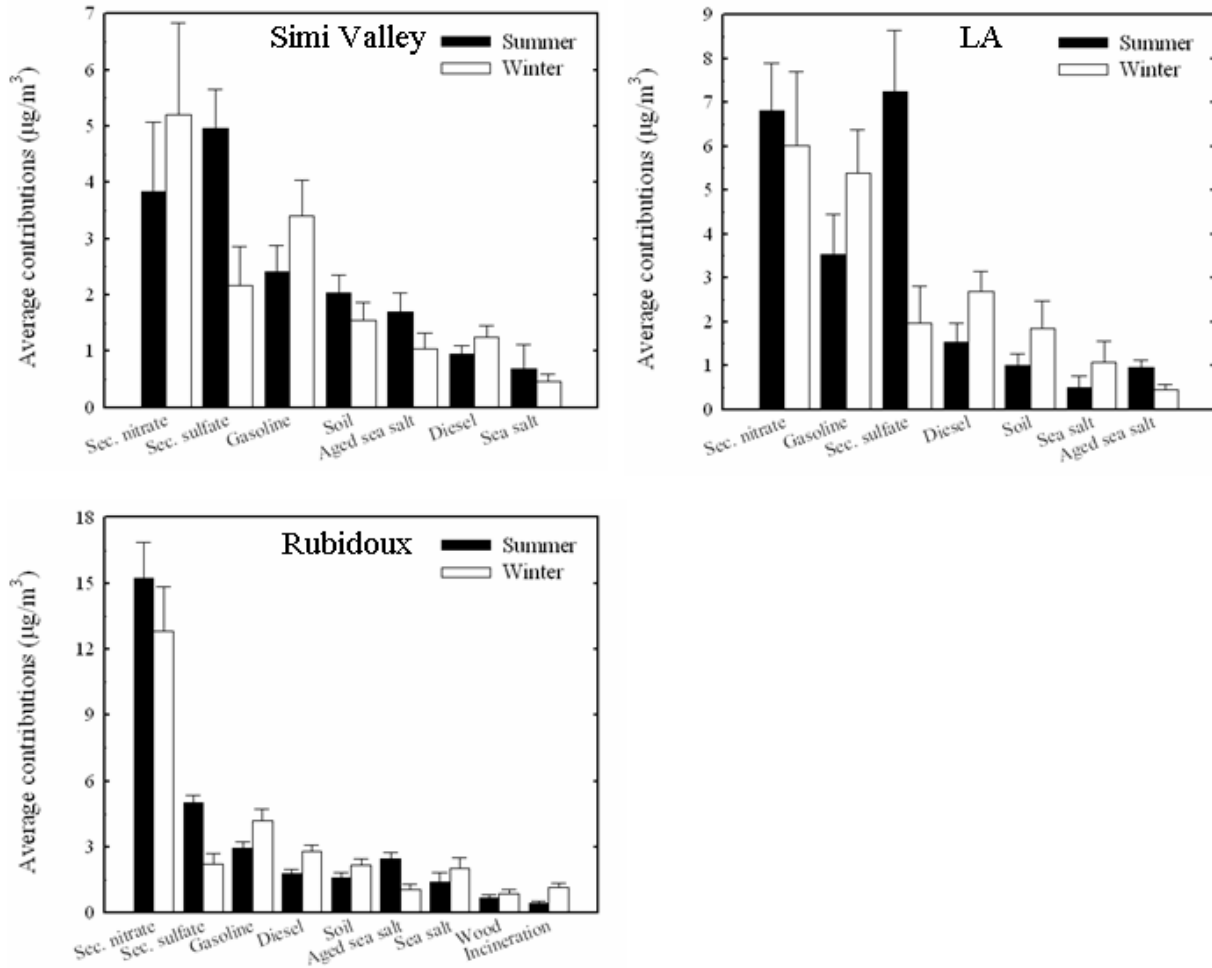


Figure 123. The seasonal comparison of source contributions to PM_{2.5} mass concentration (mean ± 95% distribution).

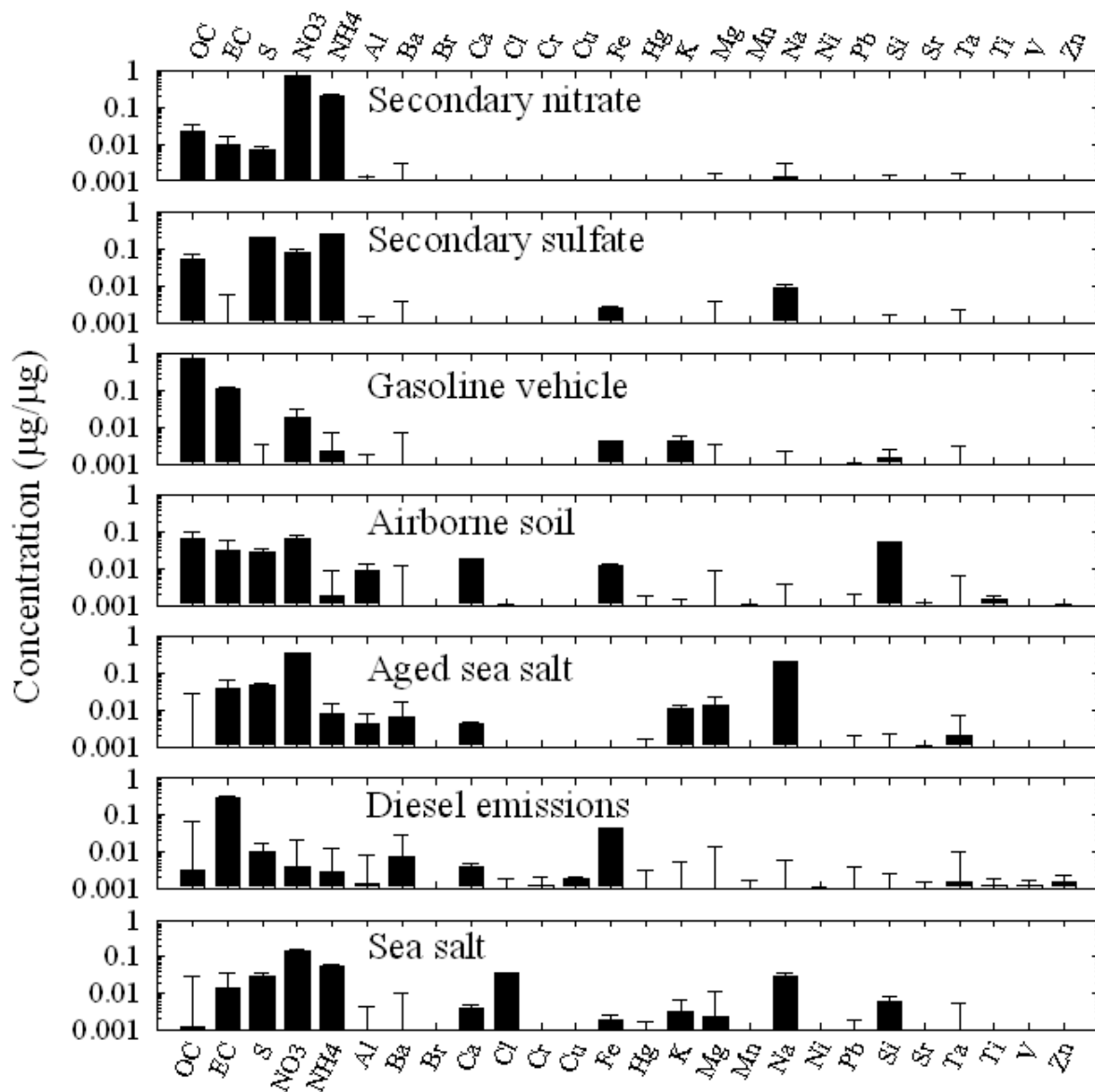


Figure 124. Source profiles deduced from PM_{2.5} samples measured at Simi Valley (prediction ± standard deviation).

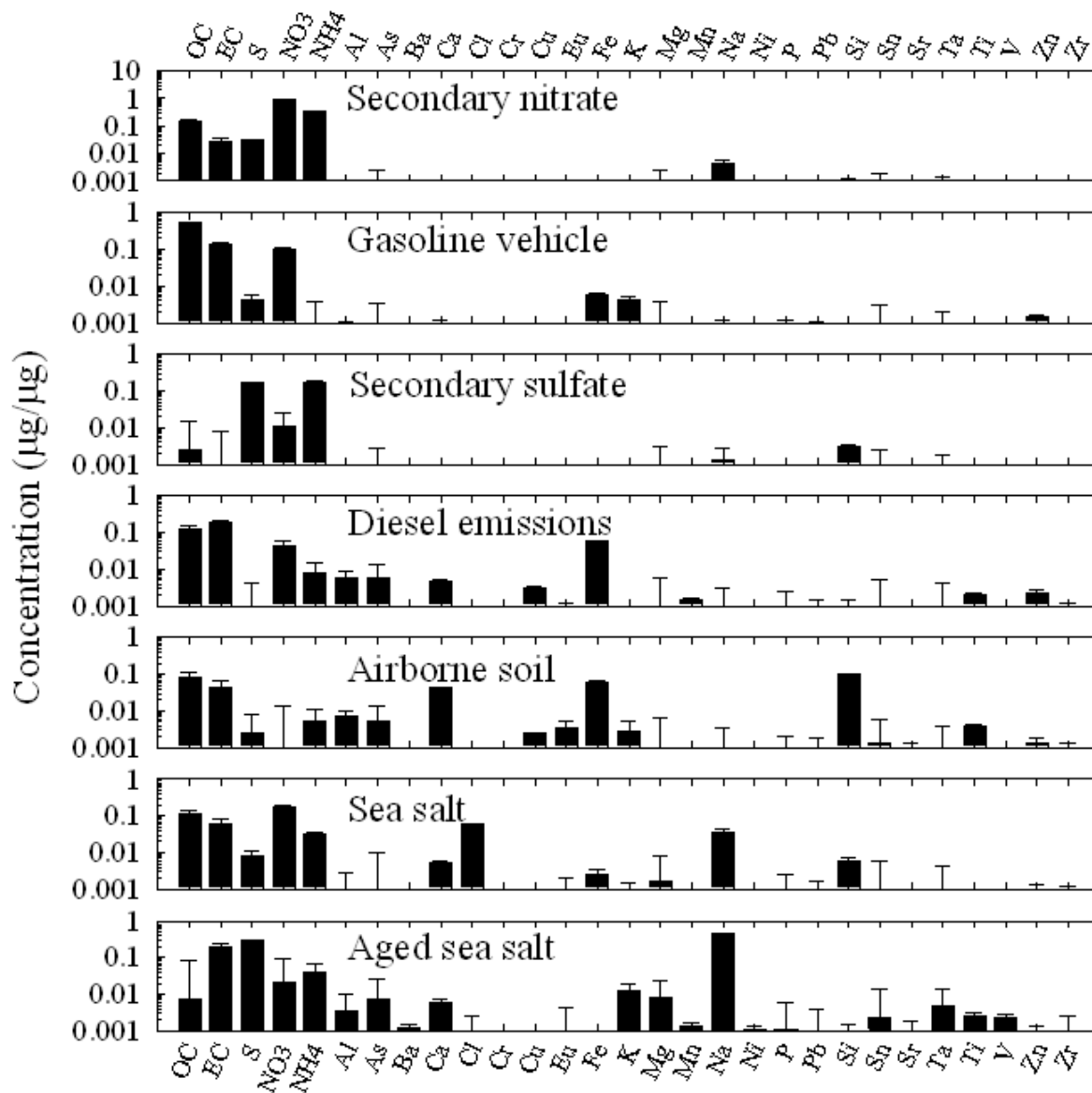


Figure 125. Source profiles deduced from PM_{2.5} samples measured at LA (prediction ± standard deviation).

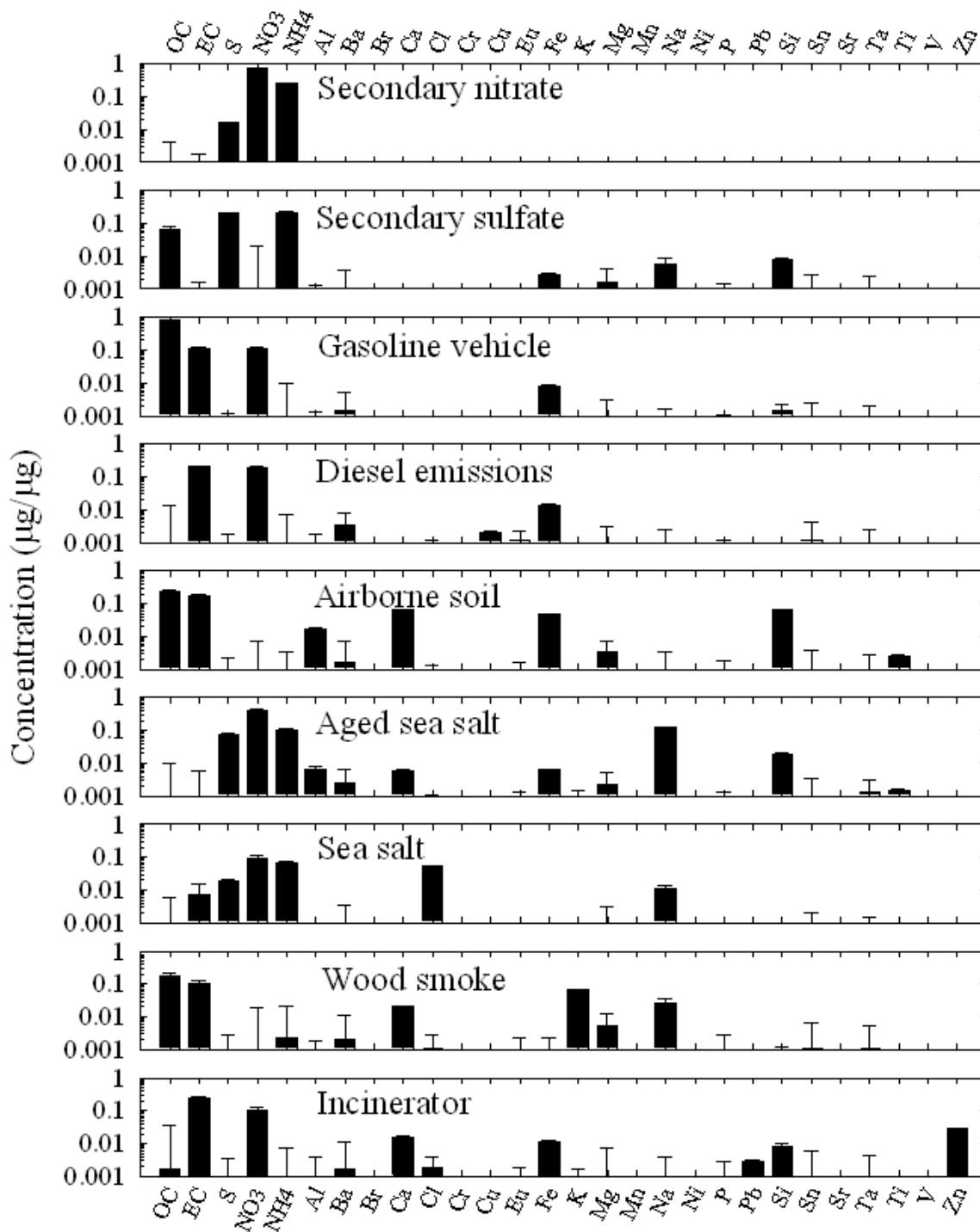


Figure 126. Source profiles deduced from PM_{2.5} samples measured at Rubidoux (prediction ± standard deviation).

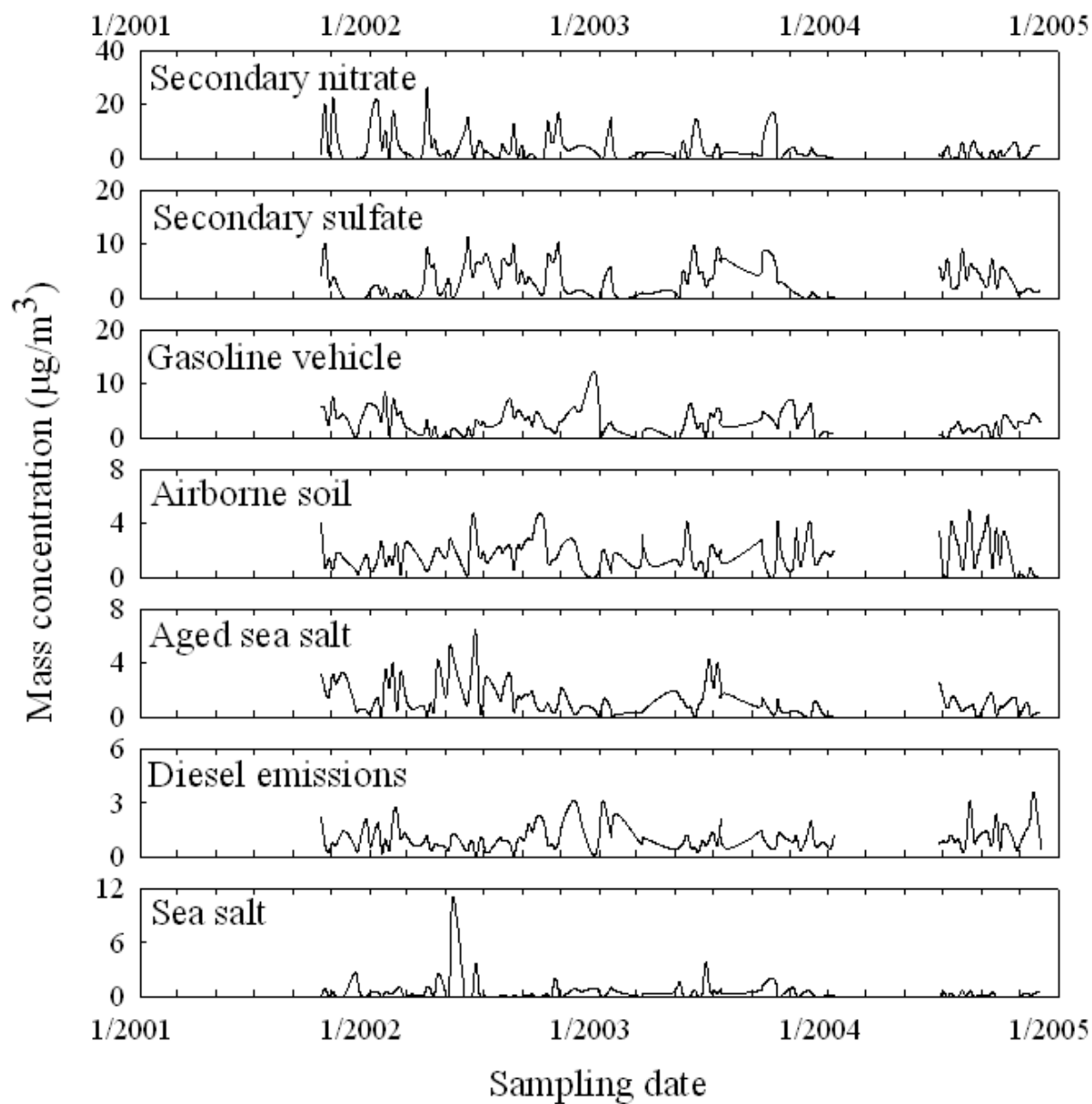


Figure 127. Time series plot of source contributions at Simi Valley.

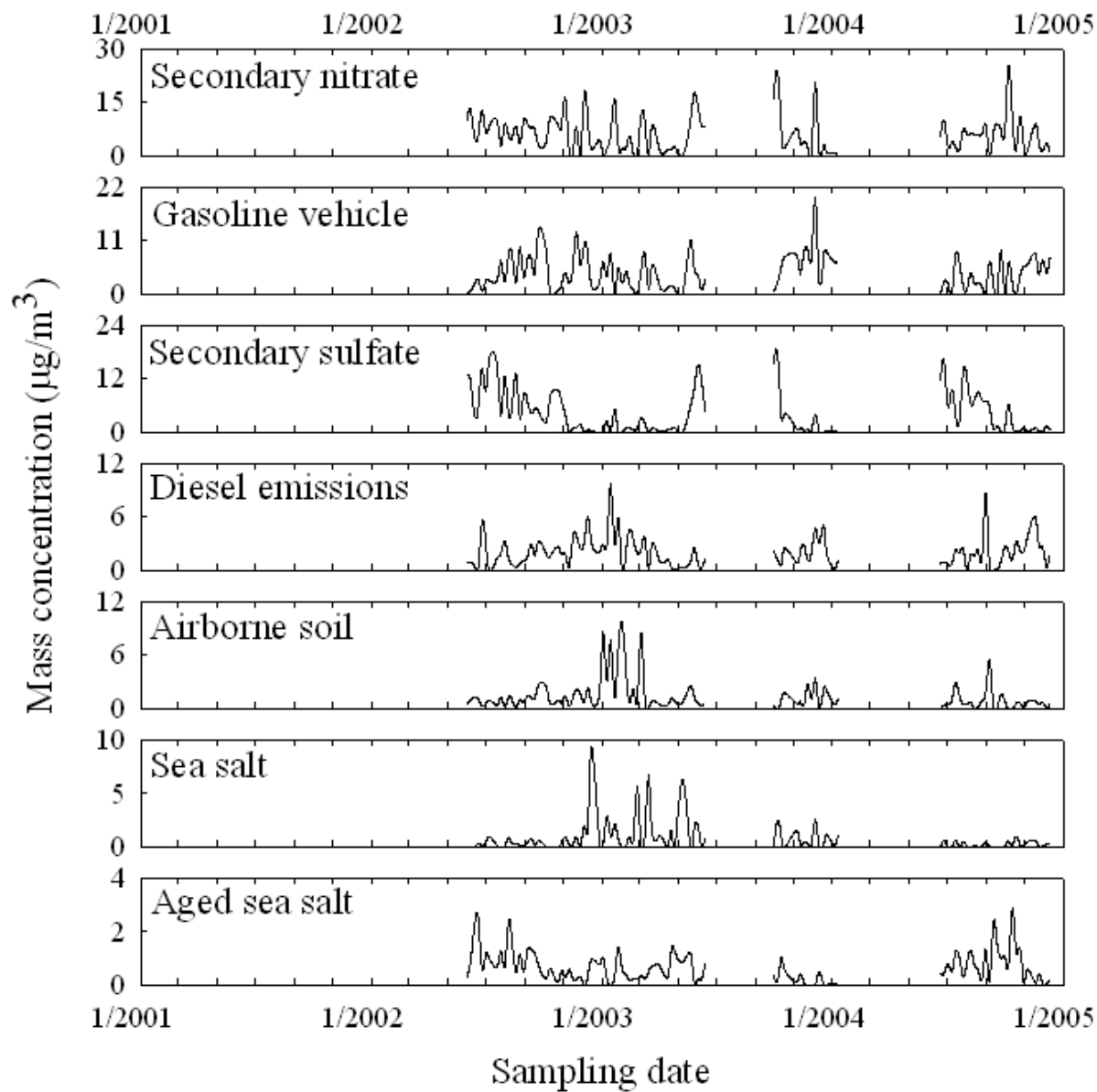


Figure 128. Time series plot of source contributions at LA.

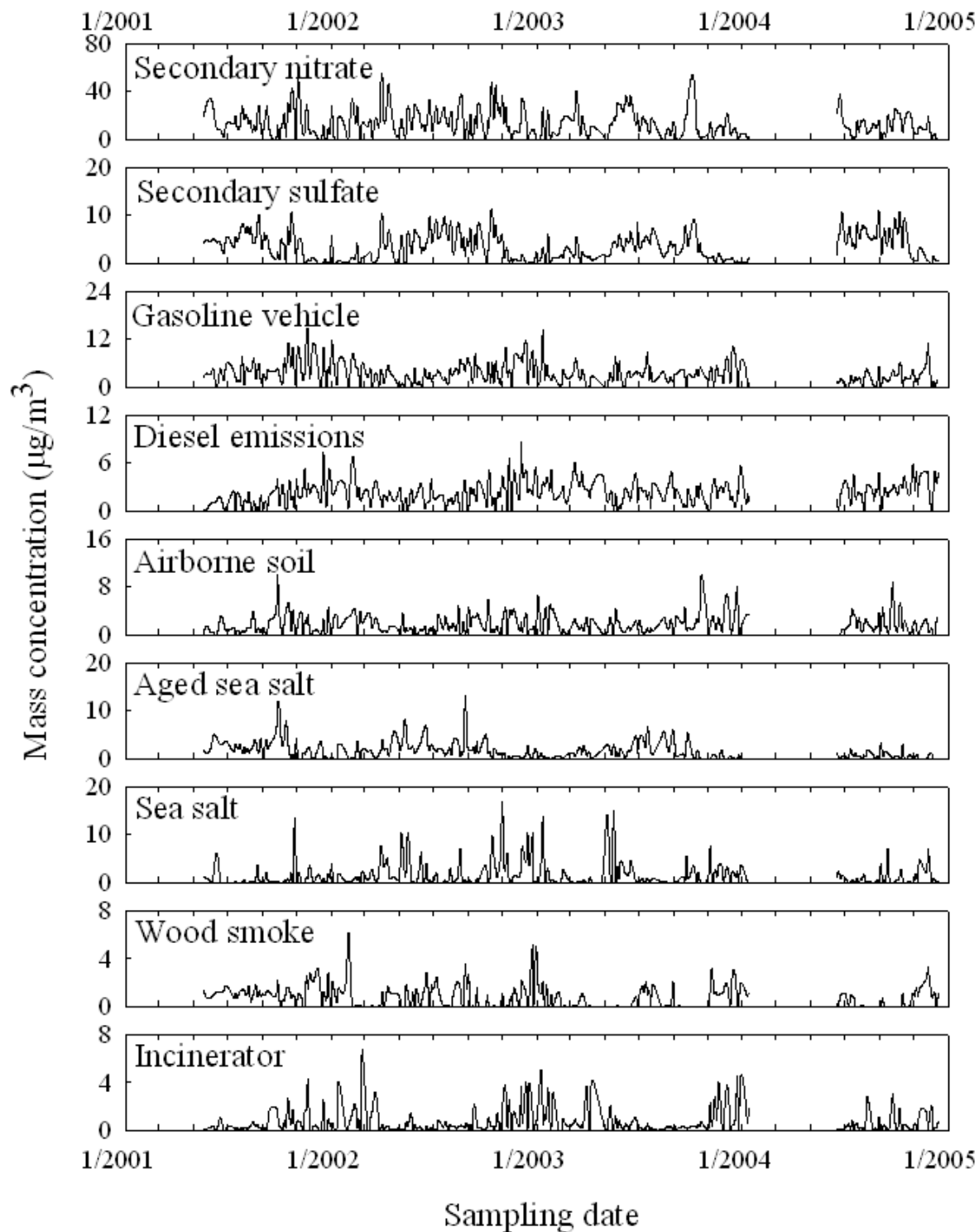


Figure 129. Time series plot of source contributions at Rubidoux.

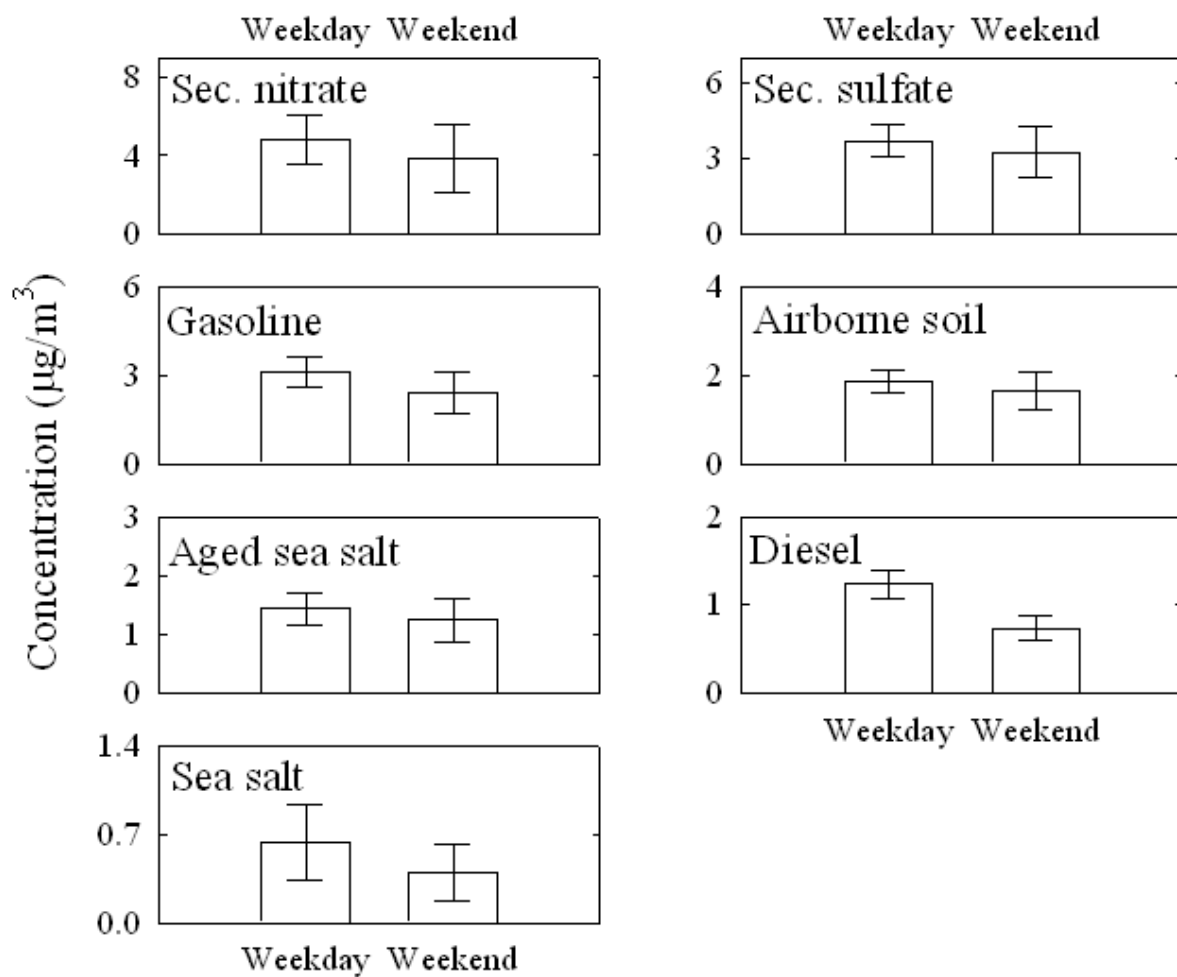


Figure 130. Weekday/weekend variations at Simi Valley (mean \pm 95% distribution).

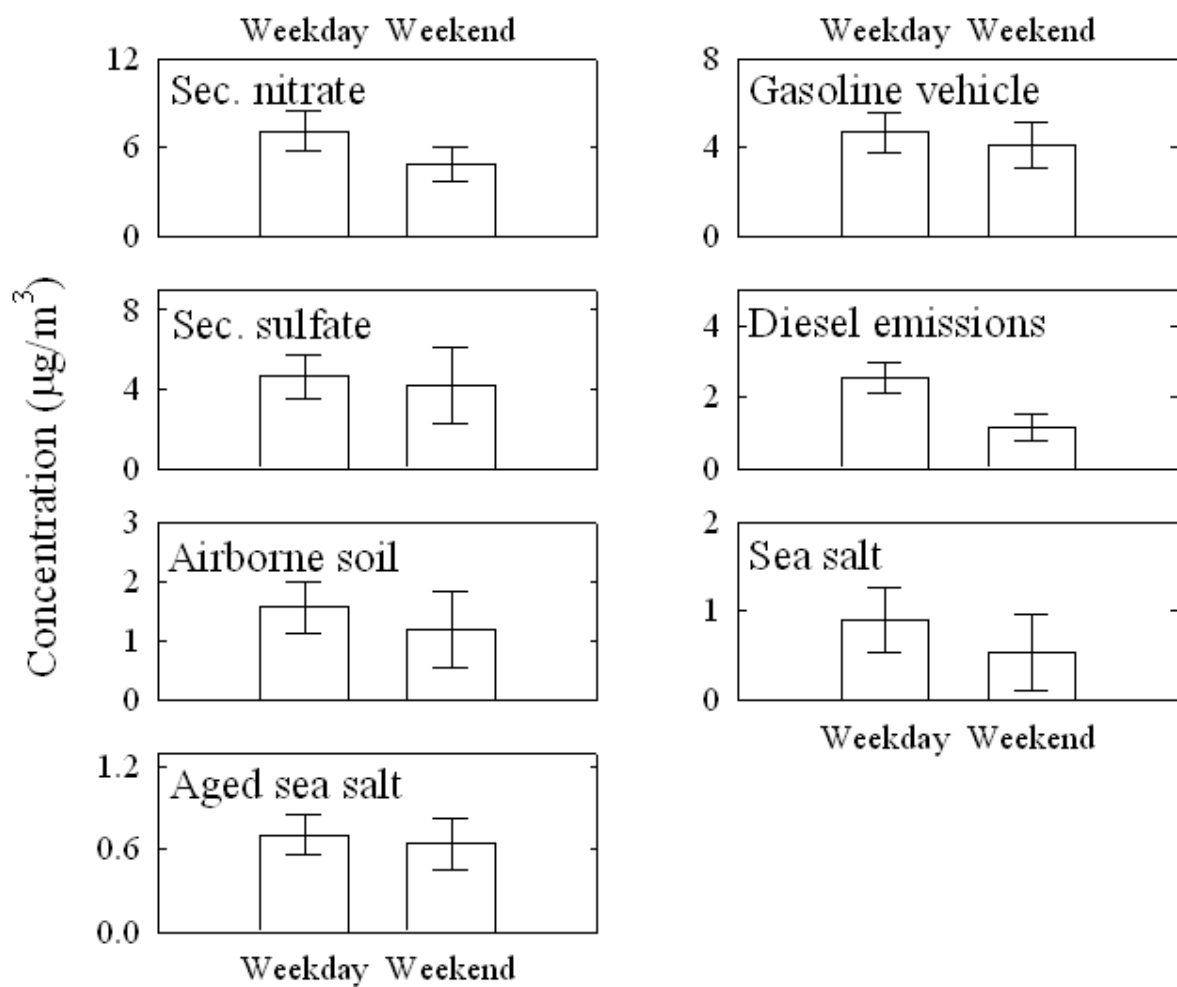


Figure 131. Weekday/weekend variations at LA (mean \pm 95% distribution).

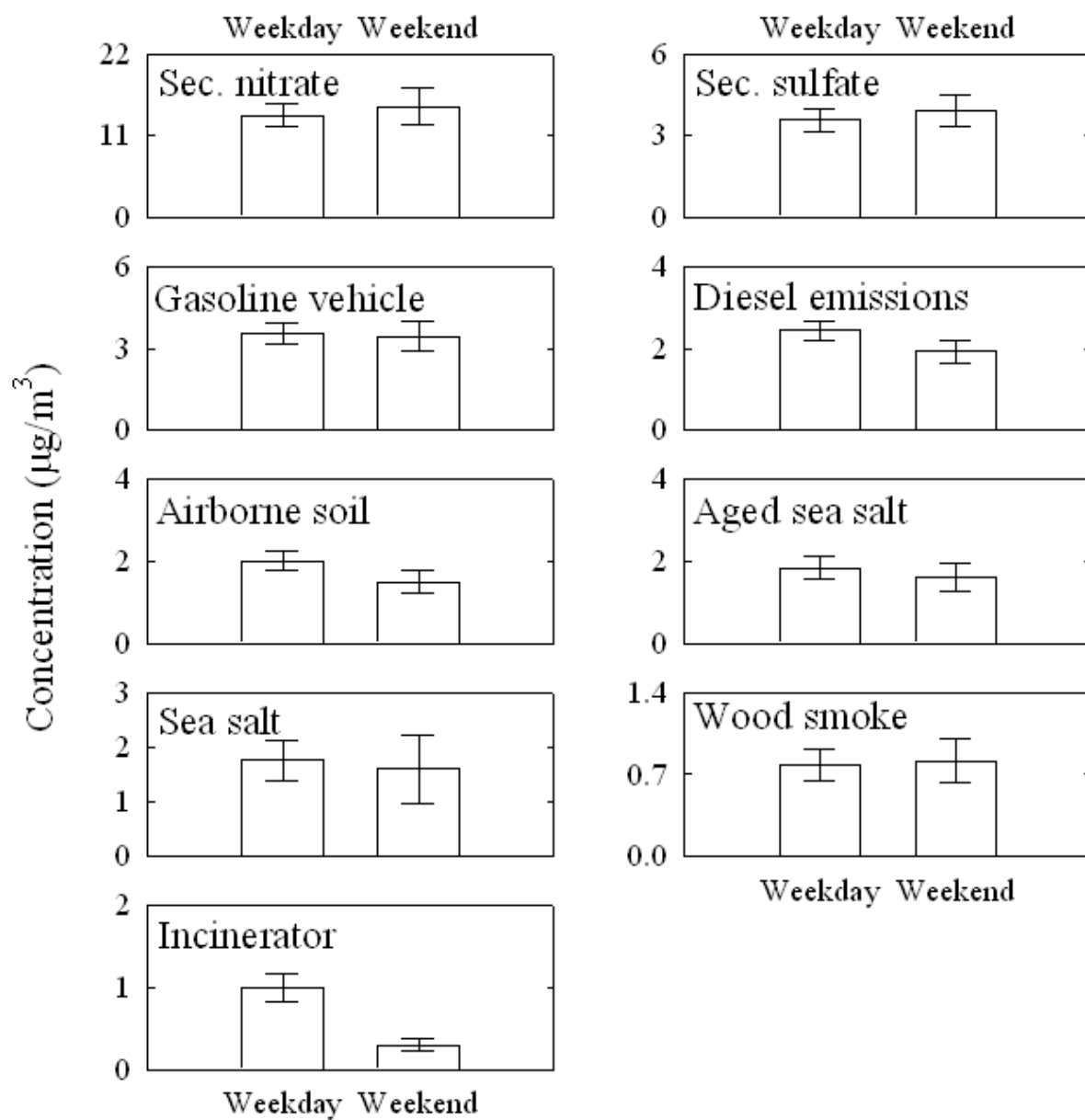


Figure 132. Weekday/weekend variations at Rubidoux (mean \pm 95% distribution).

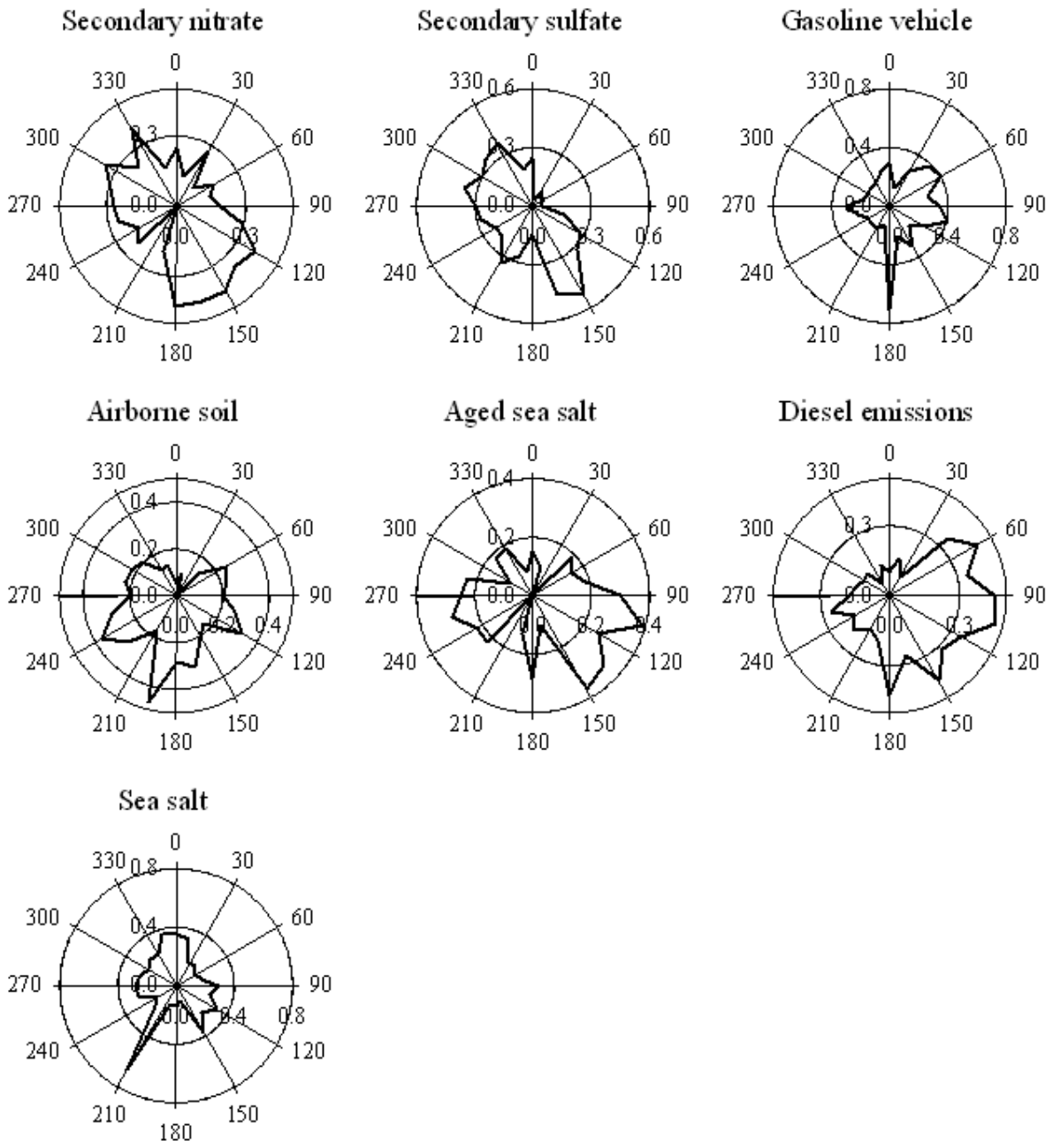


Figure 133. CPF plots for the highest 25% of the mass contributions at Simi Valley.

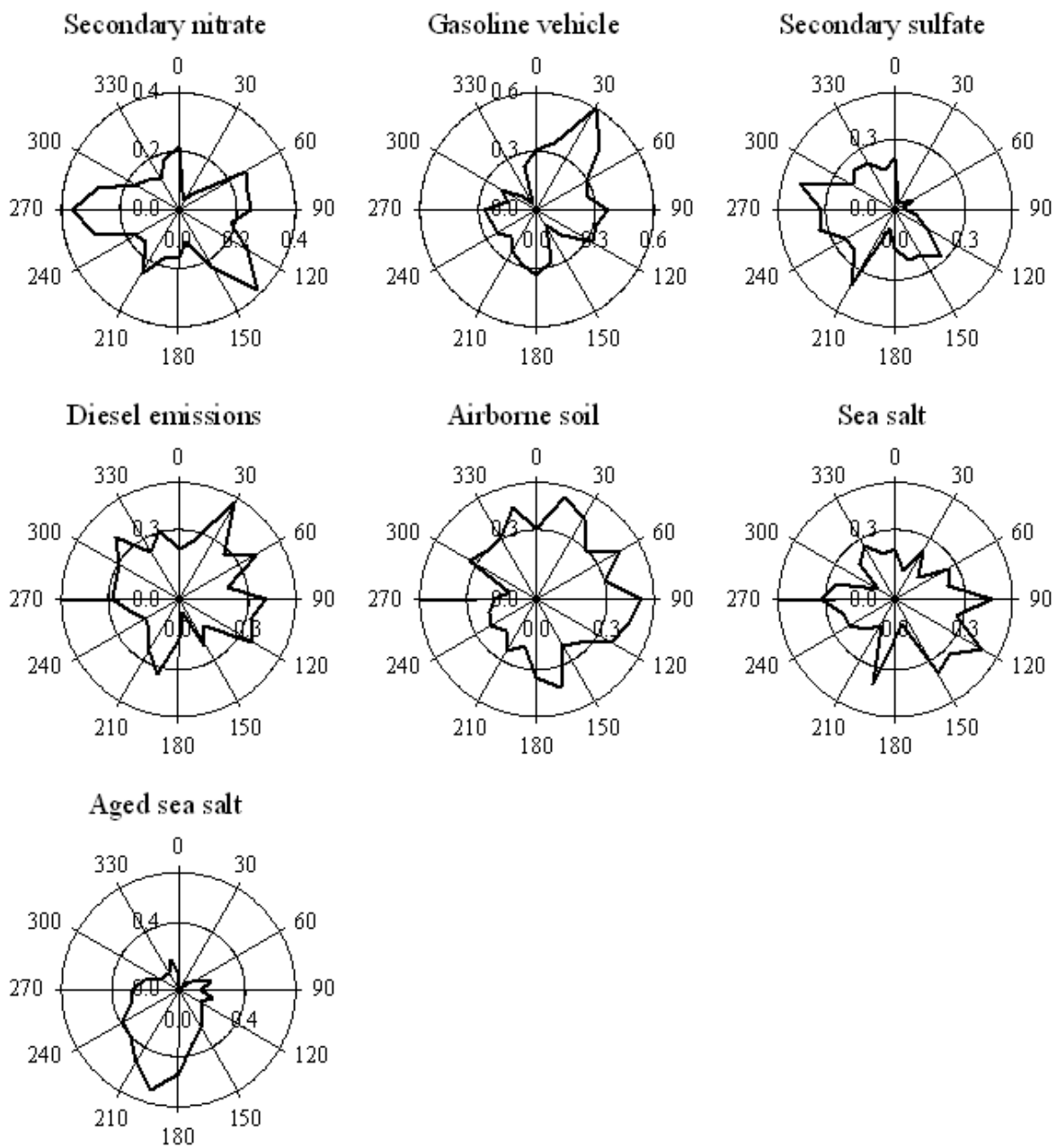


Figure 134. CPF plots for the highest 25% of the mass contributions at LA.

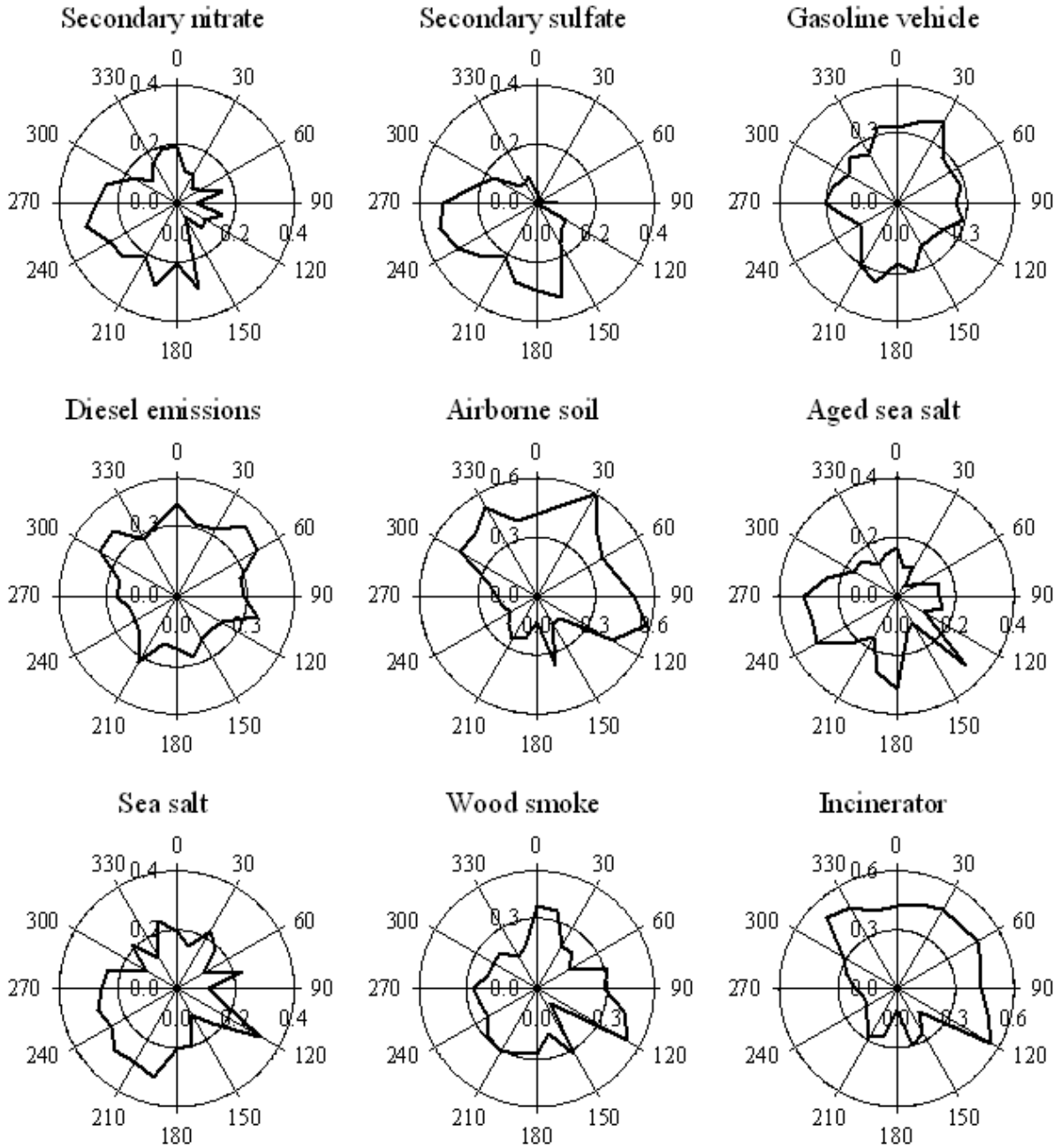


Figure 135. CPF plots for the highest 25% of the mass contributions at Rubidoux.

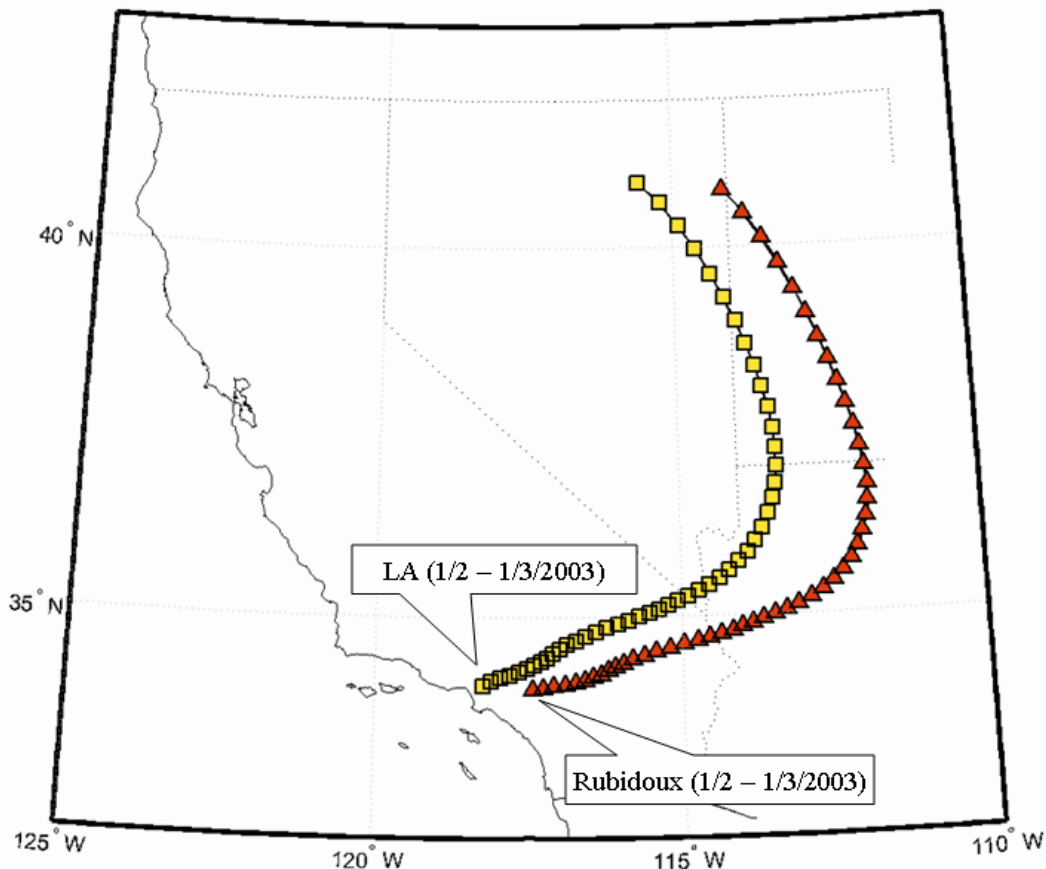


Figure 136. Backward trajectories for days with high impacts of airborne soil arriving at LA and Rubidoux on Jan. 3, 2003 (square and triangle, respectively) calculated by the HYSPLIT model (NOAA Air Resource Laboratory).

Secondary nitrate aerosol is identified by its high concentration of NO_3^- and NH_4^+ . It contributed the most at three sites accounting for 29%, 31%, and 46% of the $\text{PM}_{2.5}$ mass concentrations at Simi Valley, LA, and Rubidoux, respectively. Rubidoux, located downwind of the Los Angeles metropolitan area, had the highest average concentration ($14.06 \mu\text{g}/\text{m}^3$). Secondary nitrate aerosol does not have clear seasonal variations at any of the three sites as shown in Figure 123.

Secondary sulfate aerosol is characterized by its high concentration of SO_4^{2-} and NH_4^+ accounting for 12% - 23% of the $\text{PM}_{2.5}$ mass concentration at all three monitoring sites. Secondary sulfate shows seasonal variation with higher concentrations in summer at three monitoring sites when the photochemical activity is highest as shown in Figure 123. Secondary sulfate shows relatively constant contributions to the $\text{PM}_{2.5}$ mass concentrations at three sites (3.6 , 4.5 , and $3.7 \mu\text{g}/\text{m}^3$, respectively).

At three sites, gasoline vehicle emissions and diesel emissions were separated by different abundances of OC and EC (Watson *et al.*, 1994). Gasoline vehicles emissions have high concentration of the OC. In contrast, diesel emissions were tentatively identified on the basis of the high concentration of EC. The average contributions from gasoline vehicles to $\text{PM}_{2.5}$ mass concentration were 12 - 22% and diesel emissions were 7 - 10%. The contributions from gasoline vehicle were higher at LA ($4.5 \mu\text{g}/\text{m}^3$) than those at other sites. Diesel emissions contributed more at Rubidoux ($2.3 \mu\text{g}/\text{m}^3$) as shown in Table 45.

Airborne soil has high concentrations of Si, Fe, Al and Ca contributing 6 - 11% to the PM_{2.5} mass concentration at three sites. It could be contributed by wind-blown soil dust and re-suspended by road traffic. Airborne soil shows relatively constant contributions to the PM_{2.5} mass concentrations at three sites (1.8, 1.5, and 1.9 µg/m³ at Simi Valley, LA, and Rubidoux, respectively). Airborne soil does not clearly show either seasonal variation or weekday/weekend variation. The elevated airborne soil contributions were identified on Jan. 3, 2003 at both LA and Rubidoux sites. The two-day backward trajectories in Figure 136 showed that the airborne soil identified on Jan. 3, 2003 at LA and Rubidoux sites were likely originated from the arid area in California, Nevada, Utah, and Arizona. As shown in Figure 134 and 135, the CPF plots for the airborne soil at LA and Rubidoux that point to the north, northeast, and east likely reflecting the contributions from the arid inland area.

Aged sea salt is represented by its high concentration of Na⁺, SO₄²⁻, and NO₃⁻. Cl⁻ in the sea salt was displaced by acidic gases during the transport. Aged sea salt accounts for 3 - 9% of the PM_{2.5} mass concentrations at all three monitoring sites. This source shows a summer-high seasonal pattern. At Simi Valley, the CPF plot that points to LA downtown likely indicates the direction of the NO₃⁻ contribution. The CPF plots for the LA and Rubidoux sites point toward the direction of the Long Beach area as the major source direction.

Sea salt is represented by its high concentration of Na⁺ and Cl⁻, accounting for 4 - 6% of the PM_{2.5} mass concentration. This source does not show either seasonal or weekday/weekend variations. The CPF plot for Simi Valley shows the direction of the Pacific Ocean (southwest). At LA and Rubidoux, the CPFs plot point in the direction of the Long Beach area as well as to the southeast.

Wood smoke is characterized by OC, EC, and K (Watson *et al.*, 2001) and was identified at Rubidoux. This source contributed 3% (0.8 µg/m³) to the PM_{2.5} mass concentration. Wood smoke has a weak winter-high seasonal trend shown in Figure 123. There was not a clear weekday/weekend variation in the wood smoke contributions. Incinerator emissions that are characterized by carbon, Fe, Pb, and Zn were identified at Rubidoux. This source accounts for 3% (0.8 µg/m³) of the PM_{2.5} mass concentration. This source has both strong winter-high seasonal pattern and strong weekday-high variations.

Table 45. Average source contributions (µg/m³) to PM_{2.5} mass concentration.

Sources	Average source contribution (%)		
	Simi Valley	Los Angeles	Rubidoux
Secondary nitrate	4.51 (28.5)	6.39 (31.3)	14.06 (46.2)
Secondary sulfate	3.58 (22.6)	4.49 (22.0)	3.68 (12.1)
Gasoline vehicle	2.90 (18.3)	4.50 (22.0)	3.52 (11.6)
Diesel emissions	1.09 (6.9)	2.13 (10.4)	2.27 (7.5)
Airborne soil	1.79 (11.3)	1.45 (7.1)	1.86 (6.1)
Aged sea salt	1.37 (8.7)	0.69 (3.4)	1.78 (5.8)
Sea salt	0.57 (3.6)	0.79 (3.9)	1.71 (5.6)
Wood smoke			0.79 (2.6)
Incinerator			0.77 (2.5)

San Diego, CA

Twenty-four hour integrated airborne $PM_{2.5}$ samples were collected at an urban Escondido site (Lat 33.12778, Lon -117.074, Elevation 204 m, AIRS# 60731002) and at a suburban El Cajon site (Lat 32.79139, Lon -116.942, Elevation 143 m, AIRS# 60730003). Both sites are located in San Diego County in southern California. The city of Escondido has a population of 133,559 (US Census, 2000) that is less than 0.5% of total population in the state of California. The city of El Cajon has a population of 94,869 which represents only 0.3% of total population of California. The Escondido site is located about 40 km north-northwest from the El Cajon site. Both the sites are located near highways, so the influence of motor vehicle emissions is expected to be strong. Figure 137 shows the location of the two sampling sites.

Twenty-four hour daily integrated $PM_{2.5}$ samples were collected at the El Cajon site from 5/13/2001 to 2/12/2005 and at the Escondido site from 4/8/2002 to 2/27/2005 every 3 to 6 days. For Escondido, there were samples for which $PM_{2.5}$ mass concentration was missing or for which ions and elements were not fully analyzed. These samples comprised of 46% of the whole data set. Samples for which $PM_{2.5}$ mass concentrations diverged substantially from the 1:1 line with Federal Reference Method (FRM) $PM_{2.5}$ mass concentrations were excluded. In total, 48% of the original data were excluded from the analysis.

There were a limited number of FRM $PM_{2.5}$ mass concentrations available for the El Cajon site. Thus, instead of a comparison of the STM mass with the FRM $PM_{2.5}$ mass, mass closure was examined for the El Cajon data. About 58% of the samples had a higher sum of concentrations of the species analyzed than the observed total $PM_{2.5}$ mass concentration. This result is likely due to the volatilization of semivolatile compounds from PM mass filter. From the linear regression between total observed $PM_{2.5}$ mass and reconstructed (sum of the species measured) $PM_{2.5}$ mass concentrations, samples for which the absolute mass difference is greater than three times the estimate of the regression were defined to be outliers and excluded from the analysis. Samples for which $PM_{2.5}$ mass concentrations were missing were also excluded from the analysis. In total, 8.4% of the original data were excluded. The summary statistics of $PM_{2.5}$ mass and species concentrations used in the analysis is given in Table 46 and Table 47. The signal-to-noise (SN) ratio was utilized to determine which variables were used in the analysis (Paatero and Hopke, 2003). SO_4^{2-} had a strong linearity with elemental S ($r^2 > 0.95$) and was used instead of S in the analysis. Elemental K had a higher SN ratio than K^+ , and K was used in the analysis. In the same way, Na^+ was used in the analysis. The OC blank concentration was estimated from the regression of OC against total $PM_{2.5}$ mass concentration (Kim *et al.*, 2005), and both OC and total $PM_{2.5}$ mass concentrations were corrected with the OC blank concentration.



Figure 137. Map of sampling location for STN $PM_{2.5}$ measurements. Symbol (*) indicates the NOAA meteorological station near the sites.

Table 46. Summary statistics of the Escondido PM_{2.5} mass and species concentrations

	Concentration ($\mu\text{g}/\text{m}^3$)				Missin g (%)	BDL (%)
	Geometric mean	Arithmetic mean	Maximum	Minimu m		
PM _{2.5} mass	12.01	12.86	26.51	2.51	0	0
OC	4.433	5.317	17.51	0.908	0	0
EC	0.536	0.570	2.5	0.5	0	0
SO ₄ ²⁻	1.872	2.482	6.8	0.2	0	0
NO ₃ ⁻	2.544	3.287	11	0.38	0	0
NH ₄ ⁺	1.234	1.676	5	0.07	0	0
Al	0.034	0.051	0.31	0.003	0	17.5
Ba	0.021	0.024	0.11	0.016	0	83.5
Br	0.003	0.004	0.01	0.001	0	21.4
Ca	0.046	0.064	1.1	0.004	0	0.97
Cl	0.031	0.084	1.3	0.004	0	1.94
Co	0.004	0.004	0.005	0.001	0	13.6
Cu	0.005	0.008	0.047	0.001	0	14.6
Fe	0.082	0.101	0.41	0.018	0	0
K	0.073	0.093	0.39	0.018	0	0
Mn	0.002	0.002	0.027	0.001	0	64.0
Na ⁺	0.374	0.474	1.9	0.11	0	0
Ni	0.001	0.002	0.008	0.001	0	63.1
P	0.003	0.007	0.038	0.001	0	72.8
Pb	0.004	0.004	0.012	0.003	0	75.7
Si	0.107	0.126	0.69	0.028	0	0
Ti	0.005	0.007	0.03	0.003	0	44.7
V	0.004	0.005	0.014	0.002	0	48.5
Zn	0.009	0.012	0.048	0.001	0	3.0

Table 47. Summary statistics of the El Cajon PM_{2.5} mass and species concentrations

	Concentration ($\mu\text{g}/\text{m}^3$)				Missin g (%)	BDL (%)
	Geometric mean	Arithmetic mean	Maximum	Minimu m		
PM _{2.5} mass	11.28	12.90	37.18	1.376	0	0
OC	2.169	3.379	14.78	0.026	0	6.7
EC	0.702	0.854	3.450	0.127	0	2.6
SO ₄ ²⁻	2.053	2.860	10.60	0.208	0	0
NO ₃ ⁻	2.777	3.749	15.80	0.225	0	0
NH ₄ ⁺	1.138	1.718	7.690	0.0	0	0.3
Al	0.020	0.033	1.010	0.0	0	51
Ba	0.023	0.022	0.107	0.0	0	76
Br	0.003	0.004	0.015	0.0	0	17
Ca	0.044	0.057	1.670	0.0	0	0.6
Cl	0.024	0.080	1.210	0.0	0	31
Cr	0.001	0.002	0.031	0.0	0	67
Cu	0.005	0.006	0.037	0.0	0	15
Fe	0.087	0.105	0.644	0.0	0	0.3
K	0.067	0.081	0.530	0.010	0	0.0
Mg	0.020	0.023	0.300	0.0	0	64
Mn	0.002	0.003	0.047	0.0	0	47
Na ⁺	1.486	0.471	2.120	0.0	0.3	2.4
Ni	0.002	0.002	0.009	0.0	0	41
Pb	0.004	0.004	0.028	0.0	0	67
Si	0.087	0.121	1.600	0.0	0	4.7
Sn	0.011	0.008	0.063	0.0	0	84
Sr	0.001	0.001	0.012	0.0	0	82
Ta	0.009	0.005	0.045	0.0	0	83
Ti	0.006	0.007	0.053	0.0	0	25
V	0.003	0.004	0.018	0.0	0	37
Zn	0.005	0.007	0.054	0.0	0	17

Uncertainty estimation is a key part of PMF application. The procedure of Kim *et al.* (2005) were used to develop the uncertainties used as input to the PMF analysis. Higher uncertainties were assigned for “weak” elements based on their SN ratios. To reduce the rotational ambiguity, an adjustment was made for the parameter FPEAK as well as a matrix of FKEY values (Paatero *et al.*, 2002) in this study.

Surface wind data from the National Weather Service (NWS) sites near the two San Diego STN sites were used to calculate CPF values. There are five NWS sites in this area as shown in Figure 137. Among them, wind direction and wind speed data from San Diego Montgomery Field station (MYF, Latitude 32.8167, Longitude -117.1333) were used to calculate CPF values for both the Escondido and El Cajon sites. The MYF station is located about 20 km west of the El Cajon site and 30 km south of the Escondido site, respectively. It should be noted that since the available met data from NWS sites are not adjacent to the sampling sites and there are significant topographic features that may perturb the local wind directions, the CPF results may not provide accurate directional indications of potential emission sources that are resolved by the PMF analysis.

Escondido. Different number of factors, different initial seeds and different FPEAK values were examined and an acceptable 8-factor solution was found with an FPEAK value set to -0.2. Sources resolved are gasoline and mixed motor vehicle emissions, secondary nitrate and sulfate, aged and fresh sea salt, residual oil combustion, and airborne soil. Chemical source profiles of the factors identified from the PMF analysis are shown in Figure 138 and the estimated source contributions are shown in Figure 139. The average contributions of the sources deduced from PMF modeling were summarized in Table 48.

Gasoline emission is characterized by high OC relative to EC concentration and as much NO_3^- concentration as EC. This factor shows high peaks during winter. Those high concentrations during wintertime are likely due to low mixing height. This factor accounted for 26% of total $\text{PM}_{2.5}$ mass concentration. Mixed motor vehicle emission is represented by higher OC to EC ratio as well as various trace metals, accounting for 1% of total $\text{PM}_{2.5}$ mass concentration. It shows relatively high Cu signature. Cu is emitted from metal brake wear (Lee *et al.*, 2005), and from car motor rotors as well. Although Ba and Pb are relatively low, they are considered to be diesel-emitted metals (Lee *et al.*, 2005). The seasonal differences in the estimated mass concentrations of the sources are shown in Figure 140. Gasoline emission and mixed motor vehicle emission factor appears to show winter-higher contributions, presumably due to low atmospheric mixing layer. However, the seasonal differences were much higher for motor vehicle emission factor also shows winter-high contribution.

Secondary nitrate is represented by high NO_3^- and NH_4^+ concentration and accounted for 23% of total $\text{PM}_{2.5}$ mass concentration. This factor shows winter-high contribution. It is expected that cold temperatures favor particulate NO_3^- formation. Because lower SO_4^{2-} concentrations leave more NH_4^+ available to neutralize nitric acid (HNO_3) and form ammonium nitrate (NH_4NO_3) (Lee *et al.*, 2002). NH_4^+ in California is likely to be attributed to NH_3 emissions in large farm land in Chino and to the emissions from motor vehicles, whereas NO_3^- is more likely to be due to HNO_3 from car emissions. Chino is located northwest of the Escondido site.

Secondary sulfate has high SO_4^{2-} and NH_4^+ concentrations and shows high peaks during summertime when photochemical reactivity is enhanced. It accounted for 20% of total $\text{PM}_{2.5}$ mass concentration. Although secondary sulfate formation is known to be associated with regional transport of SO_2 and its transformation to SO_4^{2-} particles, locally-emitted and transported SO_2 may form SO_4^{2-} particles under the NH_4^+ -abundant environment with enough residence time. The geographical environment of the sampling site surrounded by mountains is likely to act as a reactor that provides enough reaction time for transformation to ammonium

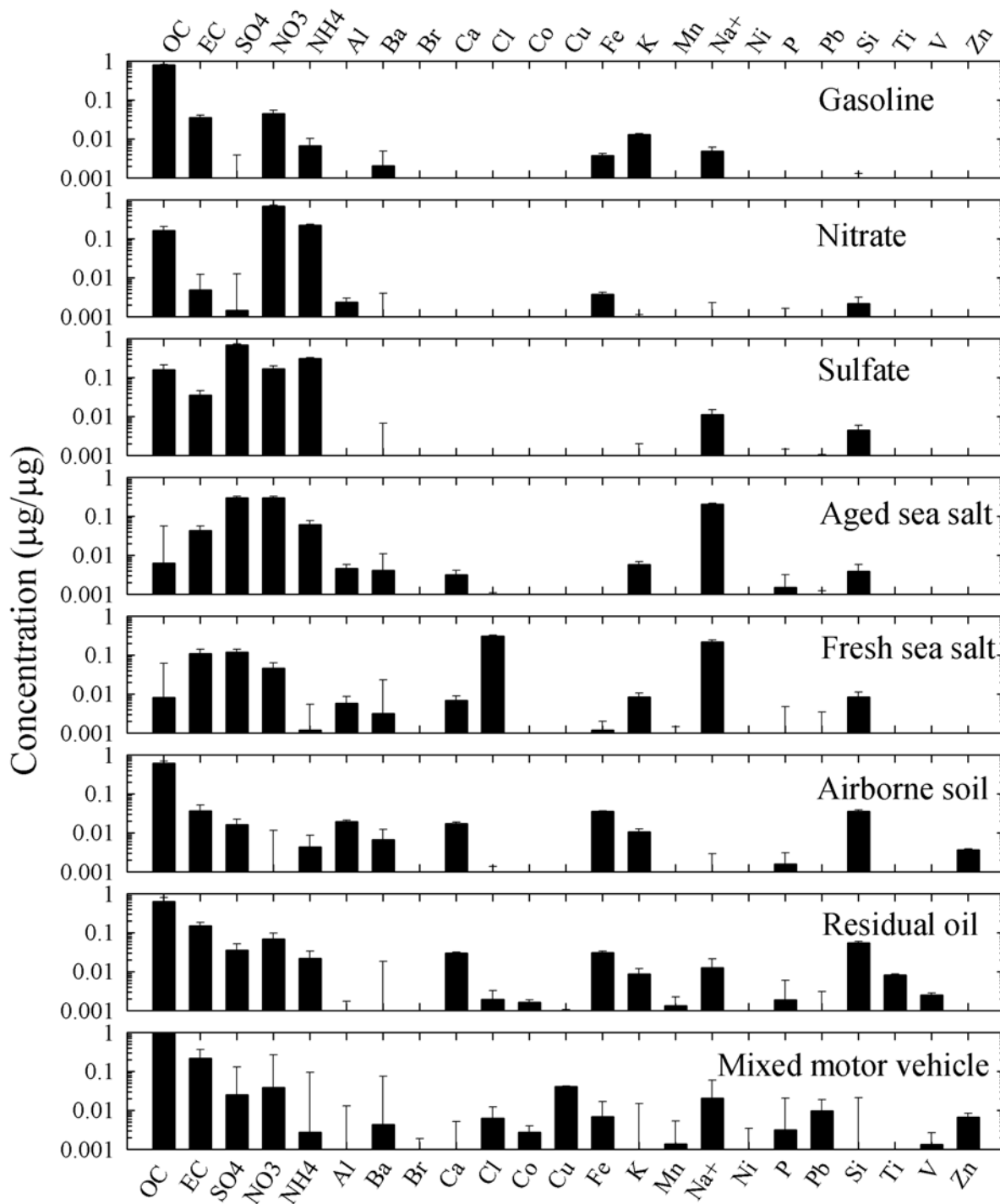


Figure 138. Source profiles of 8-factor solution deduced from PMF modeling for Escondido PM_{2.5}.

sulfate [(NH₄)₂SO₄]. The secondary sulfate factor shows higher contribution in summer than in winter as shown in Figure 142.

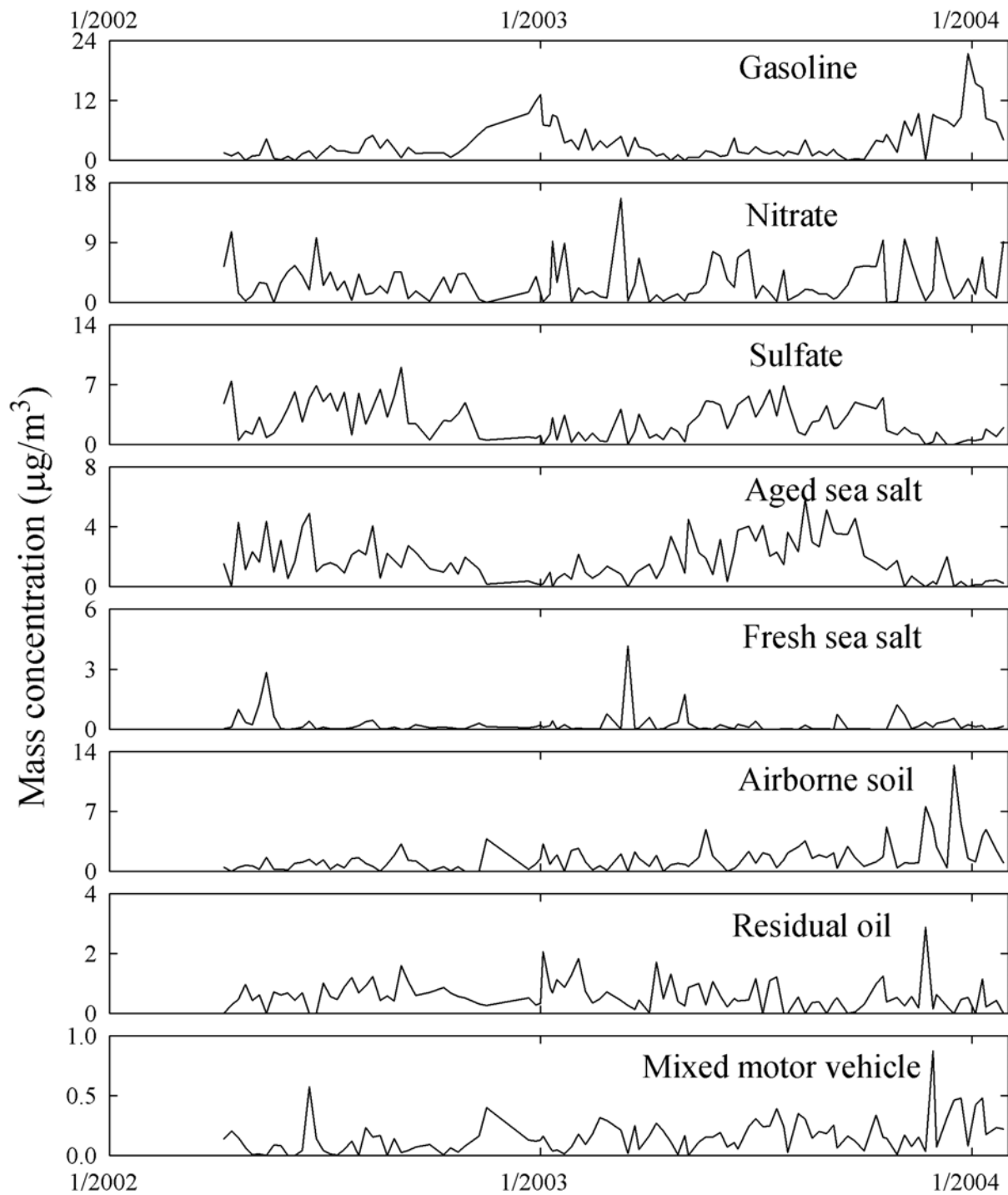


Figure 139. Source contributions of 8-factor solution deduced from PMF modeling for Escondido PM_{2.5}.

Table 48. Average source contributions from PMF to measured PM_{2.5} mass concentration at Escondido

	Average Source Contribution ($\mu\text{g}/\text{m}^3$)	Standard Error ($\mu\text{g}/\text{m}^3$)
Gasoline	3.38	0.26
Nitrate	2.92	0.19
Sulfate	2.60	0.17
Aged sea salt	1.63	0.15
Fresh sea salt	0.24	0.12
Airborne soil	1.48	0.14
Residual oil combustion	0.57	0.06
Diesel	0.15	0.01

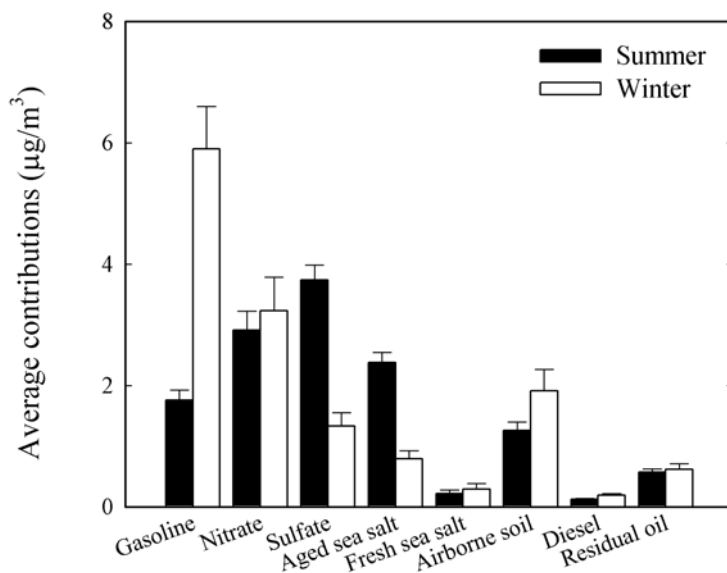


Figure 140. Seasonal average mass contributions (mean \pm 95% standard error) of each source to total PM_{2.5} mass concentration. Summer is from May to October, and winter is from November to April.

The next two profiles are sea salt factors, aged and fresh sea salt. Aged sea salt factor is characterized by high Na⁺, anthropogenic air pollutants (SO₄²⁻, NO₃⁻), and low chlorine (Cl) concentrations. The high SO₄²⁻ and low Cl suggest that sea salt particles emitted from the Pacific Ocean reacted with sulfuric acid (H₂SO₄) and/or sulfur dioxide (SO₂), leading to depletion of Cl in the sea salt particles and the formation of sodium sulfate (Na₂SO₄). The sea salt particles can also react with nitrogen oxide (NO_x) or nitric acid (HNO₃), which leads to depletion of Cl in the

sea salt particles and the formation of sodium nitrate (NaNO_3). Fresh sea salt factor shows high concentrations of Na^+ and Cl that are major components of sea salt particles and relatively low anthropogenic pollutants. These profiles indicate contributions of unprocessed sea salt particles to the site. The average mass contribution to total $\text{PM}_{2.5}$ mass concentration was 13% for aged sea salt and 2% for fresh sea salt, respectively. The aged sea salt factor showed higher contribution in summer than in winter, whereas no seasonal differences appeared for fresh sea salt factor. Although both SO_4^{2-} and NO_3^- are associated with Na^+ in the aged sea salt factor, the seasonal differences in the factor suggests the formation of Na_2SO_4 particles to be predominant since is seen summer-high contribution. No seasonal differences were shown in the fresh sea salt factor.

Airborne soil factor is characterized by high concentrations of soil components such as aluminum (Al), calcium (Ca), iron (Fe), and silicon (Si). This airborne soil accounted for 11% of total $\text{PM}_{2.5}$ mass concentration. Seasonally, it shows winter-high contributions.

The residual oil combustion factor shows the highest vanadium (V) concentration compared to the other factors. The average mass contribution to total $\text{PM}_{2.5}$ mass concentration was 4%. Ni and V are major species from residual oil combustion. Oil-fired power plants are major sources of Ni and V emissions on the east coast (Lee *et al.*, 2002; Poirot *et al.*, 2001, Song *et al.*, 2001). Huffman *et al.* (2002) suggested that during residual oil burning V and Ni were present as NiSO_4 and vanadyl sulfate ($\text{VO}\cdot\text{SO}_4\cdot x\text{H}_2\text{O}$), respectively. Thus, it is reasonable to see SO_4^{2-} along with V in the residual oil combustion factor. It is not clear why there no Ni signature was in this factor. Other elements were reported by Huffman *et al.* from residual oil combustion emissions, such as Cu, Pb, and Zn. Fe could be present as $\text{Fe}_2(\text{SO}_4)_3$. There were no Cu and Pb signatures in the residual oil combustion factor. However, those tracers are likely to be present in residual oil-burning ashes in low percentages. No clear seasonal difference was observed in the residual oil combustion factor. This residual oil combustion had somewhat similar source profiles to mixed motor vehicle emission.

The predicted $\text{PM}_{2.5}$ mass concentrations from the resolved PMF factors were compared to the measured $\text{PM}_{2.5}$ mass concentrations in Figure 141. The correlation of the linear regression was strong ($r^2 = 0.89$). However, the PMF source contributions underestimated the measured $\text{PM}_{2.5}$ mass concentration at concentration level higher than $20 \mu\text{g}/\text{m}^3$.

Different FPEAK values from -1.0 to 1.0 and FKEY matrix values were used to find the most interpretable solution. The Q value with a positive FPEAK value of 0.2 showed an abrupt rise while the Q value remained relatively flat down to a value of -0.3. FKEY values were used to pull the OC down toward zero in the mixed motor vehicle emission factor in order to see if OC could be reduced below EC. FKEY values of 2, 3, and 5 were tried. In each case, the nitrate factor disappeared and sulfate and aged sea salt appeared to be admixed in one factor. Thus, FKEY was not used in this analysis.

Figure 142 depicts the weekday/weekend effects for the PMF sources. Gasoline emission factor showed weekend-high concentrations, mixed motor vehicle factor also appeared to be higher over weekend. Meanwhile, secondary nitrate and sulfate, aged sea salt, and airborne soil

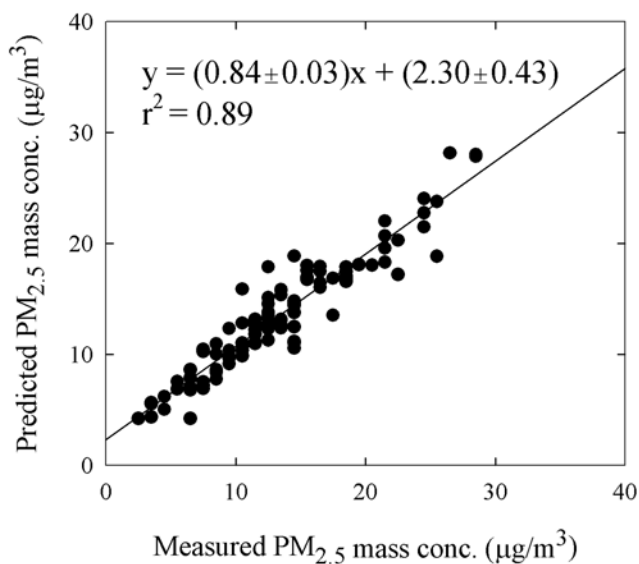


Figure 141. Comparison of measured versus predicted $\text{PM}_{2.5}$ mass concentrations for Escondido data.

appeared to be weekday-high concentrations. Residual oil combustion showed little difference in concentrations between weekday and weekend. Weekend concentration showed broader error distributions, probably due to fewer number of weekend samples than weekday samples

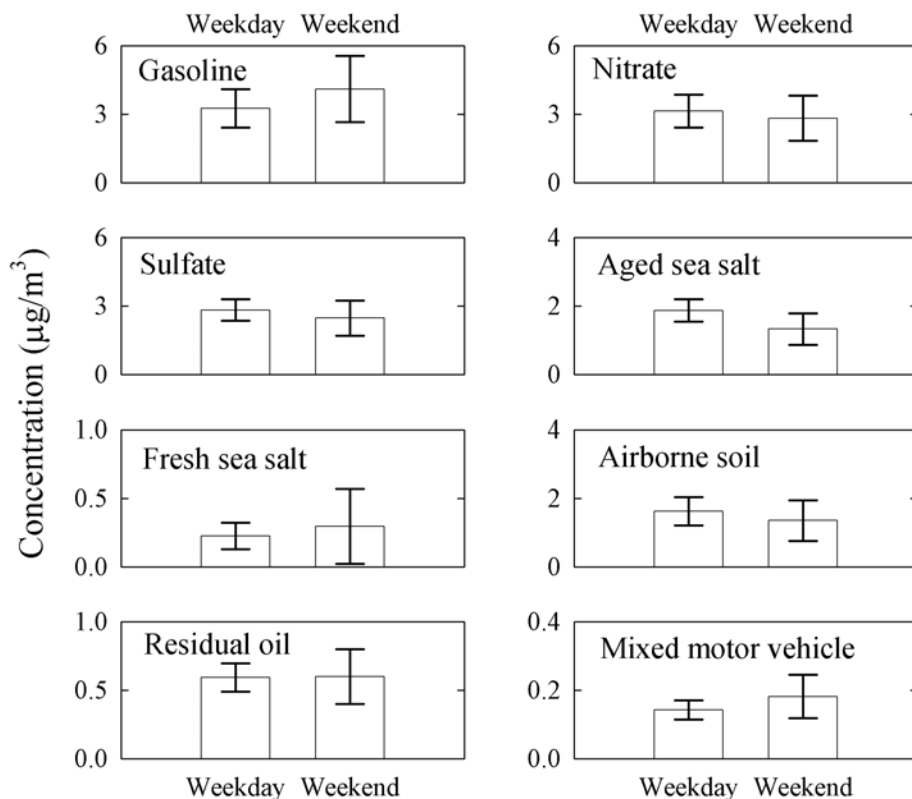


Figure 142. Average mass contributions (mean \pm 95% confidence interval) of the PMF sources for weekday and weekend $PM_{2.5}$ mass concentration at Escondido.

Figure 143 shows the CPF plots at Escondido site. The directionality of some sources do not appear well represented by CPF results. For example, the CPF for gasoline factor suggests that the Escondido site is most likely affected by sources located in the northeast of the site. However, as seen in Figure 137, there are no major roads in this direction. The nitrate factor shows northwesterly, southwesterly, and northeasterly directions as locations of potential emission sources. Considering that vehicle emissions are major sources of precursor gases of particulate nitrate, these directions are relatively well represented by the northbound and southbound state highways. The sulfate factor indicates that the Port of San Diego and downtown San Diego are potential emission areas for secondary sulfate aerosol. Local emission sources such as support vehicles, truck, and railroad engines, as well as cargo handling systems during the loading/unloading operations at the Port area and also on-road vehicles in downtown San Diego are possible sources of gaseous sulfur dioxide that react to form particulate sulfate. Both aged and fresh sea salt factors showed a southerly source direction toward the Port of San Diego. Airborne soil shows the northeasterly direction as potential emission source location, suggesting that locally blown soil dust contributed to Escondido $PM_{2.5}$. Residual oil did not show any specific directions with respect to emission sources. The CPF plot of mixed motor vehicle factor indicates the westbound local and state roads to be potential emission sources.

Thus, on-road gasoline and diesel vehicle emissions are likely attributed to mixed motor vehicle factor.

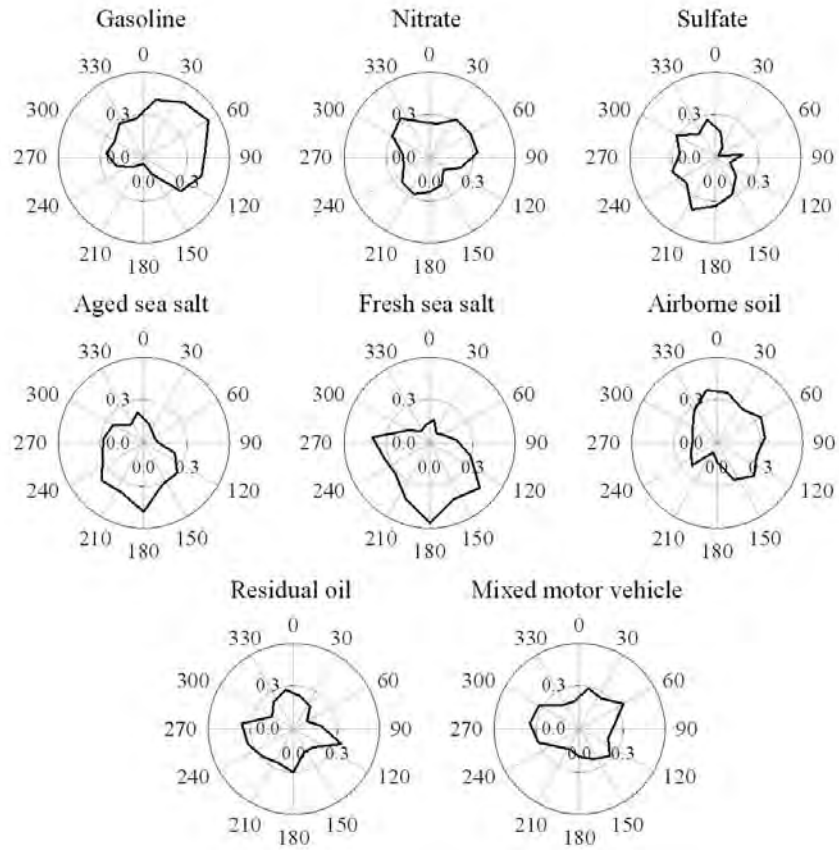


Figure 143. CPF plots of PMF-resolved sources at Escondido.

El Cajon. An 8-factor solution was preliminary achieved from PMF modeling for El Cajon PM_{2.5} speciation data. A value of FPEAK was set to -0.2 and no FKEY matrix was used. Factors deduced in this analysis include gasoline and diesel emission factors, secondary nitrate and sulfate factors, aged and fresh sea salt factors, residual oil combustion, and airborne soil factor. The source profiles of the PMF sources are given in Figure 144 and the estimated source contributions of the sources are shown in Figure 145. The average mass contributions of the sources to total PM_{2.5} mass concentration are summarized in Table 49. Seasonal differences in average mass contributions to PM_{2.5} mass concentration were also depicted in Figure 146.

Table 49. Average source contributions from PMF to measured PM_{2.5} mass concentration at El Cajon

	Average Source Contribution ($\mu\text{g}/\text{m}^3$)	Standard Error ($\mu\text{g}/\text{m}^3$)
Gasoline	3.23	0.15
Nitrate	3.39	0.12
Sulfate	2.62	0.10
Aged sea salt	1.37	0.08
Fresh sea salt	0.40	0.08
Airborne soil	0.43	0.03
Residual oil combustion	0.44	0.03
Diesel	0.15	0.01

The first factor is assigned to be gasoline emissions that are characterized by high OC relative to EC concentration. This gasoline emission factor closely resembles the gasoline factor identified at the Escondido site as shown in Figure 138. This factor also shows higher concentrations during wintertime, presumably due to low mixing height effects. The gasoline emission factor accounted for 25% to total PM_{2.5} mass concentration.

The next factor is secondary nitrate showing covariance of NO₃⁻ and NH₄⁺, and accounted for 26% to total PM_{2.5} mass concentration. This nitrate factor shows higher contribution in winter than in summer. It is expected that the formation of NH₄NO₃ is favored in cold temperatures and when less SO₄²⁻ leaves NH₄⁺ available for more neutralization to HNO₃.

The third factor is secondary sulfate in which SO₄²⁻ and NH₄⁺ highly co-vary. Secondary sulfate explains 20% of total PM_{2.5} mass concentration. Seasonal contribution was significantly high in summer, which suggests the secondary formation of sulfate aerosols from H₂SO₄ due to photochemical reactions with NH₃.

The next two factors are aged and fresh sea salt factors. The average source contribution to total PM_{2.5} mass concentration was 11% for aged sea salt and 3% for fresh sea salt, respectively. The aged sea salt factor showed higher contributions in summer, whereas fresh sea salt factor showed higher contributions in winter.

Airborne soil factor is represented by Al, Ca, Fe, K, Mg, Si, and Ti. Total PM_{2.5} mass concentration was accounted for 3% by this soil factor. Residual oil combustion is characterized by high EC concentration and covariance of Ni and V, accounting for 3% of total PM_{2.5} mass concentration. The last factor, diesel emissions are characterized by high EC to OC concentrations and various trace elements including Ba, Ca, Cu, Fe, and Pb. Those elements were also identified in the previous work (Lee *et al.*, 2005; Lee and Hopke, 2005) in the Midwest US. The diesel emission factor accounted for 1% of total PM_{2.5} mass concentration.

The predicted PM_{2.5} mass concentrations were plotted to the measured PM_{2.5} mass concentrations in Figure 147. The regression correlation (r^2) shows strong correlation between the two PM_{2.5} mass concentrations. Total measured PM_{2.5} mass concentration and associated

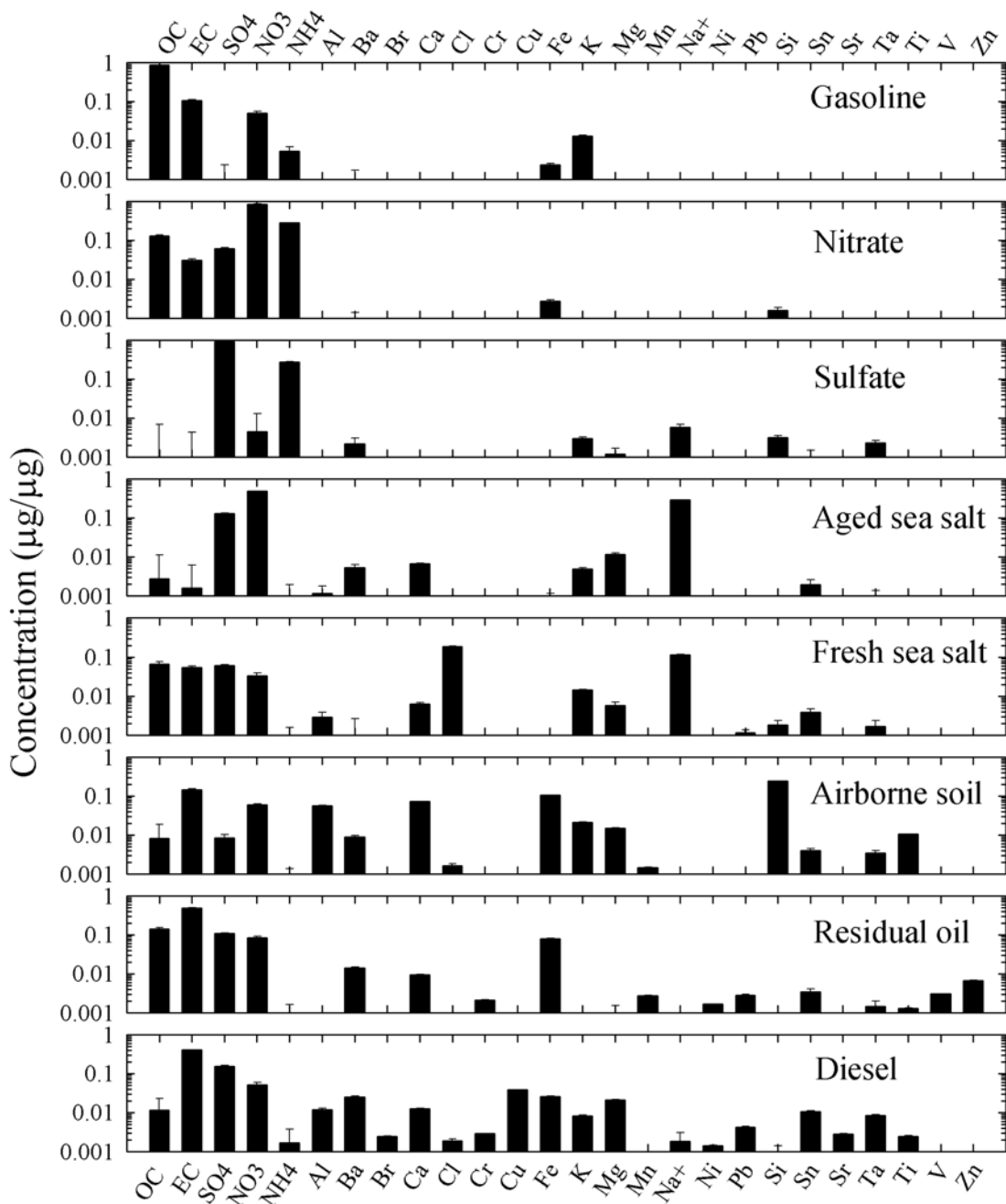


Figure 144. Source profiles of 8-factor solution deduced from PMF modeling for El Cajon PM_{2.5}.

uncertainty were included in the input to PMF modeling, but the slope of the regression was still much below 1.

The weekend/weekday effects to each source were examined and depicted in Figure 148. Gasoline emission factor and fresh sea salt factor showed higher concentrations during weekend, whereas residual oil combustion factor showed higher concentration during weekday. Other factors did not show clear differences in concentration between weekday and weekend.

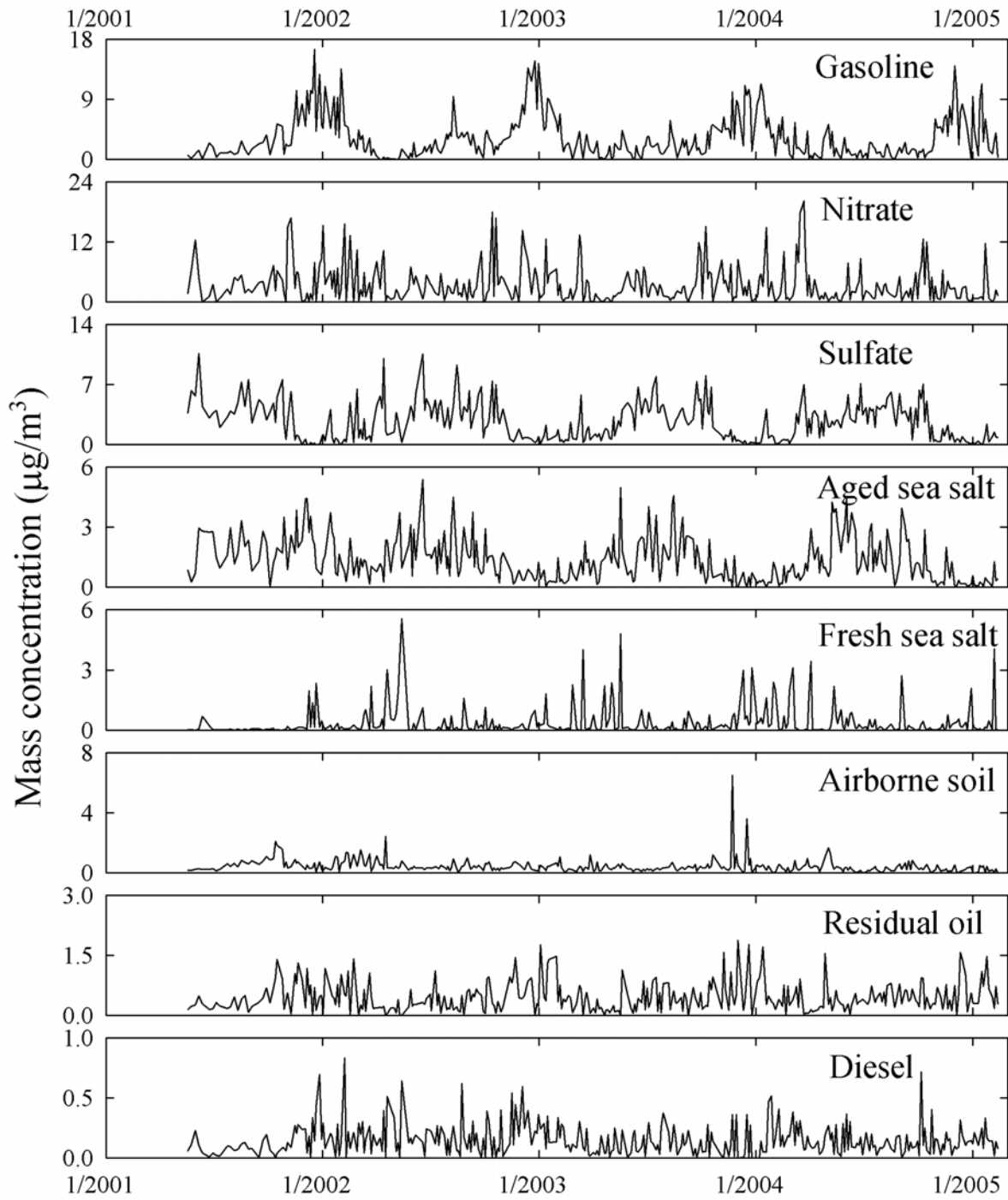


Figure 145. Source contributions of 8-factor solution deduced from PMF for El Cajon PM_{2.5}.

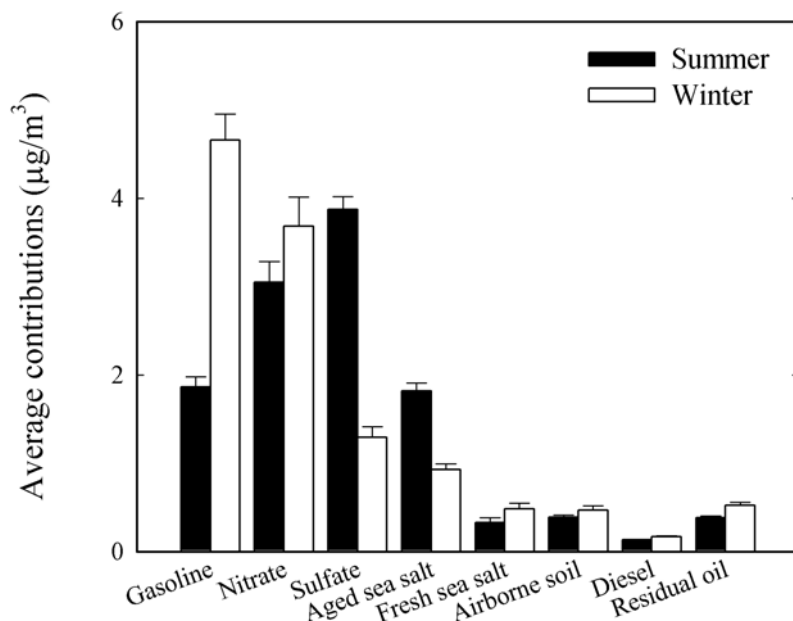


Figure 146. Seasonal average mass contributions (mean \pm 95% standard error) of each source to total $PM_{2.5}$ mass concentration. Summer is from May to October, and winter is from November to April.

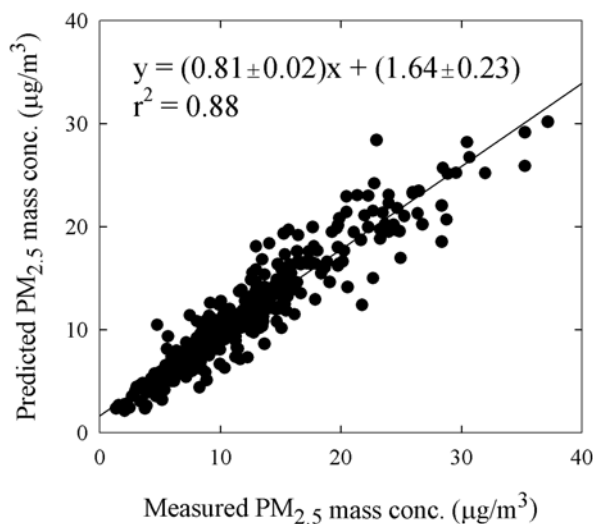


Figure 147. Comparison of measured versus predicted $PM_{2.5}$ mass concentrations for El Cajon data.

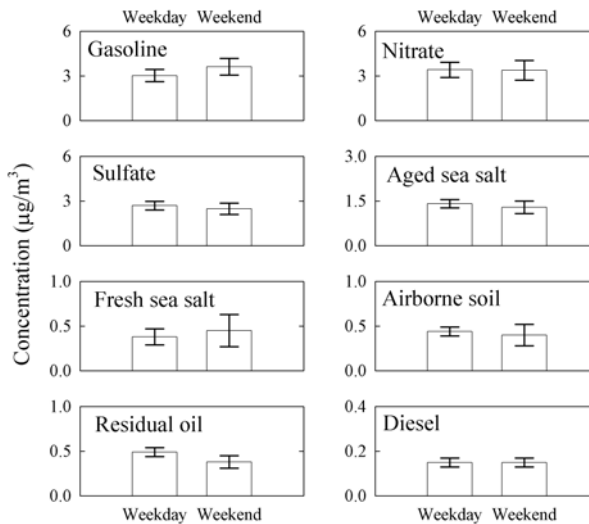


Figure 148. Average mass contributions (mean \pm 95% confidence interval) of the PMF sources for weekday and weekend $PM_{2.5}$ mass concentration at El Cajon.

Figure 149 shows the CPF plots for PMF factors at El Cajon. The CPF plot for gasoline factor suggests the exhaust from spark-ignition engine vehicles running on the state highway

(Route 8) to be a potential emission source for gasoline factor. Nitrate did not show specific directionality of sources. Sulfate factor shows the southwesterly direction of emissions from the Port of San Diego. Both aged and fresh sea salt factors indicate that potential sea salt emission sources are likely to be located in the south of the site. However, this result is not likely to happen because the Pacific ocean is located the west of the site. This outcome is another example of caveats regarding wind directions since the met data is not from the site. Airborne soil factor and diesel factor show the similar directions, the westerly, for possible location of sources. On-road mobile emissions and road dust are most likely to contribute to these factors. Residual oil factor shows the northeast of the site as a location of potential emission sources.

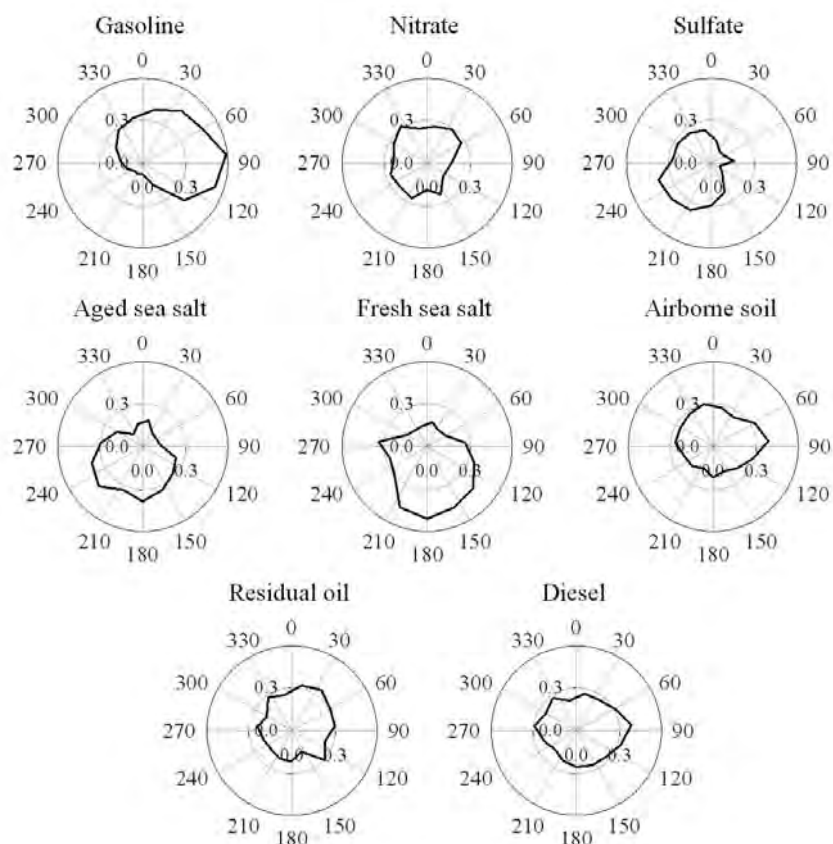


Figure 149. CPF plots of PMF-resolved sources at El Cajon.

Both the Escondido and El Cajon $PM_{2.5}$ speciation data were analyzed using PMF2 modeling, and the same number of sources (i.e., 8-factor) were preliminarily characterized. The source profiles and contributions for both the sites look very similar, so the nature of sources is expected to be similar for most of the sources at both the sites. One difference in the source nature is between diesel emission and mixed motor vehicle emission. The diesel emission was identified at the El Cajon site, whereas the mixed motor vehicle emission was identified at the Escondido site. The average contributions of the sources to total $PM_{2.5}$ mass concentration were in similar ranges for most of the sources, except fresh sea salt and airborne soil factors. The mass contribution of fresh sea salt factor was higher at El Cajon (3.1%) than at Escondido (1.9%). The contribution of airborne soil was significantly higher at Escondido (11.5%) than at El Cajon (3.3%). These differences are not quite clear at present. For each pair of sources that

have the same or similar characteristics, the estimated source contributions between the sites are compared in Figure 150.

Nitrate, sulfate, and aged and fresh sea salt factor show strong correlation ($r > 0.8$) in their source contributions between the sites. Also, gasoline and airborne soil factors show correlation of $r > 0.7$ in their contributions between the sites. The results suggest that Escondido and El Cajon $PM_{2.5}$ are likely to be affected by the similar source emissions. Diesel (or mixed motor vehicle at Escondido) and residual oil combustion factor showed highly scattered source contributions. The source contributions appeared to be randomly distributed between the sites.

To identify the location of contributing sources, further analyses utilizing wind direction and wind speed are needed. Conditional probability function (CPF) can be used to find the directions of the PMF sources. The CPF has been used in identifying the directionality of source location obtained from PMF modeling (Kim *et al.*, 2003; Kim and Hopke, 2004). On-site wind direction and speed measurement data is necessary for identifying the location of potential sources as studied in the previous work (Lee *et al.*, 2005). The two San Diego sampling sites are surrounded by mountains to the north, south, and east, and thus perturbation in wind direction is likely to occur. In addition, the nearest meteorological station for which wind data is available is approximately 20 km from the El Cajon site and 30 km away from the Escondido sites, respectively (see Figure 137). Considering the topological situation and the distance from the sampling site and the meteorological station, CPF analysis may result in incorrect directional results.

$PM_{2.5}$ mass speciation data at the two San Diego STN sites were analyzed using PMF modeling. The similar eight-factor solution was preliminarily achieved at each site. Sources are gasoline emission, diesel (or mixed motor vehicle) emission, secondary nitrate, secondary sulfate, aged sea salt, fresh sea salt, airborne soil, and residual oil combustion. The estimated source profiles and source contributions were obtained from PMF. To identify location of the sources, wind direction and speed measurement data should be utilized for the PMF source contribution results. The current meteorological data available are from a station that is ~30 km apart from the sampling sites. In order to make reliable CPF analysis, on-site or near-site meteorological data are required.

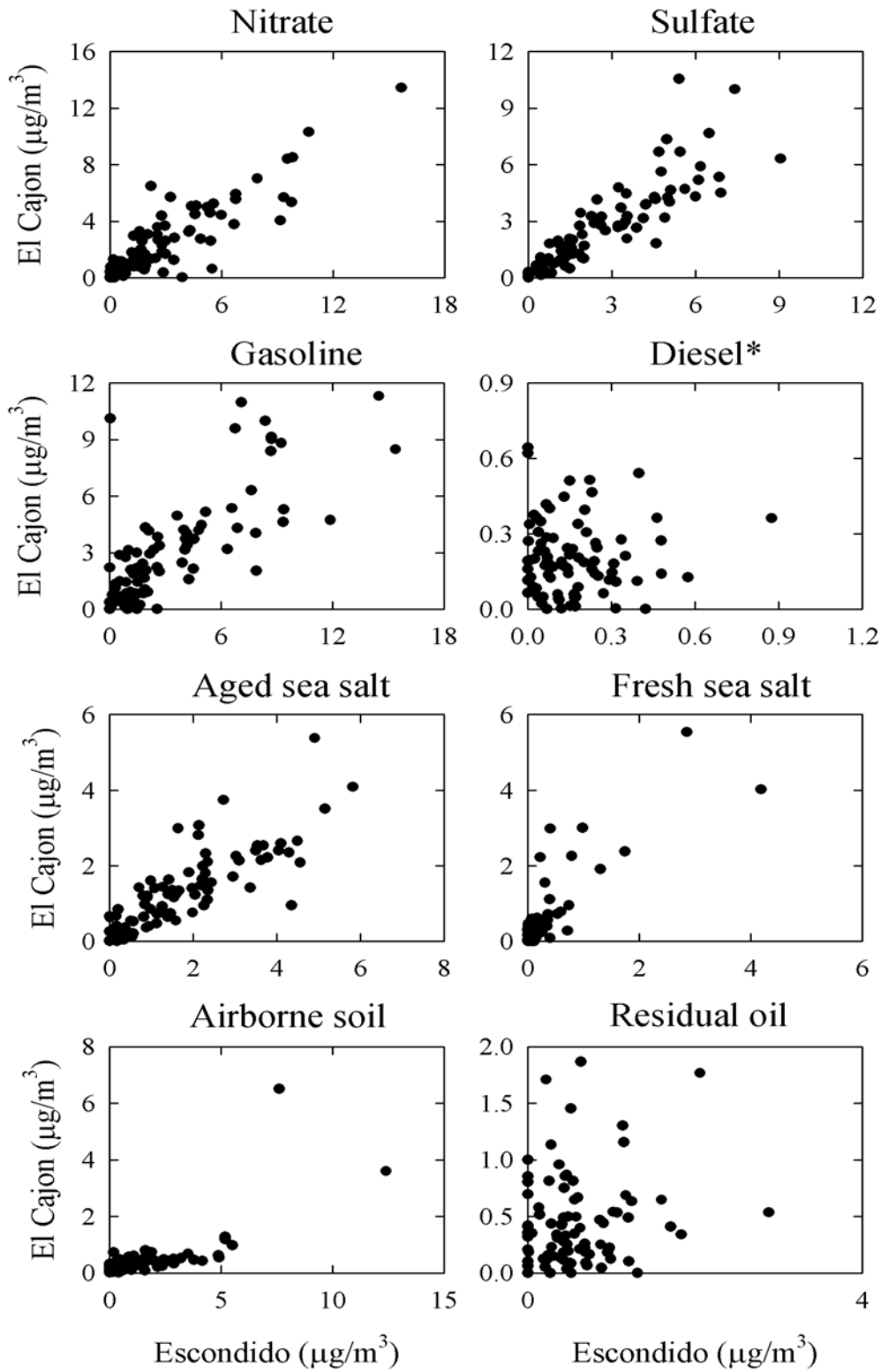


Figure 150. Comparison of the estimated source contributions between the sites. The diesel at El Cajon was compared to the mixed motor vehicle at Escondido.

Very similar CPF results were obtained for both the Escondido and El Cajon sites. The directionality of potential emission sources was generally defined for the sources resolved from the PMF analysis. However, some of the PMF sources were not clearly represented by the CPF plots probably as a result of the lack of meteorological data from the sites.

The residual oil factor CPF points to the northeast of the sites as the location of the emission sources. It is not clear why this result is obtained and what other sources could contribute to the apparent residual oil factor directionality. To further examine the sources of residual oil factor, back trajectory analysis was performed for days with high peak concentrations of the residual oil factor. There were several times peaks observed near December, 2003 as seen in Figures 139 and 145. Figure 151 shows 5-day back trajectories at a height of 500 above ground level at Escondido site on November 23, 2003 and at El Cajon site on December 2 and 20, 2003, respectively. At Escondido, air trajectories appeared to come from the Pacific Ocean passing over inland Nevada state and finally arrive at the site. Meanwhile, air trajectories on two days in December 2003 at El Cajon show that air parcels were transported over offshore Mexico. The back trajectory results suggest the possible influence of ship emissions to $PM_{2.5}$ mass in the San Diego area.

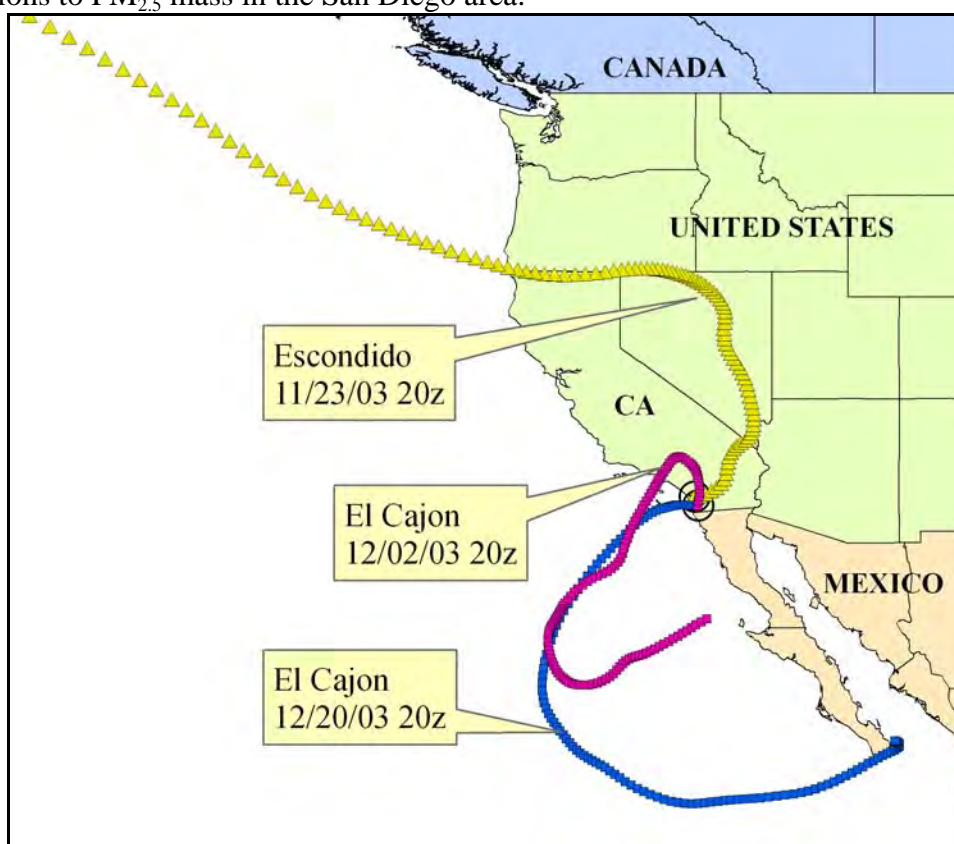


Figure 151. Back trajectories on days showing high residual oil mass concentrations at Escondido and El Cajon sites.

Relationship of Primary Combustion Emissions to Other Species

In this study, the data from the PM_{2.5} particle sampling sites along the west coast of the United States were analyzed for source apportionment by positive matrix factorization. These sites included urban sites in the U.S. Environmental Protection Agency's Speciation Trends Network and more remote sites from the IMPROVE network. Primary emissions from the combustion of residual oil produce particles containing Ni and V. Source profiles for residual oil could be observed in Seattle, Los Angeles, and San Diego. They could not be identified at the other STN sites (Anchorage, Portland, and San Jose). There were high Ni concentrations in San Jose, but no V and thus, it is highly unlikely that this source is residual oil.

The clearest influence of ship emissions was in Seattle where multiple site results point clearly at the Port of Seattle as a likely source area. However, the ship primary emissions do not represent a large source of PM_{2.5}. Secondary sulfate sources could be identified at all of the sites. Figure 153 shows a plot of the oil combustion contributions plotted against the corresponding secondary sulfate contributions at the Beacon Hill STN site. It can be seen that there is a relationship between the secondary sulfate and the primary V-Ni bearing particles. The line represents an "edge" that demonstrates this relationship (Henry, 2003). The slope of this line is 1.213 so that there appears to be 0.82 $\mu\text{g}/\text{m}^3$ of sulfate for every 1 $\mu\text{g}/\text{m}^3$ of primary oil combustion particles. Similar plots can be derived at the other two Seattle STN sites where a residual oil combustion factor was resolved as shown in Figures 153 and 154. A line with the same slope as seen in the Beacon Hill results is shown.

The situation in the Los Angeles area is unclear. A residual oil profile could not be extracted from any of the three STN sites although Ni and V could be observed in approximately the ratio seen in the residual oil combustion profiles from other locations. The average Ni and V concentrations at Rubidoux were approximately 66% of those observed at the downtown LA site. If the source was ship emissions at the Port of Los Angeles and the Port of Long Beach, there should have been a much larger decrease in the Ni and V concentrations as the air moved eastward to Rubidoux. In addition, experiments performed in Rubidoux in the summer of 2005 found high concentrations of V-bearing particles and high mercury concentrations suggesting that there is significant residual oil combustion in the Riverside-Rubidoux area even though it does not appear in the emissions inventory. In addition, there is the potential confounding of the ship emissions by the refineries in the Torrance area. The emissions inventory indicates an emission rate for Ni of 750 pounds per year and no report of V emissions. However, it is likely that the Ni comes from residual oil combustion to produce the energy needed for the refinery operations. At all three sites, the Ni and V appear most strongly in the aged sea salt factor so that it appears there is sufficient covariance among these elements and Na and nitrate that they cannot be separated.

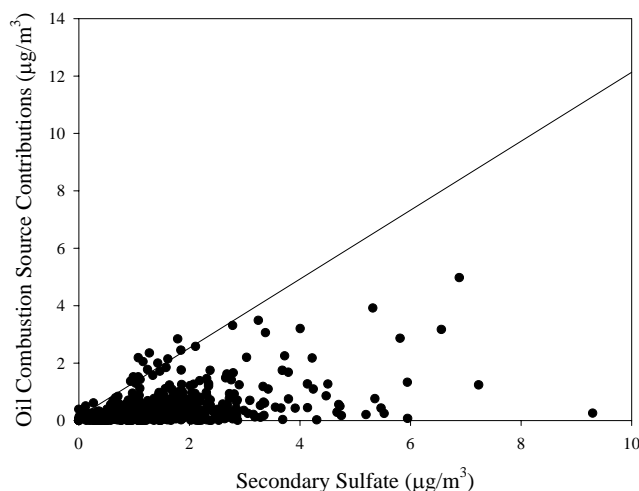


Figure 152. Plot of the contributions of oil combustion against the secondary sulfate contributions at the Beacon Hill site in Seattle.

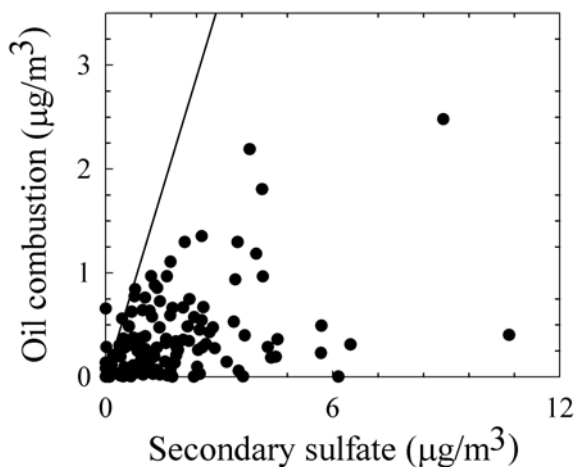


Figure 153. The residual oil combustion contribution at the Olive St. site in Seattle plotted against the secondary sulfate contributions.

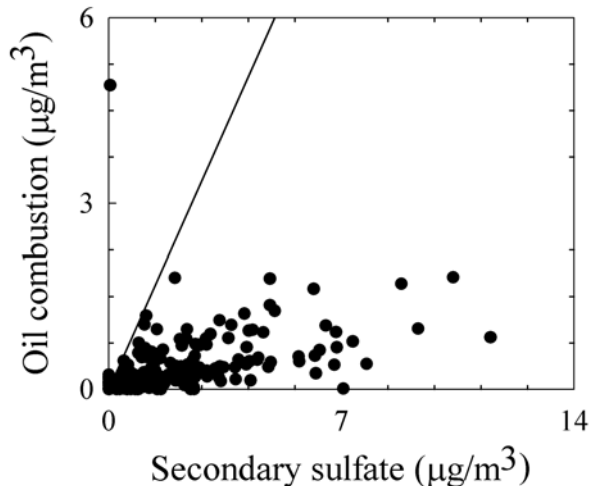


Figure 154. The residual oil combustion contribution at the Duwamish site in Seattle plotted against the secondary sulfate contributions.

At the two San Diego area sites, residual oil could be separated and the residual oil contributions are plotted against the secondary sulfate concentrations in Figures 155 and 156. It can be seen that there are no obvious edges in either of these plots. The 1.2 slope line was included as a point of comparison. At these two sites, there does not appear to be any correlation between the residual oil combustion emissions and the formation of secondary sulfate.

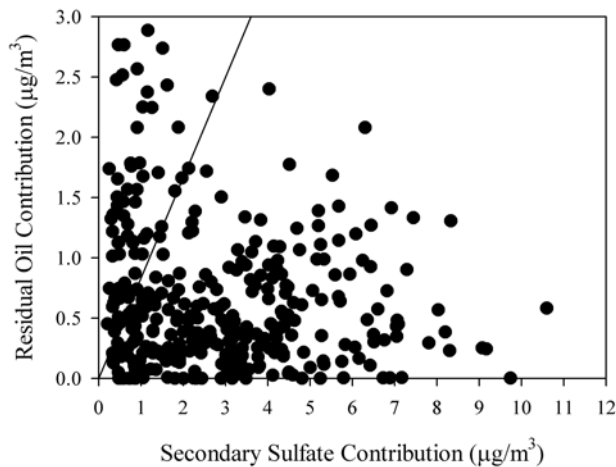


Figure 155. Plot of the residual oil contributions against the secondary sulfate contributions for the El Cajon STN site.

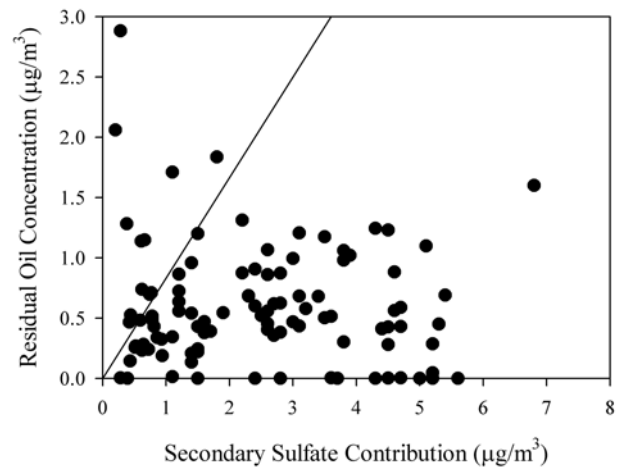


Figure 156. Plot of the residual oil contributions against the secondary sulfate contributions for the Escondito STN site.

At some of the rural IMPROVE sites (Aqua Tibia, San Rafael, Point Reyes, and Olympic), oil combustion source profiles can be identified. The clearest influence is at the Point Reyes National Seashore where it appears that the ships approaching San Francisco influence this site to the northwest of the city. At this site, the relationship between the ship emission primary particles and secondary sulfate is less well defined as shown in Figure 157. A line with

the same slope as in Seattle is shown in the figure suggesting that if there is a relationship, it has similar magnitude to that which was more clearly seen in Seattle. The plots for the other sites are more equivocal. Figure 157 shows the plot for the Olympic National Park site. In this case there is no clear edge in the plot. Thus, it is difficult to conclude that it is possible to associate a specific contribution of secondary sulfate that is clearly associated with ship diesel emissions at these sites.

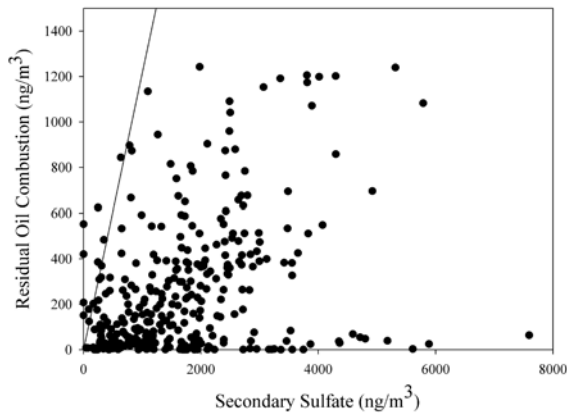


Figure 157. Residual oil combustion contributions plotted against the corresponding secondary sulfate contributions at Point Reyes National Seashore.

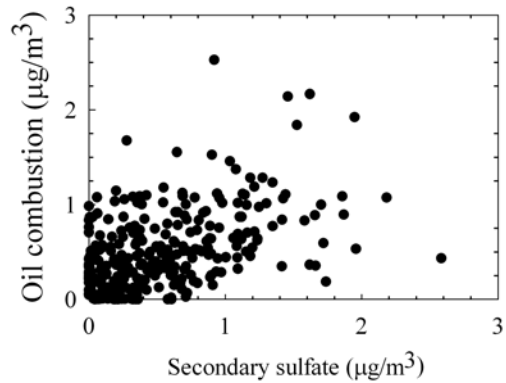


Figure 158. Residual oil combustion contributions plotted against the corresponding secondary sulfate contributions at Olympic National Park.

CONCLUSIONS

Tables 50 and 51 present the average mass apportionments derived from the PMF analyses reported previously in this report. Overall, the impacts of the ship emissions of primary particles tend to be relatively small compared to the full suite of sources identified at the sites along the western coast of the United States. The clearest influence of ship emissions was in Seattle where multiple site results point clearly at the Port of Seattle as a likely source area. However, the ship primary emissions represent a small source of PM_{2.5}. The average mass contributions ranged from 0.20 µg/m³ at Aqua Tibia to 0.60 µg/m³ at the Beacon Hill site in Seattle, WA. However, the STN data at the Beacon Hill site suggested that the mean contribution was 0.43 µg/m³. The differences appear to arise primarily from the difference in the measurement method for organic and elemental carbon as measured in the two networks.

It is also possible to identify an additional contribution of sulfate from the emission of the SO₃ from the ships. However, it appears that at most it doubles the mass contributions from the primary particle emissions.

Table 50. Summary of the average source apportionments for the IMPROVE sites along the west coast of the United States.

Site	Sulfate	Nitrate	Gasoline	Diesel	Residual Oil	Soil	Wood smoke	Sea Salt	Other
Aqua Tibia	2.67	1.44	1.28	0.26	0.20	0.80		0.94	
San Gabriel	1.04	1.05	0.50	0.08		0.37		0.28	1.34
San Rafael	1.63	0.55	1.40	0.09	0.26	0.79		0.32	0.08
Pinnacles	1.46	0.57	1.87	0.26		0.13	0.37	1.01	
Yosemite	0.89	0.20	0.23 ^a			0.73	1.11	0.65	0.23
Point Reyes	1.44	0.80	0.06	0.73	0.66	0.08	0.33	2.22	
Redwoods			1.58			0.15	0.71	1.97	
Kalmiopsis	0.85	0.24	0.06	0.04		0.27	1.22	0.33	0.16
Olympic	0.54	0.25	0.47		0.50	0.18	0.33	0.25	0.08

a. Combined contribution of motor vehicles (gasoline and diesel)

Table 51. Summary of the average source apportionments for the STN sites along the west coast of the United States.

Site	Sulfate	Nitrate	Gasoline	Diesel	Residual Oil	Soil	Wood smoke	Sea Salt	Other
Anchorage	0.89	0.91	2.66	0.33		0.32		0.33	0.67
Seattle - Beacon Hill STN	1.51	1.50	2.51	0.21	0.43	0.22	0.65	0.98	0.65
Seattle - Beacon Hill IMPROVE	1.92	1.66	0.85	0.14	0.60	0.32	1.40	1.05	0.19
Seattle - Olive Street	1.84	2.70	1.38	0.91	0.43	0.99	0.75	0.99	0.50
Seattle - Duwamish	2.48	2.87	1.59	0.65	0.44	0.70	1.21	0.92	1.38
Seattle - Georgetown	1.77	2.00	1.80	0.18		0.49	1.86	1.39	0.14
Seattle - Lake Forrest	1.70	1.19	2.67			0.23	3.07	1.20	
Portland	1.84	1.62	0.97	0.41		0.58	2.82	1.25	0.23
San Jose - 4 th St	1.58	3.29	1.07	0.57		0.99	4.73	2.14	0.37
San Jose- Jackson St	1.99	2.92	1.20	0.45		0.27	4.84	2.52	0.18
Los Angeles Downtown	4.49	6.30	4.50	4.50	2.13	1.45	0.79	1.48	0.77
Simi Valley	3.58	4.51	2.90	2.90	1.09	1.79		1.94	
Rubidoux	3.68	14.06	3.52	3.52	2.27	1.86		3.49	
El Cajon	2.62	3.39	3.23	0.15	0.44	0.43		1.77	
Escondido	2.60	2.92	3.38	0.15	0.57	1.48		1.87	

a. Combined contribution of motor vehicles (gasoline and diesel)

REFERENCES

- Alpert, D.J., Hopke, P.K., 1980. A Quantitative Determination of Sources in the Boston Urban Aerosol, *Atmospheric Environ.* 14,1137-1146.
- Begum, B.A., Kim, E., Biswas, S.K., Hopke, P.K., 2004. Investigation of sources of atmospheric aerosol at urban and semi-urban areas in Bangladesh. *Atmospheric Environment*. 38, 3025-3038.
- Begum, B.A., Kim, E., Jeong, C.-H., Lee, D.-W., Hopke, P.K., 2005. Evaluation of the Potential Source Contribution Function using the 2002 Quebec Forest Fire Episode, *Atmospheric Environ.* 39, 3719-3724.
- Bukowiecki, N., Hegedüs, F., Falkenberg, G., Gehrig, R., Hill, M., Weingartner, E., Baltensperger, U., 2004. Highly Time Resolved Elemental Ambient Concentrations of Railway Generated Aerosols, presented at the European Aerosol Conference, Budapest, September 5-10, 2004.
- California Air Resources Board. 2005. *The California Almanac of Emissions and Air Quality (2005 edition)*,
- Chow, J.C., Watson, J.G., Pritchett, L.C., Pierson, W.R., Frazier, C.A., Purcell, R.G., 1993. The DRI thermal/optical reflectance carbon analysis system, Description, evaluation and applications in U.S. air quality studies. *Atmospheric Environment* 27A, 1185-1201.
- Chueinta, W., Hopke, P.K., Paatero, P., 2000. Investigation of sources of atmospheric aerosol at urban and suburban residential area in Thailand by positive matrix factorization. *Atmospheric Environment* 34, 3319-3329.
- Corbett, J.J., Fishbeck, P.S., 2000. Emissions from Waterborne Commerce Vessels in United States Continental and Inland Waterways, *Environ. Sci. Technol.* 34, 3254- 3260.
- Corbett, J.J., Fischbeck, P.S., Pandis, S.N., 1999. Global Nitrogen and Sulfur Emissions Inventories for Oceangoing Ships. *J. Geophys. Res.*, 104, 3457-3470.
- Endresen, O., Sørge^ord, E., Sundet, J.K., Dalsøren, S.B., Isaksen, I.S.A., Berglen, T.F., Gravir, G., 2003. Emission from international sea transportation and environmental impact, *J. Geophys. Res.* 108(D17), Art. No. 4560, doi:10.1029/2002JD002898.
- Gao, N., Cheng, M.-D., Hopke, P.K., 1993. Potential Source Contribution Function Analysis and Source Apportionment of Sulfur Species Measured at Rubidoux, CA during the Southern California Air Quality Study, 1987, *Anal. Chim. Acta* 277,369-380.
- Gao, N., Cheng, M.-D., Hopke, P.K., 1994. Receptor Modeling of Airborne Ionic Species Collected in SCAQS, 1987, *Atmospheric Environ.* 28,1447-1470.
- Harma, K., Morrison, P.H., 2003. Assessment of the 2002 Biscuit fire complex in southwest Oregon and the landscape condition of the fire area. Pacific Biodiversity Institute.
- Henry, R.C., 2003. Multivariate receptor modeling by N-dimensional edge detection, *Chemom. Intell. Lab. Syst.* 65, 179– 189
- Hopke, P.K., Lamb, R.E., Natusch, D.F.S., 1980. Multielemental Characterization of Urban Roadway Dust, *Environ. Sci. Technol.* 14,164-172.
- Hopke, P.K., Gladney, E.S., Gordon, G.E., Zoller, W.H., Jones, A.G., 1976. The Use of Multivariate Analysis to Identify Sources of Selected Elements in the Boston Urban Aerosol, *Atmospheric Environ.* 10,1015-1025 (1976).
- Huffman, G.P., Huggins, F.E., Shah, N., Huggins, R., Linak, W.P., Miller, C.A., Pugmire, R.J., Meuzelaar, H.L.C., Seehra, M.S., Manivann, A., 2000. Characterization of Fine Particulate Matter Produced by Combustion of Residual Fuel Oil, *Journal of Air and Waste Management Association* 50, 1106-1114.
- Huang, S., Rahn, K.A., Arimoto, R., 1999. Testing and optimization two factor-analysis techniques on aerosol at Narragansett, Rhode Island. *Atmospheric Environment* 33, 2169-2185.
- Hwang, I.J., Hopke, P.K., 2006a. Estimation of Source Apportionment and Potential Source Locations of PM_{2.5} at a West Coastal IMPROVE Site, *Atmospheric Environ.* (In press).

- Hwang, I.J., Hopke, P.K., 2006b., Comparison of Source Apportionments of PM_{2.5} at Two San Jose Speciation Trends Network Sites, *J. Air Waste Manage. Assoc.* 56, 1287-1300.
- Jang, M., Lee, S., Kamens, R.M., 2003. Organic aerosol growth by acid-catalyzed heterogeneous reactions of octanal in a flow reactor. *Atmospheric Environment* 37, 2125-2138.
- Kim, B.M., Teffera, S., Zeldin, M., 2000. Characterization of PM_{2.5} and PM₁₀ in the South Coast Air Basin of Southern California: Part 1—Spatial Variations, *J. Air Waste Manage. Assoc.* 50, 2034-2044.
- Kim, E., Hopke, P.K., 2004a. Source apportionment of fine particles at Washington, DC utilizing temperature resolved carbon fractions. *Journal of Air and Waste Management Association* 54, 773-785.
- Kim, E., Hopke, P.K., 2004b. Improving source identification of fine particles in a rural northeastern U.S. area utilizing temperature resolved carbon fractions. *Journal of Geophysical Research* 109, D09204.
- Kim, E., Hopke, P.K., 2004c. Comparison between Conditional Probability Function and Nonparametric Regression for Fine Particle Source Directions, *Atmospheric Environ.* 38, 4667-4673.
- Kim, E., Hopke, P.K., 2006. Characterization of fine particle sources in the Great Smoky Mountains Area. *Science of the Total Environment* 368, 781-794.
- Kim, E., Hopke, P.K., 2007. Source Characterization of Ambient Fine Particles in the Los Angeles Basin, E. Kim and P.K. Hopke, *J. Environmental Engineering Science* (in press).
- Kim, E., Larson, T. V., Hopke, P.K., Slaughter, J.C., Sheppard, L.E., Claiborn, C., 2003a. Source apportionment of PM_{2.5} in an arid northwest U.S. city by positive matrix factorization. *Atmospheric Research* 66, 291-305.
- Kim, E., Hopke, P.K., Edgerton, E.S., 2003b. Source identification of Atlanta aerosol by Positive Matrix Factorization. *Journal of Air and Waste Management Association* 53, 731-739.
- Kim, E., Hopke, P.K., Paatero, P., Edgerton, E.S., 2003c. Incorporation of parametric factors into multilinear receptor model studies of Atlanta aerosol. *Atmospheric Environment* 37, 5009-5021.
- Kim, E., Hopke, P.K., Larson, T.V., Covert, D.S., 2004a. Analysis of ambient particle size distributions using positive matrix factorization and Unmix. *Environmental Science and Technology* 38, 202-209.
- Kim, E., Hopke, P.K., Edgerton, E.S., 2004b. Improving source identification of Atlanta aerosol using temperature resolved carbon fractions in Positive Matrix Factorization. *Atmospheric Environment* 38, 3349-3362.
- Kim, E., Hopke, P.K., Qin, Y., 2005a. Estimation of Organic Carbon Blank Values and Error Structures of the Speciation Trends Network Data for Source Apportionment, *Journal of Air and Waste Management Association* 55, 1190 - 1199.
- Kim, E., Hopke, P.K., Keski, D.M., Koerber, M., 2005b. Sources of Fine Particles in a Rural Midwestern U.S. Area, *Environ. Sci. Technol.* 39, 4953-4960.
- Lee, E., Chun, C.K., Paatero, P., 1999. Application of positive matrix factorization in source apportionment of particulate pollutants. *Atmospheric Environment* 33, 3201-3212.
- Lee, J.H., Yoshida, Y., Turpin, B.J., Hopke, P.K., Poirot, R.L., Liroy, P.J., Oxley, J.C., 2002. Identification of sources contributing to mid-Atlantic regional aerosol, *Journal of Air and Waste Management Association* 52, 1186-1205.
- Lee, J.H., Hopke, P.K., 2005. Apportioning Sources of PM_{2.5} in St. Louis, MO using Speciation Trends Network Data, *Atmospheric Environment* (submitted).
- Lee, J.H., Hopke, P.K., Turner, J., 2005. Source Identification of Airborne PM_{2.5} at the St. Louis-Midwest Supersite, *Journal of Geophysical Research* (submitted).
- Liu, D.Y., Prather, K.A., Hering, S.V., 2000. Variations in the size and chemical composition of nitrate-containing particles in Riverside, CA, *Aerosol Sci. Technol.* 33, 71-86.

- Liu, D., Wenzel, R.J. and Prather, K.A., 2003, Aerosol time-of-flight mass spectrometry during the Atlanta Supersite experiment: 1. Measurements, *Journal of Geophysical Research* 108(D7), 8426.
- Liu, W., Hopke, P.K., and VanCuren, R.A., 2003. Origins of Fine Aerosol Mass in the Western United States Using Positive Matrix Factorization. *J. Geophys. Res. Atmospheres*, 108 (D23), Paper No. 4716, doi:10.1029/2003JD003678.
- Maykut, N.N., Lewtas, J., Kim, E., Larson, T.V., 2003. Source apportionment of PM_{2.5} at an urban IMPROVE site in Seattle, WA., *Environ. Sci. Technol.* 37,5135-5142.
- Mason, B. (1966). *Principles of Geochemistry*, 3rd edition. Wiley, New York.
- Osan, J., Torok, S., Fekete, J., Rindby, A., 2000. Case Study of the Emissions from a Heavy-Oil-Fueled Hungarian Power Plant, *Energy & Fuels* 14, 986-983.
- Paatero, P., 1997. Least square formulation of robust non-negative factor analysis. *Chemometrics and Intelligent Laboratory Systems* 37, 23-35.
- Paatero, P., Hopke, P.K., 2003. Discarding or Downweighing High-Noise Variables in Factor Analysis Models, *Anal. Chim. Acta* 490, 277-289.
- Paatero, P., Hopke, P.K., Begum, B.A., Biswas, S.K., 2005. A Graphical Diagnostic Method For Assessing the Rotation In Factor Analytical Models Of Atmospheric Pollution, *Atmospheric Environ.* 39, 193-201.
- Peele, C., 2003. Washington State mercury chemical action plan. Washington State department of Health Publication No. 333-051.
- Polissar, A.V., Hopke, P.K., Malm, W.C., Sisler, J.F., 1998. Atmospheric Aerosol over Alaska: 2. Elemental Composition and Sources, *J. Geophys. Res.* 103, 19,045-19,057.
- Polissar, A.V., Hopke, P.K., Poirot, R.L., 2001. Atmospheric aerosol over Vermont: Chemical composition and sources. *Environmental Science and Technology* 35, 4604-4621.
- Pankow, J.F., Mader, B.T., 2001. Gas/solid partitioning of semivolatile organic compounds (SOCs) to air filters. 3. An analysis of gas adsorption artifacts in measurements of atmospheric SOC and organic carbon (OC) when using Teflon membrane filters and quartz fiber filters. *Environmental Science and Technology* 35(17), 3422-3432.
- Qin, Y., Oduyemi, K., Chan, L.Y., 2002. Comparative testing of PMF and CFA models. *Chemometrics and Intelligent Laboratory Systems* 61, 75-87.
- Ramadan, Z., Song, X. H., Hopke, P.K., 2000. Identification of sources of Phoenix aerosol by positive matrix factorization, *Journal of Air and Waste Management Association* 50, 1308-1320.
- Russell, L.M., Noone, K.J., Ferek, R.J., Pockalny, R.A., Flagan, R.C., Seinfeld, J.H., 2000. Combustion Organic Aerosol as Cloud Condensation Nuclei in Ship Tracks, *J. Atmospheric Sciences*, 57, 2591-2606.
- Schauer, J.J., Rogge, W.F., Hildemann, L.M., Mazurek, M.A., Cass, G.R., 1996. Source apportionment of airborne particulate matter using organic compounds as tracers. *Atmospheric Environment* 30, 3837-3855.
- Seinfeld, J.H., Pandis, S.N., 1998. *Atmospheric Chemistry and Physics, from Air Pollution to Climate Change*. John Wiley & Sons, New York.
- Shah, S.D., Cocker, D.R., Miller, J.W. and Norbeck, J.M. Emission rates of particulate matter and elemental and organic carbon from in-use diesel engines, *Environmental Science & Technology* 38, 2544-2550. 2004.
- Solomon, P.A., Mitchell, W., Tolocka, M., Norris, G., Gemmill, D., Wiener, R., Vanderpool, R., Murdoch, R., Natarajan, S., Hardison, E., 2000. Evaluation of PM_{2.5} Chemical Speciation Samplers for Use in the EPA National PM_{2.5} Chemical Speciation Network, EPA-454/R-01-005, Office of Air Quality Planning and Standards, U.S. Environmental Protection Agency, Research Triangle Park, NC., 456 pp.
- Song, X. H., Polissar, A.V., Hopke, P.K., 2001. Source of fine particle composition in the northeastern US, *Atmospheric Environment* 35, 5277-5286.

- Song, C.H., Chen, G., Davis, D.D., 2003. Chemical evolution and dispersion of ship plumes in the remote marine boundary layer: Investigation of sulfur chemistry, *Atmospheric Environment* 37, 2663–2679.
- Tolocka, M.P., Solomon, P.A., Mitchell, W., Norris, G.A., Gemmill, D.B., Wiener, R.W., Vanderpool, R.W., Homolya, J.B., Rice, J., 2001. East versus West in the US: Chemical characteristics of PM_{2.5} during the winter of 1999, *Aerosol Sci. Technol.* 34, 88-96.
- US Census, 2000. <http://www.census.gov/main/www/cen2000.html>.
- VanCuren, R.A., 2003. Asian aerosols in North America: Extracting the chemical composition and mass concentration of the Asian continental aerosol plume from long-term aerosol records in the western United States. *Journal of Geophysical Research* 108(D20), 4623.
- VanCuren, R.A., Cahill, T.A., 2002. Asian aerosols in North America: Frequency and concentration of fine dust, *Journal of Geophysical Research* 107 (D24), 4804.
- Watson, J.G., Chow, J.C., Lowenthal, D.H., Pritchett, L.C., Frazier, C.A., 1994. Differences in the carbon composition of source profiles for diesel and gasoline powered vehicles; *Atmospheric Environment* 28, 2493-2505.
- Watson, J.G., Chow, J.C., Houck, J.E., 2001. PM_{2.5} chemical source profiles for vehicle exhaust, vegetative burning, geological material, and coal burning in Northwestern Colorado during 1995. *Chemosphere* 43, 1141-1151
- Willis, R.D., 2000. Workshop on UNMIX and PMF as applied to PM_{2.5}. EPA 600-A-00-048.
- Xie, Y.L., Hopke, P.K., Paatero, P., Barrie, L.A., Li, S.M., 1999. Identification of source nature and seasonal variations of Arctic aerosol by positive matrix factorization. *Journal of Atmospheric Sciences* 56, 249–260
- Yli-Tuomi, T., Hopke, P.K., Paatero, P., Basumia, M.S., Landsberger, S.L., Viisanen, Y., Paatero, J., 2003. Atmospheric aerosol over Finnish Arctic: Source analysis by the multilinear engine and the potential source contribution function. *Atmospheric Environment* 37, 4381-4392.
- Yu, J.Z., Xu, J.X., Yang, J., 2002. Charring characteristics of atmospheric organic particulate matter in thermal analysis, *Environmental Science and Technology* 36, 754-761, 2002.
- Yu, K.N., Cheung, Y.P., Cheung, T., Henry, R.C., 2004. Identifying the impact of large urban airports on local air quality by nonparametric regression, *Atmospheric Environ.* 38, 4501-4507.
- Zhao, W., Hopke, P.K., 2004. Source Apportionment for Ambient Particles in the San Geronio Wilderness, *Atmospheric Environ.* 38, 5901-5910.
- Zhao, W., Hopke, P.K., 2006. Source Identification for Fine Aerosols in Mammoth Cave National Park, *Atmospheric Res.* 80, 309-322.
- Zhou, L., Kim, E., Hopke, P.K., Stanier, C., Pandis, S., 2004. Advanced factor analysis on Pittsburgh particle size distribution data. *Aerosol Sci. Technol.* 38 (S1), 118-132.